HIGH EFFICIENCY LOOSELY COUPLED WIRELESS POWER TRANSFER SYSTEM VIA MAGNETIC INDUCTION

By

ZHEN NING LOW

A DISSERTATION PRESENTED TO THE GRADUATE SCHOOL
OF THE UNIVERSITY OF FLORIDA IN PARTIAL FULFILLMENT
OF THE REQUIREMENTS FOR THE DEGREE OF
DOCTOR OF PHILOSOPHY

UNIVERSITY OF FLORIDA

2009

To my parents and wife

ACKNOWLEDGMENTS

I would like to thank my advisor Dr. Jenshan Lin for this wonderful opportunity to work under his guidance and mentoring. I have truly enjoyed working for him over the years acquiring technical knowledge as well as other soft skills. I would also like to thank Dr. William Eisenstadt, Dr. David Arnold and Dr. Sumi Helal for their time and being on my committee. I would like to thank my project teammates, both past and present for which without them this work will not be possible. They are: Joaquin Casanova for electromagnetic analysis and coil design; Jason Taylor for PCB design and fabrication; Raul Chinga for all the late night prototyping work; and Ashley Trowell for ferrites and shielding work. I would like to thank WiPower and Florida High Tech Corridor for funding this project. I would like to thank Linear Technology and Terry Decker for their support and evaluation boards. I would also like to thank Shannon Chillingworth and all of the personnel in the EE office.

Finally, I would like to thank my wife for her encouragement and unconditional support when things get rough. Without her, this would not be possible.

TABLE OF CONTENTS

page

ACKNOWLEDGMENTS 4

LIST OF TABLES 8

LIST OF FIGURES 9

ABSTRACT 15

CHAPTER

1 INTRODUCTION 16

1.1 History of Wireless Power Transmission 18
1.2 Modern Wireless Power Transmission 20
1.3 Background Information 23
1.3.1 Fundamental Theory of Operation via Phase Response 23
1.3.2 Class D Power Amplifier 26
1.3.3 Class E Power Amplifier 30

2 WIRELESS POWER TRANSFER SYSTEM 38

2.1 Single-channel Class E Power Amplifier 39
2.2 Multi-channels/Stackable Class E Power Amplifier 41
2.3 Inductive Coupling 42
2.4 Impedance Transformation Network 44
2.5 Receiver 47

3 DESIGN OF IMPEDANCE TRANSFORMATION NETWORK 50

3.1 Series-Parallel Impedance Transformation Network 50
3.1.1 Introduction 50
3.1.2 Determination of C_{rx} value 53
3.1.3 Determination of C_{out} value 58
3.1.4 Determination of C_{shunt} value 59
3.2 Parallel-Parallel Impedance Transformation Network 60
3.2.1 Introduction 60
3.2.2 Determination of C_{rx} value 61
3.2.3 Determination of C_{tx} value 63
3.2.4 Determination of C_{shunt} value 67

4 WIRELESS POWER TRANSFER SYSTEM SUPPORTING MULTIPLE RECEIVERS 69

4.1 Inductive Coupling 69
4.2 Switch Design 72
4.3 Switch Simulation 76
4.4 System Response with Receiver Switch 79

5 EXPERIMENTAL VERIFICATION 83

5.1 High Power 300W Dual Channel System using Parallel-Parallel Impedance Transformation Network Topology 83
5.2 Low Power Multiple Receivers System with decoupling Switch using Series-Parallel Impedance Transformation Network Topology 95

6 INTEROPERABILITY BETWEEN DIFFERENT PLATFORMS (COIL SIZES) 104

6.1 Test Bench Setup 105
6.2 Experimental Verification 107

7 LOAD/FAULT DETECTION AND POWER DELIVERY TRACKING 111

7.1 Load/Fault Detection Scheme 112
7.1.1 Detection Circuit 112
7.1.2 Detection Flowchart/Logic 115
7.2 Experimental Verification 117
7.2.1 Test Bench and Circuit 117
7.2.2 Experimental Results 122
7.3 Extension of Load/Fault Detection Scheme 130
7.3.1 M:N Coupling Structure 130
7.3.2 Removing L_{out} from Transmitter 139

8 RECEIVER VOLTAGE CONTROL 146

8.1 Varying Supply Voltage to Achieve Receiver Voltage Control 147
8.2 Varying Operating Frequency to Achieve Receiver Voltage Control 152
8.3 Varying C_{out} to Achieve Receiver Voltage Control 157
8.4 Conclusion 160

9 SUMMARY AND FUTURE WORK 162

9.1 Summary 162
9.2 Future Work 164

APPENDIX: FCC REGULATIONS 166

LIST OF REFERENCES 169

BIOGRAPHICAL SKETCH 172

LIST OF TABLES

Table		page
5-1	Component Values for High power 300W Dual Channel System using Parallel-Parallel Impedance Transformation Network Topology	84
5-2	Component Values for Low Power Multiple Receivers System with decoupling Switch using Series-Parallel Impedance Transformation Network Topology	96
6-1	Specification of the three different platforms	105
6-2	Coupling parameters of nine possible combinations with first three as intended pairs	106
7-1	Component Values for Load/Fault Detection Test Bench	118
A-1	FCC Part 18.307 conduction test limits	166
A-2	FCC Part 15.109 emission limits at 3 m range	167

LIST OF FIGURES

Figure		page
1-1	Block diagram of the multiple receivers wireless power transfer system using inductive coupling.	17
1-2	Complex plane of inductive and capacitive load.	24
1-3	Phasor diagram.	25
1-4	Class D power amplifier.	26
1-5	Class E power amplifier.	31
2-1	Wireless power transfer system diagram.	38
2-2	Schematic of the dual-channel Class E power amplifier.	41
2-3	Topologies for a single-element impedance transformation network.	45
2-4	Input voltage of a half wave rectifier and a full wave rectifier.	48
3-1	Windings of a 20cm x 20cm transmitting coil used for experimental verification.	51
3-2	Normalized power deliver with respect to location of transmitting coil in Figure 3-1 using a receiving coil of 9 cm x 6 cm.	52
3-3	Simplified schematic of wireless power transfer system using series-parallel impedance transformation network and Class E transmitter. Z_{tx} – Impedance looking into the transmitter load network. Z_{txcoil} – Impedance looking into the transmitting coil. Z_{rx} – Impedance looking into receiver network. R_{Load} is the equivalent resistance looking into the rectifier.	53
3-4	Resistance and reactance of Z_{rx} versus load resistance at different with different C_{rx}. (50 nF, 100 nF and 150 nF)	54
3-5	Peak resistance response looking into the transmitting coil with respect to C_{rx}.	56
3-6	Resistance and reactance looking into the transmitting coil.	56
3-7	Coupling efficiency with respect to load resistance.	57
3-8	Z_{tx} phase response with respect to load resistance for various C_{out} capacitance values.	58
3-9	Transistor drain voltage waveform for different load resistance. (C_{shunt} = 10 nF)	59

3-10 Simplified schematic of wireless power transfer system using parallel-parallel transformation network and Class E transmitter. Z_{tx} – Impedance looking into the transmitter load network. Z_{txcoil} – Impedance looking into the transmitting coil. Z_{rx} – Impedance looking into receiver network. R_{Load} is the equivalent resistance looking into the rectifier. 61

3-11 Optimum receiver capacitor value versus load resistance. 61

3-12 Coupling efficiency and transformed impedance looking into the transmitting coil. 63

3-13 Reactance of Z_{txcoil} versus load resistance with different C_{tx}. 65

3-14 Amplitude and phase of impedance of unloaded Z_{tx} versus C_{tx}. 66

3-15 R_{tx} and X_{tx} versus load resistance. (C_{tx}: 105 nF) 66

3-16 Phase of Z_{tx} versus load resistance. (C_{tx}: 105 nF) 67

3-17 Transistor drain voltage waveform for different load resistance. (C_{shunt} = 19 nF) 67

4-1 Power delivery to loads for a single receiver setup and a dual receivers setup with one of the load fixed at 1000Ω. 71

4-2 Block diagram of the proposed switch. 72

4-3 Schematic of the proposed switch circuit. 74

4-4 Schematic of the improved proposed switch circuit. 75

4-5 Schematic of the switch in Advanced System Design with a resistive as load. 76

4-6 Switch control waveform (0 V for off and 3 V for on). A minimum of 1 V is required to turn on the transistor. 77

4-7 Generated switch control waveforms. 78

4-8 Output waveform of the switch before the rectifier. 79

4-9 Proposed half-wave rectifier receiver architecture. 79

4-10 ADS schematic of test bench for receiver architecture in Figure 5-10. 81

4-11 Simulation results of test bench (Figure 4-10). Red: Low voltage control signal.Black: Receiver rectified voltage. 82

5-1 Photograph of the dual-channel Class E power amplifier. 85

5-2 Photograph of the transmitting coil – 10 turns (embedded into the table top) and receiving coil – 5 turns (placed on top). 85

5-3 Power delivery (left y-axis) and efficiency (right y-axis) of the system versus load resistance. Supply voltage: 120 V. 86

5-4 Transistor and inductor temperature with natural convection cooling and forced air cooling versus supply voltage. 87

5-5 Photograph of the dual-channel Class E power amplifier with forced air cooling. 88

5-6 Voltage and current waveforms of the Class E transmitter. 89

5-7 Power delivered to load versus load resistance. A maximum power of 69 W occurs approximately at 50Ω for dual-channel and maximum power of 10 W occurs at approximately at 75Ω for single-channel. Supply voltage: 60 V. 89

5-8 Mode-switching operation for optimized efficiency across a wide power delivery range. (1) Dual-channel mode for higher power, (2) Dual-channel mode switch-over to single-channel mode when better efficiency can be obtained at a lower power level, (3) Single-channel mode for lower power, (4) Single-channel mode switch-over to dual-channel mode when higher power delivery is needed. Supply voltage: 60 V. 90

5-9 System efficiency versus load resistance with a maximum efficiency of 64.5% for a single-channel system, and 76% for a dual-channel system - at approximately 70Ω. Supply voltage: 60 V. 91

5-10 Transmitter efficiency versus load resistance. Maximum transmitter efficiency occurs across the range of 60Ω to 100 Ω load resistance at 90% for dual -channel and 79% for single-channel. Supply voltage: 60 V. 92

5-11 System efficiency versus load resistance for single-channel and dual-channel modes achieving high efficiency at high power output. It also illustrates that a single-channel mode is more efficient at low power delivery states. Supply voltage: 60 V. 93

5-12 Transmitting coil RMS voltage versus load resistance. Supply voltage: 60 V. 93

5-13 Receiver DC voltage versus load resistance, converging to approximately 70 V in dual-channel mode and 38 V in single-channel mode. Supply voltage: 60 V. 94

5-14 Photograph of a test setup with two receivers with decoupling switch on the packaged transmitting coil. 96

5-15 Power delivery to the receiver with switch and system efficiency versus load resistance for a one-to-one setup (simulated and measured) 97

5-16 Efficiency of power delivery to the receiver with switch versus power delivered for a 1 to 1 setup (simulated and measured) 98

5-17 Comparison between receiver with switch and receiver without switch. 99

5-18 Comparison between single receiver standalone and dual-receiver setup with one receiver switched off. 99

5-19 Power delivery to receiver 1 versus its load resistance at different fixed receiver 2 load resistance. 101

5-20 Power delivery to receiver 2 versus receiver 1 load resistance at different fixed receiver 2 load resistance. (same legends as in Figure 5-20) 101

5-21 System efficiency versus total power delivery to both receivers with the load resistance of receiver 2 fixed and the load resistance of receiver 1 swept across the stated range for a dual-receiver test bench. (same legends as in Figure 5-20) 102

5-22 Measured power delivery to a dual-receiver system with load resistance varied from 10Ω to 2000Ω. 103

6-1 System efficiency and receiver voltage vs. power delivery plot for different sized receiving coil on a small sized transmitting coil. 107

6-2 System efficiency and receiver voltage vs. power delivery plot for different sized receiving coil on a medium sized transmitting coil. 109

6-3 System efficiency and receiver voltage vs. power delivery plot for different sized receiving coil on a big sized transmitting coil. 110

7-1 Block diagram of the proposed wireless power transfer system with detection circuit (detecting supply current and coil voltage) 112

7-2 Schematic of coil current extraction network using a current sense resistor. 114

7-3 Detection scheme flow chart for proposed system. 116

7-4 Photograph of the fabricated transmitter circuit with control circuit. 118

7-5 Schematic of power stage of fabricated transmitter. 119

7-6 Schematic of driver stage of fabricated transmitter. 119

7-7 Schematic of detection and control stage of fabricated transmitter. 120

7-8 Efficiency-Power plot of single receiver setup (Solid black line: Small coil. Dashed gray line: Big coil) 122

7-9 Examples of different loading conditions and fault modes on coil voltage versus supply current space. 123

7-10 Efficiency-power plot of three sets of dual load measurements and two sets of single load measurements using a combination of big and small receiving coils. 125

7-11 Transmitter coil voltage and supply current space illustrating three different zones: no-load, single load, and dual loads. 126

7-12 Transmitter coil voltage and supply current space diagram illustrating three different zones, no-load, safe and fault. 127

7-13 Linear relationship between supply current and power delivered to the loads for all 5 sets of measurements. Solid dashed line: y = 0.095x + 0.055. 129

7-14 Power delivery error distribution plot. Calculated power delivery is based on measured supply current. Solid dashed line: ideal error free calculation. 129

7-15 Examples of M:N coupling structures. 131

7-16 Measured power delivery of a dual receiver setup on a dual transmitting coil test bench with both receivers on a single coil leaving the other coil unloaded. 132

7-17 Measured power delivery of a dual receiver setup on a dual transmitting coil test bench with one receiver on each transmitting coil. 133

7-18 Efficiency-power plot of two sets of dual load measurements and two sets of single load measurements. (Green lines: Single receiver, Blue lines: Dual receivers on single transmitting coil, Red lines: Dual receivers on dual transmitting coil) 134

7-19 Transmitter coil voltage and supply current space. (Green diamond: No load, Black lines: Single receiver, Blue lines: Dual receivers on single transmitting coil, Read lines: Dual receiver on dual transmitting coil) 134

7-20 Linear relationship between supply current and power delivered to the loads for all 4 sets of measurements. Solid dashed line: y = 0.076x + 0.048. 135

7-21 Power delivery error distribution plot. Calculated power delivery is based on measured supply current. Solid dashed line: ideal error free calculation. 136

7-22 Transmitter coil voltage and supply current space with fault tests. (Green lines: Fault tests without valid receiver on one of the coil, Purple lines: Fault tests with a valid receiver on one of the transmitting coils) 137

7-23 Different methods of driving a 2:N structure. 139

7-24 Block diagram of wireless system without L_{out}. 140

7-25 Transmitter coil voltage and supply current space with fault tests with L_{out} removed. (Green lines: Fault tests without valid receiver on one of the coil, Purple lines: Fault tests with a valid receiver on one of the transmitting coils) 141

7-26 Waveform of the transmitter circuit without L_{out} when fault conditions overlaps with valid load conditions. (Red: Drain voltage, Orange: Coil voltage, Green: Coil Current) 142

7-27 Spectrum of transmitter coil voltage without L_{out} when fault conditions overlaps with valid load conditions. 142

7-28 Waveform of the transmitter circuit with L_{out} when fault conditions overlaps with valid load conditions. (Red: Drain voltage, Orange: Coil voltage, Green: Coil Current) 143

7-29 Spectrum of transmitter coil voltage with L_{out} when fault conditions overlaps with valid load conditions. 144

8-1 Block diagram of wireless power system. 146

8-2 Efficiency-power plot for supply voltage from 18 V to 30 V in steps of 1 V. 148

8-3 Receiver Voltage-Power plot for supply voltage from 18 V to 30 V in steps of 1 V. 149

8-4 Linear relationship between supply current and power delivered to the load for supply voltage from 18 V to 30 V in steps of 1 V. 151

8-5 Efficiency-power plot for operating frequency from 240 kHz to 250 kHz in steps of 2 kHz. 153

8-6 Receiver voltage-power plot for operating frequency from 240 kHz to 250 kHz in steps of 2 kHz. 153

8-7 Efficiency-power plot for operating frequency from 235 kHz to 240 kHz in steps of 1 kHz. 155

8-8 Receiver voltage-power plot for operating frequency from 235 kHz to 240 kHz in steps of 1 kHz. 156

8-9 Linear relationship between supply current and power delivered to the load for operating frequency from 235 kHz to 250 kHz in steps of 1 kHz. 156

8-10 Efficiency-power plot for different C_{out} values. 158

8-11 Receiver voltage-power plot for different C_{out} values. 158

8-12 Linear relationship between supply current and power delivered to the load for C_{out} values of 15 nF, 16 nF, 17.2 nF and 18.2 nF. 159

Abstract of Dissertation Presented to the Graduate School
of the University of Florida in Partial Fulfillment of the
Requirements for the Degree of Doctor of Philosophy

HIGH EFFICIENCY LOOSELY COUPLED WIRELESS POWER TRANSFER SYSTEM VIA MAGNETIC INDUCTION

By

Zhen Ning Low

August 2009

Chair: Jenshan Lin
Major: Electrical and Computer Engineering

After the introduction of cellular technology and WiFi technology, the power cable is the last cable that has yet to be eliminated. Magnetic induction is the leading technology to achieve wireless power transfer at high efficiencies (>75%) with power level ranging from several microwatts to thousands of watts. Using near-field operation at frequencies below 1 MHz significantly lowers the probability of interference and RF safety issues since the wavelength is extremely long and radiation is limited.

Design rules are developed to select the components of the system, which are further verified by experiments. Interoperability analysis shows that the system is sufficiently robust that coils from one platform can be used in another platform without damaging the receiver. A method of load/fault detection is proposed and verified with both hardware and software implementation. Finally, three different methods to control the unregulated receiver voltage control and power delivery is studied and it is determined that varying C_{out} in a single discrete step is able to allow the system to achieve sufficient control.

CHAPTER 1
INTRODUCTION

A wireless power transfer system is any system that has the capability to transfer electrical power from a power source to an electrical load without any interconnecting wires. A wireless power transfer system will have three basic building blocks:

1. Transmitter: DC power is converted to AC power which is used to drive the transmitting antenna (coil).
2. Energy Transfer: The AC power is transmitted through space to some point where a receiving unit is located.
3. Receiver: The transmitted AC power is collected and converted to DC by a rectification process.

Wireless power systems fall into two main categories, medium to long range, where the coverage is greater or equal to a typical Personal Area Network (PAN) which is typically a 10 m radius, and short range, where the coverage is localized within the vicinity of the transmitting device (typically a 5" distance). Although there have been attempts [1-3] to achieve long range power delivery via far-field techniques, the efficiency and power delivery is insufficient to charge even a typical cellular phone overnight. In order to provide power comparable to a typical wall mounted DC supply, the system would most likely violate RF safety regulations [4] or use a large number of transmitters resulting in an impractical implementation. Therefore, far-field techniques are most suitable for very low power applications (< 100 mW) unless they are used in less regulated environments such as military or space exploration. Inductive coupling has been one of the leading candidates in achieving wireless power transfer at power levels ranging from several microwatts to several kilowatts. Its operating range is limited as power delivery and efficiency degrades rapidly with increasing distance between the transmitting and receiving unit. Using near-field operation at frequencies below 1 MHz significantly lowers the probability of interference and RF safety issues since the wavelength is extremely long and radiation is limited.

Unlike far-fields techniques, near-field techniques are extremely sensitive to the loading conditions of the receiver(s) as well as the number of receivers. The block diagram of the wireless power transfer system using inductive coupling is show in Figure 1-1.

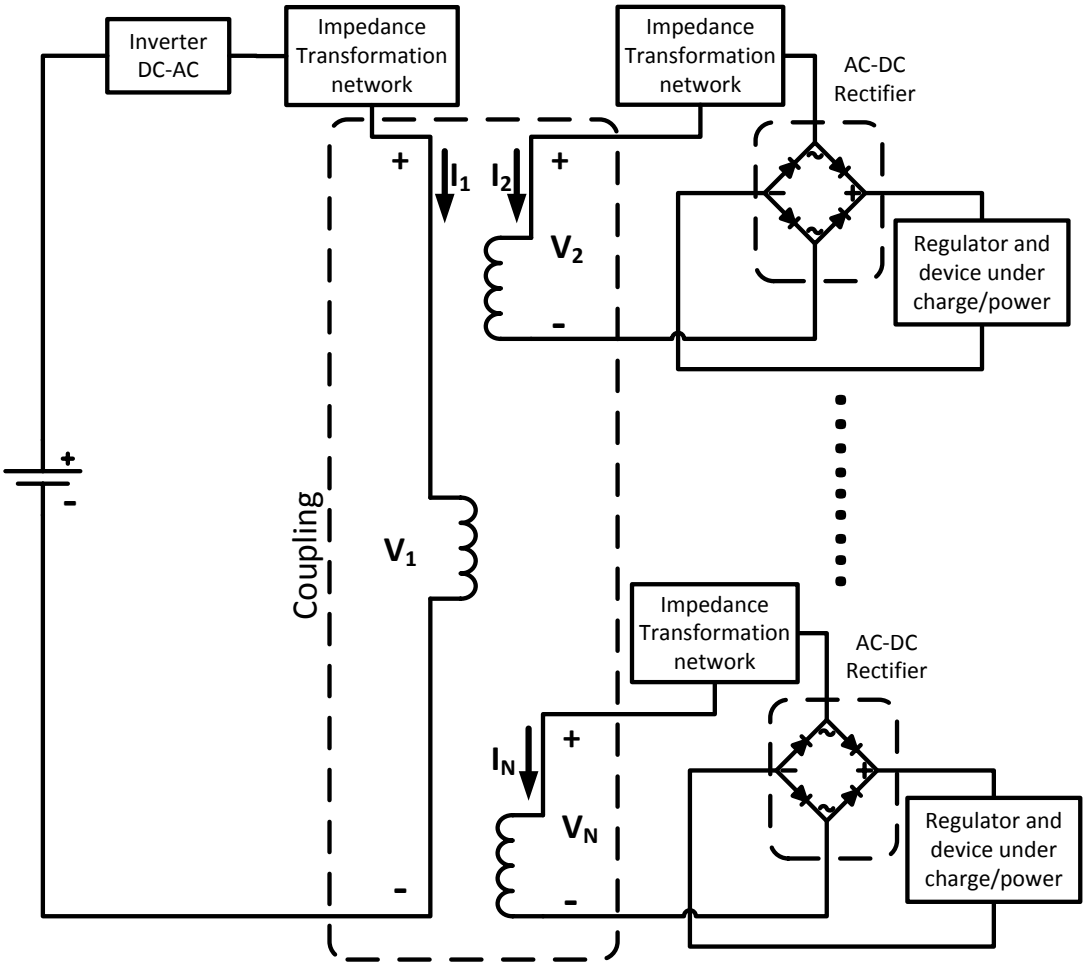

Figure 1-1. Block diagram of the multiple receivers wireless power transfer system using inductive coupling.

Other methods of wireless power transmission include using means of optics such as laser. Although, it is easy to focus a laser beam, energy conversion from electricity to laser is extremely inefficient. In addition, current state of the art photovoltaic cells used to convert the received laser to electrical energy have an efficiency of typically less than 50%.

1.1 History of Wireless Power Transmission

The beginning of wireless power transmission can be dated back to 1868 when James Clerk Maxwell developed the classical electromagnetic theory. Maxwell's equations unify previous unrelated observations of electricity, magnetism and optics into one consistent theory. Later in 1888, Heinrich Rudolf Hertz verified the existence of electromagnetic radiation by building the first radio transmitter.

The first significant breakthrough in wireless power transmission technology happened in 1897 when Nikola Tesla filed his first patents based on the Wardenclyffe Tower, which is also known as Tesla Tower in Colorado Springs. According to [2], Tesla resonated a 3 feet diameter copper ball on top of the 200 feet power with 300 kW of power from the Colorado Springs Electric Company.

There were various attempts after the Second World War to make an efficient transmission of large amount of power wirelessly but they have failed. This is because the device technology during that time was insufficient to either generate sufficient amount of power or effectively rectify the received microwave power. In 1964, William C. Brown invented the "Amplitron" [5] which is commonly known as the crossed-field amplifier. The amplifier is capable of an output of 400 kW at efficiency of 70%. With the development of silicon Schottky-barrier diodes by Hewlett-Packard Associates, high efficiency high power wireless power transfer was made possible. In 1975, the largest wireless power transfer was demonstrated at the Venus Site of JPL Goldstone Facility. 450 kW of power was transmitted across one mile using a 26m diameter parabolic antenna [2]. The 3.4 m x 7.2 m receiving rectenna array achieved a rectified DC power of 30 kW at 82.5% efficiency. The system efficiency was only 6.67% efficiency without taking the transmitter into consideration. Therefore, most of the power loss was still due to radiation. Generating a focused electromagnetic beam so that all of the energy can be projected onto a

small area remains a challenging task. The only two ways to achieve an efficient power transfer over a long distance is to increase the number of transmitting antenna elements so as to achieve a more focused beam or increase the number of elements of the receiving rectenna. Repeater stations can be used to reduce the radiation loses, but the conversion losses to retransmit the power can be so high that it is not feasible.

A more feasible alternative to the long range power transmission is via inductive coupling. However, the operating range is limited to the proximity of the transmitter. The roots of inductive coupling date back to 1831 when Michael Faraday demonstrated that in order to induce a current on a conductor the magnetic field needs to be changing [6]. Faraday did not continue to pursue the work in this area and left it for others to pick up from where he left off. Among many who have tried to study the phenomena was Joseph Henry. All the experiments were conducted by manually turning on and off DC supplies, until the introduction of dynamo in 1860s making AC supply available. Sir William Grove was the first to connect a transformer to an AC source to generate high voltage for his laboratory work.

One of the earliest successful demonstrations of a consumer product using inductive coupling with considerable power is the inductive cooker. In 1971, during the National Association of Home Builders convention in Houston, TX Westinghouse Electric Company demonstrated single burner range using a 25 kHz operating frequency [7].

On the other end of the power band, General Electric introduced the rechargeable cordless electric toothbrush in 1961, mitigating the risk of an electric shock [8]. The power transfer is achieved by splitting a transformer core into two, for which one of the core is located into the “base station” and the other is located in the toothbrush. Energy can be coupled to the toothbrush by placing it onto the “base station” with proper alignment.

The challenge of a robust inductive coupling is to be able to transfer energy to a receiving device with considerable lateral degree of freedom. In addition, portable electronics are getting very compact and lightweight, and consumers are unwilling to accept the huge heavy ferrite core. By using an air core transformer and with the receiver much smaller than the transmitter the coupling is extremely poor. The only solution is to increase the operating frequency to enhance the coupling but it is only in the recent years that power transistors are capable of achieving high power and high speed making considerable amount of power via magnetic induction possible. In addition, losses through the windings were significant due to skin depth and proximity effect until the introduction of Litz wires.

1.2 Modern Wireless Power Transmission

The first company to start working on inductive coupling wireless power system was Splashpower [9] in 2001. In order to avoid the receiving device from "blocking" the vertical field, Splashpower developed a unique coil design which enables the transmitting platform to transmit a horizontal field in both X and Y direction. This enables the receiver to be insensitive to location and rotation. However, with the introduction of many compact and low profile devices such as Apple's iPod and Motorola's Razr, modern consumer electronics are more sensitive to the thickness of the device. Therefore, the allowable extra cross sectional area on the receiving device is almost non-existent. In addition being one of the early adopters of the technology, the Splashpower system operates in tens of kilohertz making the system more inefficient than current solutions which operate at hundreds of kilohertz. Splashpower was acquired by Fulton Innovation also known as eCoupled in 2008.

eCoupled's wireless power technology was a by-product of its parent company Alticor's eSpring water purifier [10]. Approximately 10 years ago engineers at eCoupled were trying to prevent corrosion and electrical shock hazard to the ultraviolet lamp; in the end they developed a

wireless power system to solve their problem. The system designed by eCoupled involves complex control schemes and costly communication link to achieve resonance operation. Although the cost of the system is reasonable to the unique water purifier, it is considered to be high for cost sensitive consumer electronics which have very low profit margin. However, eCoupled has successfully demonstrated a power delivery up to 1000 W grilling a piece of steak on a George Foreman grill as well as powering a 2000 W blender.

ConvenientPower [11] is brainchild of Professor Ron Hui from the City University of Hong Kong. His first technical journal was dated back to 2005 which is the first published for portable electronics. Professor Hui's most significant contribution to the wireless power space is the design concept of generating an even magnetic field across a large area. Although, 7 journal papers were published and 6 patents were awarded, little was known about the system as there hasn't been any official demonstration conducted to the press. Available literature indicates that the system is a variation of magnetic induction proposed by Splashpower, eCoupled and WiPower [14] using the same underlying principles.

PowerMat [12] which is based in Israel is the newest player in the wireless power space. Neither publications nor patents have been found so far. Similar to ConvenientPower little information is known about the technology. Although, there was an official demonstration to the press during the recent Consumer Electronics Show 2009 in Las Vegas, there was little discussion about the technology. PowerMat claimed that the innovation is more of the communication protocol than the wireless power technology. Based on the limited information provided at CES and the company's website, one can deduce that their technology is also a variation of magnetic induction similar to Splashpower, eCoupled and WiPower.

WiTricity [13] was developed in a research team led by Professor Marin Soljačić in MIT. Two carefully aligned huge capacitively loaded coils with a diameter of 24 inches were used to transmit power to a 60 W light bulb at 2 m away with an approximate efficiency of 40%. The operating frequency was at 10 MHz instead of the sub megahertz range. Greater operating range was achieved by increasing operating frequency and coil size. In addition, the system was designed for resonance, thus the system will need complex control schemes to seek resonance under varying load conditions.

Research work on wireless power transmission via magnetic induction for WiPower [14] started during late 2006 at the University of Florida. Instead of seeking resonance, the system design is based on the load impedance response taking varying load impedance into account. The WiPower wireless power system ensures that the system's natural response matches closely with a typical off the shelf wall wart, ensuring unconditional stability at any load impedance. The system can be easily scaled to the required power level and power delivery up to 300 W has been demonstrated.

PowerCast [15] founded in 2003 is the only wireless power company which took the long range far field approach. Operating at ISM bands of 900 MHz and 2.4 GHz the system is able to achieve considerable coverage. However, the system suffers from the fundamental problem of power losses due to radiation resulting in mediocre power delivery. The efficiency is far worse than Brown's experiment in 1975 where Brown used a focused beam for a point to point RF link. Since the system requires covering a large area, a point to point system using a focused beam will not be practical for consumer applications. To date the PowerCast system only has the power handling capabilities of lighting LEDs or provide supplementary power to low power wireless sensor nodes.

1.3 Background Information

The purpose of this section is to provide the background information relating to the material presented in later chapters. This section starts with a discussion the fundamental theory of operating via phase response and how power control can be achieved by this technique. Following that a discussion of two popular high efficiency switch mode power amplifier topologies, the Class D and Class E, which includes their analysis equations are presented. The discussion will enable the reader to appreciate the advantages and disadvantages of each topology. Using the analysis, the Class E power amplifier is found to be a more suitable amplifier than the Class D power amplifier because it is able to achieve high efficiency operation from a phase angle of 40° to 70° while controlling the power delivered to the receiver.

1.3.1 Fundamental Theory of Operation via Phase Response

To ensure unconditionally stable operation, the system must be able to deliver the required power with respect to the load resistance closely matching that of a constant voltage power source. The transmitted power should decrease when the load impedance increases vice versa. Error in selecting component values or control scheme will result in either oscillation or undesirable power delivery trend, that is, the transmitter will increase its output when the load resistance increases. The switching buck regulator at the receiver will attempt to maintain its power delivery by increasing its input resistance or decrease its duty cycle resulting in a positive feedback. Poor efficiency will be observed due to excess power dissipated as heat and device failure may occur due to over-voltage.

There are various methods to achieve the desirable power delivery trend. A closed-loop system will require some form of control scheme and tunable components/supply voltage as well as a communication link between the receiver and transmitter. This will cause the system to be complicated, bulky in size and costly. The optimum solution to the problem is to achieve the

desired power delivery trend with respect to load resistance across a wide range of load resistances. This can be achieved by designing the system to have an effective resistance response or phase response looking into the transmitting coil. Since the class E power amplifier, which has a limited range of operating load resistance, is selected for the system and it is difficult to generate the desirable effective resistance trend while maintaining a fixed reactance using a pair of loosely coupled coils, the technique of power delivery control exploiting phase response will be more appropriate. Figure 1-2 shows the complex plane of inductive and capacitive load. Since only positive resistive loads are consider, the analysis will only consider the right half plane. The class D power amplifier [16] and class E power amplifier [18] are not suitable to drive capacitive loads, thus, the first quadrant of the Figure 1-2 will be the only valid region of operation.

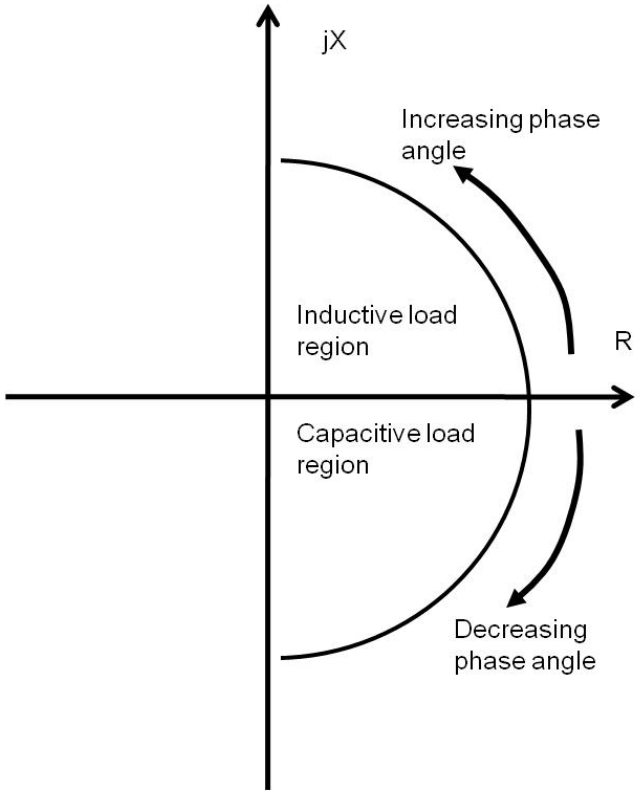

Figure 1-2. Complex plane of inductive and capacitive load.

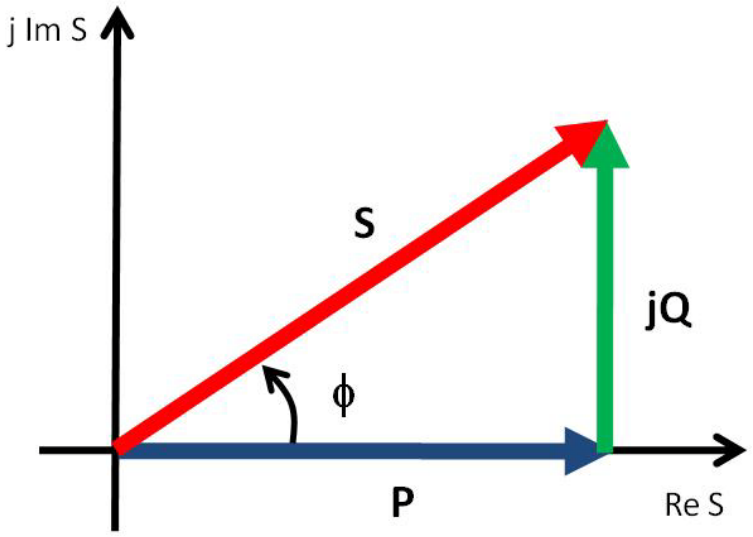

Figure 1-3. Phasor diagram.

Where

P: Real power. Unit: watts (W)

Q: Reactive power. Unit: volt-amperes reactive (VAr)

S: Complex power. Unit: volt-amperes (VA)

|S|: Apparent power. Unit: volt-amperes (VA)

ϕ: Phase angle of the load.

Figure 1-3 shows the phasor diagram to illustrate the concept of power delivery versus phase response. The real power delivered to the load is reduced when the magnitude of the apparent is kept relatively the same while increasing its phase angle to be more inductive in the anti-clockwise direction. The system can make use of such delivery trend to achieve a desirable power delivery profile with increasing load resistance. The trend can be achieved by using a series of reactive networks before the transmitting coil and after the receiving coil to shape the impedance response accordingly. The magnitude of the apparent power can also be varied to improve the power delivery trend.

1.3.2 Class D Power Amplifier

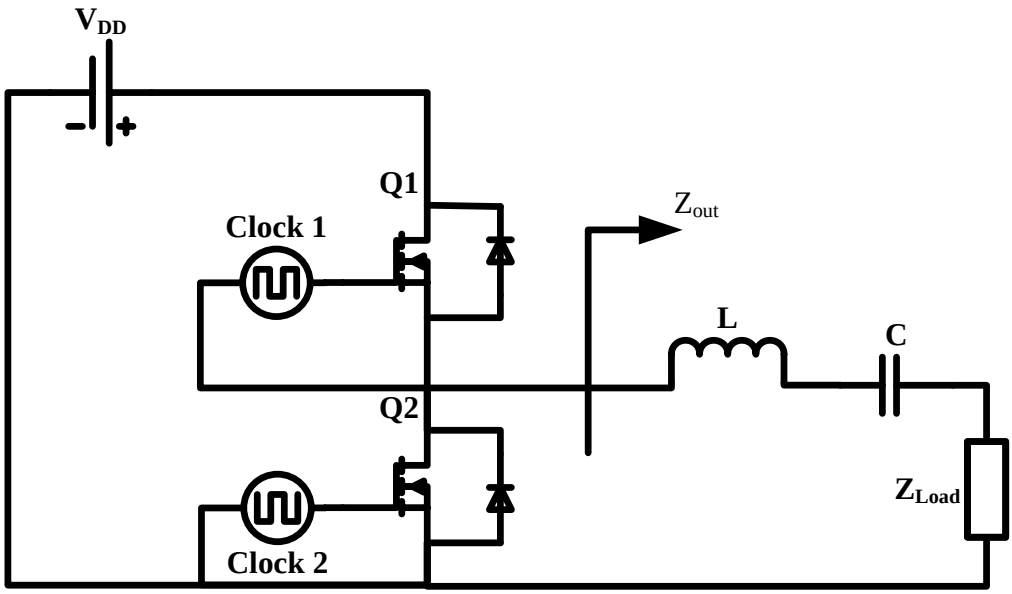

Figure 1-4. Class D power amplifier.

Driving the transmitting coil is the most crucial part of the system. In order to achieve high efficiency, only switch mode amplifier topologies will be considered for the system. Since the system should be kept simple with minimum component count, only Class D and Class E power amplifier topologies are considered. The class D power amplifier will be discussed in this section whereas the class E power amplifier will be discussed in the following section.

Class D power amplifiers have been traditionally considered as the most practical high-frequency switch mode amplifiers. The main advantage of a Class D power amplifier is that the voltage stress across the transistors is equal to the supply voltage making them suitable for either high voltage or high speed. A circuit of the Class D power amplifier consisting of two transistors Q1 and Q2 which can be modeled as two bidirectional switches, an LC output filter and a load Z_{Load} is shown in Figure 1-4. It was found that the class D power amplifier is able to drive both resistive and inductive loads but not capacitive loads [17]. The body-drain diode of the MOSFET can be used as an anti-parallel diode in case of an inductive load.

The analysis of the class D power amplifier is based on Figure 1-4 with the following four assumptions.

1. The transistor and diode forms an ideal resistive switch. All parasitic capacitance and switching time are neglected. In addition, the turn on resistance remains constant.
2. The turn on resistance of the Q1 is sufficiently small that voltage drop across Q1 can be neglected. The turn on resistance of Q1 can be moved to be part of Z_{out}.
3. The reactive components L and C are not sensitive to frequency.
4. The loaded quality factor of the output LC filter is high enough that the current through Z_{Load} is sinusoidal.

The impedance Z_{out} looking into the load network can be described by Equation 1-1

$$\begin{aligned} Z_{out} &= Z_{Load} + j\omega L + R_{L\_\text{P}arasitic} + \frac{1}{j\omega C} + \\ &\quad R_{C\_\text{P}arasitic} + R_{turn-on\ transistor} \\ &= R_{Load} + R_{L\_\text{P}arasitic} + R_{C\_\text{P}arasitic} + \\ &\quad R_{turn-on\ transistor} + j\omega\left(\frac{X_{Load}C + LC - 1}{C}\right) \end{aligned} \tag{1-1}$$

According to Figure 1-4, it can be inferred that the input voltage to the load network is a square wave from ground to V_{DD} neglecting the losses through the turn on resistance of the transistor. The square wave can be described by Equation 1-2.

$$v_{out} = \begin{cases} V_{DD} & \text{for } 0 < \omega t \le \pi \\ 0 & \text{for } \pi < \omega t \le 2\pi \end{cases} \tag{1-2}$$

It is assumed that only the fundamental tone is delivered to the load. The fundamental tone of voltage v_{out} is described in Equation 1-3 from Fourier analysis. The peak voltage is approximately 0.64 V_{DD} and the RMS voltage is approximately 0.45 V_{DD}.

$$v_{out} = \frac{2V_{DD}}{\pi}\sin\omega t \tag{1-3}$$

The current through transistor Q1 can be described as

$$i_{Q1} = \begin{cases} I_{out}\sin(\omega t - \phi) & \text{for } 0 < \omega t \le \pi \\ 0 & \text{for } \pi < \omega t \le 2\pi \end{cases} \tag{1-4}$$

By integration Equation 1-4 across a single period, we can obtain the DC component of the supply current.

$$\begin{aligned} I_{DD} &= \frac{I_{out}}{2\pi}\int_0^{\pi}\sin(\omega t - \phi)d(\omega t) \\ &= \frac{I_{out}\cos\phi}{\pi} \\ &= \frac{2V_{DD}R_{out}}{\pi^2\left|Z_{out}\right|^2} \end{aligned} \tag{1-5}$$

If the load is a purely resistive load, the DC supply current can be expressed by Equation 1-5 by setting Z_{out} of Equation 1-6 to R_{out}.

$$I_{DD} = \frac{2V_{DD}}{\pi^2 R_{out}} \tag{1-6}$$

The DC input power can be then described by Equation 1-8 from Equation 1-5.

$$P_{IN} = \frac{2V_{DD}{}^2 R_{out}}{\pi^2\left|Z_{out}\right|^2} \tag{1-8}$$

Therefore, the DC input power of a purely resistive load can be expressed by Equation 1-9 by setting Z_{out} of Equation 1-8 to R_{out}.

$$P_{IN} = \frac{2V_{DD}{}^2}{\pi^2 R_{out}} \tag{1-9}$$

I_{out} can be easily derived from Equation 1-3.

$$I_{out} = \frac{2V_{DD}}{\pi \left| Z_{out} \right|} \tag{1-10}$$

By using the same concept as above, a resistive loaded class D power amplifier will have an output current as shown in Equation 1-11.

$$I_{out} = \frac{2V_{DD}}{\pi R_{out}} \tag{1-11}$$

Power delivered to the load can be then derived by using ohm's law using Equation 1-11. Since we are only interested in the real power delivery, real power delivery can be calculated by neglecting all imaginary terms of the apparent power delivery in Equation 1-12.

$$\begin{aligned} P_{out(apparent)} &= \frac{{I_{out}}^2 Z_{Load}}{2} \\ &= \frac{{2V_{DD}}^2 Z_{Load}}{\pi^2 \left| Z_{out} \right|^2} \\ P_{out(real)} &= \frac{{2V_{DD}}^2 R_{Load}}{\pi^2 \left| Z_{out} \right|^2} \end{aligned} \tag{1-12}$$

Power loss of the class D power amplifier can be described in Equation 1-13. The three major factors contributing to the power loss of a class D power amplifier are the parasitic resistances of the series inductor and capacitor as well as the turn on resistance of both transistors.

$$P_{loss} = \frac{{I_{out}}^2 \left(R_{L\_\text{P}arasitic} + R_{C\_\text{P}arasitic} + R_{turn-on\ transistor} \right)}{2} \tag{1-13}$$

From Equation 1-14, it can be seen that an ideal class D power amplifier is able to achieve 100% efficiency which is desirable for this application.

$$\eta = \frac{P_{out(real)}}{P_{in}} = \frac{R_{Load}}{R_{L-\text{Parasitic}} + R_{C-\text{Parasitic}} + R_{turn-on\ transistor} + R_{Load}} \quad (1\text{-}14)$$

1.3.3 Class E Power Amplifier

The class E power amplifier [17] consists of a single switch with a load network. The main advantage of the class E is that it only consists of a single transistor and does not require a pair of out-of-phase gate drive for the transistors as shown in Figure 2-3 for the class D. Therefore, a clock signal with sufficient drivability can be directly fed to the gate of the transistor without a gate driver to control the driving signal to the high side and low side of the amplifier (Class D). However, the voltage stress on the transistor of an ideal class E power amplifier is 3.562 times the supply voltage, making the power amplifier unattractive at high supply voltage. For example, if the supply voltage of an optimized class E power amplifier is 48V, the drain voltage can swing up to approximately 170 V. Therefore, by providing a 80% safety margin, one need to use a transistor with a breakdown voltage of approximately 220 V. In addition, the high drain voltage might cause higher noise levels in the system due to poor PCB design and if appropriate noise reduction is not implemented. Reference [17] stated three objectives for the transistor's drain voltage and current waveform to achieve class E operation.

1. The rise of the voltage across the drain of the transistor should only occur when the transistor is turned off.
2. The drain voltage across the transistor should be zero at the time when the transistor is turned on. (Zero Voltage Switching operation – ZVS)
3. The gradient of the drain voltage should be zero at the time the transistor is turned on. (Zero Derivative Switching – ZDS)

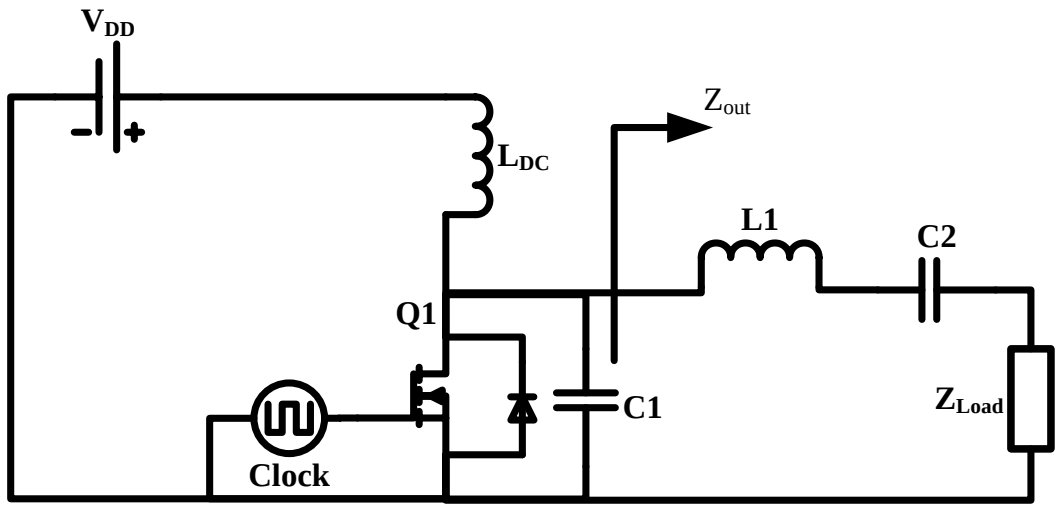

Figure 1-5. Class E power amplifier.

The detail analysis of an ideal class E power amplifier is based on Figure 1-5 which was first discussed in [18] – [19] by Frederick H. Raab with the following five assumptions.

1. The RF choke L_{DC} is sufficiently large that the current flowing through has negligible AC components.
2. The series LC filter of L1 and C2 has sufficiently high Q that the output current to the load can be considered to be a sinusoid (single tone). Therefore, it can be assumed that the filter is an open circuit at higher harmonic frequencies.
3. The shunt capacitance of the transistor is independent of the drain voltage or small enough to be neglected.
4. The transistor is an ideal switch and has only 3 different states
    a. On state with zero resistance.
    b. Off state with infinite resistance.
    c. Transition state for which the response time is zero.
5. The load will always be a resistive load. Any extra reactance can be added to the series LC filter.

Using assumption 2 the output voltage and currents across the load should be sinusoidal (single tone, free of higher order harmonics) and can be described by Equation 1-15 and 1-16 respectively.

$$v_{Load}(\omega t) = c\sin(\omega t + \phi) \tag{1-15}$$

$$i_{Load}(\omega t) = \frac{c}{R_{Load}}\sin(\omega t + \phi) \tag{1-16}$$

The drain voltage should be also a sinusoid when the transistor is turned off but with a phase shift due to extra reactance X introduced by the series LC filter. Therefore, the drain voltage is expressed in Equation 1-17 as the summation of the voltage drop across the load and the series LC filter.

$$\begin{aligned} v_{drain}(\omega t) &= c\sin(\omega t + \phi) + \frac{cj\left(\omega L1 - \frac{1}{\omega C2}\right)}{R_{Load}}\sin(\omega t + \phi) \\ &= c_1\sin\left(\omega t + \phi_1\right) \end{aligned} \tag{1-17}$$

Where,

$$c_1 = c\sqrt{1 + \frac{\left(\omega L1 - \frac{1}{\omega C2}\right)^2}{R_{Load}^{\ 2}}} = \rho c \tag{1-18}$$

$$\phi_1 = \phi + \Psi = \phi + \tan^{-1}\left(\frac{\omega L1 - \frac{1}{\omega C2}}{R_{Load}}\right) \tag{1-19}$$

When switch is off, the drain voltage is produced by the charging of capacitor C1 by the difference in current between the supply current and the current driving the load network. Therefore the drain voltage can be obtained by integrating the across the window when the switch is turned off as shown in Equation 1-20.

$$
\begin{aligned}
v_{drain}(\omega t) &= \frac{1}{\omega C1}\int_{\omega t_o}^{\omega t} i_{C1}(u)du \\
&= \frac{1}{B}\int_{\left(\frac{\pi}{2}\right)-y}^{\omega t}\left[I_{CC}-\frac{c}{R_{Load}}\sin(u+\phi)\right]du \\
&= \left[\frac{I_{CC}}{B}\left(-\frac{\pi}{2}+y\right)+\frac{c}{BR_{Load}}\sin(\phi-y)\right]+ \\
&\frac{I_{CC}}{B}\omega t+\frac{c}{BR_{Load}}\cos(\phi+\omega t)
\end{aligned}
\tag{1-20}
$$

Where B is ωC1 and y is half of the transistor turn off time.

The magnitude of the fundamental tone can be obtained by Fourier integral. Since, the drain voltage waveform is not symmetrical around π/2, there will be an unknown phase offset with respect to the load voltage waveform.

$$
\begin{aligned}
c_1 &= \frac{1}{\pi}\int_0^{2\pi} v_{drain}(\omega t)\sin\left(\omega t+\phi_1\right)d\omega t \\
&= -2\left[\frac{I_{CC}}{\pi B}\left(\frac{\pi}{2}-y+\phi_1\right)+\frac{c}{\pi BR_{Load}}\sin\left(y-\phi_1\right)\right]\cos\phi_1\sin y \\
&+\frac{I_{CC}}{B}\left[-2\sin\phi_1\sin y+2\left(\frac{\pi}{2}+\phi_1\right)\cos\phi_1\sin y+2y\sin\phi_1\cos y\right] \\
&-\frac{c}{2\pi BR_{Load}}\left[\sin(2\phi+\psi)\sin 2y-2y\sin\psi\right]
\end{aligned}
\tag{1-21}
$$

Using Equation 1-21 we can solve for c by substituting ρc for c_1 and rearranging to obtain Equation 1-22.

$$
\begin{aligned}
c &= I_{CC}R_{Load}\frac{2y\sin y\cos\phi_1+(2y\cos y-2\sin y)\sin\phi_1}{\pi BR_{Load}\rho+\frac{1}{2}\sin(2\phi+\psi)\sin 2y-y\sin\psi+2(y-\phi)\cos\phi_1\sin y} \\
&= I_{CC}R_{Load}h(\phi,\psi,y,B,R,\rho)
\end{aligned}
\tag{1-22}
$$

Since the fundamental tone at the drain is defined by a sinewave of phase φ_1, there can be no cosine or quadrature component with respect to phase φ_1. Replacing the sine term with a cosine term in Equation 1-21, Equation 1-23 is obtained.

$$\begin{aligned} 0 &= \frac{1}{\pi}\int_0^{2\pi} v_{drain}(\omega t)\cos\left(\omega t+\phi_1\right)\, d\omega t \\ &= -\left[\frac{I_{CC}}{\pi B}\left(y-\frac{\pi}{2}-\phi_1\right)+\frac{c}{\pi BR_{Load}}\sin(\phi-y)\right]2\sin\phi_1\sin y \\ &+\frac{I_{CC}}{\pi B}\left[-2\cos\phi_1\sin y-2\left(\frac{\pi}{2}+\phi_1\right)\sin\phi_1\sin y+2y\sin\phi_1\cos y\right] \\ &-\frac{c}{2\pi BR_{Load}}\cos(2\phi+\psi)\sin 2y+\frac{yc\cos\psi}{\pi BR_{Load}} \end{aligned} \tag{1-23}$$

Therefore, by rearranging the terms in Equation 1-23 and solving for c, Equation 1-24 is obtained.

$$\begin{aligned} c &= I_{CC}R_{Load}\frac{2y\sin\phi_1\sin y-2y\cos\phi_1\cos y+2\cos\phi_1\sin y}{-2\sin(\phi-y)\sin y\sin\phi_1-\frac{1}{2}\sin 2y\cos(2\phi+\psi)+y\cos\psi} \\ c &= I_{CC}R_{Load}\,g(\phi,\psi,y) \end{aligned} \tag{1-24}$$

Since both Equation 1-22 and Equation 1-24 describes c, by substituting Equation 1-22 into Equation 1-24, Equation 1-25 is obtained.

$$g(\phi,\psi,y)=h(\phi,\psi,y,B,R,\rho) \tag{1-25}$$

In order to solve equation 1-25, we need to cross multiple the denominators of the two functions g and h and break down the higher order terms of sine and cosine to their first order equivalent. Since the only unknown in Equation 1-25 is ϕ, after rearranging the terms we can obtain a solution for ϕ by either Equation 1-26 or Equation 1-27 and they provide a single consistent answer.

$$\phi = \tan^{-1}\left(-\frac{\begin{array}{l}\left(2y\sin y\cos\psi + 2y\cos y\sin\psi - 2\sin y\sin\psi\right)\left(-2\sin\psi\sin^2 y\right) \\ +\left(2y\sin y\sin\psi - 2y\cos y\cos\psi + 2\sin y\cos\psi\right) \\ \left(\pi BR\rho - y\sin\psi + \sin\psi\sin y\cos y\right) \\ +\left(2y\sin y\sin\psi - 2y\cos y\cos\psi + 2\sin y\cos\psi\right)\left(2\sin^2 y\cos\psi\right) \\ -\left(2y\sin y\cos\psi + 2y\cos y\sin\psi - 2\sin y\sin\psi\right) \\ \left(y\cos\psi - \sin y\cos y\cos\psi\right)\end{array}}{\begin{array}{l}\left(2y\sin y\cos\psi + 2y\cos y\sin\psi - 2\sin y\sin\psi\right) \\ \left(\pi BR\rho - y\sin\psi + \sin\psi\sin y\cos y\right) \\ +\left(2y\sin y\sin\psi - 2y\cos y\cos\psi + 2\sin y\cos\psi\right) \\ \left(y\cos\psi - \sin y\cos y\cos\psi\right)\end{array}} \right) \tag{1-26}$$

$$\phi = \tan^{-1}\left(-\frac{\begin{array}{l}\left(2y\sin y\sin\psi - 2y\cos y\cos\psi + 2\sin y\cos\psi\right) \\ \left(\pi BR\rho - y\sin\psi + \sin\psi\sin y\cos y + 2\cos\psi\sin^2 y\right) \\ -\left(2y\sin y\cos\psi + 2y\cos y\sin\psi - 2\sin y\sin\psi\right) \\ \left(y\cos\psi + 2\sin^2 y\sin\psi - \sin y\cos y\cos\psi\right)\end{array}}{\begin{array}{l}\left(2y\sin y\cos\psi + 2y\cos y\sin\psi - 2\sin y\sin\psi\right) \\ \left(\pi BR\rho - y\sin\psi + \sin\psi\sin y\cos y + 2\cos\psi\sin^2 y\right) \\ +\left(2y\sin y\sin\psi - 2y\cos y\cos\psi + 2\sin y\cos\psi\right)\left(-2\sin\psi\sin^2 y\right) \\ +\left(2y\sin y\sin\psi - 2y\cos y\cos\psi + 2\sin y\cos\psi\right) \\ \left(y\cos\psi + 2\sin^2 y\sin\psi - \sin y\cos y\cos\psi\right) \\ -\left(2y\sin y\cos\psi + 2y\cos y\sin\psi - 2\sin y\sin\psi\right)\left(2\sin^2 y\cos\psi\right)\end{array}} \right) \tag{1-27}$$

Once we obtained ϕ from either Equation 1-26 or Equation 1-27, we can obtain either g or h by substituting ϕ into Equation 1-22 or Equation 1-24 to get c. Since we assume that there is no voltage drop across RF choke, we can assume that the integrated drain voltage across one period is equal to the value of the DC supply voltage as shown in Equation 1-28 where R_{dc} is the input resistance of the class E power amplifier looking into from the supply voltage port.

$$\begin{aligned} V_{cc} &= \frac{1}{2\pi}\int_0^{2\pi} v_{drain}(\omega t)\, d\omega t \\ &= \frac{I_{CC}}{2\pi B}\int_{\left(\frac{\pi}{2}\right)-y}^{\left(\frac{\pi}{2}\right)+y}\left[\left(y-\frac{\pi}{2}+g\sin(\phi-y)\right)+\omega t+g\cos(\omega t+\phi)\right]d\omega t \\ &= \frac{I_{CC}}{2\pi B}\left[\left(2y^2+2yg\sin(\phi-y)\right)-2g\sin\phi\sin y\right] \\ &= I_{CC}R_{dc} \end{aligned} \tag{1-28}$$

Using Equation 1-15, Equation 1-22, Equation 1-24 and Equation 1-28. Power delivery and efficiency can be derived as followed.

$$R_{dc} = \frac{1}{2\pi B}\left[\left(2y^2+2yg\sin(\phi-y)\right)-2g\sin\phi\sin y\right] \tag{1-29}$$

$$\begin{aligned} P_o &= \frac{1}{2}\frac{c^2}{R_{Load}} \\ &= \frac{{I_{CC}}^2 g^2 R_{Load}}{2} \\ &= \frac{{V_{cc}}^2 g^2 R_{Load}}{2{R_{dc}}^2} \end{aligned} \tag{1-30}$$

$$\begin{aligned} P_i &= V_{cc}I_{CC} \\ &= \frac{{V_{cc}}^2}{R_{dc}} \end{aligned} \tag{1-31}$$

$$\eta = \frac{P_o}{P_i} = \frac{V_{cc}{}^2 g^2 R_{Load}}{2R_{dc}{}^2} \tag{1-32}$$

Although, it is known that an optimized ideal single-ended class E power amplifier requires its switching transistor to have a 3.562 times higher breakdown voltage than that of the Class D, it is often overlooked that the output power of an optimized ideal single-ended Class E power amplifier as shown in Equation 1-33 from [20] is 2.847 times higher than that of typical optimized ideal Class D power amplifier as shown in Equation 1-34.

$$P_{out-ClassE} = \frac{8}{\pi^2 + 4}\frac{V_{CC}{}^2}{R} = 0.5768\left(\frac{V_{CC}{}^2}{R}\right) \tag{1-33}$$

$$P_{out-ClassD} = \frac{2}{\pi^2}\frac{V_{CC}{}^2}{R} = 0.2026\left(\frac{V_{CC}{}^2}{R}\right) \tag{1-34}$$

From Equation 2-33 and Equation 2-34 we can conclude that in order to achieve similar output power, the Class D power amplifier requires a supply voltage that is 1.687 times higher than that of Class E power amplifier. When supply voltage is constrained, a Class E transmitter power amplifier is preferred to a class D transmitter because of higher output power at the same supply voltage.

CHAPTER 2
WIRELESS POWER TRANSFER SYSTEM

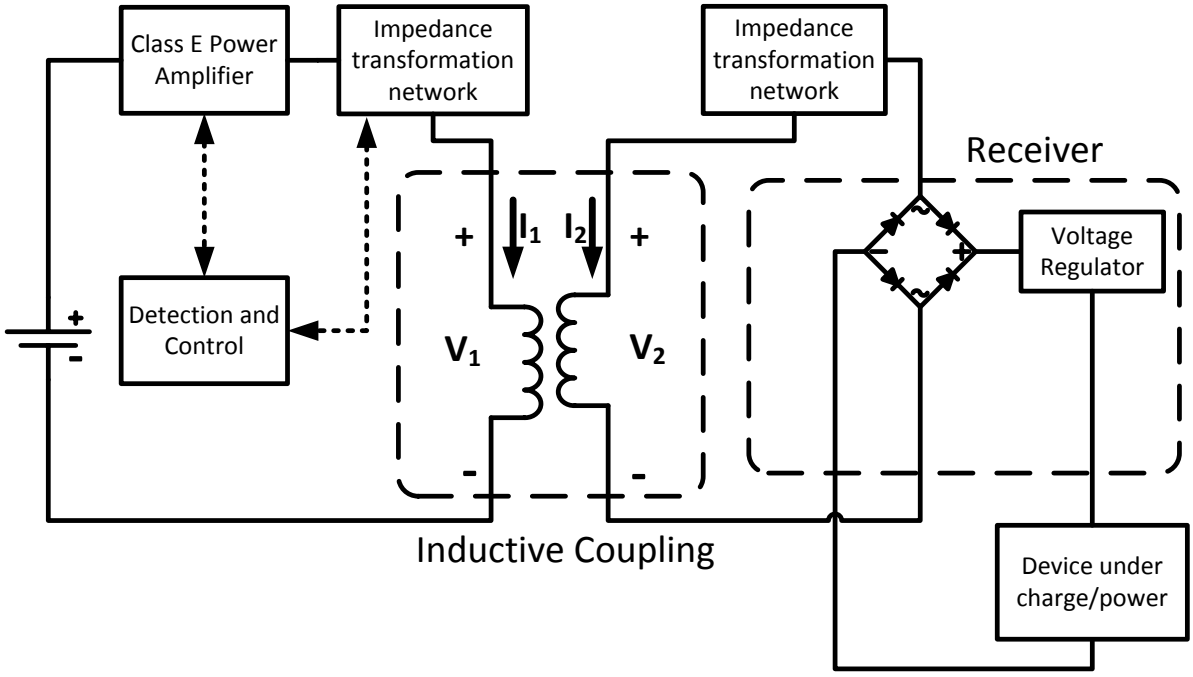

Figure 2-1. Wireless power transfer system diagram.

The system diagram of the proposed wireless power transfer system via magnetic induction is shown in Figure 2-1. Energy transfer between the transmitter and receiver is achieved by inductive coupling using a pair of air core coils. The class E power amplifier discussed in Chapter 1 under background information is used as an inverter to convert the input DC power to high frequency AC power of several hundred kilohertz. In order to achieve the desirable power delivery trend and impedance looking into the transmitter's load network, an impedance transformation network is inserted before the transmitting coil and after the receiving coil. The received AC power is converted to DC by the receiver's rectifier. A full wave rectifier can be used to reduce device stress on the diodes or a half wave rectifier can be used to reduce the receiver PCB footprint. Depending on loading conditions, the rectified DC voltage after the rectifier varies across a wide range. Therefore, a voltage regulator is used to regulate the

fluctuating DC voltage to a stable DC voltage before it is used to power the receiving device. A detection scheme using a micro-controller and sensing circuits is required to ensure the transmitter is in its nominal operating conditions. Such a detection scheme is proposed and discussed in Chapter 7. Control signals can be used to disable the transmitter or tune the system power delivery profile to enhance system efficiency and robustness. Techniques to control power delivery profile as well as receiver voltage are discussed in Chapter 8.

2.1 Single-channel Class E Power Amplifier

The class E power amplifier is an elegant design with minimum number of components. Theory of operation of the class E power amplifier is discussed in Chapter 1. The amplifier consists of three main sections, the DC feed network (typically a single choke inductor), the switch (typically a single N channel MOSFET) and the load network. The network from C1 towards the load in Figure 1-5 can be considered part of the load network and will be discussed in Chapter 3.

It is preferred that the choke inductor of the DC feed network (L_{DC}) to have a sufficiently large reactance so that it can be considered as an open circuit for the AC signal. Since impedances looking into the load network under most operating conditions will not exceed 50 Ω, an effective impedance of 500 Ω or better for the DC feed network is sufficient. Therefore, for a system operating at 250 kHz, the minimum inductance value should be 330 µH. Although, it is desirable to have the inductance value as high as possible, the parasitic resistance will be large resulting in poor efficiency and heating issues. In addition, an inductor with a larger inductance will typically of a larger size making the transmitter bulky.

The switch is the core of the class E power amplifier. Selecting the correct switch is very important, it needs to be sufficiently fast, have a low turn on resistance and have a sufficiently high breakdown voltage. To achieve a high breakdown voltage, the most practical candidate for

the switch is the N channel power MOSFET. The theoretical maximum voltage across the switch for a class E power amplifier is slightly more than 3.5 times of the supply voltage if it is optimized to drive a fix load. As seen from Figure 3-9 and Figure 3-17, the drain voltage can be up to 20% higher than the theoretical maximum while driving a varying load. Therefore, the maximum voltage across the switch should be approximately 4.2 times of the supply voltage during nominal operation instead of 3.5 times. However, the selected MOSFET should have a break down voltage of at least 5.5 times of the supply voltage to achieve a 0.8 factor of safety margin for various fault conditions. A wireless power transfer system with a supply voltage of 15V will require a transistor with a breakdown of 100 V or better. Although, a higher breakdown voltage will ensure the system to be more robust, a transistor with a higher breakdown voltage tends to be slower in speed and have a larger turn on resistance. In an ideal case the voltage across the transistor should be 0 V when a large current is driven across the transistor in its turn on state. To achieve this operating condition, the turn on resistance of the transistor needs to be sufficiently small. This also helps in reducing energy being dissipated as heat across the turn on resistance. A turn on resistance of 0.1Ω or less is a good starting point . The capacitance between the drain and source of a MOSFET varies with the drain voltage. To ensure than the fluctuation of drain to source capacitance with respect to the drain voltage can be neglected, the variation should be much smaller than C1 (typically <5% of C1). If the gate to source capacitance is too large, a gate driver is required to provide sufficient drivability to effectively turn on and off the transistor. Finally, the transistor must be able to switch sufficiently fast to reduce switching losses, the rise time and fall time of the transistor should be better than 1% of the period of the operating frequency (better than 40 ns for operating frequency of 250 kHz).

2.2 Multi-channels/Stackable Class E Power Amplifier

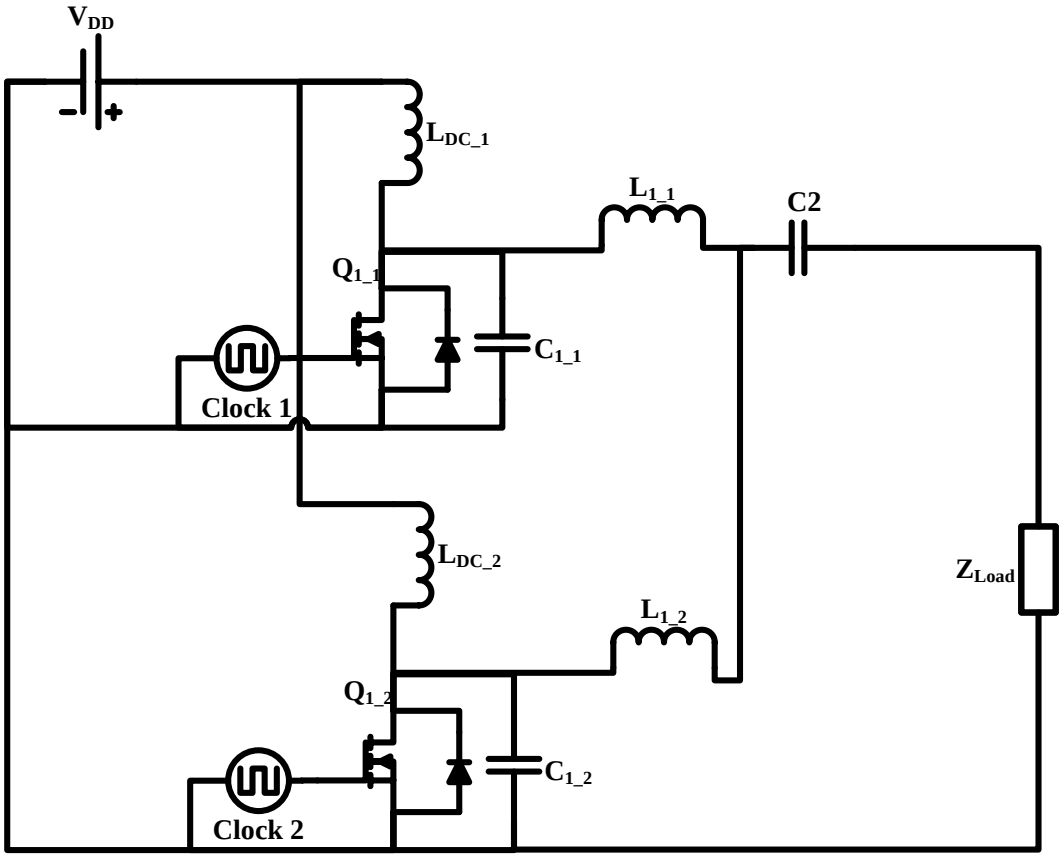

Figure 2-2. Schematic of the dual-channel Class E power amplifier.

In addition to the typical single-ended class E transmitter, a multiple channel class E transmitter with independent gate drive is shown in Figure 2-2 (Dual-channel). The dual-channel class E allows the system to shut down one of the channels to switch to a lower power mode so that the receiver's regulator responds by reducing its input resistance. The analysis of the dual-channel class E is straightforward. If both the channels are enabled, the equivalent inductance across both L_1 is $L_1/2$, while if one channel is enabled, the equivalent inductance is simply L_1 making Z_{out} more inductive while keeping the real components of Z_{out} the same. If Z_{out} is more inductive, more reactive power and less real power is transmitted to Z_{Load} reducing power delivery. Likewise, the equivalent value of C_{shunt} is doubled for a dual-channel configuration.

The dual-channel class E transmitter can be easily scaled to multiple channels, but the size increases along with a higher probability of device mismatches. As the number of channels increases, the problems caused by device mismatches might far outweigh the benefits. It was found empirically that the number of channels should be kept at a maximum of three. The observed efficiency improvement was negligible when the number of channels was increased from three to four and the efficiency started to degrade at five channels, predominately due to variations in inductance value. Although this technique enables the system to operate at a higher efficiency, the tradeoff is that the power delivered to the load network is fed across a single inductor instead of two for a dual-channel case, thus the equivalent parasitic resistance of L_{out} is doubled for a dual-channel topology, reducing the potential enhancement of the system efficiency as power loss via the inductor remains the same in regardless of the number of channels.

2.3 Inductive Coupling

Power transfer for the system is achieved via magnetic induction between two air core coils. Vertical magnetic field is the dominate component of power transfer because both the transmitting and receiving coils have large surface area. By having a larger surface area, the coil is able to intercept more of the magnetic flux and receive more power. In addition, modern portable electronic devices are extremely thin in profile having limited cross sectional area for any magnetic flux to cut through the cross sectional area. Appropriate shielding [21] at the expense of weight and thickness can be used to make the system more robust in environments where the system's magnetic field is likely to interact with other nearby objects. However, shielding is not the focus of this dissertation and it is assumed that the system will be working in an environment free of structures and materials that will significantly affect the system performance or is sufficiently shielded to begin with.

Although it would be ideal for both the transmitting coil and the receiving coil to be of the same size to ensure maximum coupling as shown in [22] – [24], a practical system will tend to use a receiver coil significantly smaller than the transmitting coil. This allows a user to freely place a device in any orientation without intentionally "docking" it as well as to place multiple devices on the transmitting coil. Therefore, in order to achieve consistent power delivery and impedance response regardless of the receiving coil's location, the transmitting coil must be able to generate a magnetic field that has relatively even distribution. This is achieved by using the method proposed in [25]. Alternative methods are also proposed in [26] – [27].

The voltage and current of the transmitting coil and the receiving coil can be described using Equation 2-1, Equation 2-2 and Equation 2-3 from [22] [27] neglecting any second order effects such as skin depth and proximity effect which can be mitigated by using Litz wires.

$$V_1 = j\omega M_{11} I_1 + j\omega M_{12} I_2 \tag{2-1}$$

$$V_2 = j\omega M_{21} I_1 + j\omega M_{22} I_2 \tag{2-2}$$

$$M_{12} = k\sqrt{M_{11} M_{22}} \tag{2-3}$$

Where

V_1 is the voltage at the transmitting coil. (Figure 2-1)

I_1 is the current at the transmitting coil. (Figure 2-1)

V_2 is the voltage at the receiving coil. (Figure 2-1)

I_2 is the current at the receiving coil. (Figure 2-1)

M_{11} is the self inductance of the transmitting coil.

M_{22} is the self inductance of the receiving coil.

$M_{12} = M_{21}$ is the mutual inductance of the two coils.

k is the coupling coefficient between the two coils.

By Ohm's law:

$$Z_{tx} = R_{tx} + jX_{tx} = \frac{V_1}{I_1} \tag{2-4}$$

$$Z_{rx} = R_{rx} + jX_{rx} = \frac{V_2}{I_2} \tag{2-5}$$

Using Equation 2-1, Equation 2-2 and Equation 2-4 and assuming a time-harmonic operation with frequency ω, impedance looking into the transmitting coil for a single receiver is derived as Equation 2-6.

$$Z_{tx} = \frac{\omega^2 M_{12}^2 R_{rx}}{R_{rx}^2 + \left(\omega M_{22} + X_{rx}\right)^2} + j\left(\omega M_{11} - \frac{\omega^2 M_{12}^2 \left(\omega M_{22} + X_{rx}\right)}{R_{rx}^2 + \left(\omega M_{22} + X_{rx}\right)^2}\right) \tag{2-6}$$

2.4 Impedance Transformation Network

The purpose of impedance transformation network on the primary and secondary sides of the coupling is to achieve maximum power transmission and efficiency by operating within the optimum impedance range looking into the transmitter load network [29] over a wide range of load resistances.

In consideration of size and efficiency, capacitors instead of resistors and inductors should be used for the network. This is because resistors dissipate power and the size of a low loss inductor is generally large. Although, a multi-element transformation network might achieve a better response, for simplicity and low component count, the system uses a single-element transformation network. The four possible topologies of the single-element transformation network are shown in Figure 2-3.

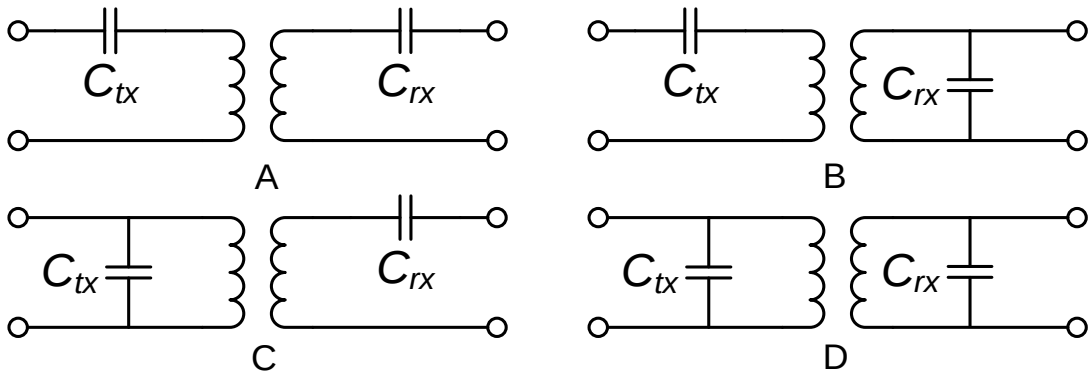

Figure 2-3. Topologies for a single-element impedance transformation network. A) Series-Series Topology, B) Series-Parallel Topology, C) Parallel-Series Topology and D) Parallel-Parallel Topology

Fundamentally, a series capacitor only introduces a negative reactance and does not change the real part of the impedance. On the other hand, a parallel capacitor changes both the real and imaginary parts of the impedance. To simplify the analysis, the receiver input impedance is modeled using a variable resistor load and Equation 2-7 illustrates the transformation performed by the parallel capacitor.

$$Z_{rx} = \frac{R_{rx}}{1+\omega^2 C_{rx}^{\ 2} R_{rx}^{\ 2}} - j\frac{\omega C_{rx} R_{rx}^{\ 2}}{1+\omega^2 C_{rx}^{\ 2} R_{rx}^{\ 2}} \tag{2-7}$$

Equation 2-7 shows that the resistance R_{rx} is "compressed" by a factor of $1/(1+\omega^2 C_{rx}^{\ 2} R_{rx}^{\ 2})$. Thus, the equivalent resistance R_{rx} decreases with increasing load resistance. At high load resistance, the transformed resistance is small. Therefore, a significant part of the received power is dissipated across the receiving coil as heat. This phenomenon is desirable if the receiver is in a state that requires very little power or during trickle charge. Therefore, it has a "decoupling" effect regulating the power delivery with increasing load resistance. However, this should occur if and only if the transmitter is designed to output limited power under this operation condition because heating can become a problem if too much power

is being dissipated across the receiving coil. Due to the parallel capacitor, a reactive term jX_{rx} is introduced to the equation. The reactive term jX_{rx} decreases nonlinearly from null with increasing load resistance with an asymptote of $-1/\omega C_{rx}$. This is used to compensate the receiving coil's self inductance.

From Equation 2-6 it can be observed that the resistance looking into the transmitter coil is reduced significantly if the resistance looking from the receiver coil into the receiver is increased. R_{tx} is further reduced because the mutual inductance is relatively small. If the total resistance looking into the transmitting coil is mainly the parasitic resistance of the transmitting coil, limited power is transmitted to the receiver as most of the power is dissipated across the transmitting coil as heat. Therefore, it is preferred for a wireless power transmission system using loosely coupled coils to have a parallel capacitor across the receiving coil. By substituting Equation 2-7 into Equation 2-6, the expression of impedance looking into the transmitting coil with a parallel capacitor across the receiving coil is shown in Equation 2-8.

$$Z_{tx} = \left(\frac{\omega^2 M_{12}^2 \left(\frac{R}{1+\omega^2 C^2 R^2} \right)}{\left(\frac{R}{1+\omega^2 C^2 R^2} \right)^2 + \left(\omega M_{22} - \frac{\omega C R^2}{1+\omega^2 C^2 R^2} \right)^2} \right) + j \left(\omega M_{11} - \frac{\omega^2 M_{12}^2 \left(\omega M_{22} - \frac{\omega C R^2}{1+\omega^2 C^2 R^2} \right)}{\left(\frac{R}{1+\omega^2 C^2 R^2} \right)^2 + \left(\omega M_{22} - \frac{\omega C R^2}{1+\omega^2 C^2 R^2} \right)^2} \right) \tag{2-8}$$

For the transmitter transformation network, a series or parallel topology can be used. To maintain an ideal efficiency above 95%, the allowable variation of load resistance of an ideal class E amplifier should be kept within +55% and -37% [18]. If the variation of resistance

looking into the transmitter coil is too large, it is preferred that a parallel capacitor is used instead of a series capacitor to “compress” the resistance. A suitable capacitor value is needed to ensure that the transmitter does not suffer immediate failure when there is no receiving coil, and to produce an increasing reactance trend with increasing load resistance so as to ensure the preferred power delivery trend.

On the other hand, an appropriate receiver capacitance value can also be selected so that the resistance looking into the transmitting coil is kept within a reasonable bound but not too small to impact on the coupling efficiency and to produce an increasing reactance trend with increasing load resistance so as to ensure the preferred power delivery trend. A suitable series transmitting capacitor is then needed to translate the reactance looking into the transmitting coil to cancel part of the self inductance of the transmitting coil. Based on the above analysis, both the parallel-parallel and series-parallel impedance transformation network topologies can be used for the system.

2.5 Receiver

Since more receivers will be paired up with a single transmitter and most receivers are intended to be integrated into compact portable electronics, the receiver of the wireless power transfer system needs to be low cost and compact in size. Therefore, the receiver will only consist of a rectifier to convert the AC power to DC power and a voltage regulator to ensure a stable DC voltage is use to power the device. The effort of attaining universality for cell phone power port still faces huge resistance from the OEMs. By having a proprietorship communication protocol for a wireless power transfer system will work against a universal charging/power platform to reduce waste and power consumption. Therefore, a communication link should be avoided unless it is the last resort and the wireless power receiver is integrated into the device tapping into its existing wireless communication system.

Reverse recovery time of the diodes used for the rectifier is critical because the operating frequency is much higher than the typical 50/60 Hz AC power lines. A good rule of thumb is to select a diode with a reverse recovery time less than 1% of the operating frequency's period. For example, a 200 kHz system should use a rectifying diode with a reverse recovery not slower than 50 ns. It is easy to find schottky diodes with negligible reverse recovery time at breakdown voltages below 100 V for low to medium power applications (< 100W). However, for high power applications either an ultrafast recovery diode or schottky diodes in series are required to ensure they are not damaged by the reverse biased voltage.

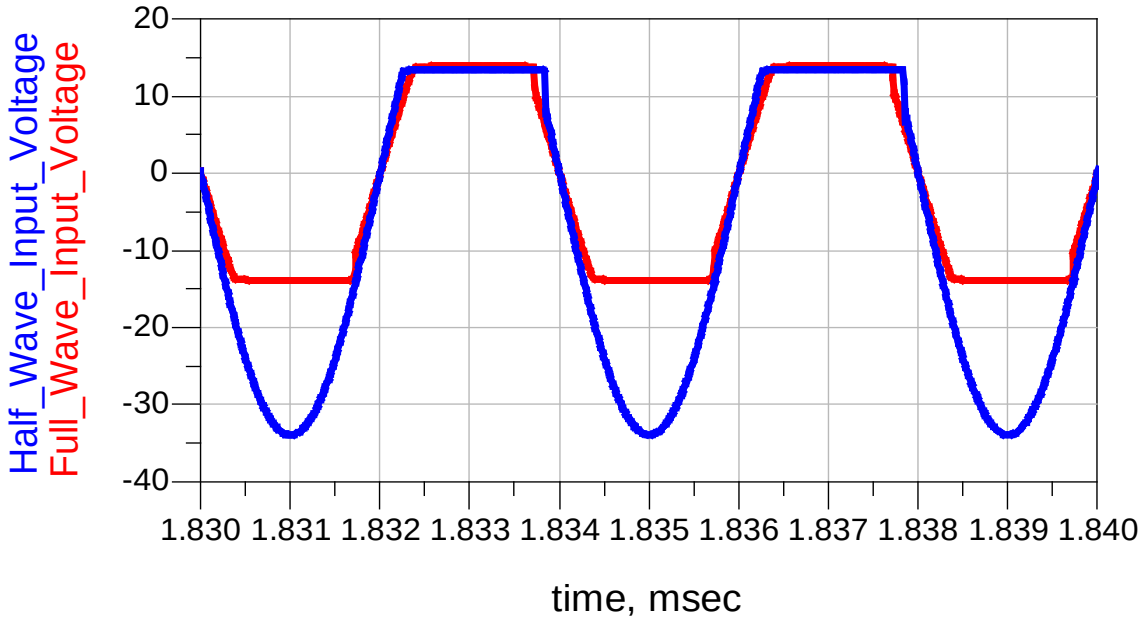

Figure 2-4. Input voltage of a half wave rectifier and a full wave rectifier.

Figure 2-4 shows the input voltage of both a half wave rectifier and a full wave rectifier where the flat section of the waveform is when the rectifying diode conducts charging the charging holding capacitor used to smooth out the voltage ripples at the output of the rectifier. The diodes for a full wave rectifier conducts during both the positive and negative cycle of the waveform whereas the diodes for the half wave rectifier only conducts during either cycle depending on the orientation of the diode. For the specific load condition shown in Figure 2-4,

the full wave rectifier requires a diode with a breakdown voltage of 20 V and better to operate. On the other hand the half wave rectifier will require a diode with a breakdown voltage of 40 V and better to operate which is a lot higher than a full wave rectifier. Although, a half wave rectifier helps to reduce the size of the receiver PCB by reducing the number of diodes from four to one, it will require a diode of a much higher voltage rating to operate. Under most situations, a full wave rectifier is preferred for high power applications where a slight increase in PCB size is not an issue.

A switching buck regulator is preferred over low dropout regulators for this application because the input voltage swings across a considerable range and high efficiency must be maintained. In order to keep the receiver compact the output inductor of the switching regulator should be kept below 10 µH, which can be achieved by selecting regulators with switching frequencies above 500 kHz. Although, increasing the switching frequency will result in the voltage regulator being more compact, the efficiency starts to degrades losing power to heat.

CHAPTER 3
DESIGN OF IMPEDANCE TRANSFORMATION NETWORK

The design of the proposed wireless power system starts by setting constraints of the dimensions of the transmitting and receiving coil as well as operating frequency. This chapter presents the design rules for two systems using the parallel-parallel impedance transformation network and the series-parallel impedance transformation network achieving desirable power delivery profile. The parallel-parallel impedance transformation network design rule is based on the dual-channel transmitter topology to achieve high power transfer while the series-parallel impedance transformation network design rule is based on the single-channel transmitter topology to achieve compact low power design. A different operating frequency is used to illustrate that the design rule applies to a wide frequency range.

3.1 Series-Parallel Impedance Transformation Network

3.1.1 Introduction

An operating frequency of 240 kHz is used for the design of the series-parallel impedance transformation network topology. Since high efficiency schottky diodes are used for the receiver rectifier, the resistance looking into the rectifier should be very close to the resistance after the rectifier as very little energy is lost. Therefore, to simplify the analysis, the load resistance is defined as the equivalent resistance looking into the rectifier instead of after the rectifier. It is desirable for the receiving coil to be much smaller than the transmitting coil, but efficiency and power transfer capabilities start to degrade significantly due to poor coupling if the receiver is too small. Therefore, it is preferred to keep the coupling coefficient k above 0.1. To minimize space usage as well as ease of integration into the target device, the receiving coil is typically tightly wound. However, due to the requirement of ensuring a consistent coupling coefficient regardless of position and orientation the windings of the transmitting coil are very different

from the receiving coil. The gaps between each turn of the transmitting coil are spaced in a non uniform manner with the windings more spaced out when it gets to the middle of the coil so as to achieve even field distribution. Thus, achieving consistent performance regardless of the placement of receiving coil.

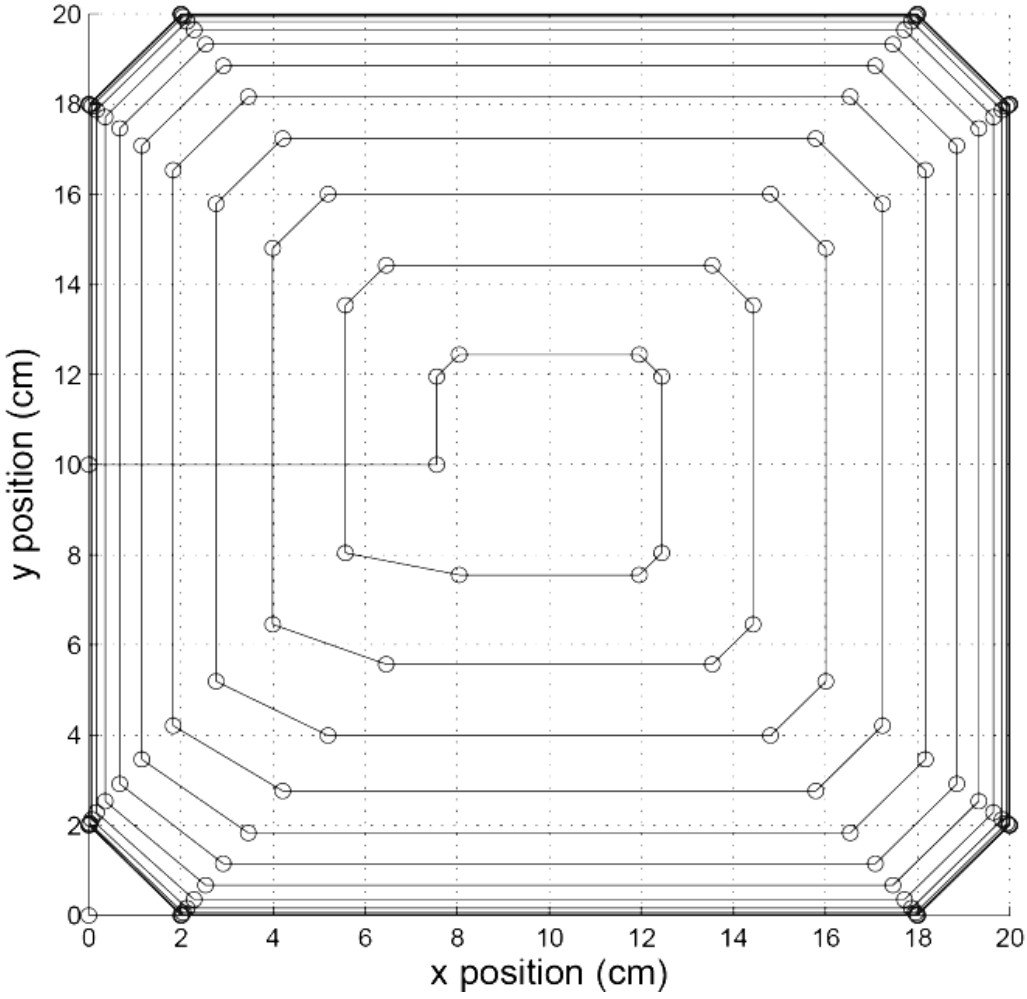

Figure 3-1. Windings of a 20cm x 20cm transmitting coil used for experimental verification.

Figure 3-1 shows the windings of a 13 turns 20 cm x 20 cm transmitting coil from [25] which will be use for later experimental verification, the last 3 turns are overlapped onto each other. Designing of the transmitting coil windings to achieve an even magnetic field distribution is not the scope of this dissertation. The normalized power delivery with respect to location of the transmitting coil in Figure 3-1 using a tightly wounded receiving coil of 9 cm x 6 cm with 6

turns is shown in Figure 3-2 using the centre of the receiving coil as reference. The receiver is 13.5% of the size of the transmitter. Power delivery variation is kept within ± 5% with a standard deviation of 2.2%. Since there is no obvious distribution of power delivery trend with respect to receiver location, it can be assumed that the generated magnetic field is even and the variations are due to measurement errors.

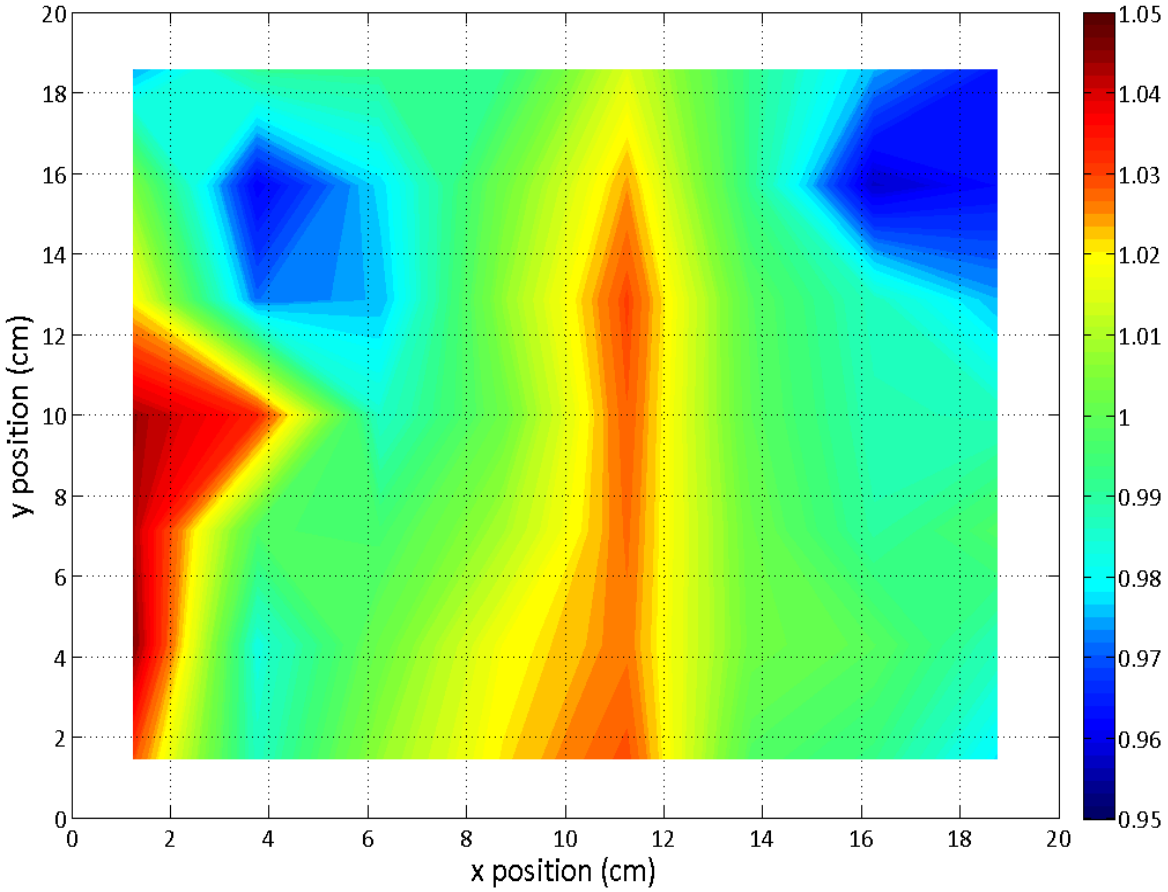

Figure 3-2. Normalized power deliver with respect to location of transmitting coil in Figure 3-1 using a receiving coil of 9 cm x 6 cm.

Key parameters of the coils including self inductances, mutual inductance, and parasitic resistances can be extracted by measuring the fabricated coil with an impedance analyzer or analyzing with electromagnetic simulation tools. The coils were fabricated using 100/40 round served Litz wires for the experiment to mitigate proximity effect and skin effect. The 100/40 round served Litz wires consists of 100 strands of 40 gauge wires insulated from each other. The

self inductance of the transmitting coil is 45.3 µH with a parasitic resistance of 0.5 Ω. The self inductance of the receiving coil is 5.2 µH with a parasitic resistance of 0.1 Ω. Mutual inductance between the coils is 2.8 µH with a coupling coefficient of 0.1824. Measurements of the coils were measured using the HP4192A LF Impedance Analyzer. The design rule for the series-parallel impedance transformation network will be based on Figure 3-3. Although C_{out} and C_{tx} are two separate capacitors, C_{tx} will be considered to be part of C_{out}.

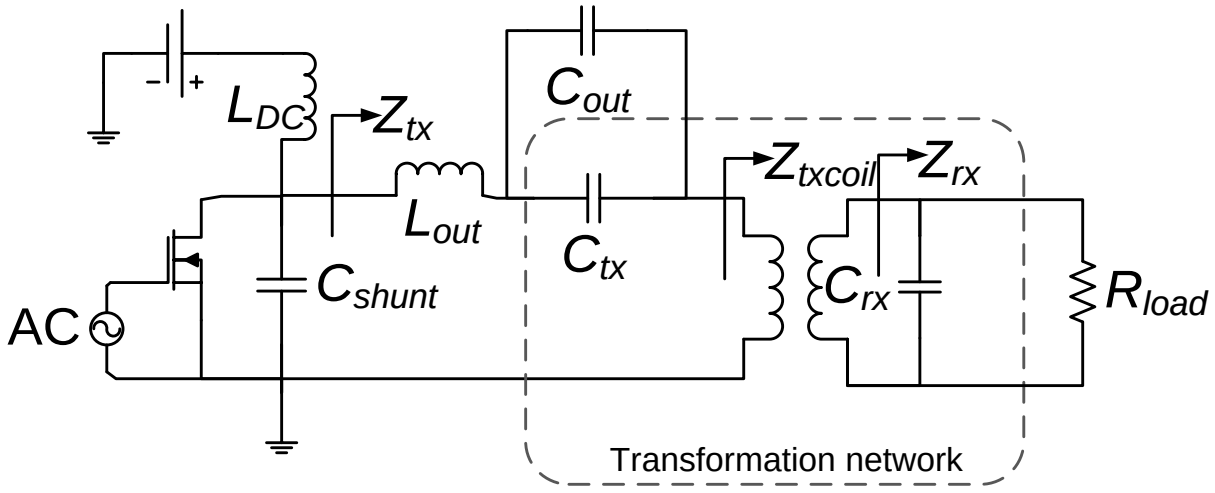

Figure 3-3. Simplified schematic of wireless power transfer system using series-parallel impedance transformation network and Class E transmitter. Z_{tx} – Impedance looking into the transmitter load network. Z_{txcoil} – Impedance looking into the transmitting coil. Z_{rx} – Impedance looking into receiver network. R_{Load} is the equivalent resistance looking into the rectifier.

3.1.2 Determination of C_{rx} value

The design of the system starts from the receiver looking into the load. The typical impedance response for different parallel capacitors is shown in Figure 3-4. The capacitance value is selected based on the inductance of the receiving coil as well as the mutual inductance between the coils. Although, it will be desirable to achieve a maximum resistance looking into the transmitting coil across a wide range of load resistances [29], the resistance variation looking into the transmitting coil might be too large, thus requiring a shunt capacitor across the

transmitting coil to “compress” the resistance resulting in the parallel-parallel impedance transformation network topology which will be discussed later. Therefore, it will be more practical to select a capacitor value that will generate the desirable resistance range looking into the transmitter load network Z_{tx} as shown in Figure 3-3.

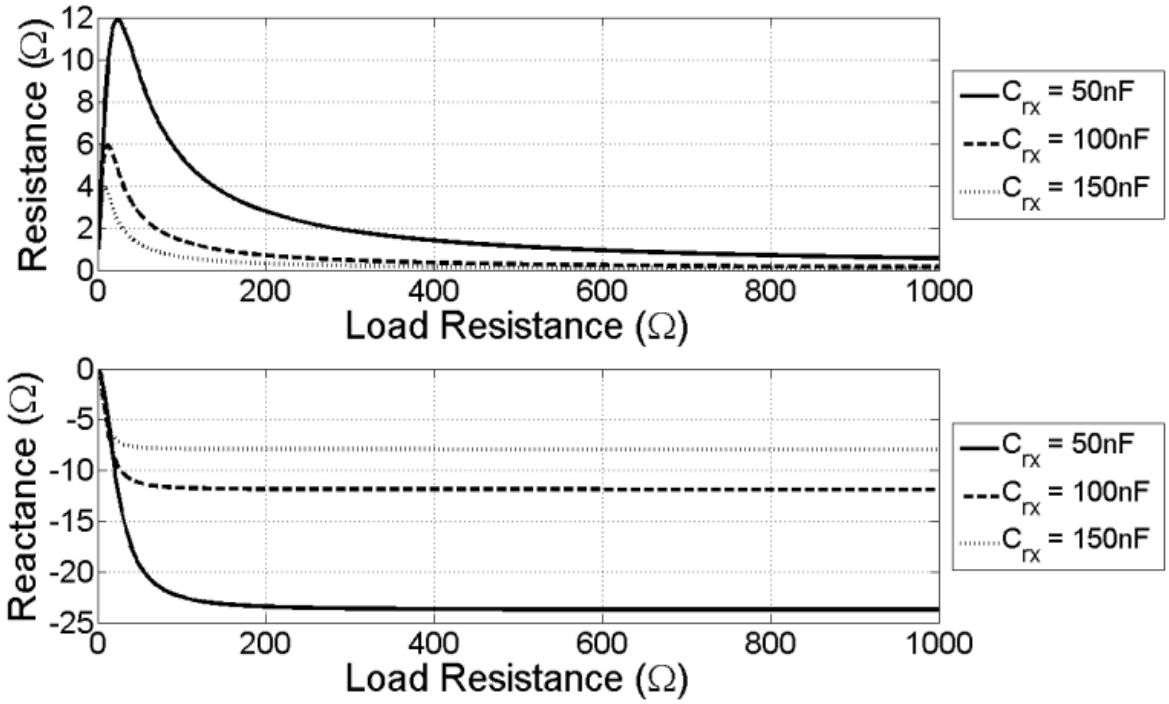

Figure 3-4. Resistance and reactance of Z_{rx} versus load resistance at different with different C_{rx}. (50 nF, 100 nF and 150 nF)

Shifting of the reactance value to achieve a desirable phase response so as to achieve a desirable power delivery profile can be done by varying C_{out} or L_{out} in Figure 3-3. In order to determine the range of resistance looking into the transmitting coil an appropriate L_{out} value needs to be selected first. The class E transmitter requires a minimum loaded Q of 1.7879 to operate [20]. There are two factors that affect the decision of L_{out}. For the same loaded Q value it will be desirable to have L_{out} as large as possible so that the resistance looking into the transmitting coil will be larger. Therefore, the parasitic resistance of the transmitting coil can be neglected. However, if L_{out} is too large the parasitic resistance of the inductor will be relatively

large unless a better inductor of lower parasitic resistance is used. However, when the parasitic resistance of the inductor of the same inductance value gets lower, the size of the inductor also gets bigger. The lowest loss inductor will be an air core inductor using Litz wire but its size will be larger. In addition, based on Equation 3-1 if the resistance looking into the transmitting coil is too large limited power will be delivered to the receiver. On the other hand, if L_{out} is too small the maximum value of the resistance looking into the transmitting coil will be limited. Therefore, with a small resistance looking into the transmitting coil, the parasitic resistance of L_{out} and the transmitting coil will get more significant affecting the system efficiency and power delivery as most of the voltages will drop across the parasitic resistance and not across the reflected resistance by the receiver looking into the transmitting coil.

$$P = \frac{V^2}{Z_{tx}} \cos\theta = \frac{V^2 R_{tx}}{Z_{tx}^2} \tag{3-1}$$

For an operating frequency of 240 kHz the system will be able to operate well with a L_{out} value from 6.8µH to 22µH depending on the parasitic resistance of the transmitting coil, the parasitic resistance of L_{out} and C_{out} as well as size constrain. For this design a 10 µH inductor (RL-5480-5-10 from Renco) is selected. The inductor has low loss, 0.16 Ω of parasitic resistance at 240 kHz and is considerable small in size (15.875 mm diameter and 17.78 mm height). However, due to de-rating at higher operating frequency the effective inductance of the inductor is 9.5 µH instead of 10 µH at 240 kHz. The inductance will further decrease with higher current and temperature. This is predominately due to the temperate sensitive nature of most ferrous cores used in inductors.

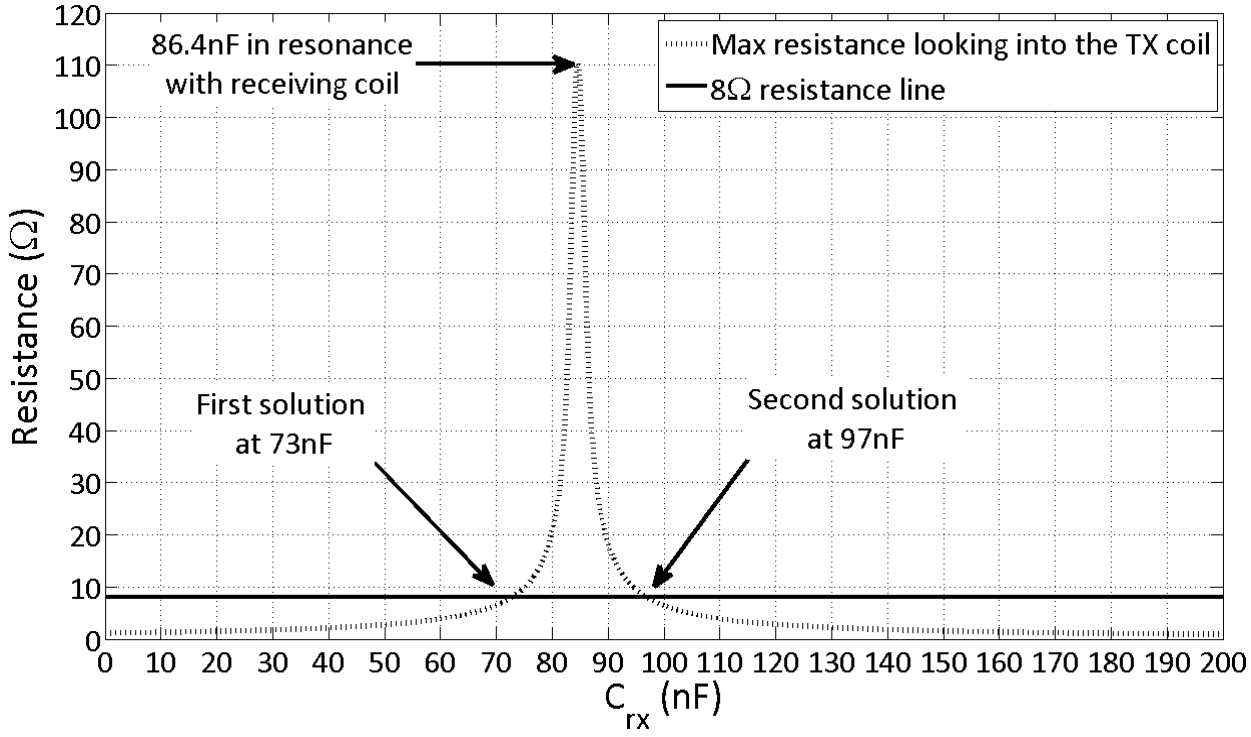

Figure 3-5. Peak resistance response looking into the transmitting coil with respect to C_{rx}.

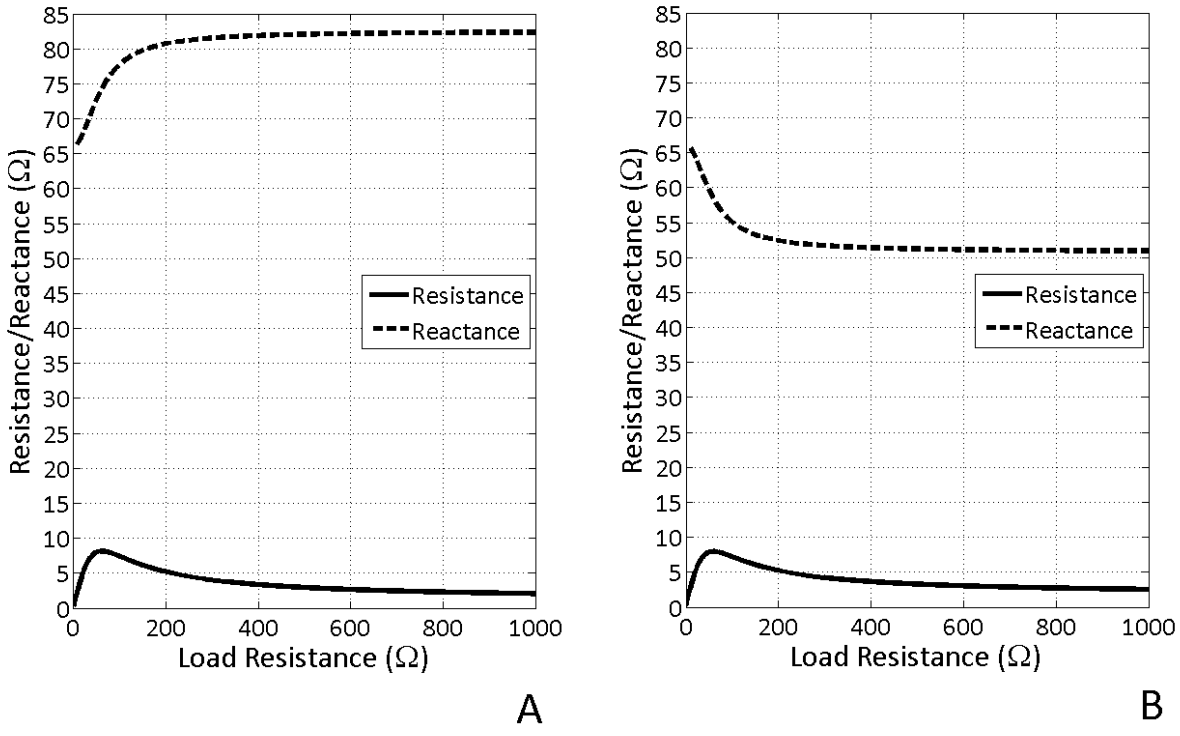

Figure 3-6. Resistance and reactance looking into the transmitting coil. A) with receiver capacitance of 73 nF and B) with receiver capacitance of 97 nF.

Although both receiver capacitance values provide the same resistance trend looking into the transmitting coil, the reactance trend is different. Using a capacitance value of 73 nF before the resonance capacitance value of 86.4 nF results in an increasing trend of reactance with increasing load resistance converging at approximate 82 Ω. On the other hand, a capacitance value of 97 nF will result in a decreasing trend of reactance with increasing load resistance converging at approximately 51 Ω. According to Equation 3-1, increasing the reactance while keeping the resistance relatively the same will decrease the power delivery. Therefore, in order to obtain the desirable trend of decreasing power delivery with respect to increase load resistance the first solution of 73 nF before the resonance capacitor value with the receiving coil is selected.

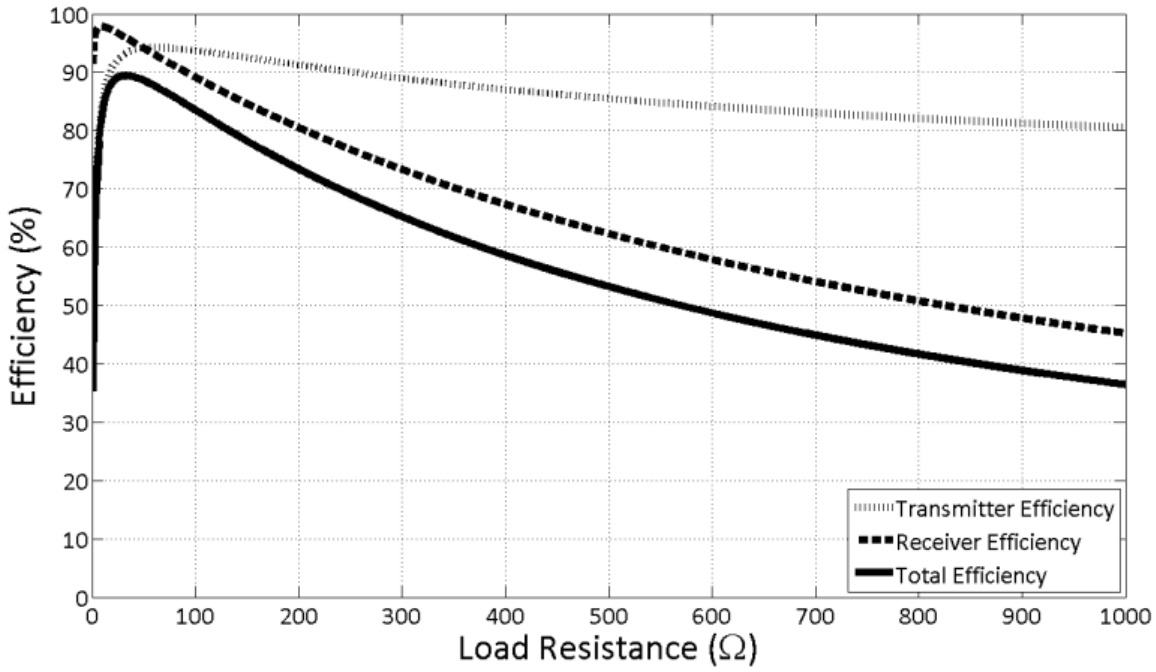

Figure 3-7. Coupling efficiency with respect to load resistance.

Based on the selected receiver capacitance value, the efficiency of the coupling with respect to load resistance shown in Figure 3-7 can be calculated using the parasitic resistance of the coil. Coupling efficiency peaks at close to 90% at a load resistance of 30 Ω. Although efficiency rolls off to an approximate 36% at 1 kΩ, power delivered at the resistance is

extremely low. The gradual degradation in receiver efficiency is desirable as it helps to regulate the power during trickle charge. Power delivered by the transmitter remains consistent at high load resistances because the equivalent load impedance Z_{tx} looking into the transmitter load network does not change much.

3.1.3 Determination of C_{out} value

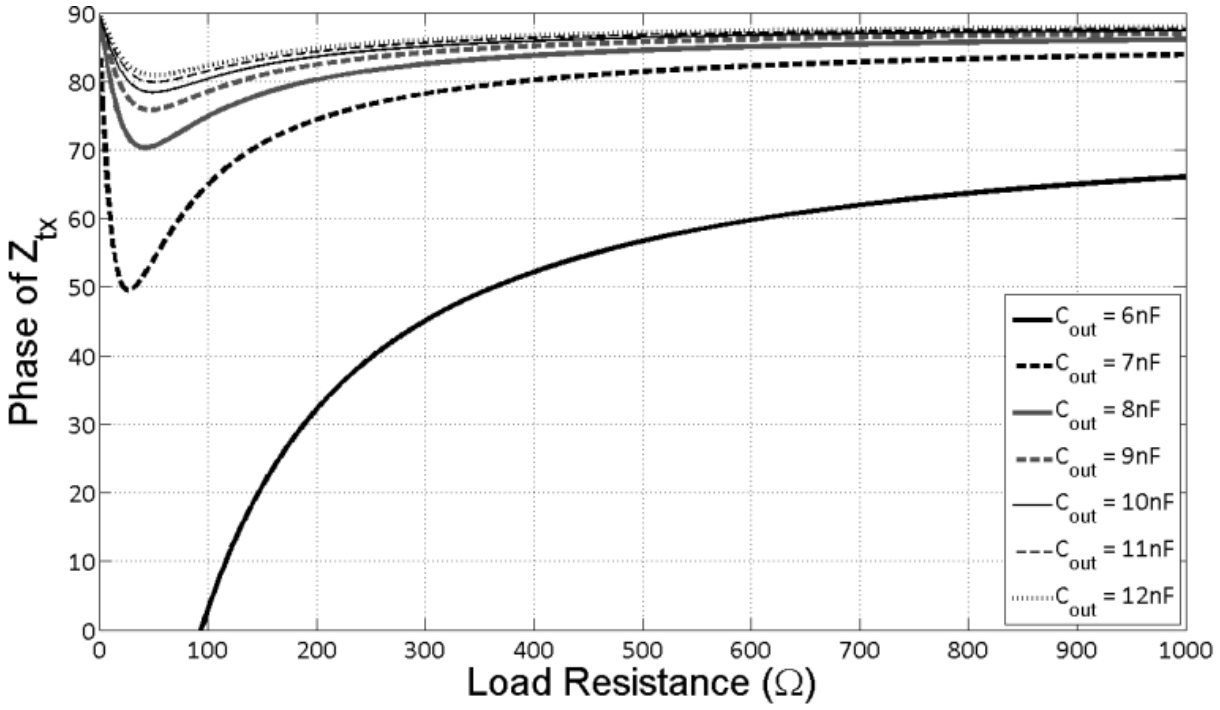

Figure 3-8. Z_{tx} phase response with respect to load resistance for various C_{out} capacitance values.

Figure 3-8 shows the phase response of Z_{tx} with respect to load resistance for different C_{out} values with increasing phase angle with increasing capacitance value. The Class E power amplifier does not perform well under capacitive loads and high efficiency is achieved at a range of phase angle from 40° to 70° [18]. Therefore, any value 7 nF and above can be used for C_{out}. Since the coil inductance is large, the phase response is sensitive to the component values. This can be verified by the large phase response swing observed in Figure 3-8 when C_{out} is changed from 6 nF to 7 nF. Since C_{out} should be selected to achieve maximum power delivery and

stability, C_{out} is selected to be 8 nF because the variation in phase response when C_{out} changes from 7 nF to 8 nF and from 8 nF to 9 nF is less than from 6 nF to 7 nF. This ensures that the fluctuation in power delivery due to component tolerance is limited. However, a higher C_{out} can be selected to limit the power delivery as shown in Equation 3-1.

3.1.4 Determination of C_{shunt} value

Once the values of the inductors and capacitors in the transmitter load network and the receiver network are determined, the remaining step is to determine C_{shunt} to achieve ZVS and ZDS operation so as to minimize switching losses. The optimum C_{shunt} value can be determined using the equations derived in Chapter 2 and [18]-[19] which are implemented in Matlab code. The optimum C_{shunt} is found to be 10 nF and the variation of transistor drain voltage versus load resistance is shown in Figure 3-9. It can be seen that the transistor drain voltages are kept very close to zero when the transistor is being switched on at a phase of 180°. In addition, the negative voltages do not occur because the built in diode will start to conduct and restrict the voltage at the negative of its turn on voltage which is around -1.3V.

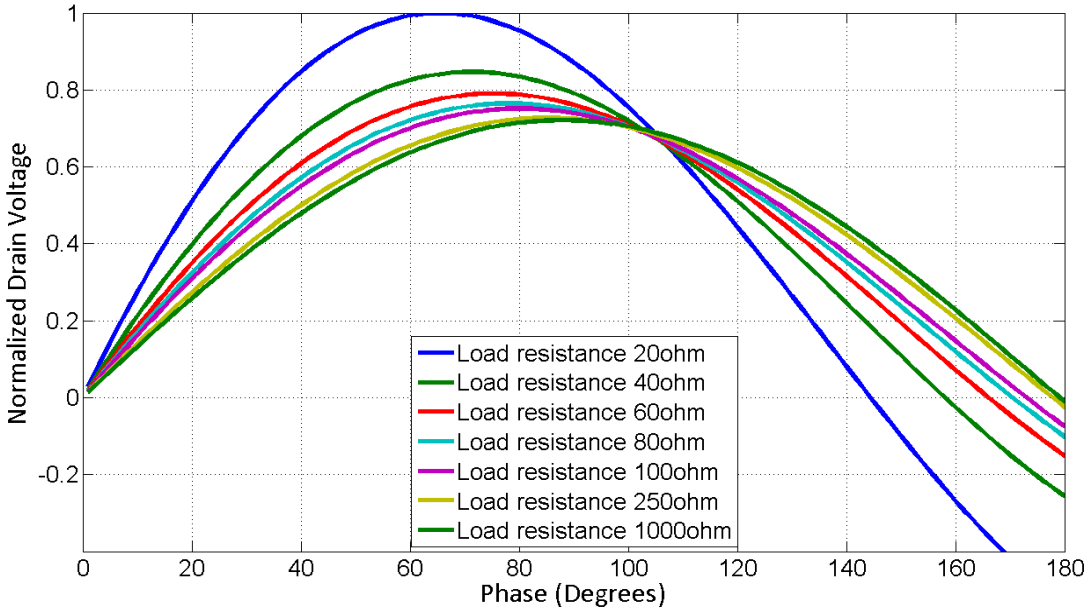

Figure 3-9. Transistor drain voltage waveform for different load resistance. (C_{shunt} = 10 nF).

3.2 Parallel-Parallel Impedance Transformation Network

3.2.1 Introduction

Instead of 240 kHz, an operating frequency of 134 kHz is used for this design rule. Operating frequency should not affect the design rules unless it is extremely high, for example more than 5 MHz. Similar to the series-parallel impedance transformation network design rule, the load resistance is defined as the equivalent resistance looking into the rectifier instead of after the rectifier. Key parameters of the coils including self inductances, mutual inductance, and parasitic resistances can be extracted by measuring the fabricated coil with an impedance analyzer or analyzing with electromagnetic simulation tools. A pair of coils was fabricated using 16 AWG magnetic wires instead of Litz wires for the experiment. The transmitting coil is 21 cm by 21 cm with 10 turns while the receiving coil is 13 cm by 13 cm with 5 turns tightly wounded together. The transmitting coil is designed with the appropriate spacing between the turns to achieve 5% variation of the received power at all different locations. Therefore, it can be reasonably assumed that the coupling is constant regardless of receiving coil position. The self inductance of the transmitting coil is 31.95 µH with a parasitic resistance of 0.32Ω. The receiving coil is 12.52 µH with a parasitic resistance of 0.2Ω. Mutual inductance between the coils is 7.454 µH with a coupling coefficient of 0.373. Measurement of the coils was measured using the HP4192A LF Impedance Analyzer. Since the coils are fabricated using magnetic wires instead of Litz wires, the actual parasitic resistance of both coils during power transfer will be larger than the low voltage signal measured values. This is due to both proximity and skin depth effects. The design rule for the parallel-parallel impedance transformation network will be based on Figure 3-10 which has an extra capacitor C_{tx} shunt across the transmitting coil relative to Figure 3-3.

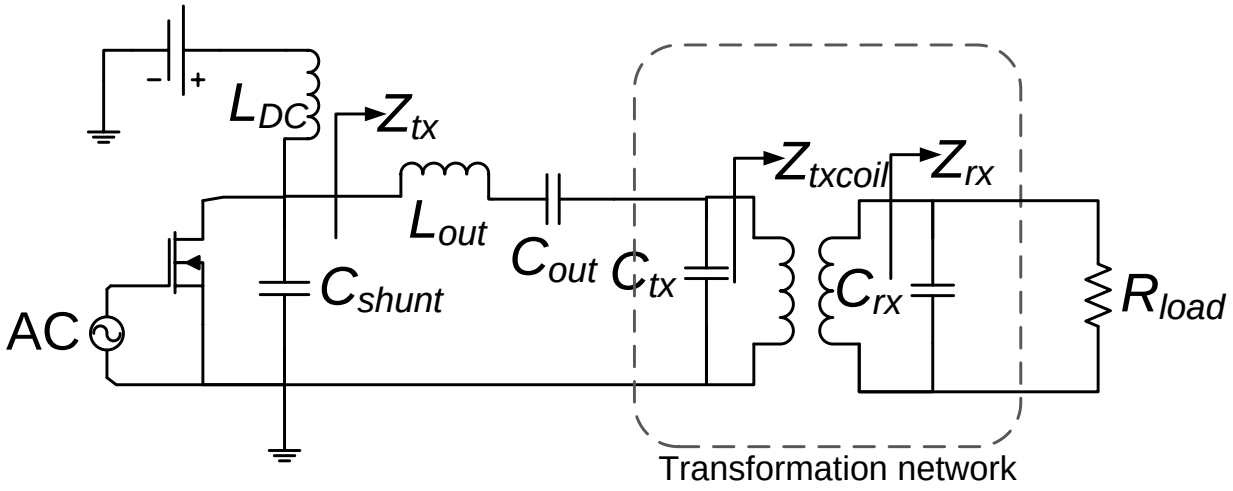

Figure 3-10. Simplified schematic of wireless power transfer system using parallel-parallel transformation network and Class E transmitter. Z_{tx} – Impedance looking into the transmitter load network. Z_{txcoil} – Impedance looking into the transmitting coil. Z_{rx} – Impedance looking into receiver network. R_{Load} is the equivalent resistance looking into the rectifier.

3.2.2 Determination of C_{rx} value

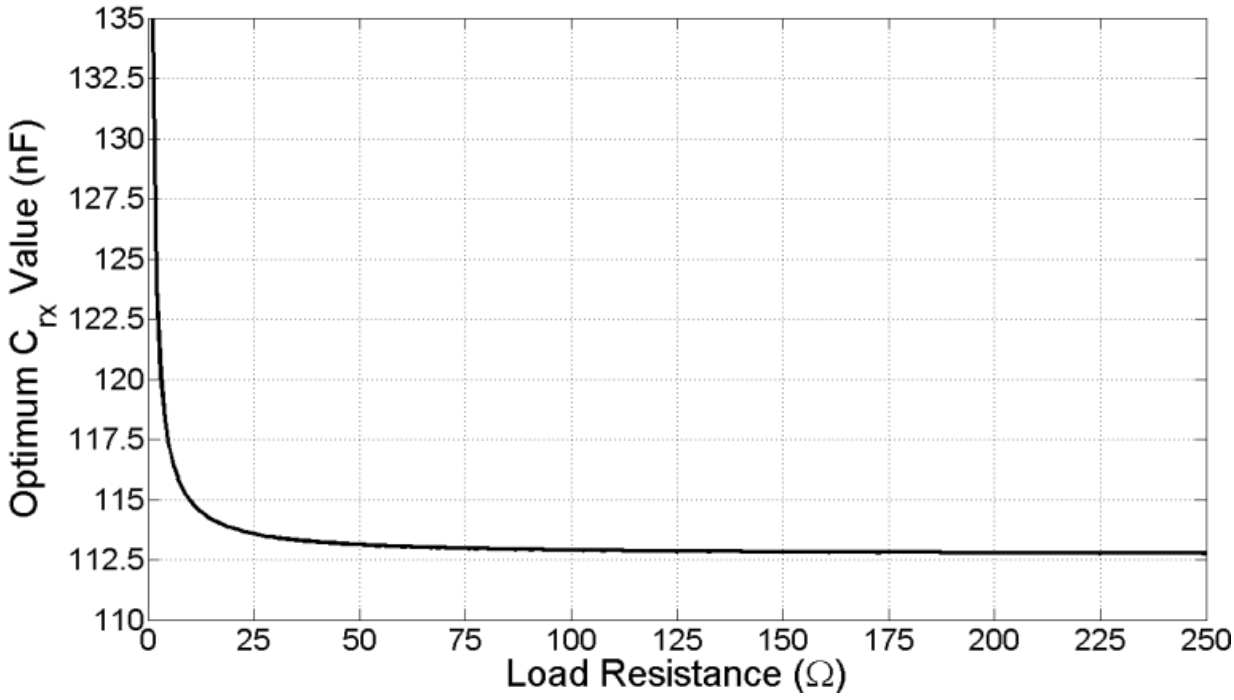

Figure. 3-11. Optimum receiver capacitor value versus load resistance.

The capacitance value is selected based on the inductance of the receiving coil as well as the mutual inductance between the coils. It is ideal to achieve a maximum resistance looking into the transmitting coil across a wide range of load resistances. However, in reality, the optimum capacitance value is different for their respective load resistances. In addition, there is no closed form analytical solution. Differentiating the real part of Equation 2-8 and solving for the optimum receiver capacitance value is not straightforward. Therefore, a simple parameter sweep of Matlab code is used to sweep through a range of receiver resistances and capacitance values to extract the optimum value.

Based on the coil parameters, Figure 3-11 shows the optimum C_{rx} value versus load resistance. The optimum C_{rx} value decreases rapidly from 135 nF to 113 nF with increasing load resistance. The typical operation of a switching voltage regulator used for this application does not present a very low resistance at its input. For example, it can be safely concluded that to power a typical USB enabled device at 5 V, 500 mA (input resistance of 10Ω) , the regulator input resistance should not drop below 25Ω by assuming that the regulator has 100% efficiency and the minimum input regulation voltage is 8 V. Since it is likely that the regulator will operate with load resistance between 25Ω to 100 Ω during high power transfer, it is be important to achieve high efficiency across this impedance range. 113 nF is chosen as the preferred receiver capacitance value.

Figure 3-12 shows the coupling efficiency between the coils and the impedance looking into the transmitting coil (Z_{txcoil}). The efficiency is calculated using the ratio of the power delivered to the resistance R_{txcoil} over the power delivered to both the parasitic resistance and the effective resistance R_{txcoil}. The above method is used to determine the transmitting and receiving coil efficiencies. The coupling efficiency is the combination of both the transmitting coil and

receiving coil efficiencies. It can be seen that the efficiency of the transmitting coil remains high for all cases, which is desirable. This is because the transmitter puts out a large amount of power and should have a higher efficiency to mitigate heat loss. The gradual degradation in receiver efficiency is desirable as it helps to regulate the power during trickle charge. This can be seen in later analysis that the power delivered by the transmitter remains consistent at high load resistances. This is because the equivalent load impedance Z_{tx} looking into the transmitter load network does not change much.

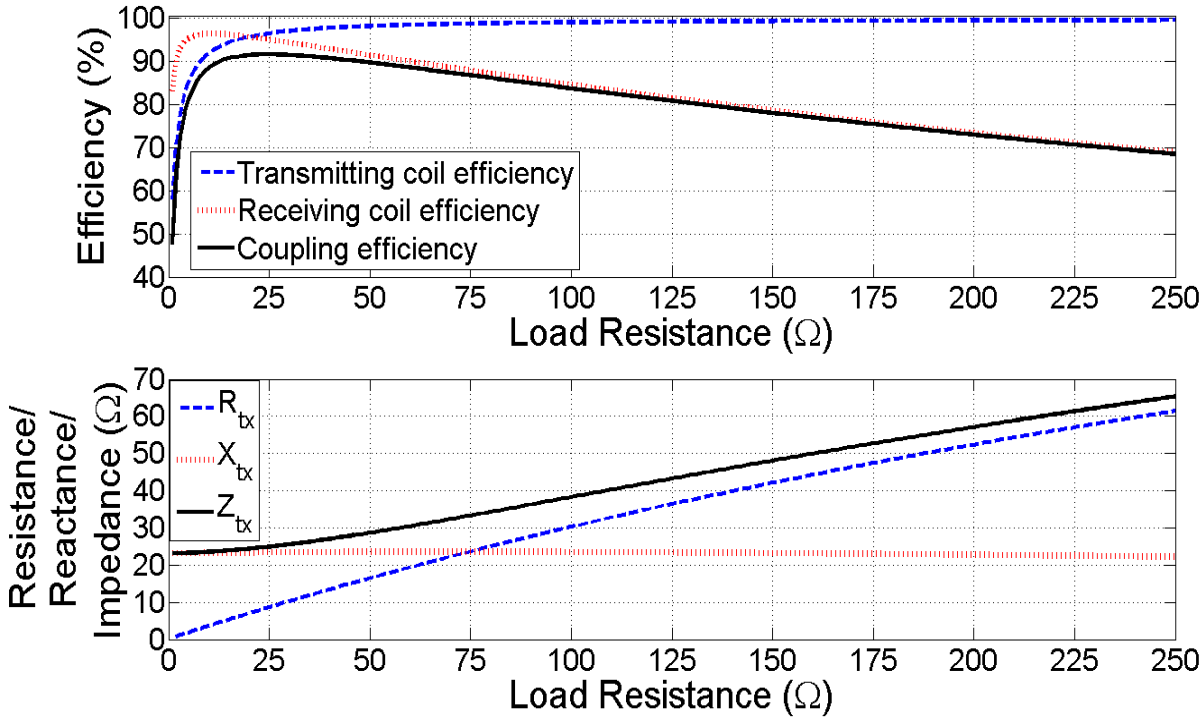

Figure 3-12. Coupling efficiency and transformed impedance looking into the transmitting coil.

3.2.3 Determination of C_{tx} value

Selecting an appropriate transmitting coil parallel capacitor value requires to fulfill two constraints. First, the system must not fail catastrophically when the receiving coil is removed from the transmitting coil (Z_{tx} should not be capacitive and preferably has a phase angle of greater than 40°). Although it is possible to implement a load detection scheme as discussed in

Chapter 7 to turn off the transmitter and reduce unloaded power losses, it is still desirable for the unloaded power consumption to be minimal to begin with. By repeatedly stressing the components with excessive voltage and current will cause them to have a shorter life cycle. In addition, lower power consumption during unloaded condition, will further reduce power consumption during the standby mode.

Limiting unloaded power loss can be achieved by ensuring the unloaded Z_{tx} has equivalent impedance similar to the case with a high load resistance (high impedance with large phase angle). From the schematic of the Class E circuit in Figure 3-10, it can be deduced that most of the power loss is due to the transmitting coil and inductor parasitic resistances as they are in the path of power transfer. Therefore, one way to reduce the unloaded power loss is to use an inductor with lower parasitic resistance or Litz wire for the transmitting coil.

For the second constraint, the reactance of the transformed impedance must have an increasing trend with respect to the load resistance in order to achieve an increasing phase response. Harmonics rejection as well as any phase shifting to bring the impedance of the transmitter load network to the appropriate range is realized by C_{out} and L_{out}. C_{out} and L_{out} are selected based on the operating frequency. Since inductors are typically larger than capacitors, it is not recommended to put more than one inductor on each channel. For the selected operating frequency, L_{out} is selected to be 100 µH (50 µH equivalent single channel) with a parasitic resistance of 1.3Ω at 134 kHz and C_{out} is selected to be 68nF. Since inductors have typically poorer tolerance than capacitors, they can be placed next to each other so that the mutual inductance between the inductors will force the current in the inductors to be synchronized. C_{out} can be tuned to vary the power delivery profile after the design is completed. If C_{out} is too low Z_{tx}

phase will be too small affecting the ZVS operation. If C_{out} is too high the large Z_{tx} phase will limit power delivery.

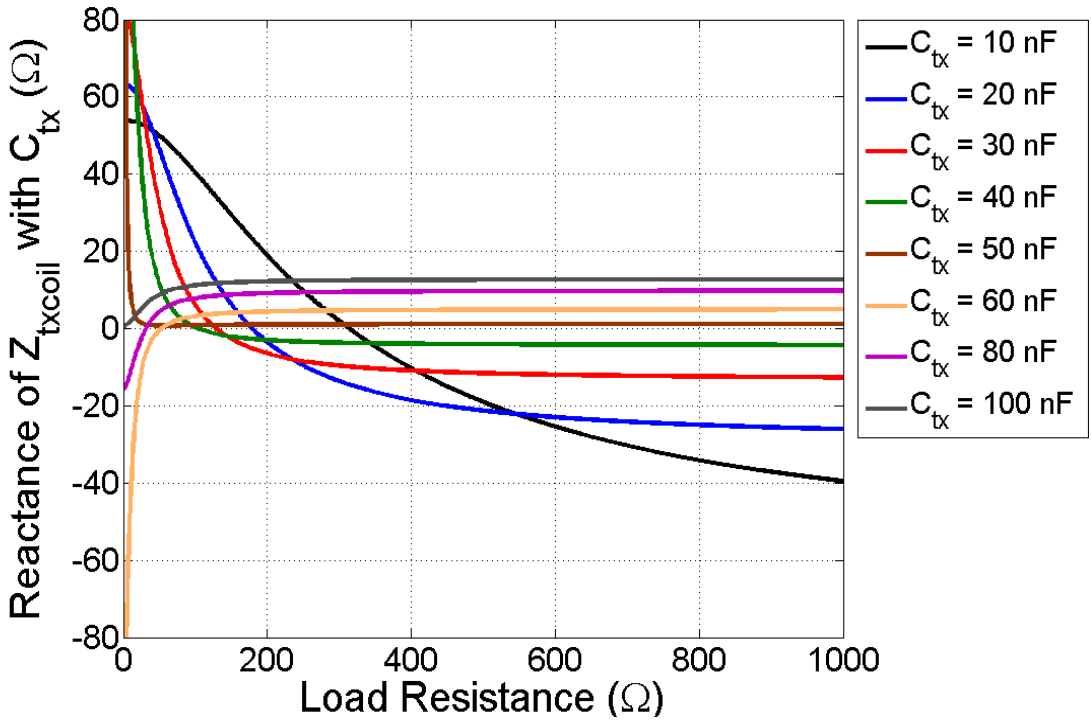

Figure 3-13. Reactance of Z_{txcoil} versus load resistance with different C_{tx}.

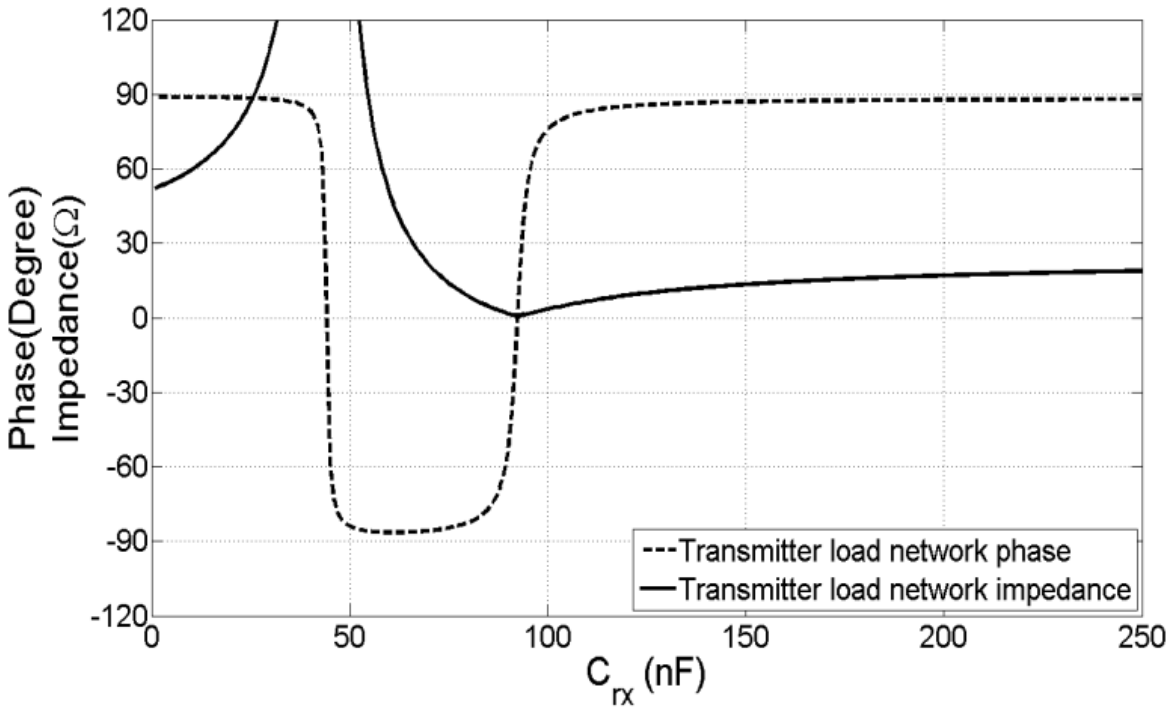

Figure 3-14. Amplitude and phase of impedance of unloaded Z_{tx} versus C_{tx}.

From Figure 3-13, it can be determined that C_{tx} must be at least 60 nF to ensure proper phase response. Figure 3-14 shows the amplitude and phase of the unloaded Z_{tx} with different C_{tx}. Since the class E power amplifier does not work well when driving capacitive load [18] and might even result in a system failure due to heating, C_{tx} values between 44 nF to 93 nF should be avoided. Based on both conditions, it can be concluded that C_{tx} should be above 93 nF. Although it would be ideal to have a large C_{tx} value so that the unloaded power loss is minimized, the variation of the load network reactance decreases, as seen in Figure 3-13, when the value of capacitance increases. If the variation of both resistance and reactance are small, the phase shift across the load resistance is small, resulting in little variation in the power delivery versus load resistance. If the power delivered to the receiver is not reduced to a manageable level at high load resistance, power will be dissipated in the receiving coil creating heating problems. Based on a minimum magnitude of unload Z_{tx} of 10 Ω, a capacitance value of 105 nF is selected for C_{tx}.

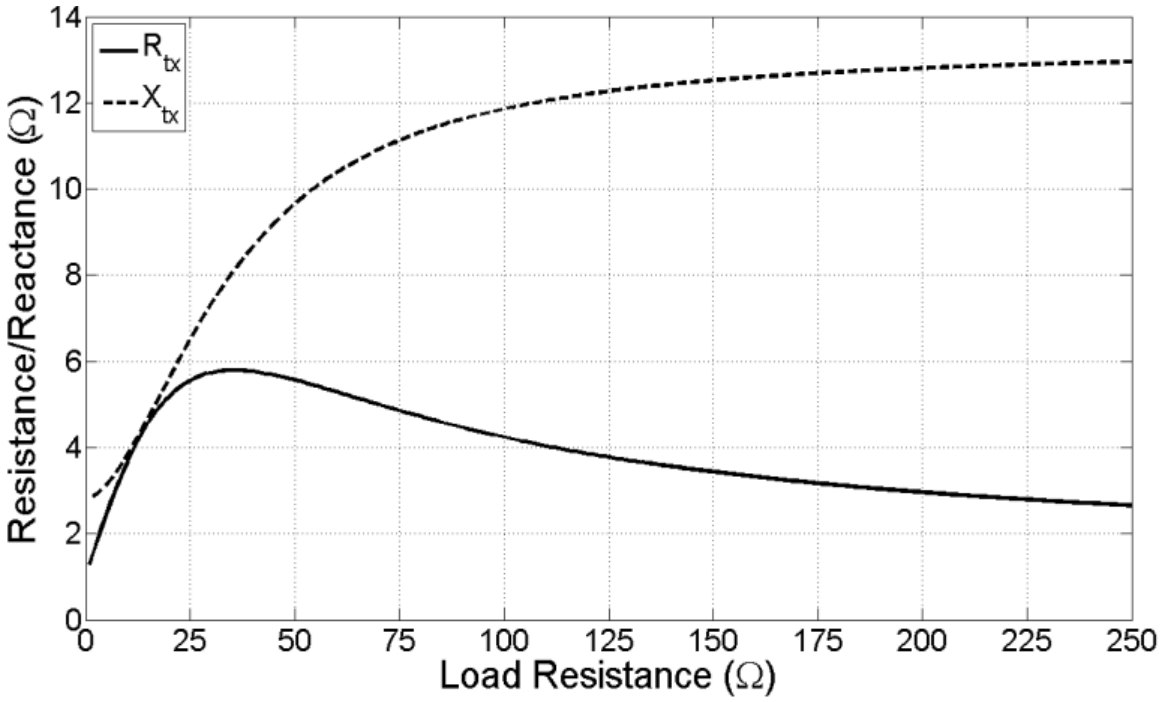

Figure 3-15. R_{tx} and X_{tx} versus load resistance. (C_{tx}: 105 nF)

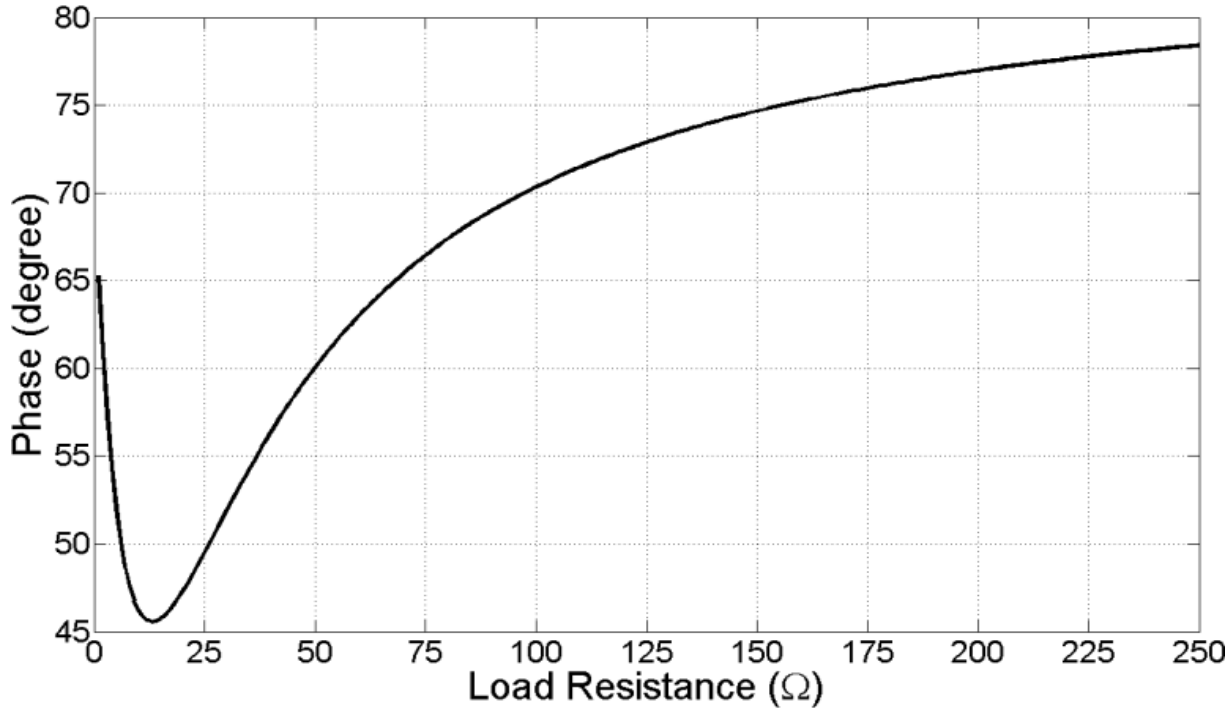

Figure 3-16. Phase of Z_{tx} versus load resistance. (C_{tx}: 105 nF)

3.2.4 Determination of C_{shunt} value

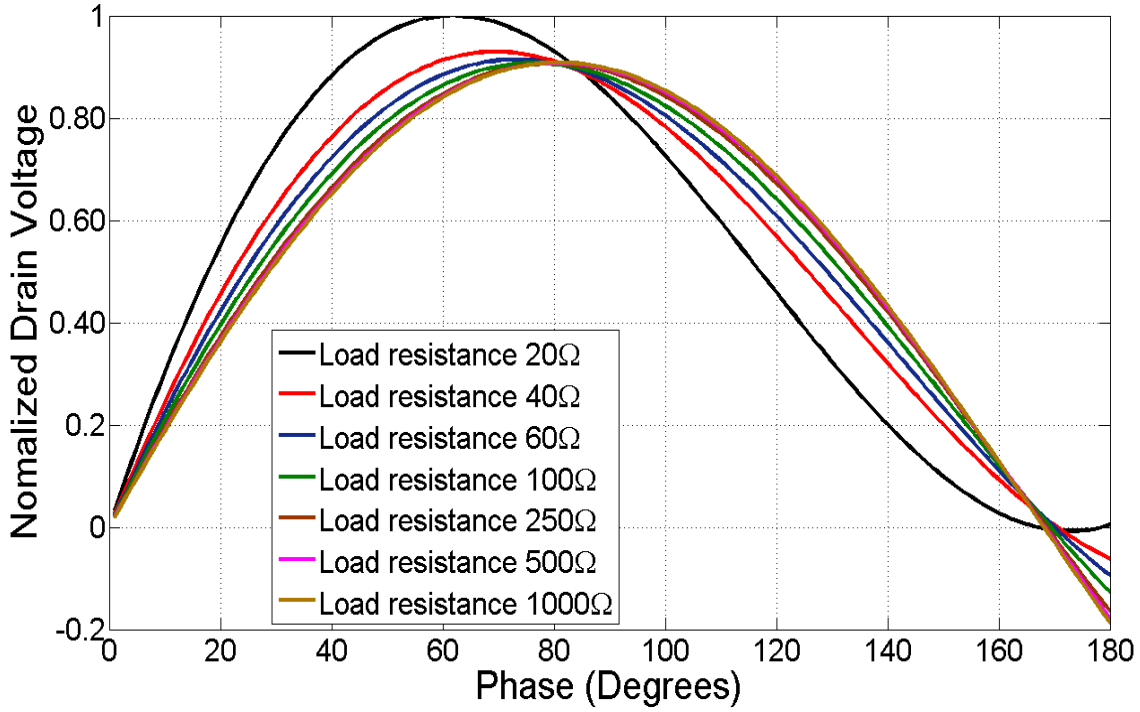

Figure 3-17. Transistor drain voltage waveform for different load resistance. (C_{shunt} = 19 nF).

The method to determine C_{shunt} is the same as the design rule of the series-parallel impedance transformation network topology. The optimum C_{shunt} is found to be 19 nF and the variation of transistor drain voltage versus load resistance is shown in Figure 3-17. If the system is to be reduced to a single channel topology the optimum C_{shunt} value will be double of 19 nF, 38 nF. On the other end the optimum C_{shunt} value for a triple channel topology will be 12.67 nF. The optimum value of C_{shunt} can be easily scaled to the desired number of channels.

CHAPTER 4
WIRELESS POWER TRANSFER SYSTEM SUPPORTING MULTIPLE RECEIVERS

4.1 Inductive Coupling

The analysis of a 1:N coupling structure for a single transmitting coil delivering power to multiple receivers extends from the analysis in Chapter 2. Since the receivers are intended to be integrated into portable devices, it is highly unlikely that the receivers will be overlapped. In addition due to the physical constraint of the devices, they should be sufficiently spaced apart. Therefore, the mutual inductance between the receiving coils can be neglected as the coupling between the receiving coils will be significantly weaker than the coupling between the transmitting coil and receiving coils.

The voltage and current characteristics of the transmitting coil and X number of receiving coils can be described using the following equations:

$$V_1 = j\omega M_{11} I_1 + j\omega \sum_{N=1}^{X} M_{1N} I_N \tag{4-1}$$

$$V_N = j\omega M_{N1} I_1 + j\omega M_{NN} I_N \tag{4-2}$$

$$M_{1N} = k_N \sqrt{M_{11} M_{NN}} \tag{4-3}$$

Where

V_1 is the voltage at the transmitting coil. (Figure 1-1)

I_1 is the current at the transmitting coil. (Figure 1-1)

V_N is the voltage at N receiving coil. (Figure 1-1)

I_N is the current at N receiving coil. (Figure 1-1)

M_{11} is the self inductance of the transmitting coil.

M_{NN} is the self inductance of N receiving coil.

$M_{1N} = M_{N1}$ is the mutual inductance of the transmitting coil and Nth receiving coil.

k_N is the coupling coefficient between the transmitting coil and Nth receiving coil.

X is the total number of receivers.

By Ohm's law:

$$\begin{aligned} Z_{tx} &= R_{tx} + jX_{tx} \\ &= \frac{V_1}{I_1} \end{aligned} \tag{4-4}$$

$$\begin{aligned} Z_{rxN} &= R_{rxN} + jX_{rxN} \\ &= \frac{V_N}{I_N} \end{aligned} \tag{4-5}$$

Using Equation 4-1, Equation 4-2 and Equation 4-4 and assuming a time-harmonic operation with frequency ω, the impedance looking into the transmitting coil for multiple receivers is derived as Equation 4-6.

$$\begin{aligned} Z_{tx} = & \sum_{N=1}^{X} \frac{\omega^2 M_{1N}^2 R_{rxN}}{R_{rxN}^2 + \left(\omega M_{NN} + X_{rxN}\right)^2} \\ & + j\left(\omega M_{11} - \sum_{N=1}^{X} \frac{\omega^2 M_{1N}^2 \left(\omega M_{NN} + X_{rxN}\right)}{R_{rxN}^2 + \left(\omega M_{NN} + X_{rxN}\right)^2}\right) \end{aligned} \tag{4-6}$$

A typical buck switching regulator requires a higher input voltage to operate and tends to "amplify" the load resistance. The "amplification" of load resistance will tend to "choke" the other receivers in a multiple receivers setup especially when one of the receivers is in a high resistance/trickle charge state. The trend can be observed from Equation 4-6 and Equation 3-1 which also can be observed from Figure 4-1. In order to achieve considerable power delivery when one of the receiving devices is fully charged, it needs to decouple itself from the system.

The decoupling can be achieved by a switch either in series of the power path to break the connection or in parallel with the receiving coil to create a short across the receiving coil so that the transmitter does not see the transformed impedance due to the receiver.

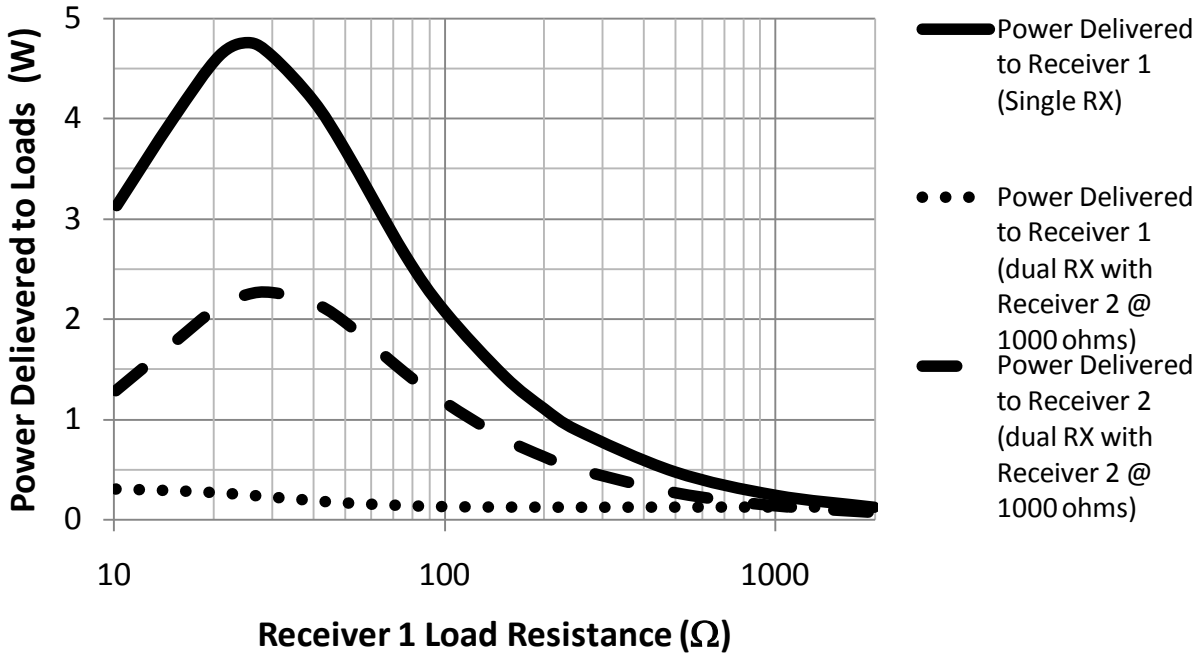

Figure 4-1. Power delivery to loads for a single receiver setup and a dual receivers setup with one of the load fixed at 1000Ω.

Since the receiver will be a portable device such as cellular phone, mp3 player, etc, the receiver switch used to "decouple" the receiver needs to be compact and able to be driven by a low voltage, e.g. not more than 3 V. Although, most electromechanical switches are able to tolerate large voltages and currents, they are typically large for portable electronics and generate a "clicking" sound during switching which is not acceptable. Off the shelf solid state switches are typically designed for 50/60 Hz AC line application. They are relatively larger in size and do not offer sufficient isolation for hundreds of kilohertz signals. It is possible to find switches which operate at high frequencies but the power handling starts to drop with increase in frequency as shown in [30] unless novel materials are used as shown in [31] which will make the switch expensive. In addition, it is difficult to control the switch with voltages lower than the

voltage being switched using a simple transmission gate topology or switch transistors. A new switch architecture which is an extension of a transmission gate switch is proposed to control a large voltage/current signal with a low voltage control signal. The discussion of the switch circuit in this section is independent of the decoupling architecture.

4.2 Switch Design

The block diagram is shown in Figure 4-2. The proposed switch should be able to handle voltages up 25 Vrms and current up to 2 Arms with an operating frequency up to 1 MHz. In addition, the proposed design should not use any inductors so that it can be easily integrated into an IC or single package solution with the voltage regulator.

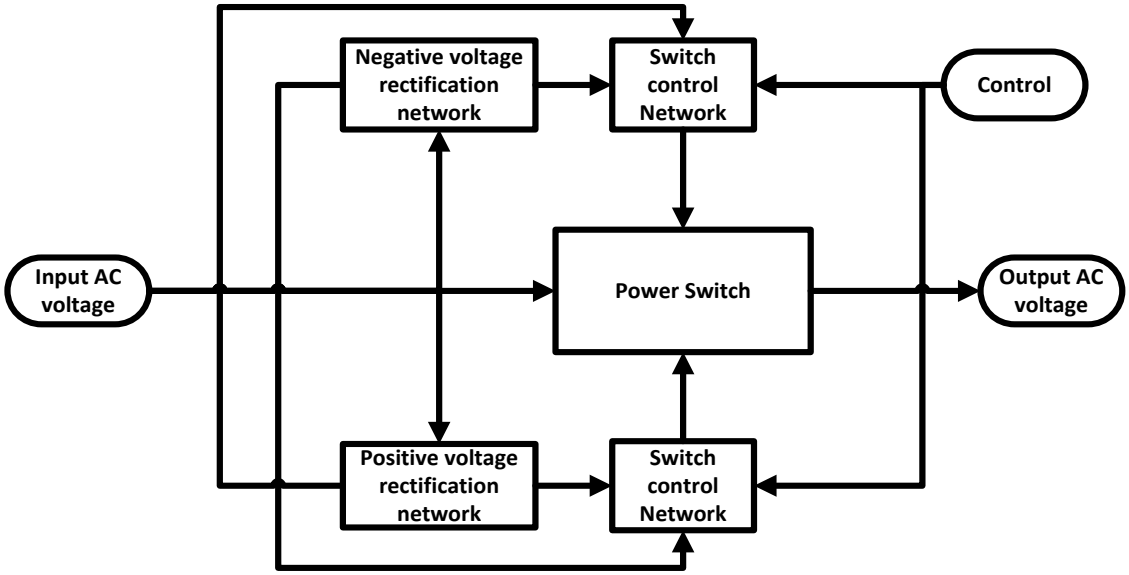

Figure 4-2. Block diagram of the proposed switch.

The power switch block in Figure 4-2 uses a typical transmission gate architecture which is a NMOS and a PMOS in parallel. A schottky diode must be added to either before or after the transistor to counter the effect of the body diode of the power MOSFET. The schottky diode selected must have power handling comparable to the body diode of the transistor. The control signals to the gate of both of the transistors are provided via their respective switch control

network. Two rectification circuits extract the maximum voltage and minimum voltage of the input AC voltage. The maximum voltage and minimum voltage are used as an input for the respective switch control network in a cross-coupled topology. Based on the control signal provided by the receiver, the switch control network will switch between the maximum voltage and the minimum voltage to either turn the transmission gate on or off. Schematic of the proposed switch circuit is shown in Figure 4-3. A single package dual N and P channel MOSFET (IRF7343) from International Rectifier is used. The transistors have an absolute V_{gs} of 20 V and an absolute V_{ds} of 55 V. The peak continuous drain current of the N channel MOSFET is 4.7 A and P channel MOSFET is 3.4 A. Turn on resistance for both transistors are typically better than 0.1 Ω. Therefore, the transistors are able to handle considerable amount of power at high efficiency. Rise time and fall time of both transistors are better than 22 ns, giving it a fast response time. The input capacitor of both transistors is typically better than 750 pF which makes driving the transistor feasible. The C_{gd} of both transistors are less than 100pF and the C_{ds} of both transistors are less than 125 pF, reducing the leakage current at high frequency when the switch is turned off. MBRA340T3 is selected for both the rectification network diode and switch because it is able to handle voltages up to 40 V and currents up to 3 A. In addition, it has a small forward voltage drop of 0.45 V and being a schottky diode it has negligible reverse recovery time.

Notation for resistors and capacitors are in the form of RX_X and CX_X. The number after the underscore is used to differentiate between the two switch control networks which are similar, namely channel 1 for the P channel MOSFET of the transmission gate and channel 2 for the N channel MOSFET of the transmission gate. Value for C1 is 100 nF, C2 is 10 nF, R1 is 10 kΩ and R2 is 47 kΩ.

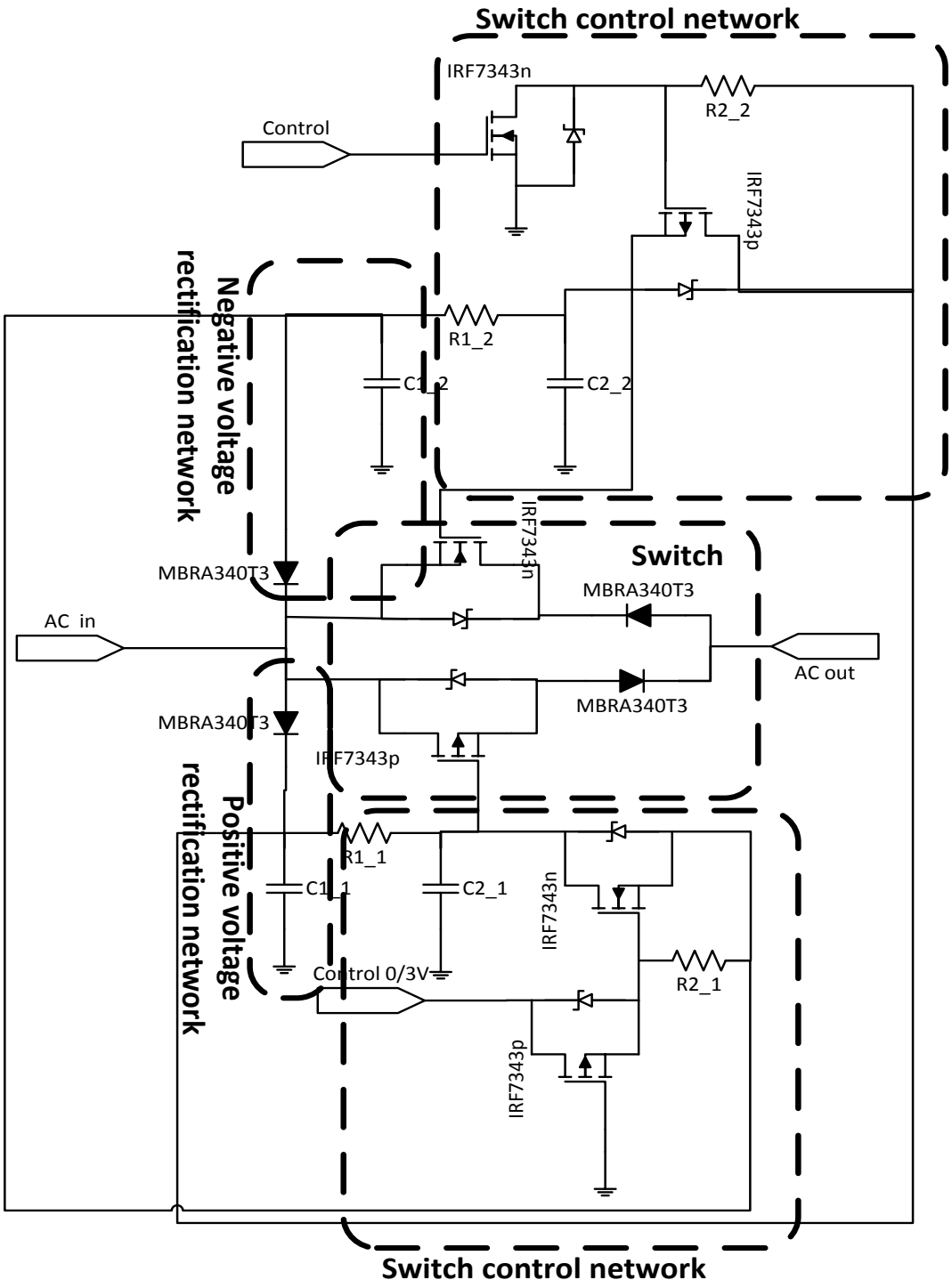

Figure 4-3. Schematic of the proposed switch circuit.

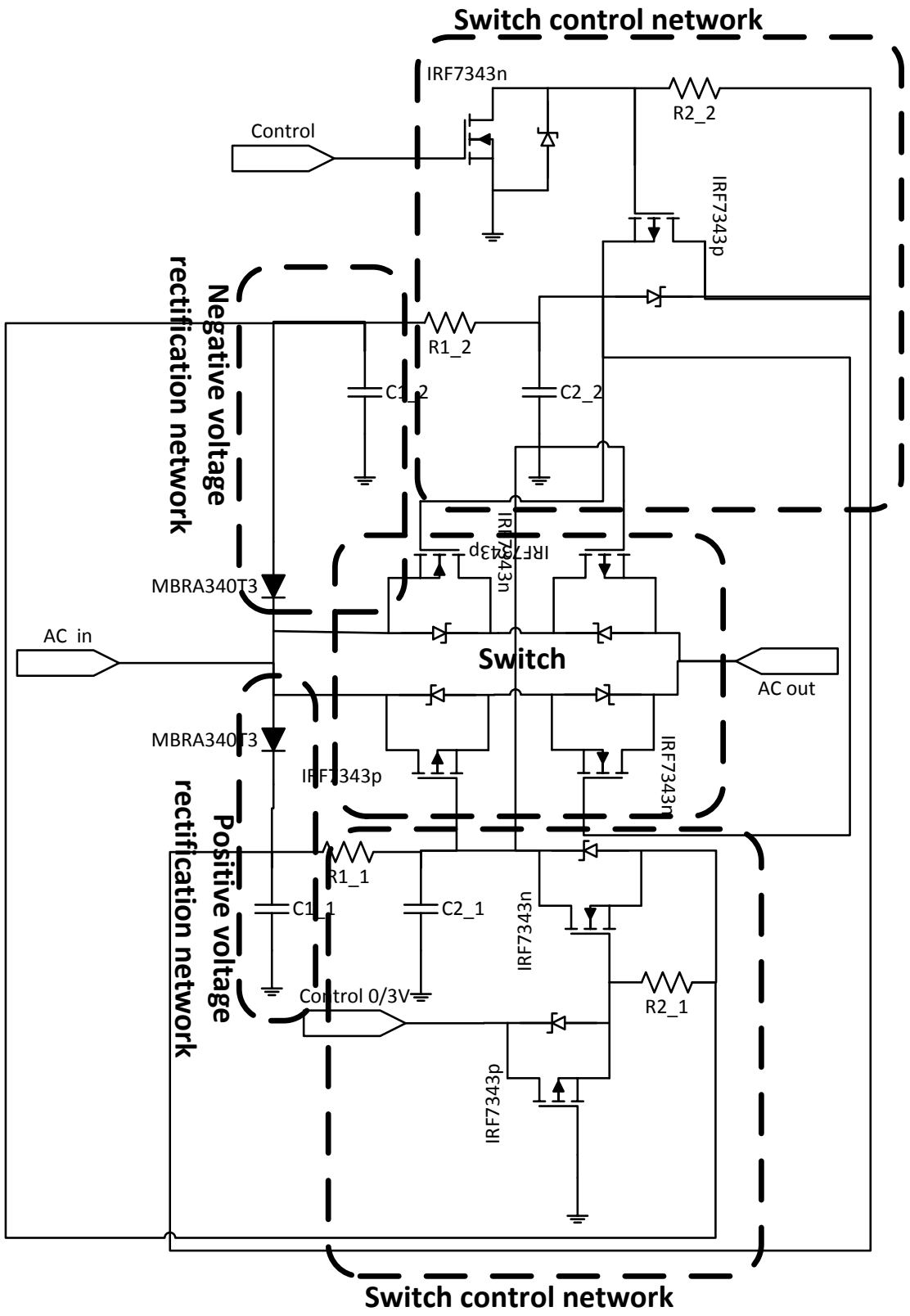

Figure 4-4. Schematic of the improved proposed switch circuit.

An improved version of the proposed switch is to replace the diode in series with the transmission gate transistors with a transistor as shown in Figure 4-4. By doing so, the power signal will not suffer a forward voltage diode drop, reducing the losses through the switch. However, the switch control network must ensure that it is able to drive the extra gate loading the two rectification networks. Since the diodes used have a low forward drop voltage, and for simplicity, the switch will use the schematic on Figure 4-3 instead of Figure 4-4.

4.3 Switch Simulation

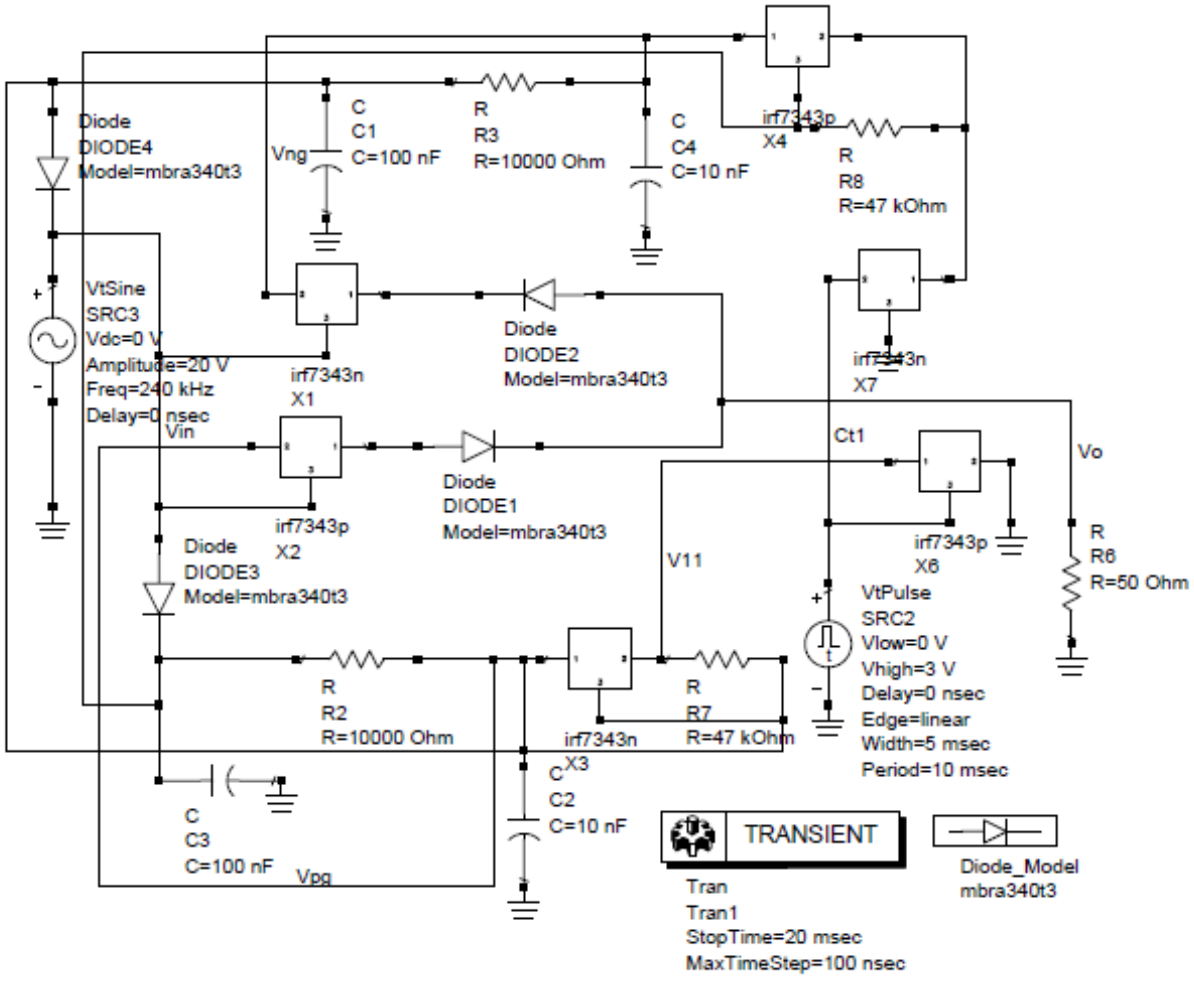

Figure 4-5. Schematic of the switch in Advanced System Design with a resistive as load.

Simulation and verification of the switch is done using Advanced System Design by Agilent. The simulation schematic to analyze the performance of the switch with a 50 Ω resistive load is shown in Figure 4-5. Transistor and diode model in the simulation are obtained from the manufacturer. Therefore, the simulation results should match the performance of the fabricated circuit.

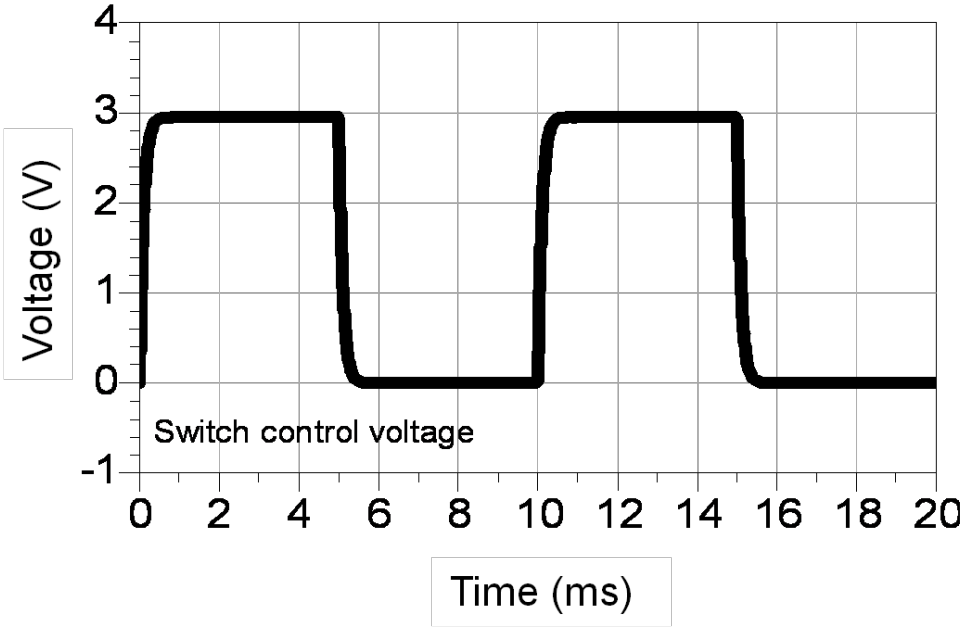

Figure 4-6. Switch control waveform (0 V for off and 3 V for on). A minimum of 1 V is required to turn on the transistor.

Figure 4-6 shows with switch control waveform which is 0 V for off state and 3 V for on state at a duty cycle of 50% and a frequency of 100 Hz. Based on the transistor used (IRF7343), the switch is able to operate at turn on voltages as low as 1 V. Figure 4-7 shows the switch control voltage for each respective channel. The turn off response time for channel 1 is approximately 630 µS and turn off response time for channel 2 is approximately 700 µS. The turn on response time for channel 1 is approximately 60 µS and turn on response time for channel 2 is approximately 70 µS. Therefore, the switch can operate up to 1 kHz switching frequency, which is way beyond the application of the circuit which is to turn off the receiver

when the device is fully charged. The turn on time is significantly faster than the turn off time because the voltage across C1 and C2 are the same when the switch is turned off and when the switch transits from the off stage to on stage C2 is charged/discharged via the low resistance path through the transistor whereas when the switch transits from the on stage to the off stage C2 is charged/discharged via resistor R1 which increases the time constant significantly. Response time can be improved by decreasing R1 at the expense of power loss through the switch. Decreasing either C1 or C2 also helps to improve the response time. However, the ripples on the rectified voltage might become significant and affect the operation of the circuit.

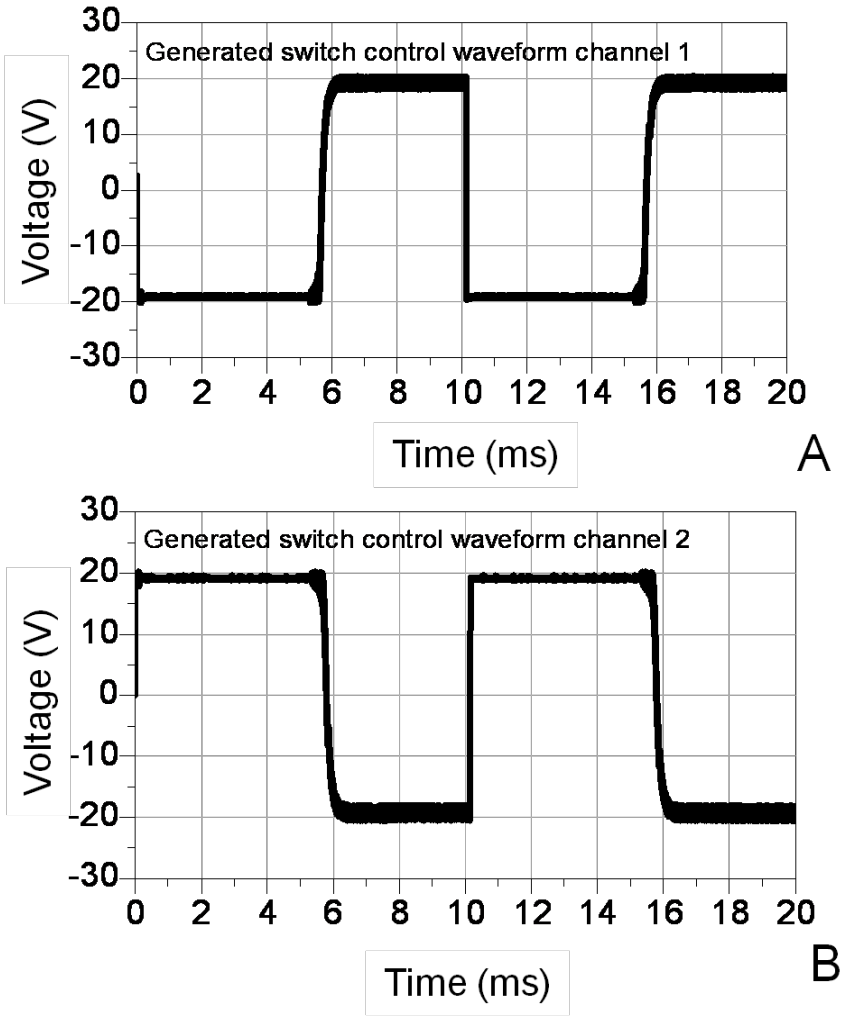

Figure 4-7. Generated switch control waveforms. A) Channel 1 (P channel MOSFET of the transmission gate) and, B) Channel 2 (N channel MOSFET of the transmission gate).

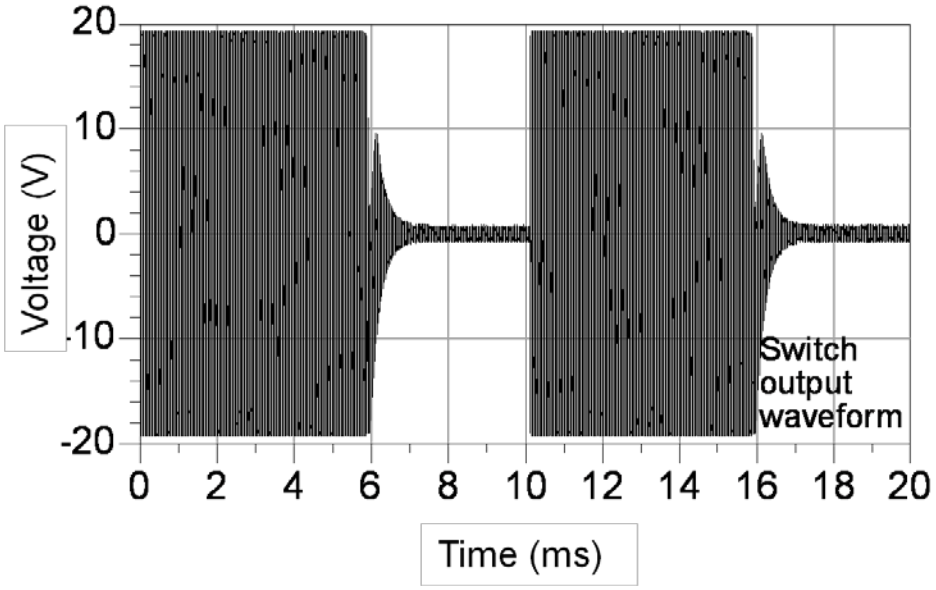

Figure 4-8. Output waveform of the switch before the rectifier.

Figure 4-8 shows the output AC waveform of the switch across the 50 Ω resistive load. The switch is capable of breaking the high voltage/current AC signal path with reasonable turn on and turn off time with the time off time slightly slower than the turn on time. The reason for the difference in timing is the same reason for those of the switch control network waveform.

4.4 System Response with Receiver Switch

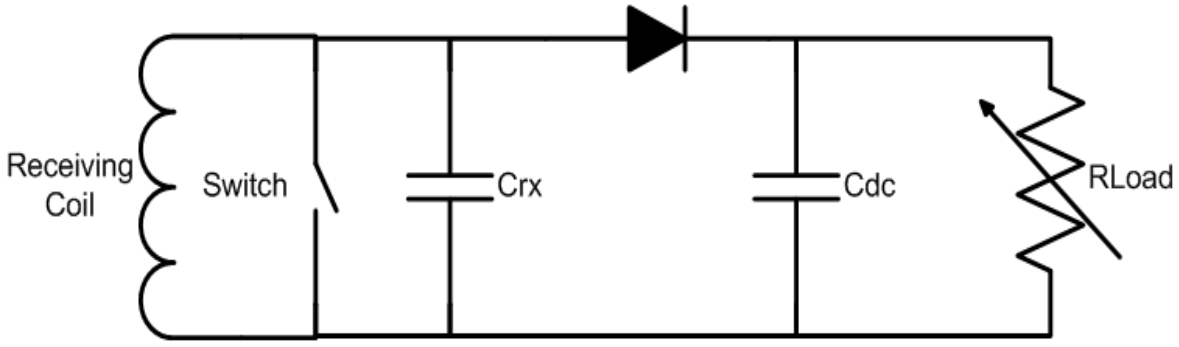

Figure 4-9. Proposed half-wave rectifier receiver architecture.

Figure 4-10 shows the proposed receiver architecture. A half wave rectifier is used instead of a full wave rectifier because the circuit will be more compact using a single diode instead of four. Another benefit is that the rectification process only suffers a single diode forward voltage

drop instead of two. In addition, the operating frequency will be in the range of hundreds of kilohertz, thus it will not require a very large charge holding capacitor. Instead of using the switch in the power path, the switch is placed shunt across the coil. There are two reasons in using such a topology. Firstly, by shorting the receiving coil, the receiver coil sees a short. Therefore, R_{rx} and X_{rx} in Equation 2-7 will be extremely small that their value can be assumed to be zero.

Let X_{rx} in Equation 2-7 be zero.

$$Z_{tx} = \frac{\omega^2 M_{12}^2 R_{rx}}{R_{rx}^2 + \left(\omega M_{22}\right)^2} + j\left(\omega M_{11} - \frac{\omega^3 M_{12}^2 M_{22}}{R_{rx}^2 + \left(\omega M_{22}\right)^2}\right) \tag{4-7}$$

Next let R_{rx} in Equation 4-7 to be zero.

$$Z_{tx} = j\left(\omega M_{11} - \frac{\omega M_{12}^2}{M_{22}}\right) \tag{4-8}$$

Substituting Equation 2-3 into Equation 4-8.

$$Z_{tx} = j\left(\omega M_{11} - \omega k^2 M_{11}\right) \tag{4-9}$$

In order for the system to be able to support multiple devices and provide sufficient lateral freedom, it is reasonable for the coupling coefficient to be much less than 0.25. By assuming the coupling coefficient to be 0.25, k^2 will be 0.0625 which is much lower than 1. Therefore, if the receiving coils are shorted under loosely coupled condition, the transmitter only sees the self inductance of the transmitting coil. However, if the coupling coefficient between the coils starts to increase there will be a reduction in self inductance of the transmitting coil. This will cause Z_{tx} to be less inductive and potentially causing the class E power amplifier to be no operating under ZVS/ZDS condition.

The second reason is that the switch's natural state is open when no voltage is applied to the control port. Therefore, the receiver will allow power to pass through when the control port is left floating. This is critical especially when the battery on the receiver is fully drained and is unable to control the switch. By using the proposed architecture in Figure 4-9, the receiver does not require any bootstrapping even when there is no power, because the switch will be in a naturally on state.

Figure 4-10 shows the test bench to verify the performance of the switch when used in this specific scenario. A similar clock control source is used as well. The switch circuit in Figure 4-5 is converted to the modular block X1. Instead of using a full Class E driver, the transmitter is simplified as an AC current source with 1A peak current at 240kHz. The transmitter coil is modeled as inductor L1 and receiving coil as inductor L2, mutual inductance is modeled via "Mutual1" block.

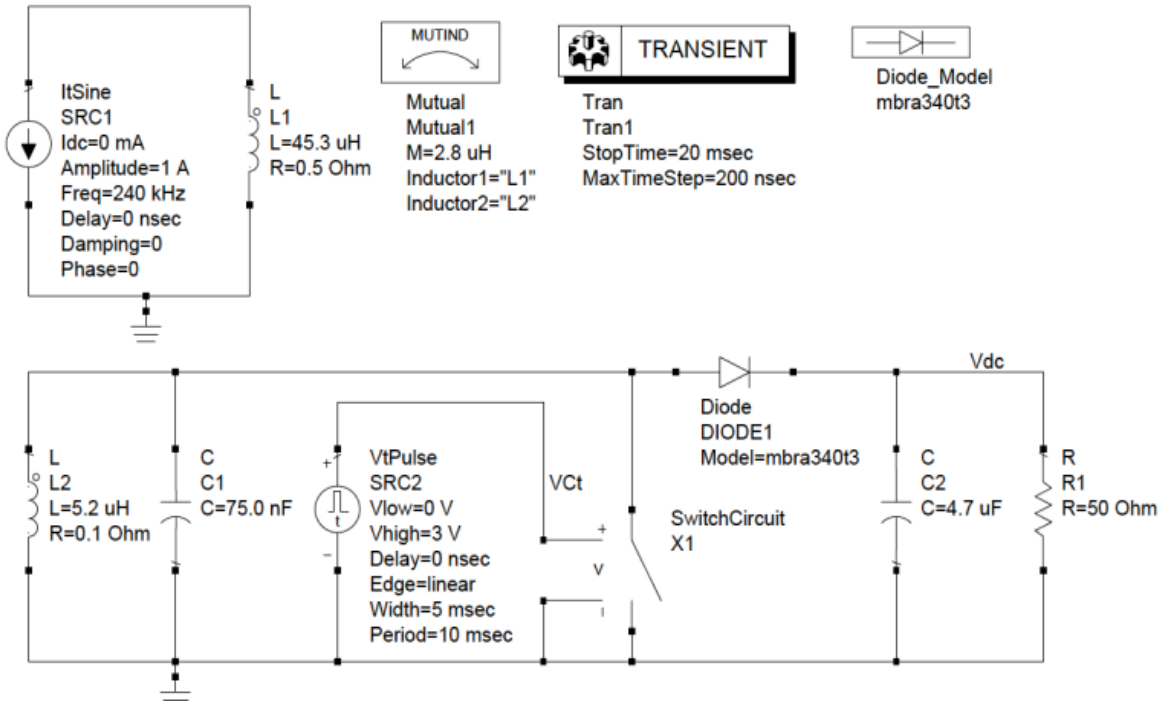

Figure 4-10. ADS schematic of test bench for receiver architecture in Figure 5-10.

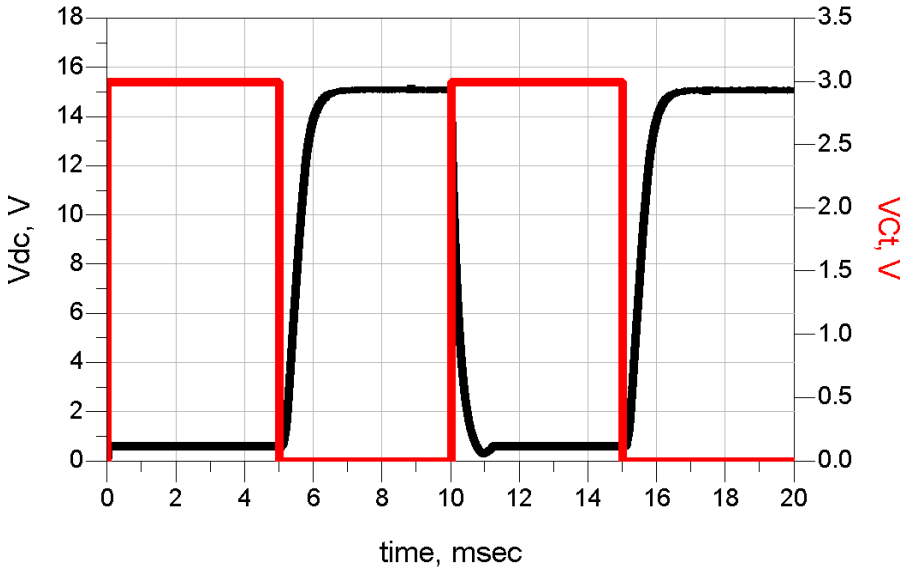

Figure 4-11. Simulation results of test bench (Figure 4-10). Red: Low voltage control signal. Black: Receiver rectified voltage.

Figure 4-11 shows the simulation results of the test bench of Figure 4-10 with the control voltage in red and output rectified voltage in black. As predicted in switch standalone simulations, the switch closing time is faster than the opening time, resulting in a faster decoupling response time. Although the receiver is supposed to be fully decoupled when the switch closes, a 0.5V DC voltage still can be observed at the load. This is because the switch is not an ideal switch and a potential drop will be observed across the parasitic resistance of the transmission gate transistor as well as the series diodes used to counter the effect of the body diode. The 0.5V DC voltage should not be a concern because it is not sufficient to turn on the voltage regulator which is typically used to provide a stable DC voltage. From the simulation results, it can be concluded that the switch circuit can be used in scenarios where a control voltage is significantly smaller than the input AC voltage at high frequencies regardless of topologies.

CHAPTER 5
EXPERIMENTAL VERIFICATION

5.1 High Power 300W Dual Channel System using Parallel-Parallel Impedance Transformation Network Topology

Based on the parallel-parallel impedance transformation network topology design rule, a dual-channel Class E transmitter test system capable of delivering nearly 300 W with a supply voltage of 120 V is fabricated using the IRFP21N60L HEXFET® power MOSFET from International Rectifier. A full wave rectifier with a shunt charge holding capacitor at the output using MUR420 from Vishay is fabricated to convert the AC power to DC power. Since the forward voltage drop is 0.875 V and the reverse recovery is 30 ns, power loss due to the voltage drop and reverse recovery is small compared to the amount of power delivered to the load. Load resistance in this section is the equivalent resistance looking into the regulator or device being charged/powered as shown in Figure 1-1 instead of the equivalent resistance looking into the rectifier as shown in Figure 3-3.

In order to reduce losses through parasitic resistance, low loss polypropylene capacitors are used. To achieve a balance between size and efficiency, a 100 µH inductor (1140-101K-RC) by Bourns Jw Miller is selected for L_{out}. Since most of the loss of the transmitter is due to the parasitic resistance of L_{out}, a larger and more efficient inductor can be used if space permits. Table 5-1 shows the calculated value of each component with respect to the actual component value used in the experimental setup. The calculated values obtain from Chapter 3 are initially used and further tuned to achieve optimum power delivery and efficiency across a wide range of load resistance. Most of the values follow closely to the calculated value from Matlab. The only exception is C_{shunt}. The main reason for such a discrepancy is that the equation used in [18]-[19] assumes the transistor to be an ideal switch. Therefore, while calculating the drain voltage, the built-in diode in the transistor was not taken into account. The other parameters of the transistor

do not have any significant effect on the calculated values since the rise and fall times of the transistor are significantly faster than the switching time and the drain-to-source capacitance is less than 1 nF. In addition, the turn-on resistance of the transistor is extremely small. Another reason is that during the calculation, the DC feed inductor (L_{DC}) is assumed to be infinitely large, which is not true in experiment.

Table 5-1. Component Values for High power 300W Dual Channel System using Parallel-Parallel Impedance Transformation Network Topology

	Calculated	Experimental	% Variation
C_{rx}	113 nF	115 nF	+1.8%
Ct_x	105 nF	100 nF	-4.8%
C_{out}	68 nF	68 nF	0%
L_{out}	100 µH	100 µH	0%
L_{out} parasitic resistance	-	1.3 Ω	-
C_{shunt}	19 nF	15 nF	-21%
TX coil inductance	-	31.95 µH	-
TX coil dimension	-	21 cm x 21 cm	-
TX coil parasitic resistance	-	0.32 Ω	-
RX coil Inductance	-	12.52 µH	-
RX coil dimension	-	13cm x 13 cm	
RX coil parasitic resistance	-	0.20 Ω	-
Mutual Inductance	-	7.475 µH	-
Coupling Coefficient	-	0.374	
L_{DC}	-	500 µH	-

The fabricated dual-channel transmitter with a dimension of 10 cm x 8.5 cm is shown in Figure 5-1. The two inductors of L_{out} occupy a significant amount of space due to the requirement of low parasitic resistance so as to maintain high efficiency in power delivery. Figure 5-2 shows the transmitting coil (21 cm x 21 cm) embedded inside a table top case, and the receiving coil (13 cm x 13 cm) placed on top of the case. The actual separation between the two coils is 10 mm. The setup enables the user to have a large degree of translational freedom both in the X and Y direction. It should be noted that there is no ferrite core in either the transmitting coil or receiving coil.

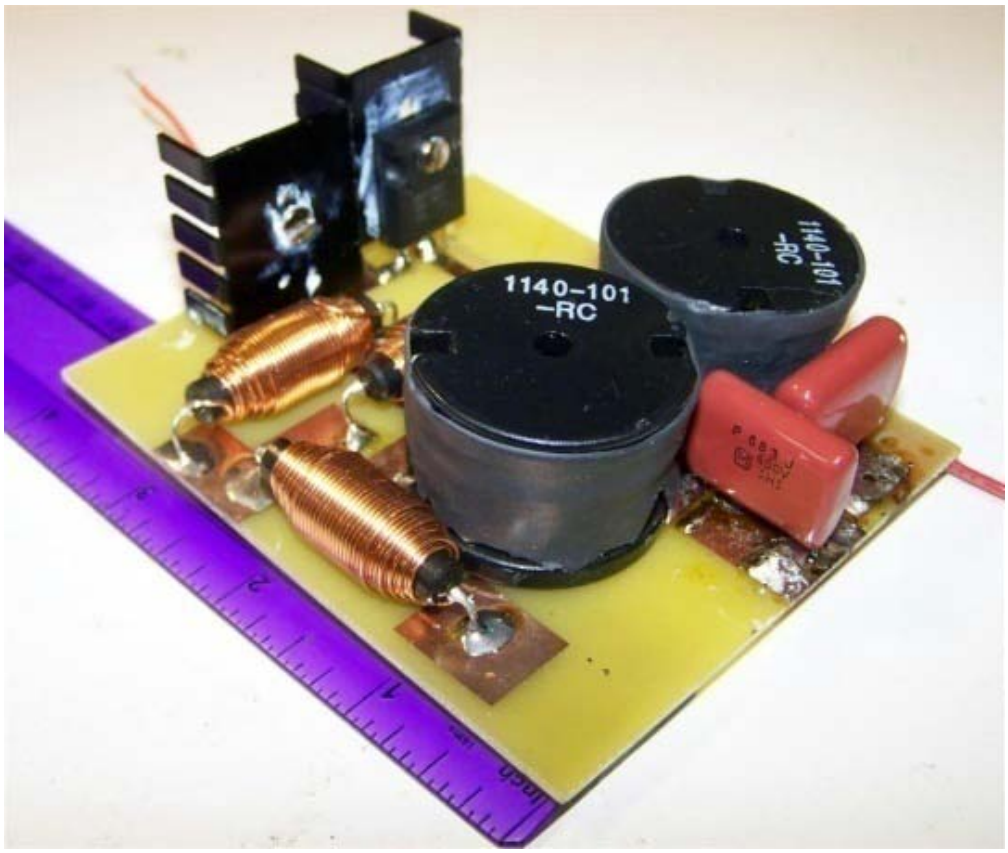

Figure 5-1. Photograph of the dual-channel Class E power amplifier.

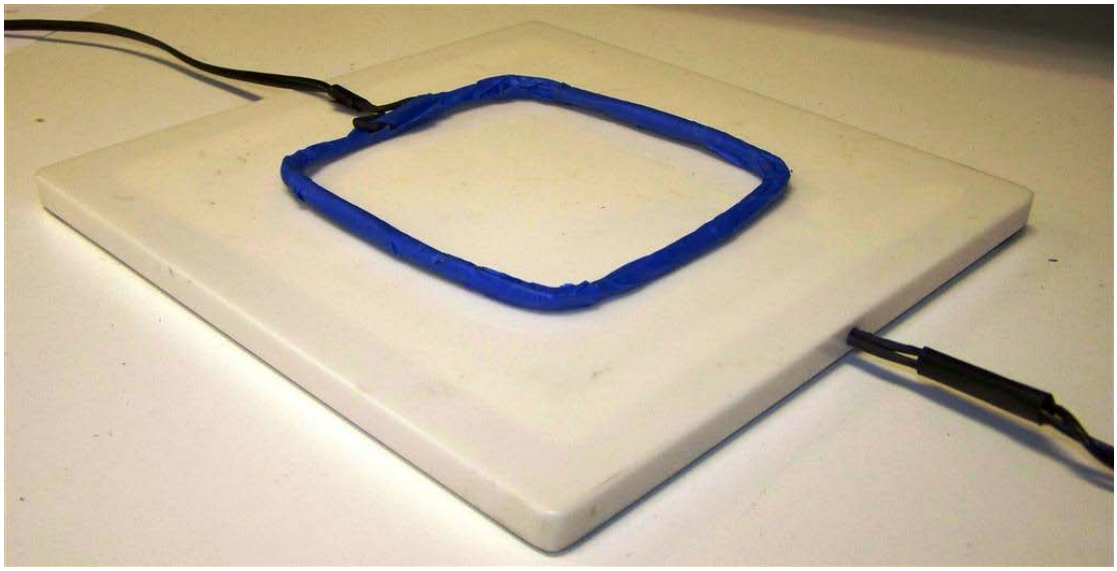

Figure 5-2. Photograph of the transmitting coil – 10 turns (embedded into the table top) and receiving coil – 5 turns (placed on top).

Using a 120V power supply, power delivery of 295 W to a 50Ω load with a DC voltage of 121.5 V and current of 2.43 A is achieved. The input current from the power supply is 3.25 A. The end-to-end system efficiency is 75.7%. Peak drain voltage is 460 V which is 25% lower than the rated maximum voltage of the transistor. Figure 5-3 shows the efficiency and power delivery of the 120 V system versus load resistance. Although the maximum power of 295 W occurs at 50 Ω load resistance, a high efficiency of at least 77% is achieved across the range of 60 Ω to 140 Ω, which matches the optimum range of power delivery above 200 W. The power delivered is proportional to the square of the supply voltage. The power delivery of the system can be increased by increasing the supply voltage as long as the DC power supply driving system is able to provide sufficient power and the drain voltage across the transistor stays within its breakdown voltage.

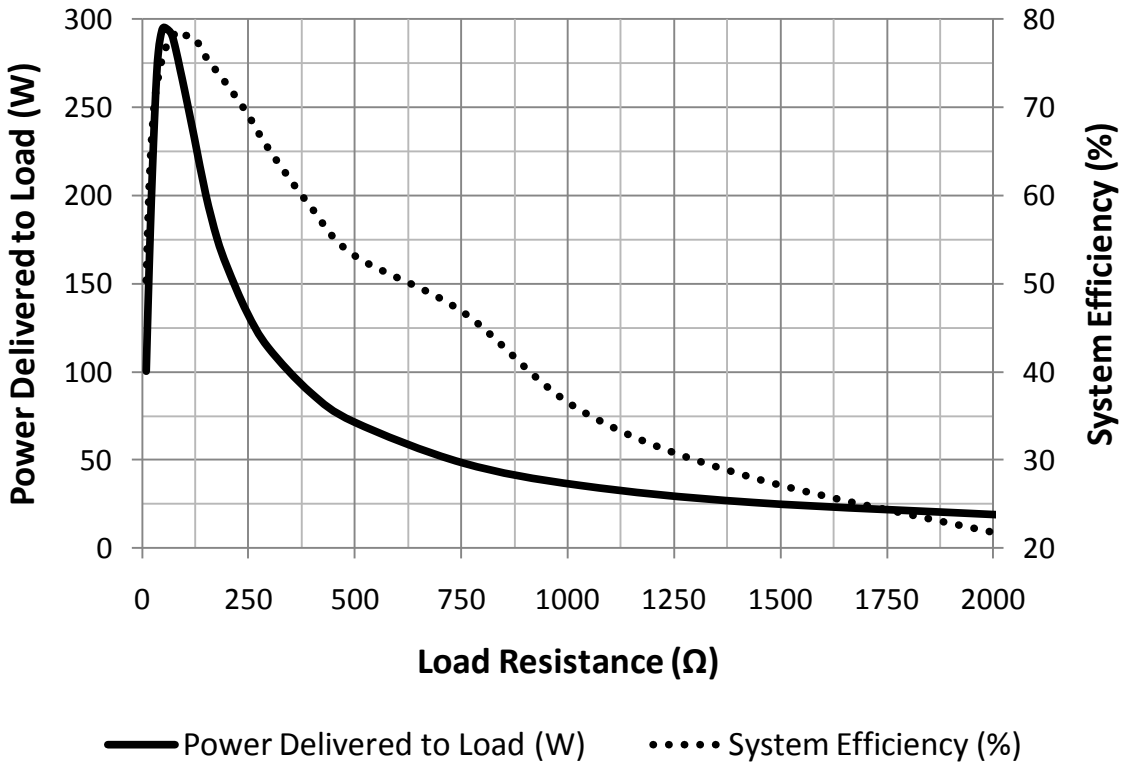

Figure 5-3. Power delivery (left y-axis) and efficiency (right y-axis) of the system versus load resistance. Supply voltage: 120 V.

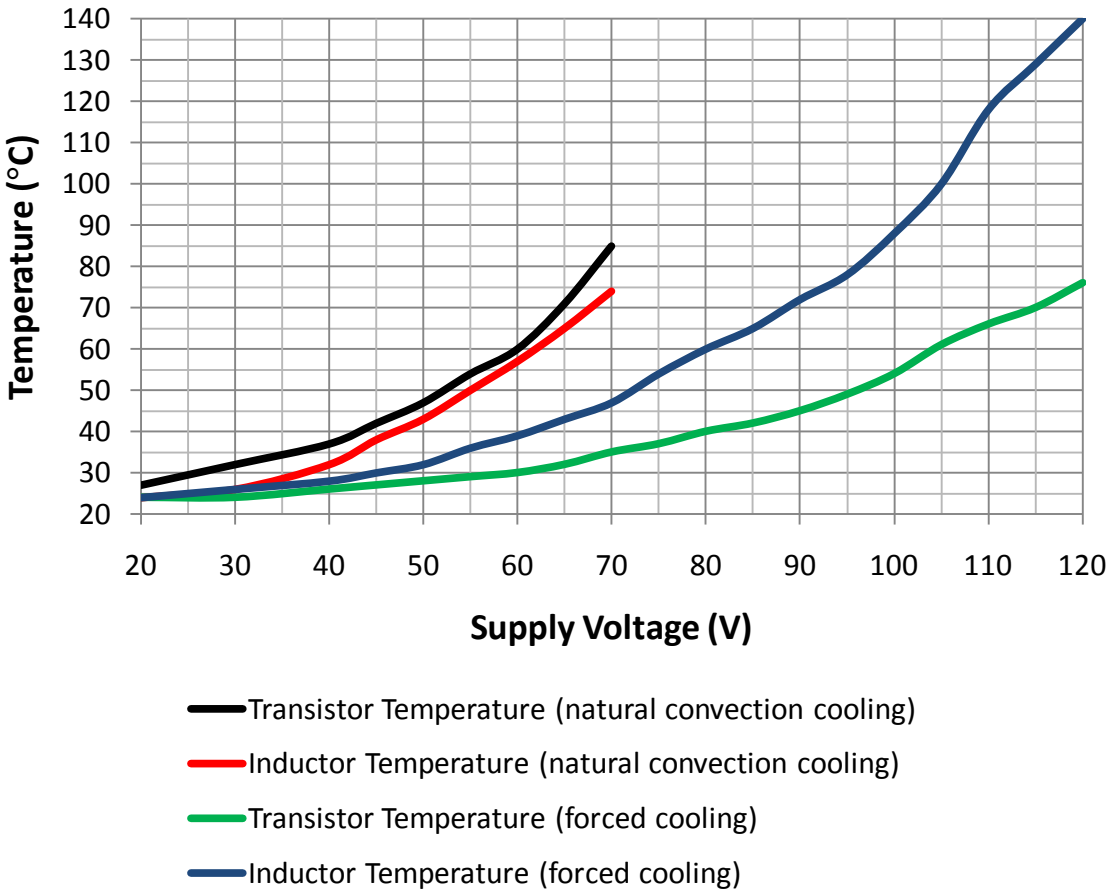

Figure 5-4. Transistor and inductor temperature with natural convection cooling and forced air cooling versus supply voltage.

The transmitter is able to operate under natural convection cooling with up to 95 W of power delivery to the load using a supply voltage of 65 V. Power levels above 95 W requires forced air cooling on the transmitter to keep the temperature of the transistors below 70 ℃. Although most of the loss due to heat occurs at the transistor or inductor, a temperature increase at the inductor is not critical because it is a passive component and more resilient to heat. However, this will cause a drop in inductance value which will decrease the load network phase angle increasing the power delivery slightly. The slight increase in power delivery should be taken care by the receiver's regulator. Temperatures of both the transistor and inductor for natural convection cooling and forced air cooling were measured using the Fluke 62 mini

infrared thermometer at extremely close proximity is shown in Figure 5-4. A 12 V DC dual ball bearing fan of size 90 mm x 90 mm x 25 mm with a speed of 2700 rpm achieving an air flow of 44 cfm is used for forced air cooling (shown in Figure 5-5). Since the power consumption of the fan is only 2.4 W, it can be neglected for the efficiency calculations. In addition, the heat sinks on the transistors further enhance the heat dissipation capabilities. As seen in Figure 5-4, the transistor temperature reaches a practical limit of 75 ℃ for a supply voltage of 120 V. Although higher power can be achieved by increasing the supply voltage using a higher power output power supply, more effective heat dissipation methods are required to prevent the transistors from overheating.

A compact system operating without forced air cooling is often preferred. Therefore, the following measurements based on a supply voltage of 60 V operating under natural convection cooling are presented. Figure 5-6 shows the transmitting coil current and voltage when it is driving a 50 Ω load at the receiver. It can be seen that the current is lagging the voltage. As seen from the drain waveform, ZVS operation is achieved.

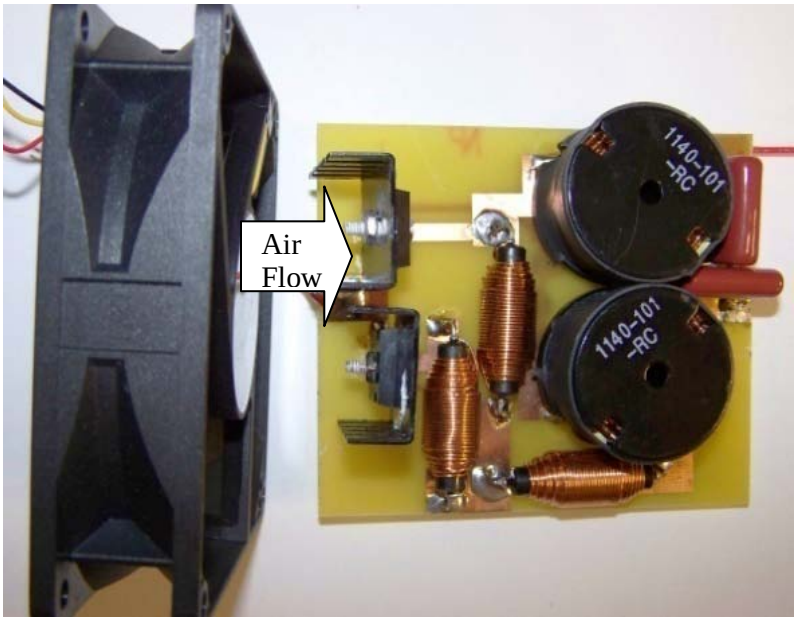

Figure 5-5. Photograph of the dual-channel Class E power amplifier with forced air cooling.

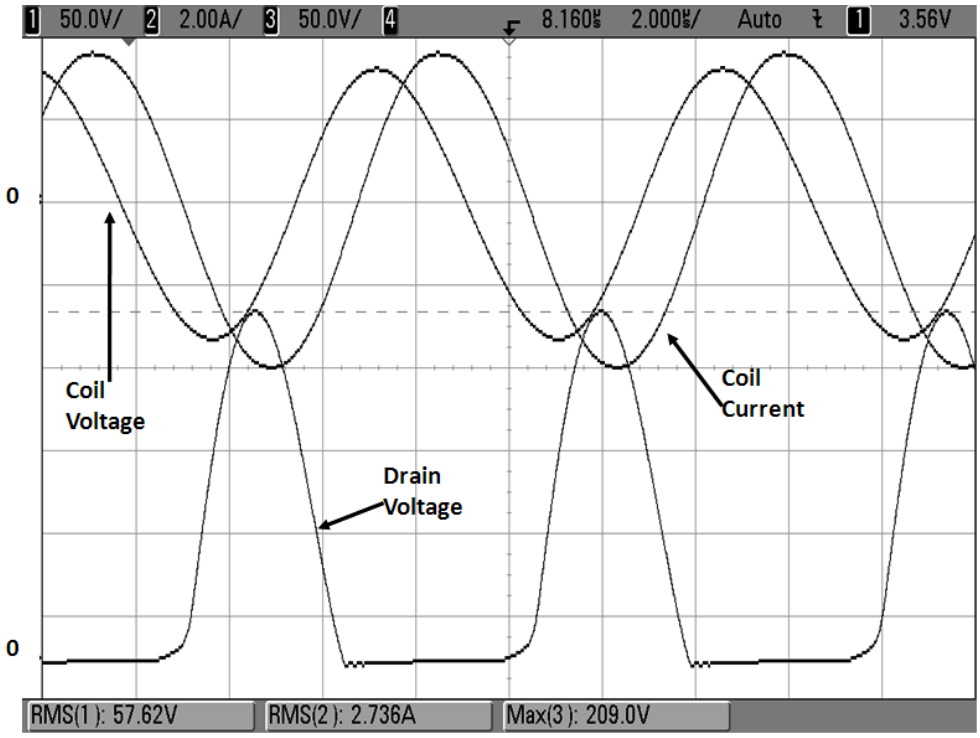

Figure 5-6. Voltage and current waveforms of the Class E transmitter.

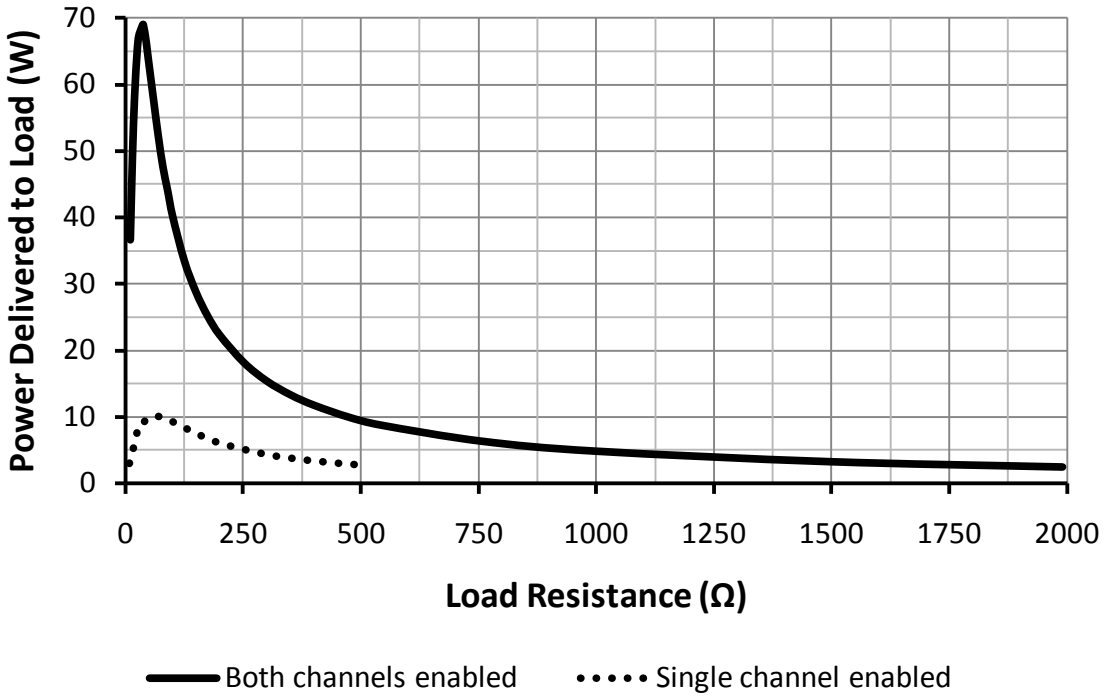

Figure 5-7. Power delivered to load versus load resistance. A maximum power of 69 W occurs approximately at 50 Ω for dual-channel and maximum power of 10 W occurs at approximately at 75 Ω for single-channel. Supply voltage: 60 V.

Figure 5-7 shows the power delivery versus load resistance of both dual-channel (solid line) and single-channel (dotted line) modes. Power delivery for both modes peak at about 50 Ω load resistance, the dual channel mode peak power is close to 70 W while the single channel mode is at 10 W. The system efficiency versus load resistance is shown in Figure 5-9 which verifies that the resistance looking into the network of the transmitting coil in parallel with the shunt capacitor decreases with increasing load resistance. This results in a larger voltage drop across the parasitic resistance of the inductor and a lower efficiency.

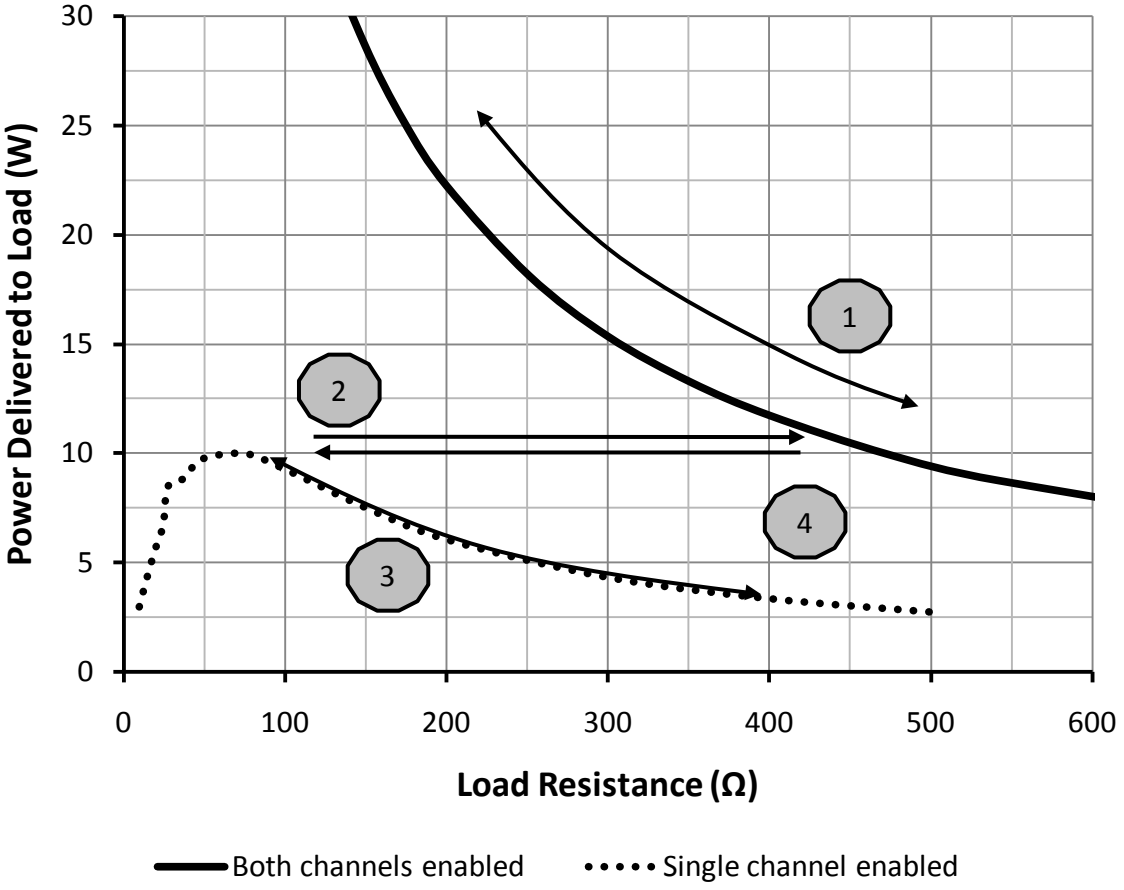

Figure 5-8. Mode-switching operation for optimized efficiency across a wide power delivery range. (1) Dual-channel mode for higher power, (2) Dual-channel mode switch-over to single-channel mode when better efficiency can be obtained at a lower power level, (3) Single-channel mode for lower power, (4) Single-channel mode switch-over to dual-channel mode when higher power delivery is needed. Supply voltage: 60 V.

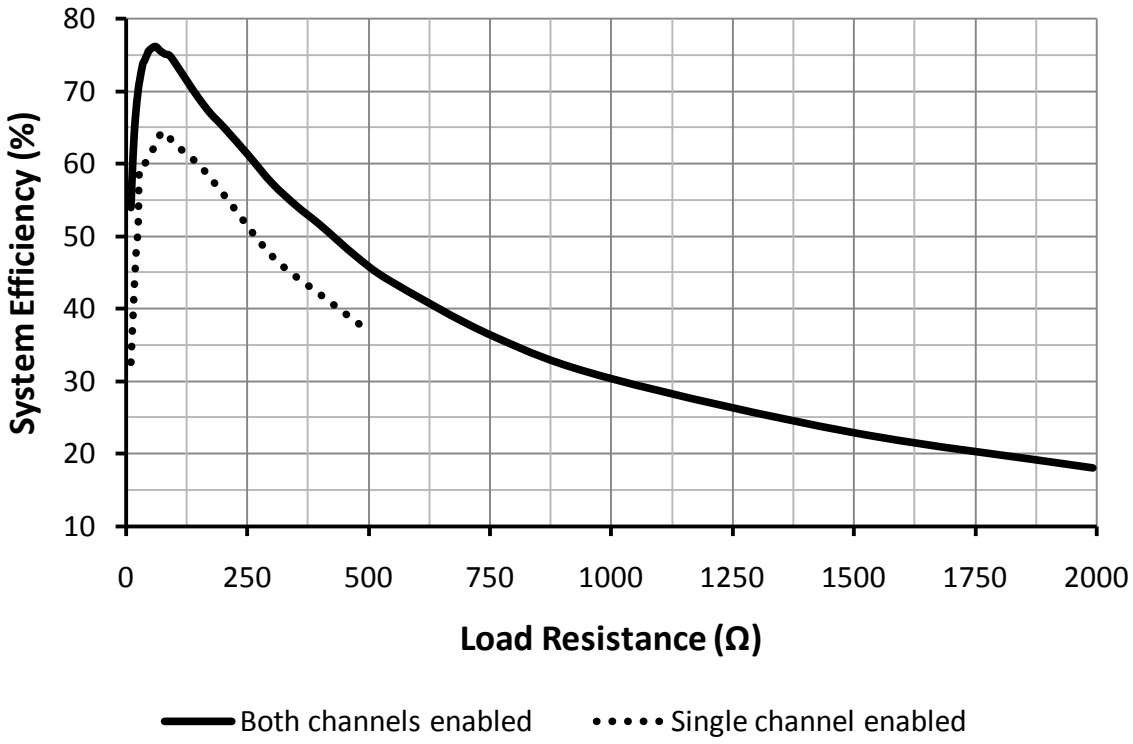

Figure 5-9. System efficiency versus load resistance with a maximum efficiency of 64.5% for a single-channel system, and 76% for a dual-channel system - at approximately 70Ω. Supply voltage: 60 V.

The efficiency of the single-channel mode is approximately 10-15% lower than the efficiency of the dual-channel mode for the same load resistance because the current is flowing through a single L_{out} inductor instead of a pair of them. The parasitic resistance is doubled, thus resulting in lower system and transmitter efficiencies as shown in Figure 5-9 and Figure 5-10 respectively. However, when the system enters light load mode or trickle charge mode, it is desirable to switch to the single-channel mode. It can be seen from Figure 5-11 that the system efficiency is approximately 15% higher than the dual-channel mode for delivering the same amount of power below 10 W. Instead of operating at high load resistance for a dual-channel mode resulting in high receiver DC voltage as shown in Figure 5-13, it is possible to achieve similar power delivery at much lower load resistance for a single-channel mode, resulting in a lower receiver DC voltage and higher system efficiency. In addition, a typical buck regulator has

higher DC-DC efficiency when the input voltage is lower. Therefore, a load detection scheme is required to determine the switch-over point from dual-channel mode to single-channel mode. It can be seen from Figure 5-7 that a power delivery of 10 W occurs at 500Ω load resistance in the dual-channel mode making it a good switch-over point to single-channel mode ((2) in Figure 5-8). It can be seen that a 500Ω load resistance translates to an approximate RMS voltage of 20 V across transmitting coil for the dual-channel mode as shown in Figure 5-12. Likewise, if the power requirement for the single-channel mode is too high, it is required to switch to the dual-channel mode. It can be inferred from Figure 5-7 that the switch-over point to dual-channel mode is approximately 75Ω ((4) in Fig ure 5-8) where the efficiency peaks in single-channel mode, which translates to a RMS coil voltage of 22 V in Figure 5-12.

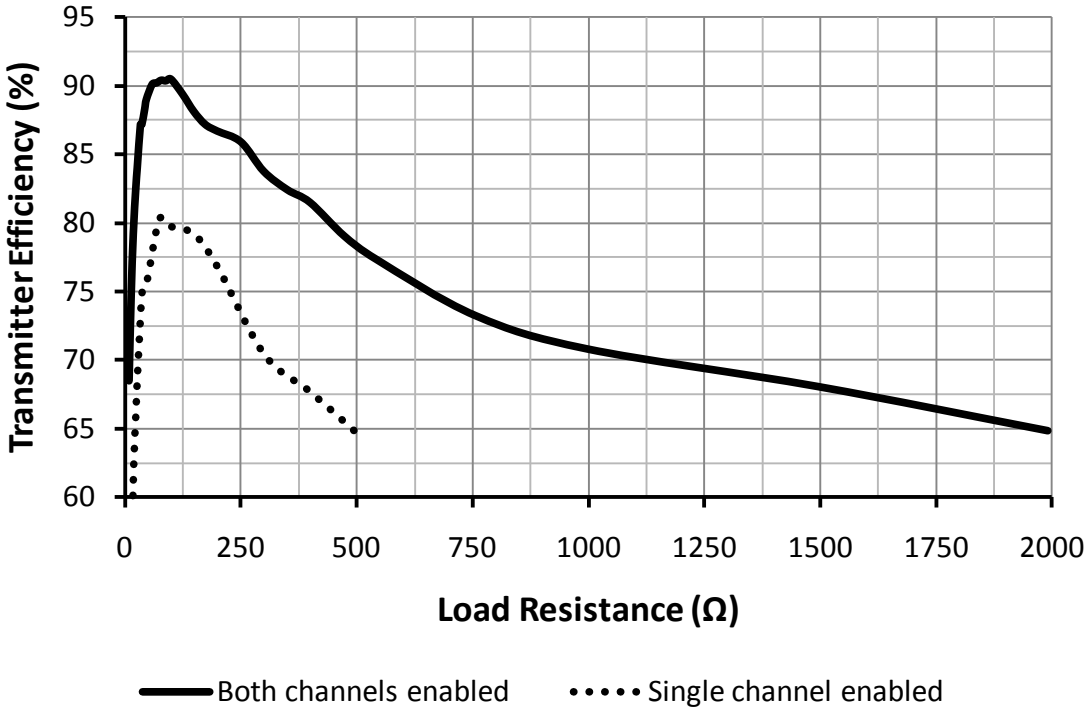

Figure 5-10. Transmitter efficiency versus load resistance. Maximum transmitter efficiency occurs across the range of 60Ω to 100 Ω load resistance at 90% for dual -channel and 79% for single-channel. Supply voltage: 60 V.

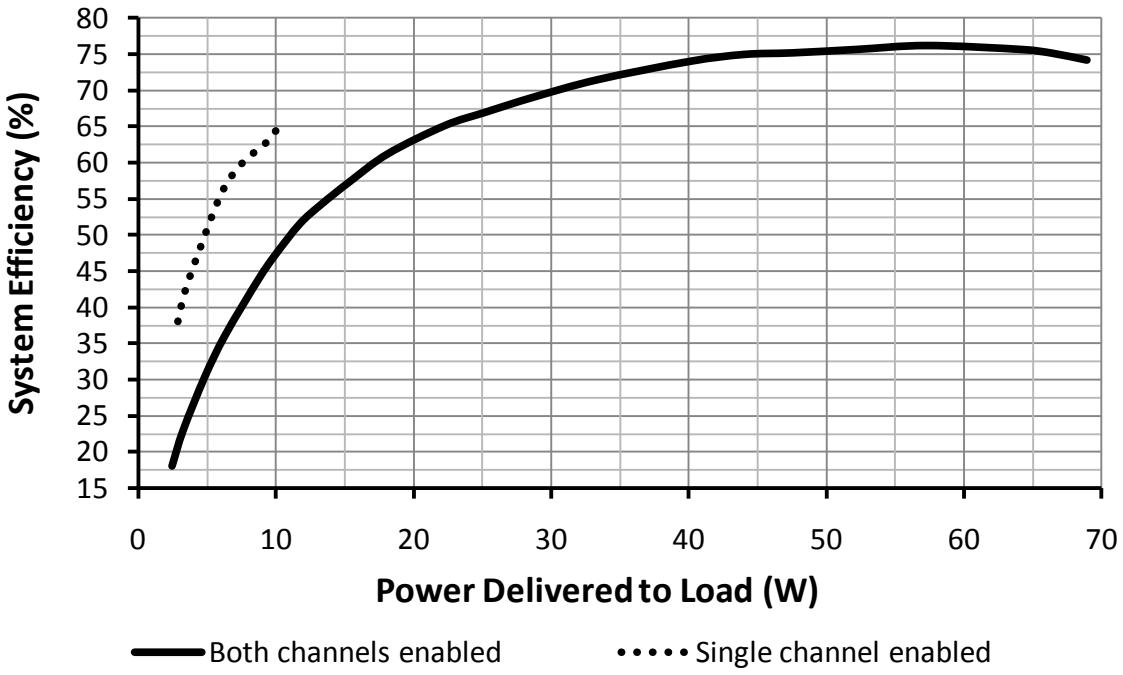

Figure 5-11. System efficiency versus load resistance for single-channel and dual-channel modes achieving high efficiency at high power output. It also illustrates that a single-channel mode is more efficient at low power delivery states. Supply voltage: 60 V.

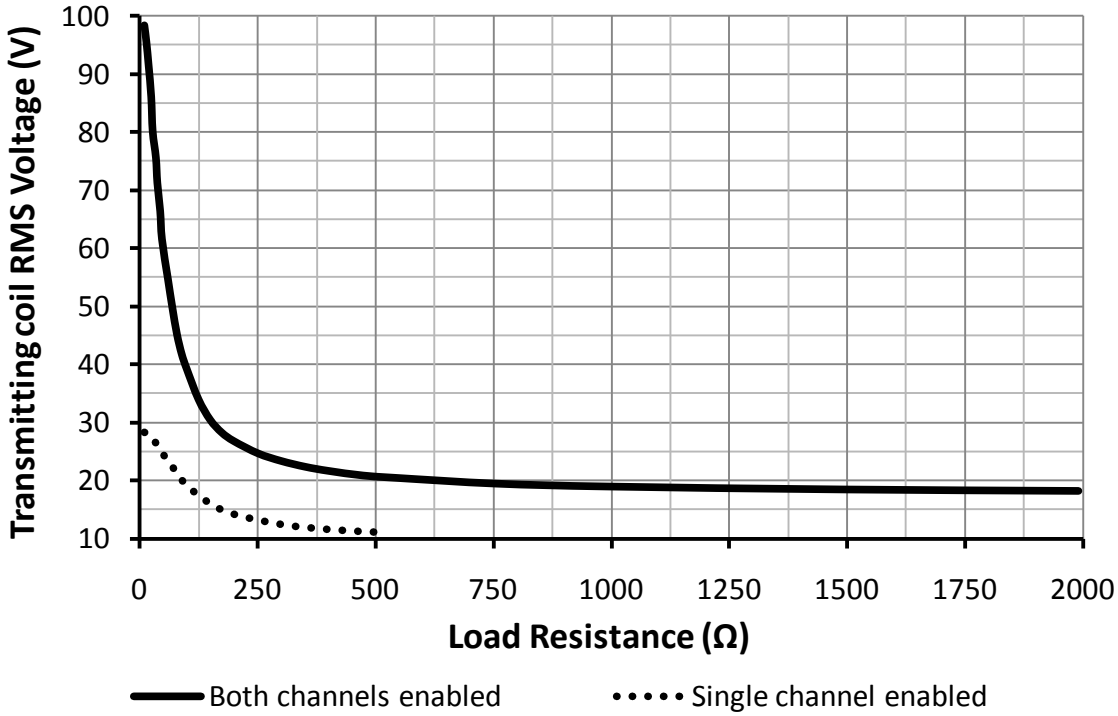

Figure 5-12. Transmitting coil RMS voltage versus load resistance. Supply voltage: 60 V.

Figure 5-13 shows the receiver DC voltage versus load resistance for both the dual-channel mode and the single-channel mode. It can be seen that there is no over voltage issue as the voltage starts to converge to a value of approximately 70 V when the load resistance is high. The receiver open-circuit voltage is 73.4 V and open-circuit power consumption is 10 W in the dual-channel mode. However, during single-channel operation, the receiver open-circuit voltage is only 38.3 V and its open-circuit power consumption is only 4 W which is 6 W less than that of the dual-channel mode. Therefore, it is preferred to perform load detection using the single-channel mode and increase the output power by enabling the dual-channel mode if more power is required to reduce standby power consumption. By controlling the maximum receiver DC voltage, the requirement for the receiver's regulator is relaxed enabling the system designer a wider range of selection.

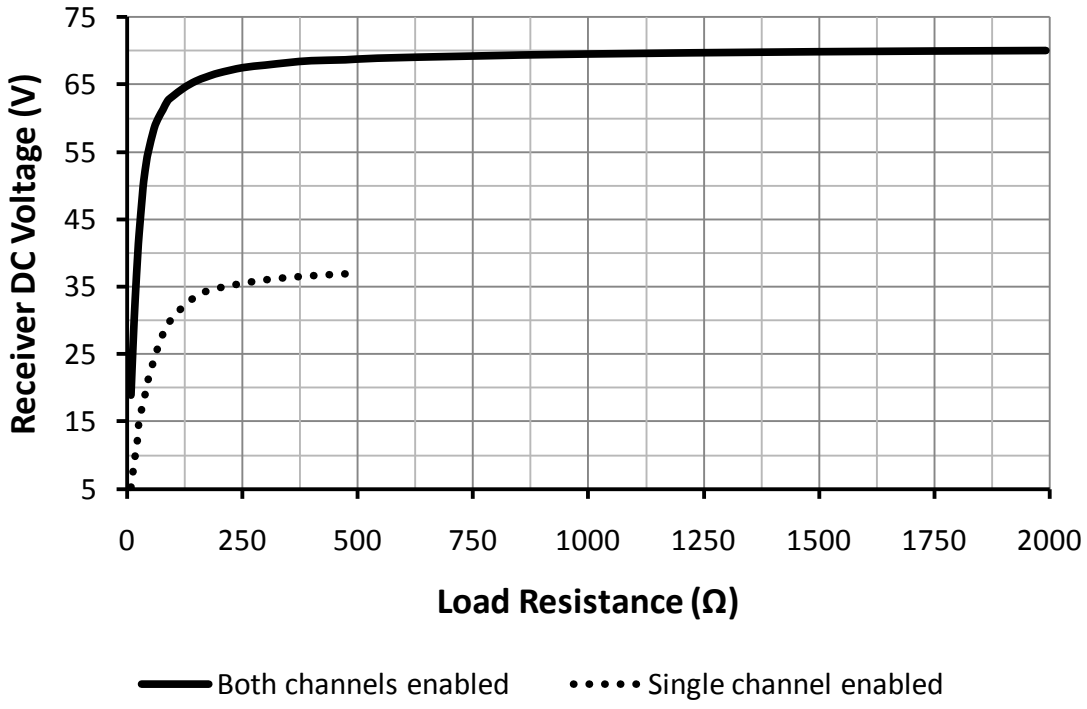

Figure 5-13. Receiver DC voltage versus load resistance, converging to approximately 70 V in dual-channel mode and 38 V in single-channel mode. Supply voltage: 60 V.

5.2 Low Power Multiple Receivers System with decoupling Switch using Series-Parallel Impedance Transformation Network Topology

The Class E transmitter test system operating at 240 kHz was fabricated using the IRLR/U3410 power MOSFET. A 13-turn 20 cm x 20 cm transmitting coil which was described in the design rules and two 6-turn 9 cm x 6 cm receiving coils were used. The platform is capable of simultaneously charging up to four independent devices. Although it is possible to extend the experiment to more than two receivers, for better understanding of the system response and easier analysis, experiments of charging two receivers were conducted. A Matlab code was also written based on the equations derived in [18]-[19] to study the efficiency and power delivery. All measurements and simulation results are based on a 12V power supply. The 12V power supply is selected because the supply voltage is readily available from the DC supply plugs in vehicles and several other AC-DC converters.

Table 5-2 shows the value of each component used in the experiment. Component values are selected by matching the closest available component value and further tuned to achieve optimum performance. C_{rx} is selected to be 75 nF. Since the switch contributes 3.5 nF of capacitance and the rectifier contributes another 3.5 nF of capacitance, a 68 nF capacitor is used to achieve an effective capacitance of 75nF. Capacitance contributed to the receiver due to the switch and rectifier is measured using the HP4192A LF Impedance Analyzer in small signal operation. Therefore, the actual capacitance under large signal operation will be slightly different depending on the load conditions and voltage at the switch and rectifier. In order to reduce losses and heat through the parasitic resistance of the capacitors, low loss polypropylene capacitors are used. Alternatively, C0G/NP0 surface mount capacitors can be used as well. However, they are physically small and tend to heat up faster than the larger leaded polypropylene capacitors making them not suitable for high power applications.

Table 5-2. Component Values for Low Power Multiple Receivers System with decoupling Switch using Series-Parallel Impedance Transformation Network Topology

	Calculated	Experimental	% Variation
C_{rx}	73nF	75nF	+2.7%
C_{out}	8nF	9.4nF	+17.5%
L_{out}	9.5µH	9.5µH	0%
L_{out} parasitic resistance	-	0.16Ω	-
C_{shunt}	10nF	12nF	+20%
TX coil inductance	-	45.3µH	-
TX coil dimension	-	20cm x 20cm	-
TX coil parasitic resistance	-	0.5Ω	-
RX coil Inductance	-	5.2µH	-
RX coil dimension	-	9cm x 6cm	
RX coil parasitic resistance	-	0.1Ω	-
Mutual Inductance	-	2.8 µH	-
Coupling Coefficient	-	0.182	-
L_{DC}	-	500 µH	-

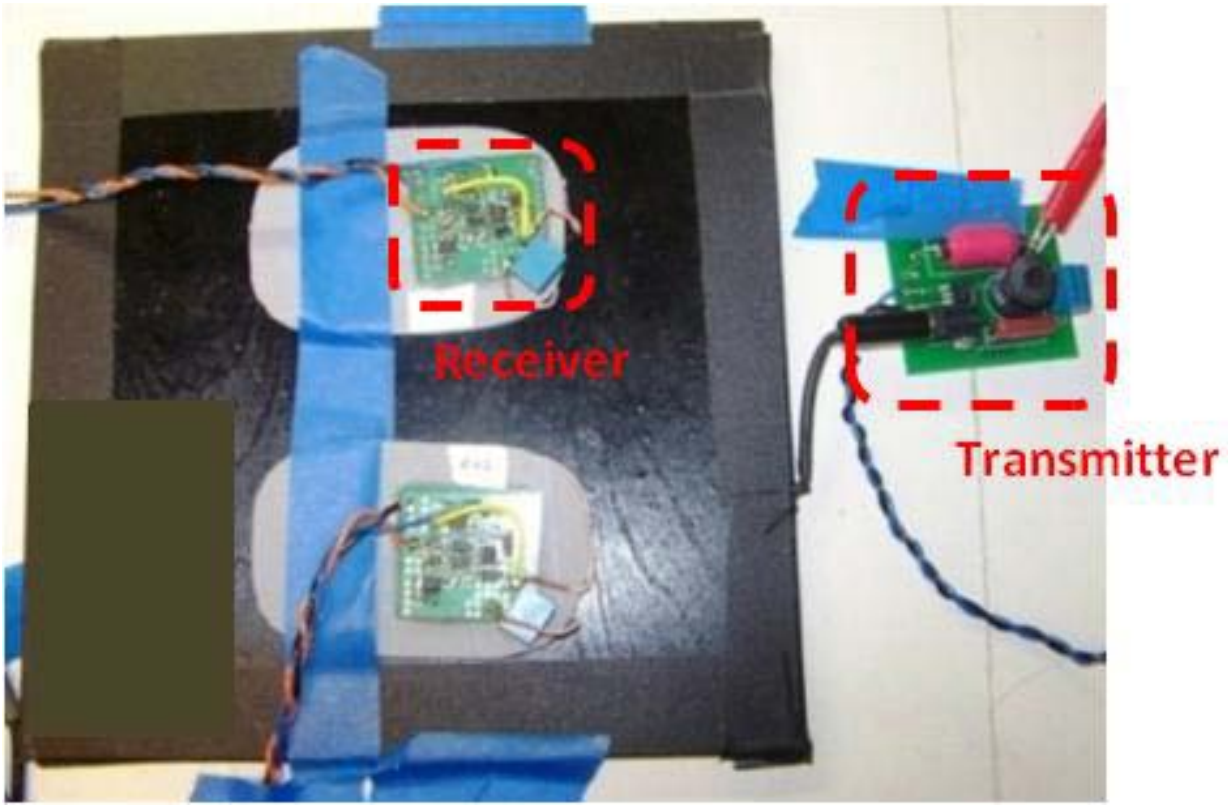

Figure 5-14. Photograph of a test setup with two receivers with decoupling switch on the packaged transmitting coil.

Figure 5-14 shows the photograph of the test setup with two receivers on the packaged transmitting coil. The vertical separation between the transmitting coil and receiving coils is about 2 mm. The locations of receivers on the transmitting coil were fixed by the blue tapes to ensure the same conditions for all measurements.

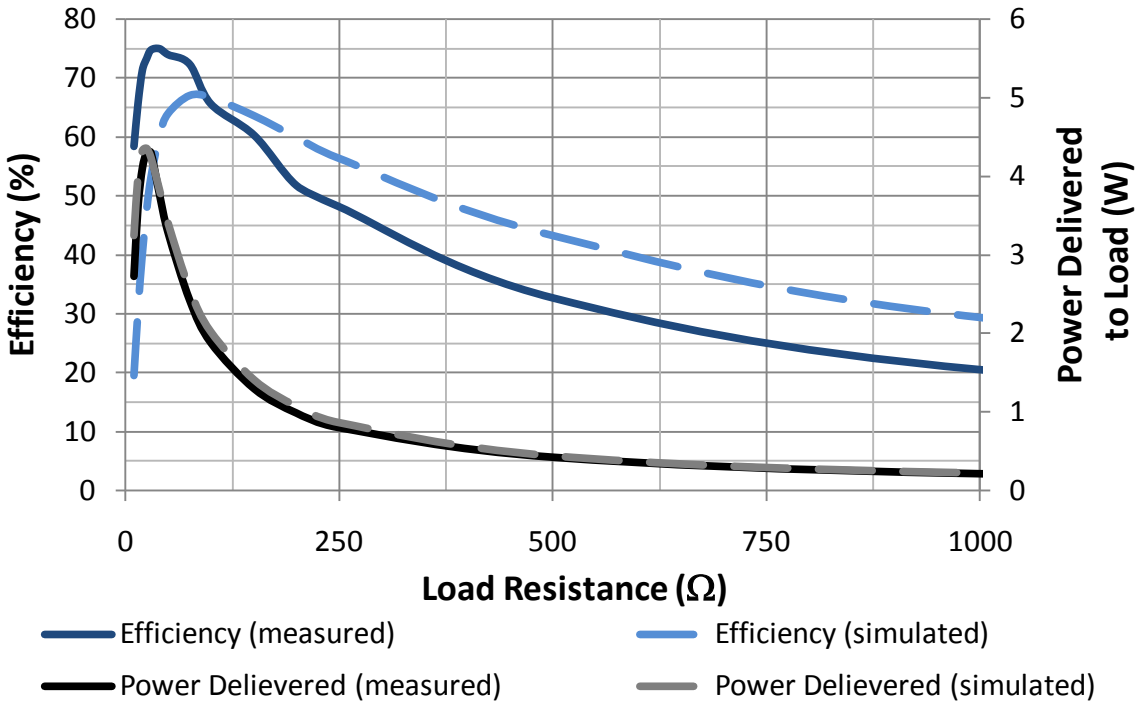

Figure 5-15. Power delivery to the receiver with switch and system efficiency versus load resistance for a one-to-one setup (simulated and measured)

Comparison of power delivery to the receiver and system efficiency versus load resistance of a one-to-one setup between the simulated results and the experimental results is shown in Figure 5-15. Measurements are conducted by connecting the receiver to a rheostat for which the resistance is varied manually in predetermined steps. The simulation and measured trend of a single receiver setup agree well with peak measured power at around 4.75 W. There is a slight discrepancy between the measured and simulated efficiencies because the transistor and DC feed inductor are assumed to be ideal in the simulation model. In addition, the effect of the build in

body diode of the transistor is also not taken into consideration. The assumption affects the calculated supply current and the calculated efficiency. Power delivery is not affected because it depends on Z_{tx} rather than the transistor during nominal operation. A comprehensive plot presenting the performance of the system in Figure 5-16 shows the system efficiency versus power delivery.

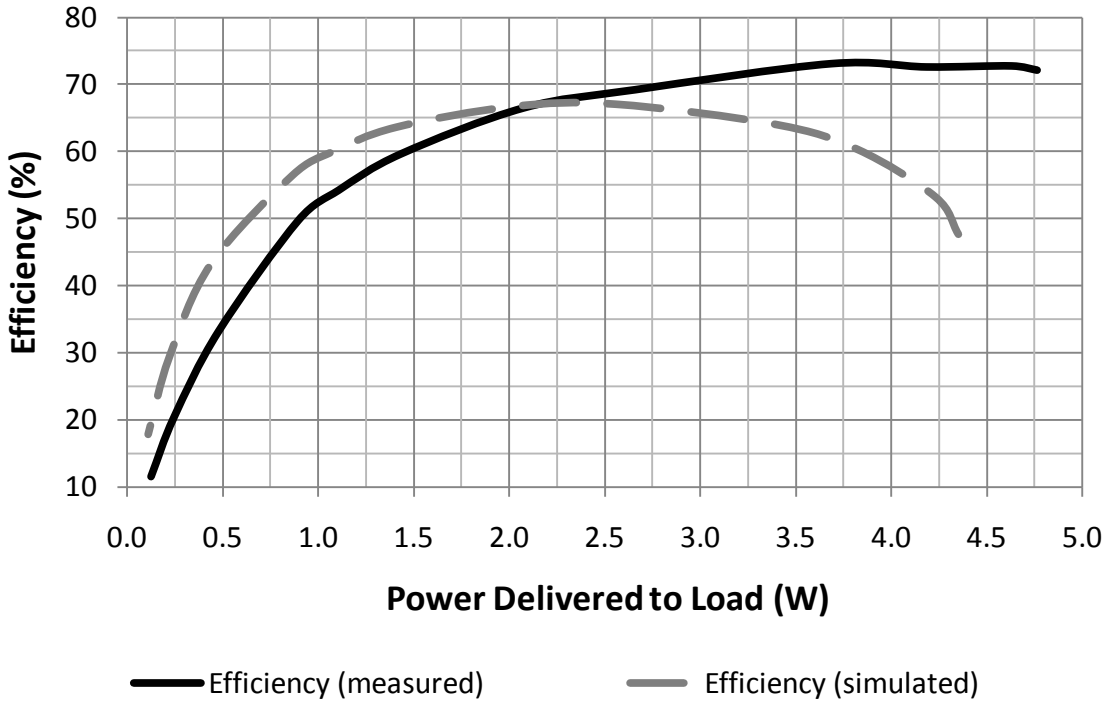

Figure 5-16. Efficiency of power delivery to the receiver with switch versus power delivered for a 1 to 1 setup (simulated and measured)

Figure 5-17 compares the performance of the receiver with and without the switch with power delivery capabilities of both receivers are nearly the same. They peak at around 4.75 W with the efficiency of the receiver with switch slightly lowered by 1 to 2%. The impact of the switch in the receiving mode is minimal because it is in shunt with the receiver. In addition, it can be concluded that the leakage through the switch is negligible. Figure 5-18 compares the performance of a single receiver with the decoupling switch architecture and dual-receiver setup with one of the receivers decoupled from the transmitter. The efficiency degrades by an average

of 5% and no more than 10% overall even though the second receiver is turned off. Although the receiver is decoupled from the system, the switch circuitry still has some turn-on resistance when it attempts to short the receiving coil. Therefore, a small amount of power is still dissipated across the switch.

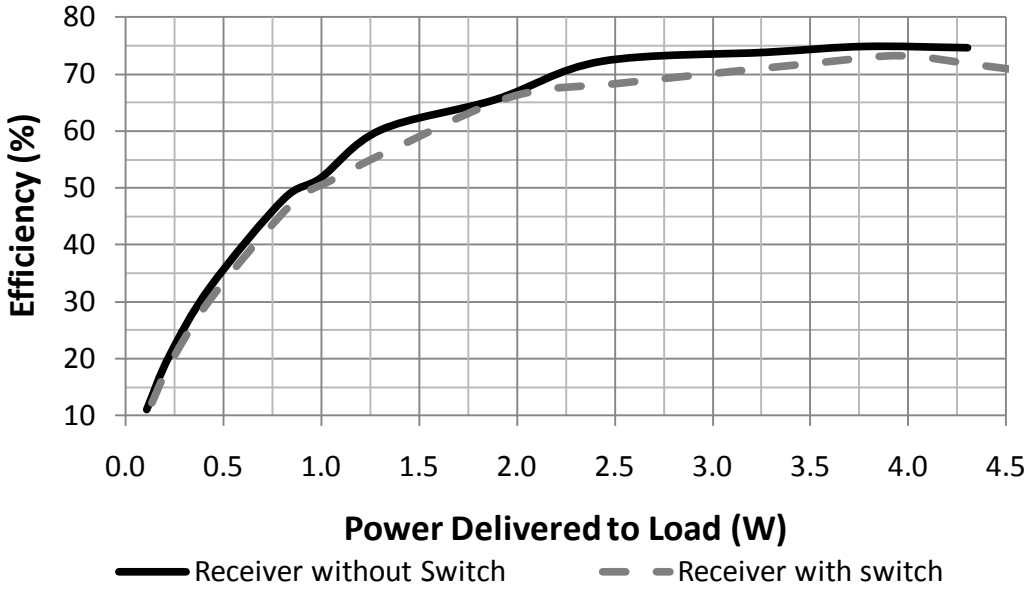

Figure 5-17. Comparison between receiver with switch and receiver without switch.

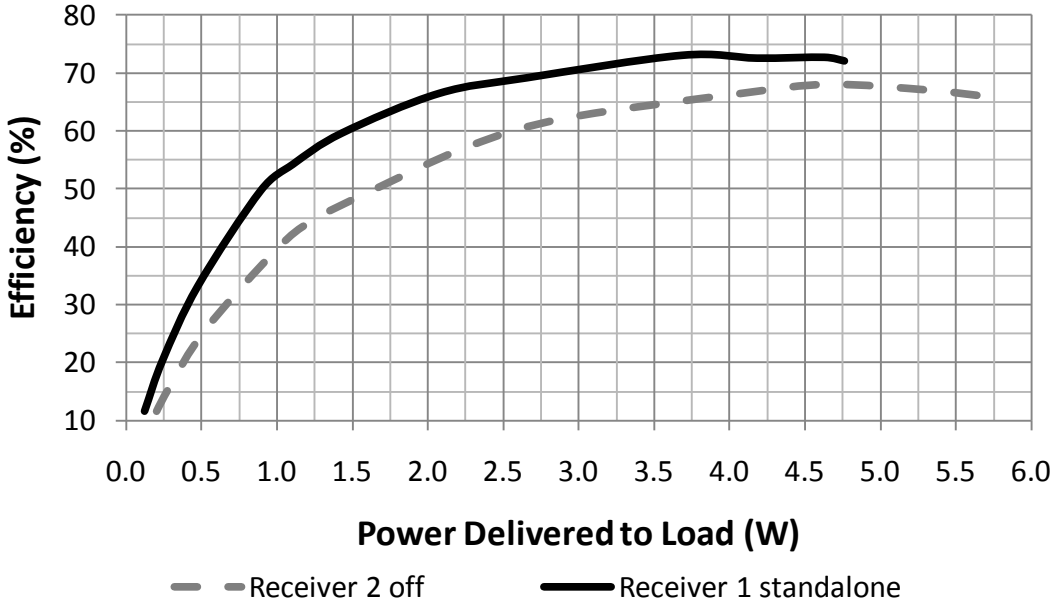

Figure 5-18. Comparison between single receiver standalone and dual-receiver setup with one receiver switched off.

To study the power delivery of a dual-receiver platform, the load resistance of one of the receivers (receiver 2) is fixed while the load resistance of the other receiver (receiver 1) is swept across the range of 10Ω to 2000 Ω in 15 discrete steps (10 Ω, 15 Ω, 20 Ω, 25 Ω, 30 Ω, 40 Ω, 50 Ω, 75 Ω, 100 Ω, 150 Ω, 200 Ω, 250 Ω, 500 Ω, 1000 Ω and 2000 Ω) in an experiment using the same method for the single receiver measurement. Figure 5-19 shows the power delivery to the receiver 1 versus its load resistance at different receiver 2 load resistance values, while Figure 5-20 shows the power delivery to receiver 2 versus receiver 1 load resistance at different fixed receiver 2 load resistance values. When the load resistance of receiver 2 is kept above 50 Ω, the variation of power delivery to receiver 1 due to receiver 2 is limited, but peak power drops to around 2.5 W. In addition, power delivery to receiver 2 also stays consistent regardless of the load resistance or power delivery to receiver 1, as long as the load resistance of receiver 1 stays above 50 Ω. To reduce the dependency of the receivers on each other due to a single driving coil, the minimum load resistance should be greater than 50 Ω. However, this will result in a reduction of maximum power delivered to the load by the system. The dependency of the receivers is due to the collective impedance looking into the transmitting coil due to the multiple receivers and not the mutual inductance between the receiving coils. The minimum load resistance can be designed by selecting an appropriate receiver regulator and setting the appropriate power delivery profile by changing C_{tx}, or the supply voltage. This will set the unregulated input voltage before the regulator to achieve the specified load resistance looking into the regulator while at its maximum power delivery condition so that the load resistance will not fall below minimum value mitigating the power choking effect. The experimental verification and analysis is limited to two receivers but similar trends are expected for multiple receivers of three or more.

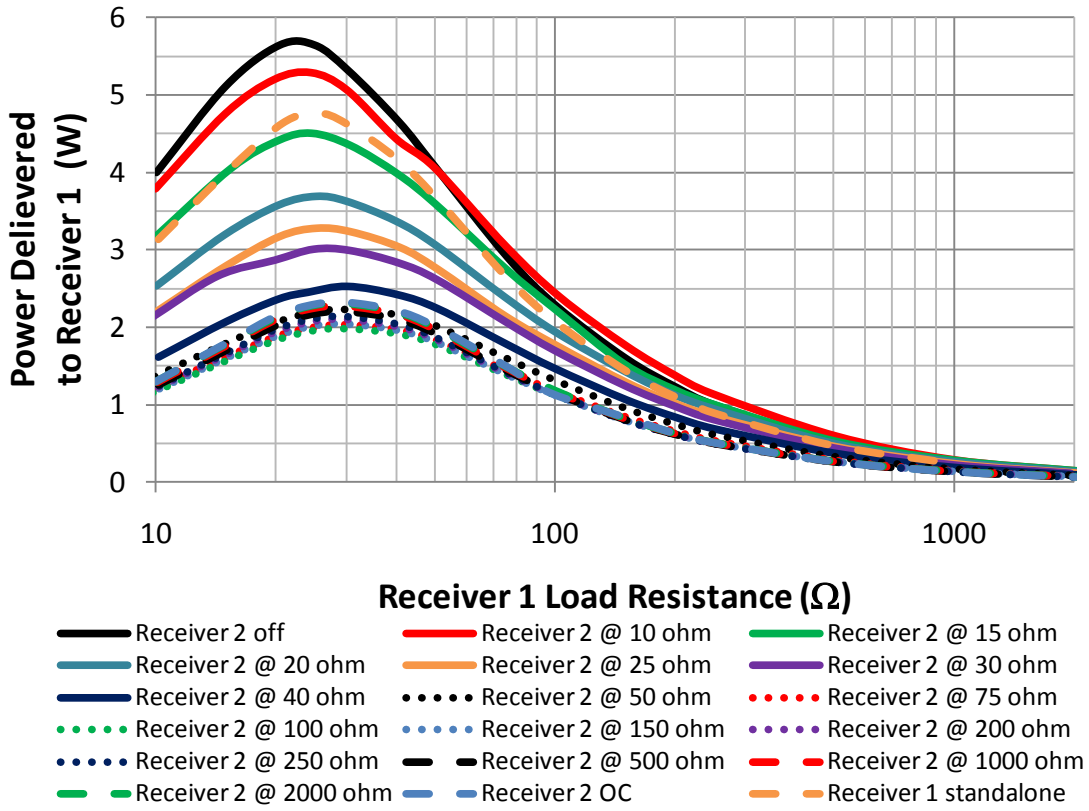

Figure 5-19. Power delivery to receiver 1 versus its load resistance at different fixed receiver 2 load resistance.

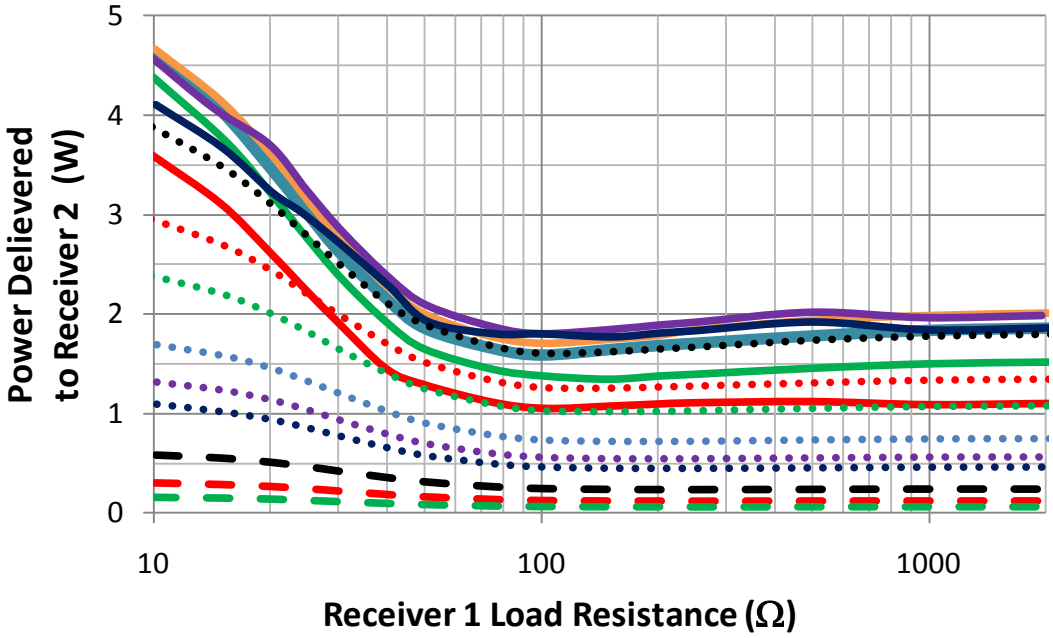

Figure 5-20. Power delivery to receiver 2 versus receiver 1 load resistance at different fixed receiver 2 load resistance. (same legends as in Figure 5-19)

Once the fully charged receiver (receiver 2) is decoupled from the system using the switch circuit, power delivery to the other receiver (receiver 1) increases significantly. Therefore, the switch circuit can be used to prevent the receiver that is fully charged to "choke" the other receiver of the power it requires. This will mitigate the effect of reduced charge rate for the receiving devices so that the system will be able to deliver sufficient power to the receiver.

Figure 5-21 shows the system efficiency versus total power delivered to the loads with receiver 2 fixed at a specific load resistance while sweeping the resistance of receiver 1 from 10Ω to 2000Ω. System efficiency is above 55% for power delivery above 2 W. Although the efficiency starts to degrade significantly at lower power delivery, the absolute system power loss is low. Therefore, no heating issues were observed during the experiment. All components were operating below 36°C.

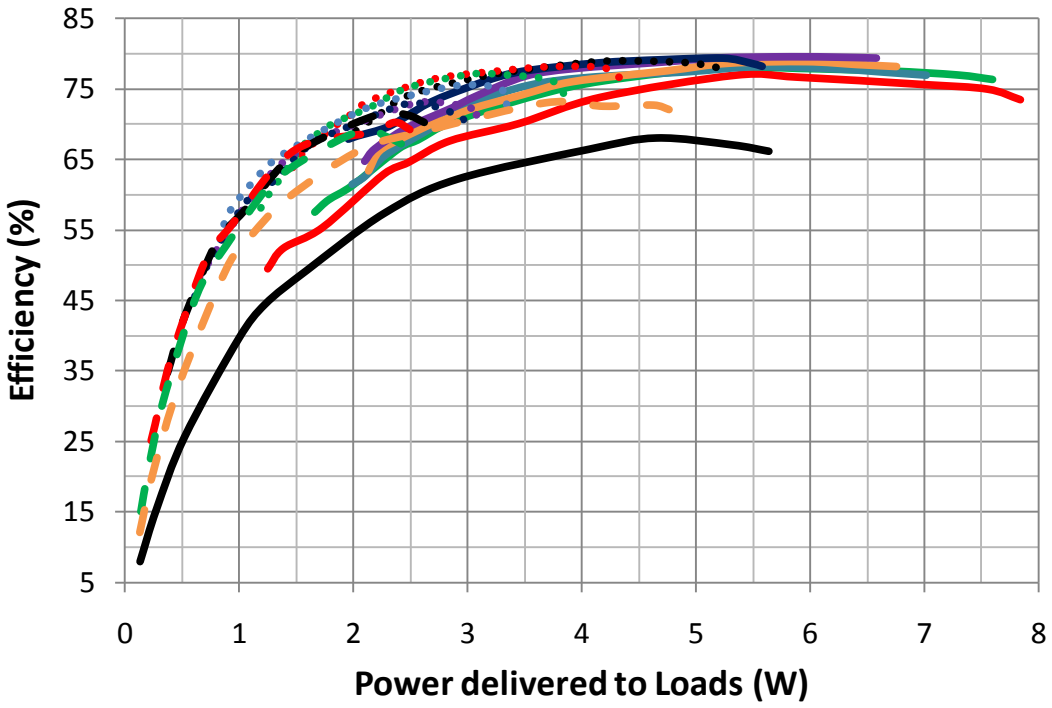

Figure 5-21. System efficiency versus total power delivery to both receivers with the load resistance of receiver 2 fixed and the load resistance of receiver 1 swept across the stated range for a dual-receiver test bench. (same legends as in Figure 5-19)

Figure 5-22 shows the measured power delivery space of receiver 1 and receiver 2. Under all loading conditions the guaranteed power delivery is approximately 2W. The guaranteed power delivery can also be observed in Figure 5-19 and Figure 5-20 in another form as discussed previously. Therefore, the system is capable of delivering 2W of power under all conditions which is close to the specified power delivery of 2.5W in the design. Higher power delivery can be achieved by reducing the capacitance of C_{tx} slightly or by increasing the supply voltage. Care must be taken during reduction of C_{tx} to keep the phase of Z_{tx} within the high efficiency/low loss operation above 40°.

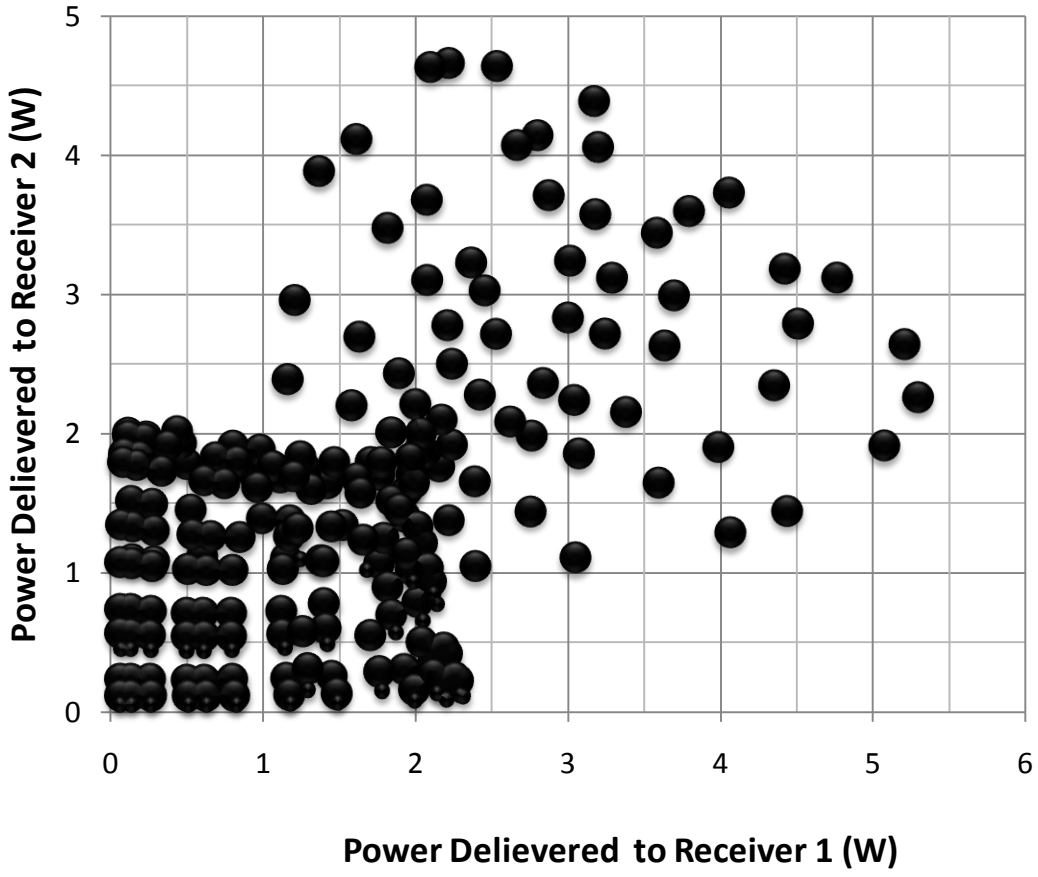

Figure 5-22. Measured power delivery to a dual-receiver system with load resistance varied from 10Ω to 2000Ω.

CHAPTER 6
INTEROPERABILITY BETWEEN DIFFERENT PLATFORMS (COIL SIZES)

The design rules of the wireless power system are presented in Chapter 3. They are further verified with experimental results in Chapter 5. However, the presented design rules and results only verify the operation of a specific one to one device pairing between the transmitting coil and receiving coil. This does not include operation between another pair of coils of different sizes and might result in a cross platform interoperability issue. It might not be a critical problem if power delivery is insufficient, but it will be a major problem if it results in damaging the receiver. For a practical system, it is expected that the same transmitter for a certain cell phone/device to be able to work for all other different cell phones/device which might have a different receiving coil size due to its physical dimensions. In addition, it will be desirable if the cell phone's transmitter is be able to transfer power to a smaller device which requires less power such as an mp3 player or a Bluetooth headset. As companies start to expand their product lines or try to differentiate from one another, there will be transmitters with different sized transmitting coils. Therefore, it is critical to ensure there is some level of interoperability between the different platforms. Without interoperability between the different platforms, the consumer will be forced to purchase a different transmitter for each of the product he or she owns, not achieving the purpose of a universal charging platform to reduce power consumption and wastage. Regardless of providing sufficient power to drive the receiver, the transmitter should not damage the receiver via overvoltage at the input of the receiver's voltage regulator. The interoperability can be further enhanced by creating a wireless power standards body to regulate the different systems. A wireless power consortium is being set up by Phillips in December 2008 but has yet to gain sufficient momentum to ensure some form of interoperability between different products and platforms.

6.1 Test Bench Setup

The interoperability study is performed by using three different sets of transmitting and receiving coils with components selected using the series-parallel topology design rules in Chapter 3. Transmitter and receiver units are then interchanged between the respective platform without changing any component or automatic tuning to study the interoperability of the system. Table 6-1 shows the sizes of the different pairs of coils and their respective components values, for consistency a L_{out} of 10 µH is used for all the platforms. C_{rx} being in shunt with the receiving coil gets smaller with the increase of receiving coil size as the self inductance of the receiving coil increases. C_{out} which is in series with the transmitting coil gets smaller when the transmitting coil increases in size as the self inductance of the transmitting coil increases. This is because more negative reactance is required to offset the increase in self inductance of the transmitting coil. Since the Z_{tx} for all 3 cases are designed to be relatively close to each other, C_{shunt} is kept the same for all three different platforms.

Table 6-1. Specification of the three different platforms

	Value
Small platform	
Transmitting coil size	11 cm x 8 cm (88 cm^2)
Receiving coil size	5 cm x 4 cm (20 cm^2)
C_{rx}	103.3 nF
C_{out}	27 nF
C_{shunt}	15 nF
Medium platform	
Transmitting coil size	16 cm x 16 cm (256 cm^2)
Receiving coil size	6 cm x 5.5 cm (33 cm^2)
C_{rx}	94.7 nF
C_{out}	10 nF
C_{shunt}	15 nF
Big platform	
Transmitting coil size	20 cm x 20 cm (400 cm^2)
Receiving coil size	9 cm x 6 cm (54 cm^2)
C_{rx}	68 nF
C_{out}	9 nF
C_{shunt}	15 nF

Table 6-2. Coupling parameters of nine possible combinations with first three as intended pairs

TX Size	RX Size	L1 (µH)	L2 (µH)	M (µH)	K	Size Ratio
Small	Small	10.96	3.70	2.21	0.347	4
Medium	Medium	40.53	4.10	2.28	0.176	8
Big	Big	46.00	5.45	2.81	0.178	7
Small	Medium	10.96	4.10	3.05	0.455	3
Small	Big	10.96	5.45	4.66	0.603	2
Medium	Small	40.53	3.70	1.65	0.135	13
Medium	Big	40.53	5.45	3.45	0.232	5
Big	Small	46.00	3.70	1.37	0.105	20
Big	Medium	46.00	4.10	1.88	0.137	12

With three different platforms, it is possible to come up with nine possible combinations as shown in Table 6-2. The original pairs of the transmitting and receiving coils for the three platforms designed using the design rules in Chapter 3 are shown as the first three rows. From Equation 2-40, it can be inferred that the self inductance of the receiving coil is compensated by C_{rx} and has little effect on the coupling between the coils when they are swapped between each other. By looking at the real part of Equation 2-6, it is independent of the transmitting coil's self inductance. Since most of the effects of the receiving coil's self inductance is being compensated by C_{rx} the power transfer is more dependent on the mutual inductance between the pair of transmitting and receiving coils used. Similar analysis can be used for the imaginary part of Z_{tx} as C_{out} is used to cancel out most of the effects of self inductance of the transmitting coil. Other than the setup with a small transmitting coil and a big transmitting coil, the mutual inductances between the transmitting and receiving coil are kept to around 2 µH. Once the appropriate capacitor and inductor values are selected via the design rule presented in Chapter 3, the Class E transmitter is rather robust under most loading conditions. No control mechanism is required to achieve correct power delivery trend and high efficiency. The variation of mutual inductance should be acceptable to still maintain relatively high efficiency power transfer with the correct power delivery trend with respect to load resistance.

6.2 Experimental Verification

Using the nine different combinations of the three platforms on a one transmitter to one receiver setup, nine different data sets were collected. The supply voltage is selected to be 12 V but the analysis should be independent of the supply voltage. For this experiment, the setups should be able to deliver at least 5 W of power and a receiver voltage of not more than 25 V and not less than 8 V for nominal operation of the voltage regulator to achieve a 5 V regulated output. The results are described using the notation of transmitting coil size as the first word and the receiving coil size as the second word. Therefore, it means that a small sized receiving coil is being placed on top of a medium sized transmitting coil for the notation “medium small”.

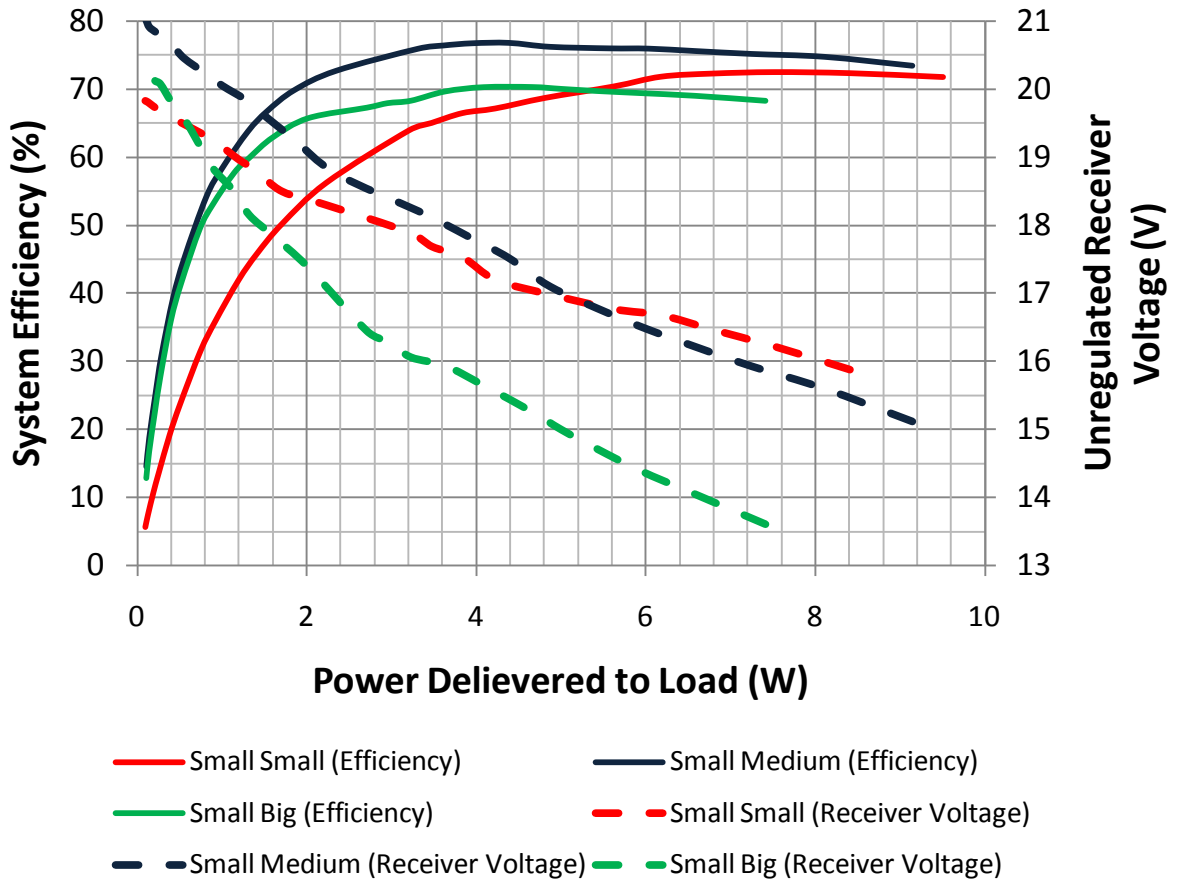

Figure 6-1. System efficiency and receiver voltage vs. power delivery plot for different sized receiving coil on a small sized transmitting coil.

The results are presented in three different graphs each for a different transmitting coil size. All results using the small receiving coil are presented in red, medium receiving coil are presented in blue and big receiving coil are presented in green. Dashed lines are used for the unregulated receiver voltage (right axis) while solid lines are used for system efficiency excluding the voltage regulator (left axis).

Figure 6-1 shows the experimental results of three different sized coils being placed on a transmitter with a small transmitting coil. When a larger receiving coil is placed on top of the small transmitting coil the real part of Z_{tx} becomes larger, reducing the losses through the transmitting coil's parasitic resistance and L_{out}'s parasitic resistance. Therefore, the setup for "small medium" is more efficient than "small small". However, when the real part of Z_{tx} becomes too large due to high mutual inductance between the coils (4.66 µH for "small big" setup), the phase angle of Z_{tx} becomes too low that the class E transmitter. Therefore, the class E transmitter is working at the borderline case of ZVS/ZDS with increased losses at the transmitter across the switching transistor. This occurs when the green efficiency line starts to deviate from the blue line with increase in power delivery (decreasing in phase angle) at approximately 1 W power level. However, the efficiency is still acceptable and no significant heating issue is observed. The receiver voltage under a specific loading condition is kept approximately the same for all three cases with the maximum unregulated receiver voltage at slightly less than 21 V and the minimum unregulated receiver voltage above 13 V, no over-voltage was observed. The lower unregulated receiver voltage for the "small big" setup is due to the same reason for the lower efficiency phenomena as more power is being dissipated at the transmitter than transmitted to the receiver as useful power. All three setups are able to achieve at least the stated 5 W of power delivery to the receiver.

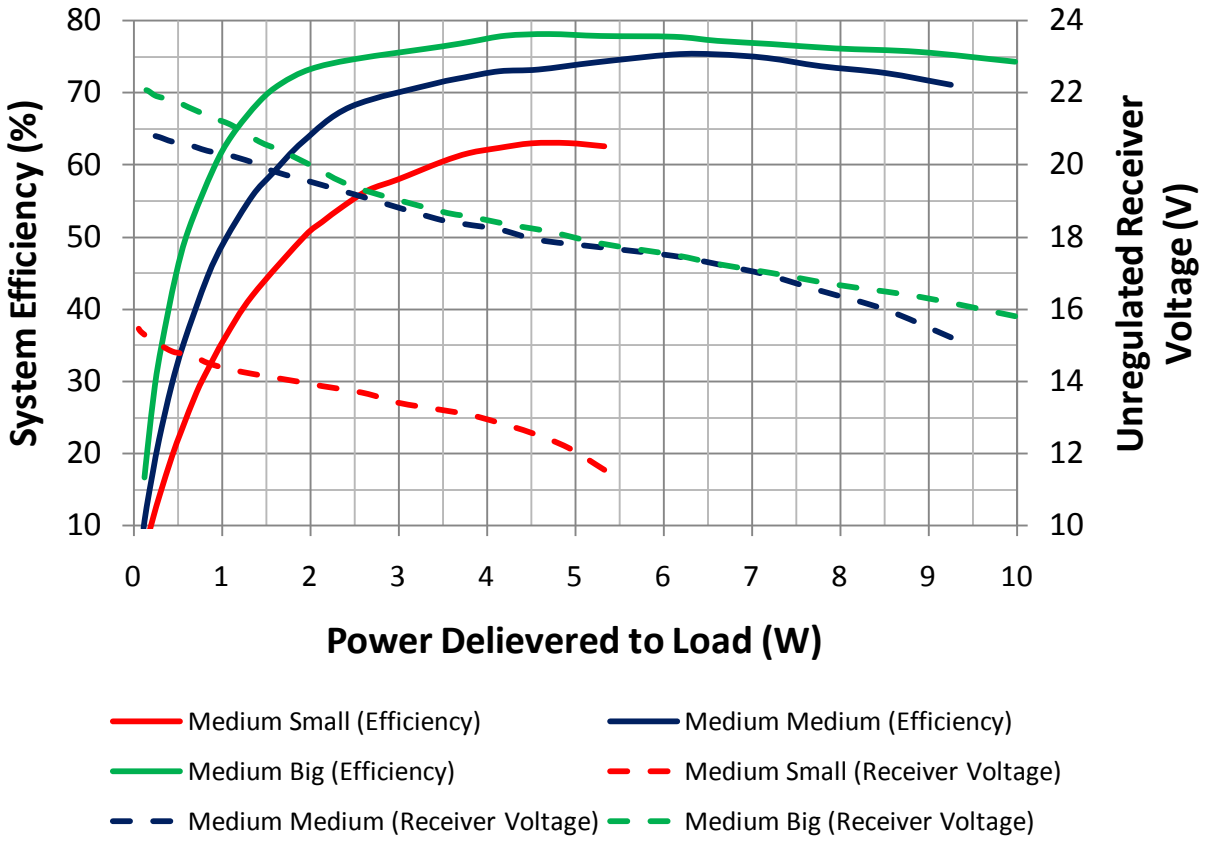

Figure 6-2. System efficiency and receiver voltage vs. power delivery plot for different sized receiving coil on a medium sized transmitting coil.

Figure 6-2 shows the same experimental results as Figure 6-1 but with the transmitting coil replaced with the medium sized transmitting coil. Based on the previous observation with "small medium" the trend of increasing efficiency of "medium big" is expected. With the decrease in mutual inductance between the coils, the real part of Z_{tx} is reduced for this setup resulting in more energy being dissipated across the parasitic resistance of L_{out} and the transmitting coil. Therefore, the trend of reduction on efficiency is also expected for the "medium small" setup. In addition due to the same reasons less power is expected to be transferred to the receiver. All three setups are able to achieve at least 5 W of power delivery with "medium small" slightly above 5 W. The unregulated receiver voltage is still kept within the nominal operating range of 8 V to 25 V.

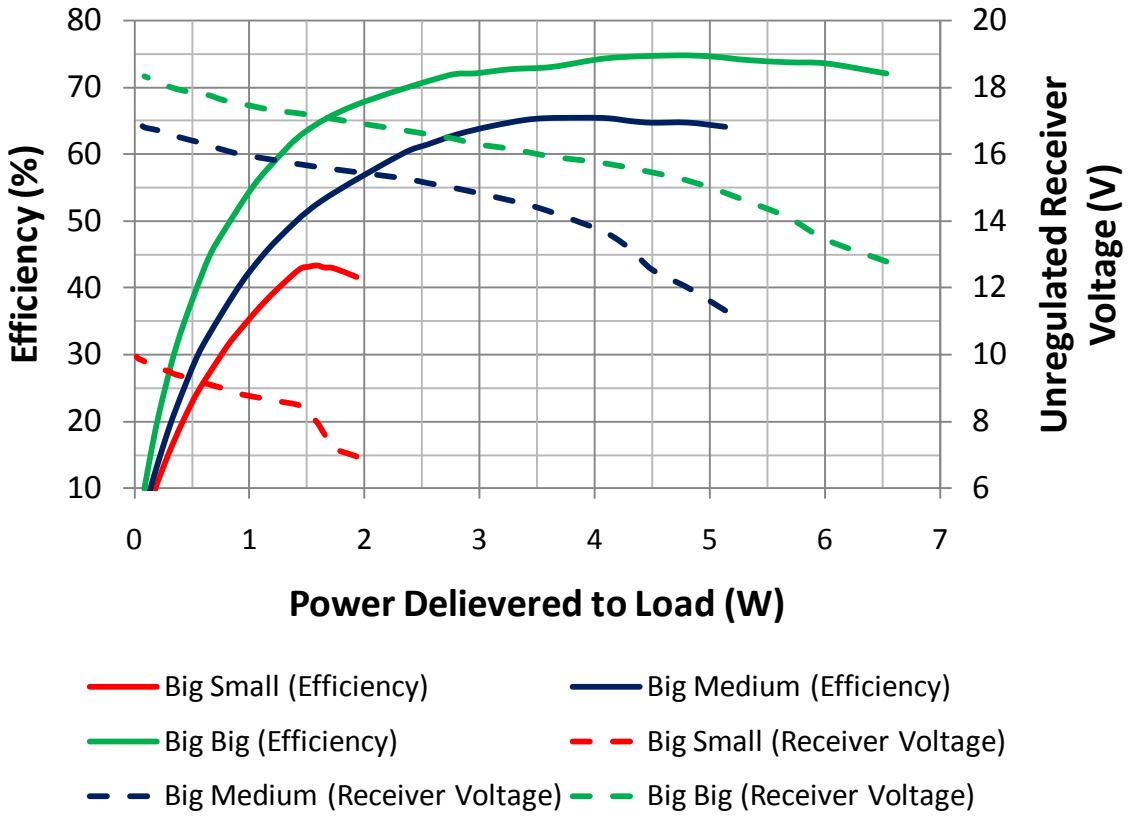

Figure 6-3. System efficiency and receiver voltage vs. power delivery plot for different sized receiving coil on a big sized transmitting coil.

Following the same approach, the medium sized transmitting coil is replaced with a big sized transmitting coil and results are show in Figure 6-3. The efficiency and power delivery degrades for both the smaller receiving coils. The coupling is so weak for the "big small" setup that very little power (up to 2 W) is being transmitted to the receiver. In addition, the unregulated receiver voltage drops below 8 V which is too low to achieve voltage regulation for a 5 V output. Since eight out of nine of the combinations except "big small" meet the specification of at least 5 W of the power delivery and unregulated receiver voltage range of 8 V to 25 V, we can infer that a desirable range of size ratio between the receiving coil and transmitting coil is approximately 1:2 to 1:12. This also translates to a coupling coefficient of 0.137 to 0.603.

CHAPTER 7
LOAD/FAULT DETECTION AND POWER DELIVERY TRACKING

The proposed near-field wireless power transfer system is sensitive to nearby conductive or magnetic objects as both the mutual inductance and the self inductances of the transmitting and receiving coils will be affected. Although it is possible to shield the transmitting coil from interferences behind or beneath it, the shield does not prevent a user from potentially damaging the system by placing objects such as a metal sheet on the transmitting coil or simply flipping the transmitting coil over a metal table. Therefore, to ensure robust operation of the system, a method of fault mode detection must be implemented so that the transmitter circuitry will not be damaged due to undesirable actions by the user.

In addition to protecting the transmitting platform from being damaged by conductive or magnetic objects, it is also desirable to reduce power consumption by turning off the transmitter when no valid receiving device is placed on the transmitting platform. The system will wake up for a very short period of time which is long enough for it to reach steady state. The time is predominately dependant on the self inductance of the transmitting coil and operating frequency. It is typically in the range of 0.5 ms to 5.0 ms. Probing the system with a rate of 1 Hz to 2 Hz speed is sufficiently fast for the user not to feel much latency. Therefore, the worst case duty cycle is 1% and is sufficient to reduce no load power consumption considerably. Although, one could use a communication link to perform authentication and handshaking, there would be a considerable increase in cost and component count. An alternative is to detect the system loading condition by the voltages and currents of the transmitter. To ensure low power consumption and cost, the voltages and currents to be detected must be either DC or be converted to DC so that a low speed analog-to-digital convertor (ADC) can be used to accurately extract the information and convert to digital domain.

7.1 Load/Fault Detection Scheme

7.1.1 Detection Circuit

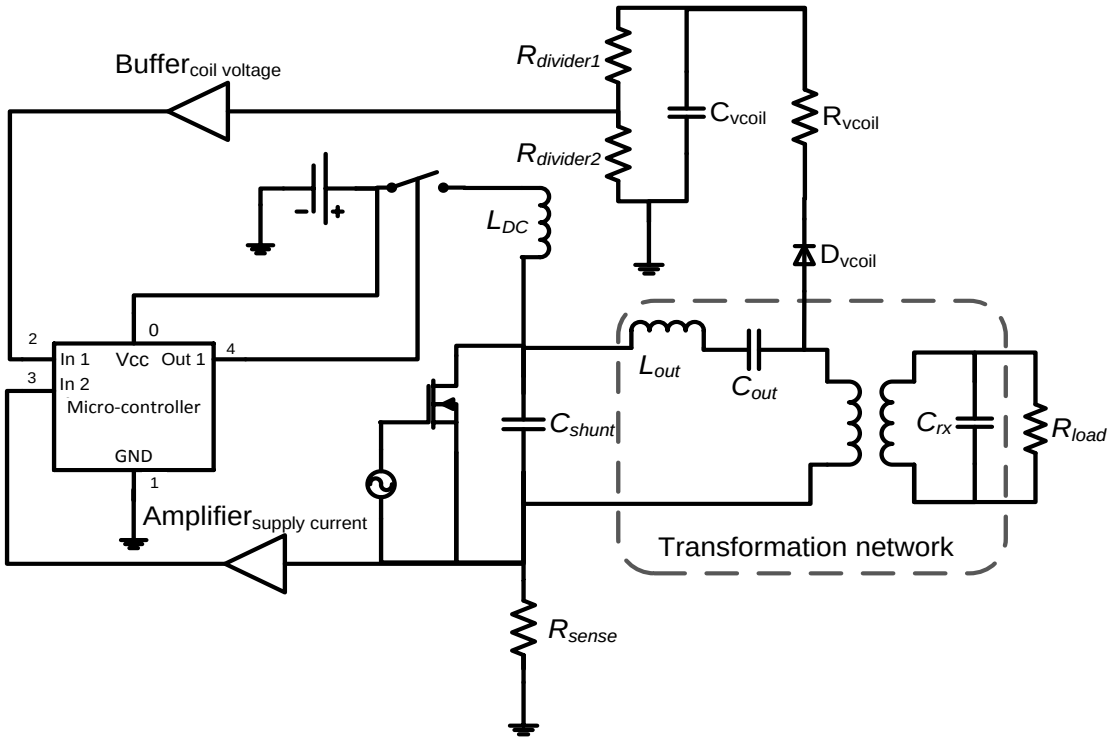

Figure 7-1. Block diagram of the proposed wireless power transfer system with detection circuit (detecting supply current and coil voltage)

Figure 7-1 shows the block diagram of the proposed wireless power transfer system with detection circuit. The class E transmitter operates at 240 kHz. There are three parameters that can be extracted from the wireless power transfer system without establishing a communication link between the transmitter and receiver. They are namely, the coil voltage, the supply current, and the coil current.

Coil voltage is extracted by rectifying the coil voltage via a high impedance path using a half wave rectifier. R_{vcoil} and C_{vcoil} shown in Figure 7-1 are used to smooth out the rectified voltage. R_{vcoil} is also used to regulate the current flow in the rectifying diode to prevent sudden and large current spikes from damaging the components. The voltage is then stepped down via a

potential divider using $R_{divider1}$ and $R_{divider2}$ to a workable voltage without damaging the input port of the micro-controller. To mitigate loading effects and reduce high frequency noise, a buffer using a low speed operational amplifier, e.g., LM324, in the voltage follower configuration can be used before the micro-controller's ADC port. Higher order low pass can be achieved by adding appropriate capacitors to the operational amplifier as a simple first order low pass filter.

Supply current is extracted from the circuit via the current sense resistor R_{sense} in Figure 7-1. The R_{sense} resistor is located at the class E transmitter ground before returning to the system ground, instead of locating at the high side before L_{DC}. Therefore, any voltage drop across the resistor will be referenced to the system ground instead of the supply voltage. Since the voltage drop will be extremely small (0.1V or less), a non-inverting amplifier using an operational amplifier LM324 can be used to amplify the voltage, mitigating any loading effects and reducing high frequency noise. Similar to the extraction of coil voltage, extra low pass filter can be added by the same technique discussed.

Measurements of the coil current can be realized by using either current sense transformers or current sense resistors. Current sensing transformers are typically large in size and operate at frequencies lower than 100 kHz, making them impractical for this system. A current sense resistor can be added to the low side of the coil to measure the voltage drop across the resistor. This is more practical than placing the current sense resistor on the high side as shown in Figure 7-2. This is because extremely high tolerance resistors are needed for the potential dividers if they are placed on the high side. Detecting a high frequency AC current with respect to ground is difficult because the ground of such a high voltage and current system is extremely noisy relative to the high side of the transmitting coil. The ground noise will contain frequencies including the operating frequency making it not possible to mitigate its effects via filtering. Unlike measuring

the supply current, which does not require rectification, both the high frequency voltage signal and the ground noise will be rectified. Therefore, it is not possible to perform low pass filtering to mitigate the effects of ground noise using a low speed operational amplifier. Since the ground noise is unpredictable and changes according to loading conditions, it is difficult to perform precise and stable measurement of the coil current. For the above reasons, only the coil voltage and supply current will be extracted.

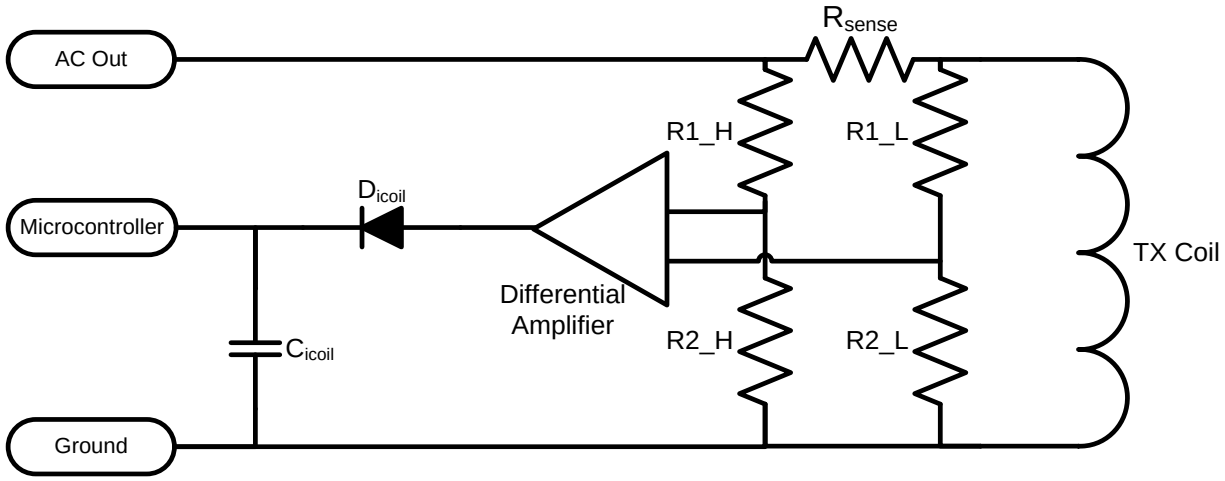

Figure 7-2. Schematic of coil current extraction network using a current sense resistor.

A DC switch shown in Figure 7-1 before the choke inductor L_{DC} is used to turn off the transmitter under no-load mode or fault mode which includes over current. A low turn-on resistance PMOS transistor using a low power NMOS transistor to pull down its gate voltage can be used as the switch. Additional over current protection can be implemented by using a polymeric positive temperature coefficient device (PPTC) at the supply as a second level protection. Reverse polarity voltage protection can also be implemented by adding a reverse biased diode in shunt with the supply voltage. If a reverse voltage is applied, the diode will cause a short circuit and the PPTC will be activated to disconnect the supply path. Over-voltage protection of sudden spiking can be implemented by using a transient voltage suppression (TVS)

diode commonly referred as a transorb across the supply. The TVS diode can also be doubled as the diode for reverse voltage protection. To prevent thermal runaway, a thermistor can be located next to the transistor of the power stage. By using the thermistor as part of a potential divider on which the supply voltage is applied, the temperature can be tracked by reading the voltage across the thermistor using the micro-controller's ADC.

7.1.2 Detection Flowchart/Logic

The detection scheme flowchart is shown in Figure 7-3. It can be implemented using a low cost micro-controller, such as 16F688 by Microchip. It is found experimentally that the system reaches a steady state after it is being powered on for 1 ms. This is when a decision to power on or off the transmitter can be made. The time to steady state is dependent on the operating frequency as well as the self inductance of the transmitting coil.

The no-load and safe modes follow a similar logic flow. The only difference is that the transmitter is powered down if no-load mode is detected whereas the transmitter is powered up if the safe mode is detected. Both modes will probe the circuit for supply current and coil voltage after each predetermined X seconds to determine its operating mode, (a reasonable number for X is 1). Increasing X will incur higher latency to make the system response slow and decreasing X will incur higher no-load power consumption. The operating modes are determined by the supply voltage and coil voltage space, which will be discussed later. The thresholds are dependent on the supply voltage, transmitter’s component values, and transmitting coil parameters. The dependence of the parameters on the receiver is found to be weak. Therefore, the thresholds work independent of receivers as well. Hysteresis needs to be implemented in the code so that the system does not oscillate when its operating mode is at the borderline case. The fault counter Z is reset if the system ends up in either mode.

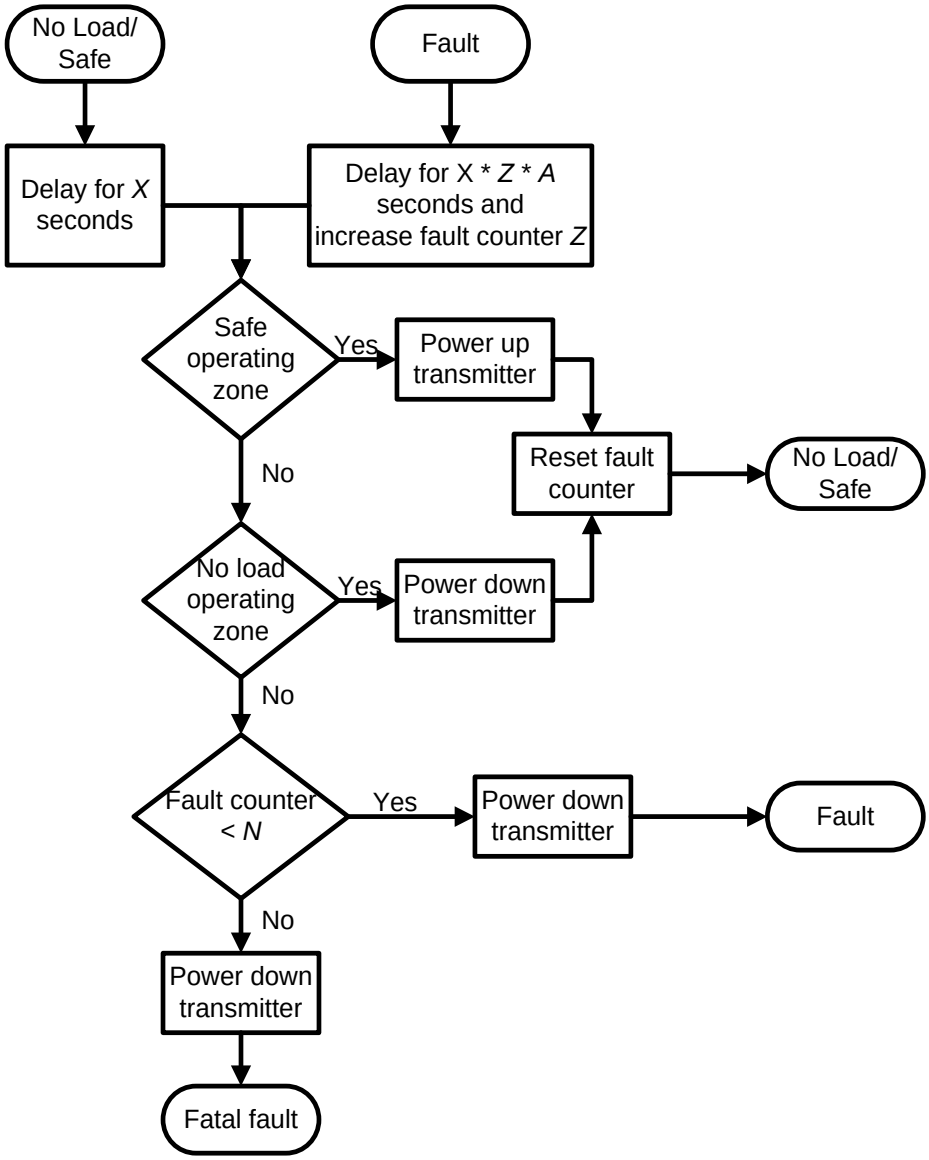

Figure 7-3. Detection scheme flow chart for proposed system.

When the coil voltage and supply current is excessive, the system enters its fault mode. A common cause of fault mode is when a huge piece of metal is placed over the transmitting coil, which decreases the total effective inductance of the transmitting coil significantly. When this happens, the class E ZVS/ZDS operation is no longer valid. If the transmitter is not powered down immediately, the transistor will be damaged due to excessive power dissipating as heat. The delay to probe the system to determine if the cause of the fault has been rectified is increased by a factor *A* on top of the original X delay. The delay is increased with increasing occurrence of

fault so that the system does not need to repeatedly stress the system within such a short window of time. Once the number of tries reaches N, the system will enter into the fatal fault mode, and the only way to exit from the mode is to perform a hard reset which involves disconnecting the DC supply of the system.

Other fault modes which are not covered by the flowchart include thermal run away mode due to excessive heating at the power stage and battery fault mode for a one-to-one system. As will be shown in the experimental verification, it is possible to track the charge/power received status of a receiving unit for a one-to-one power system. If the trend of the power delivered over time deviates from the expected trend, the system will enter a battery/receiver fault mode which also requires a hard reset. This also prevents possible damage when a user places a non-compliant receiver of a different charging profile on the transmitter. Brownout and over-voltage at the supply can also be detected by a supply voltage monitoring network so that the transmitter can be powered down under fault mode. A supply monitoring network is simply a potential divider to drop the supply voltage to the range of the micro-controller's ADC so that the micro-controller can make a decision based on the ADC's input.

7.2 Experimental Verification

7.2.1 Test Bench and Circuit

The wireless power transfer system is fabricated based on the component values shown in Table 7-1 which was selected using design rules presented in Chapter 3. The transmitting coil used is similar to the one used in Figure 3-1. To ensure that the proposed detection scheme can be applied to the same transmitter platform regardless of the receiver size, two different receiver sizes were used in the experimental verification. All coils were fabricated using 100/40 round served Litz wires. The supply voltage for the system is selected to be 12 V and can be varied depending on the power level requirements. Supply voltage should not be considered as a factor

during the analysis. The fabricated transmitter shown in Figure 7-4 has a size of 15 cm x 2 cm. It is designed to be long and narrow so that it can be placed beside the transmitting coil as a single integrated unit. The low power detection and control block is located away from the high voltage power stage to reduce noise and coupling effects. The power input jack is located between the two blocks for the same reasons.

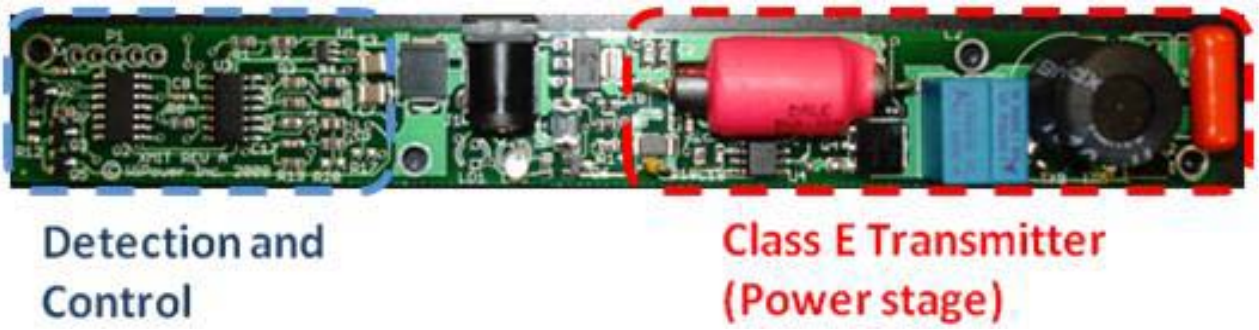

Figure 7-4. Photograph of the fabricated transmitter circuit with control circuit.

Table 7-1. Component Values for Load/Fault Detection Test Bench

	Value
Coil Specifications	
TX coil inductance	45.3 µH
TX coil dimension	20 cm x 20 cm
TX coil parasitic resistance	0.5 Ω
RX coil inductance (big RX)	5.45 µH
RX coil dimension (big RX)	9 cm x 6 cm
RX coil parasitic resistance (big RX)	0.235 Ω
Mutual inductance (big RX)	2.81 µH
Coupling coefficient (big RX)	0.178
RX coil inductance (small RX)	4.00 µH
RX coil dimension (small RX)	6 cm x 5.5 cm
RX coil parasitic resistance (small RX)	0.22 Ω
Mutual inductance (small RX)	1.88 µH
Coupling coefficient (small RX)	0.140
Circuit Specifications	
L_{DC}	500 µH
C_{rx} (big RX)	68 nF
C_{rx} (small RX)	95 nF
C_{out}	9.4 nF
L_{out}	10 µH
Lout parasitic resistance	0.16 Ω
C_{shunt}	12 nF

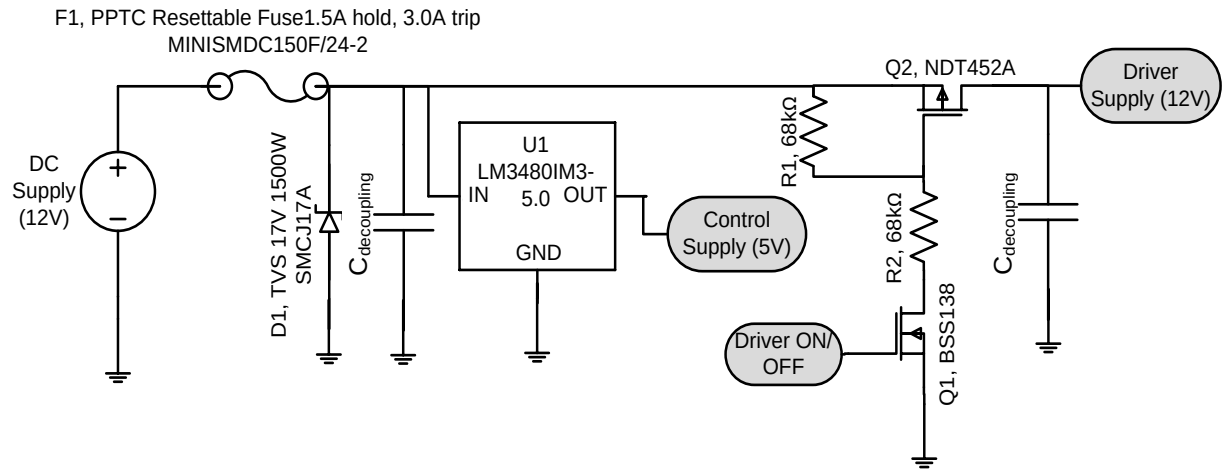

Figure 7-5. Schematic of power stage of fabricated transmitter.

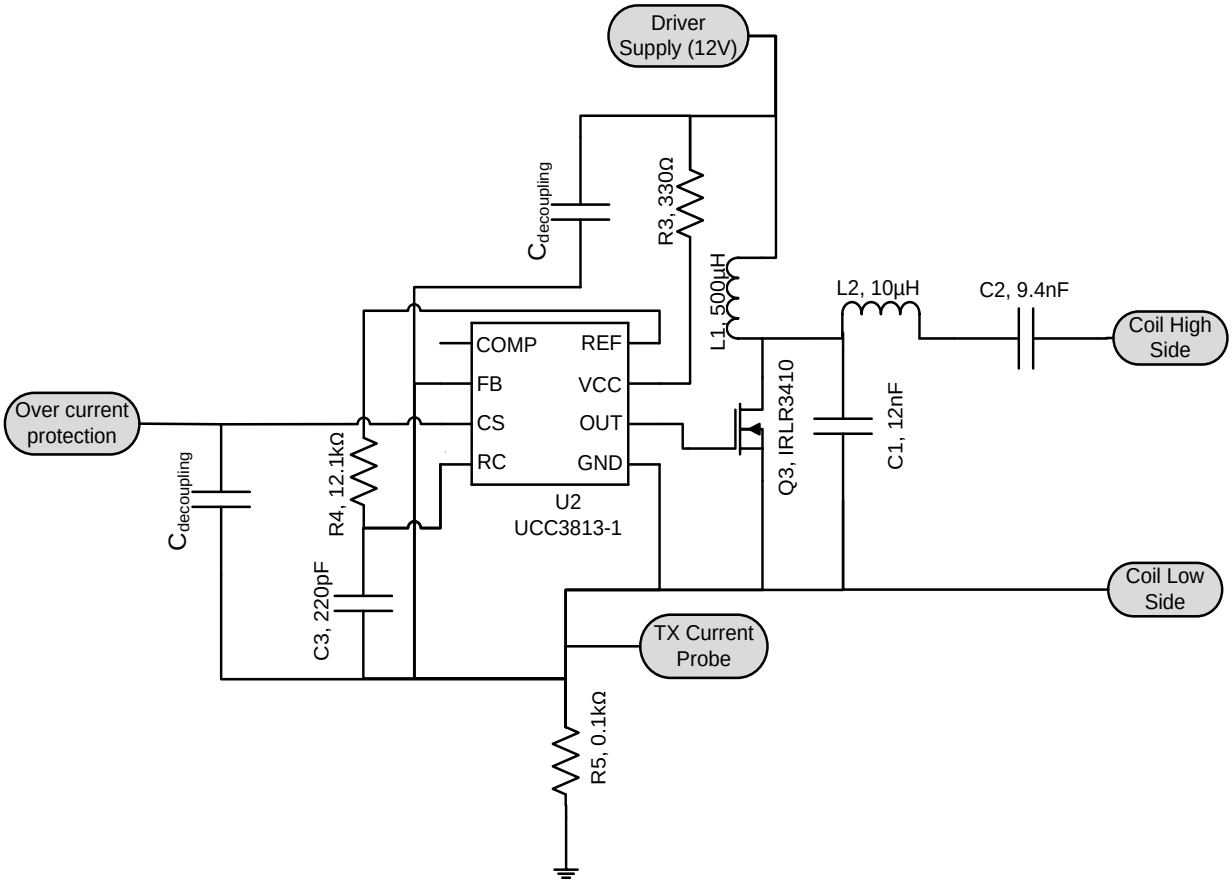

Figure 7-6. Schematic of driver stage of fabricated transmitter.

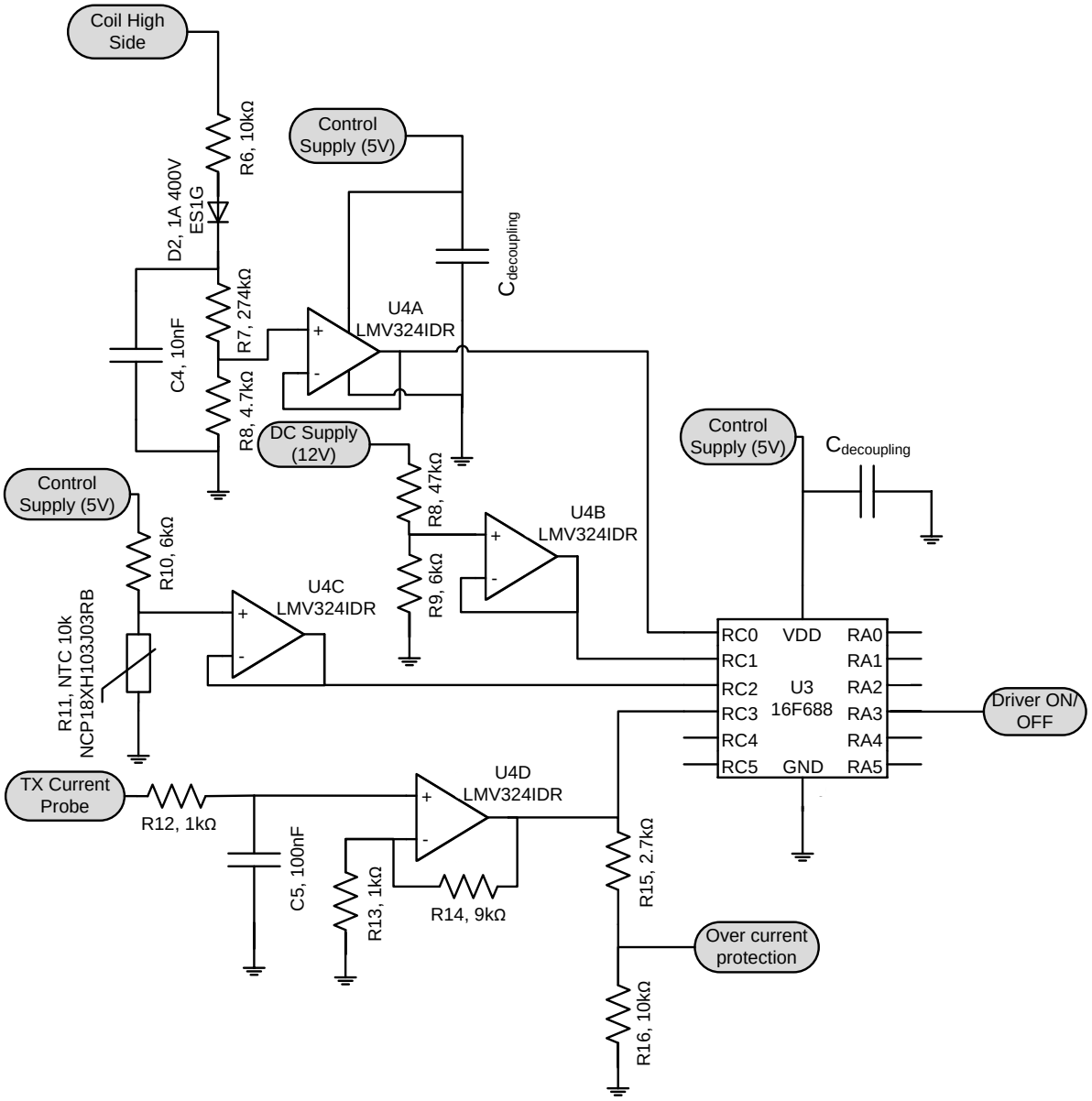

Figure 7-7. Schematic of detection and control stage of fabricated transmitter.

Figure 7-5 to Figure 7-7 shows the schematic of the fabricated transmitter. Figure 7-5 shows the power stage which handles the over current protection, reverse voltage protection and on/off control of the transmitter. Figure 7-6 shows the driver stage which includes the class E transmitter and clock. Figure 7-7 shows the detection and control stage. The transmitter has two levels of protection, hardware protection and software controlled protection.

Hardware protection is used as a last resort protection for which the thresholds are set to be higher than the software controlled protection. It should only be triggered when the micro-controller (U3) in Figure 7-7 fails. Over current protection is realized by a PPTC fuse, F1 as shown in Figure 7-5 which has a 1.5 A hold and 3.0 A trip. The transient voltage suppression (TVS) diode, D1 in Figure 7-5 serves two purposes. It helps to eliminate any transient voltage spikes due to discharge from the energized coil during powering down, and protects the transmitter from over-voltage. In addition, if the user accidentally connects the DC supply in reverse polarity it will attempt to short out the supply and load excessive current. The fuse F1 will be activated to break the connection protecting the transmitter.

An intermediate stage of over current protection is added to the transmitter via disabling the PWM clock, U2 in Figure 7-6. This is achieved by pulling the CS pin to high. Values of R15 and R16 in Figure 7-7 are selected to shut down the clock when supply current exceeds 1.2 A which is higher than the software determined maximum current of 0.85A as shown in Figure 7-12.

The transmitter should rely on software control protection for its nominal operation. This is achieved by turning on and off the PMOS transistor Q2 via a low voltage control generated by the micro-controller (U3) using a NMOS transistor to pull down the gate voltage of Q2 via R1 and R2. It is important that the regulator for the detection and control stage U1 is placed before the Q2 transistor so that the detection and control stage is still in operation even when power is being cut to the driver stage. Using a quad operational amplifier LMV324IDR as shown in Figure 7-7, the micro-controller (U3) is able to read in 4 different parameters of the system. They are coil voltage (U4A), supply voltage (U4B), driver temperature (U4C) and driver stage current (U4D).

Coil voltage and driver stage current extraction has already been discussed in the previous section. The thresholds are predetermined by sweeping the loads as shown in Figure 7-12. By extracting the supply voltage, the transmitter is able to prevent over-voltage conditions as well as under-voltage conditions that might cause the system to deviate from its nominal operation. The system is set to a supply voltage operating range of 9 V to 15 V. In addition to detecting the supply voltage, the transmitter is able to vary its thresholds accordingly to make it more robust. The thresholds can be stored in the flash memory of the micro-controller (U3). A 0.5V resolution is sufficient to prevent any false alarm or damage to the system. Finally, a thermistor (R11) is placed next to the class E driver's transistor to monitor its temperature. The system will shut down when temperature exceeds 75°C and only resume nominal operation when the temperature drops below 60°C.

7.2.2 Experimental Results

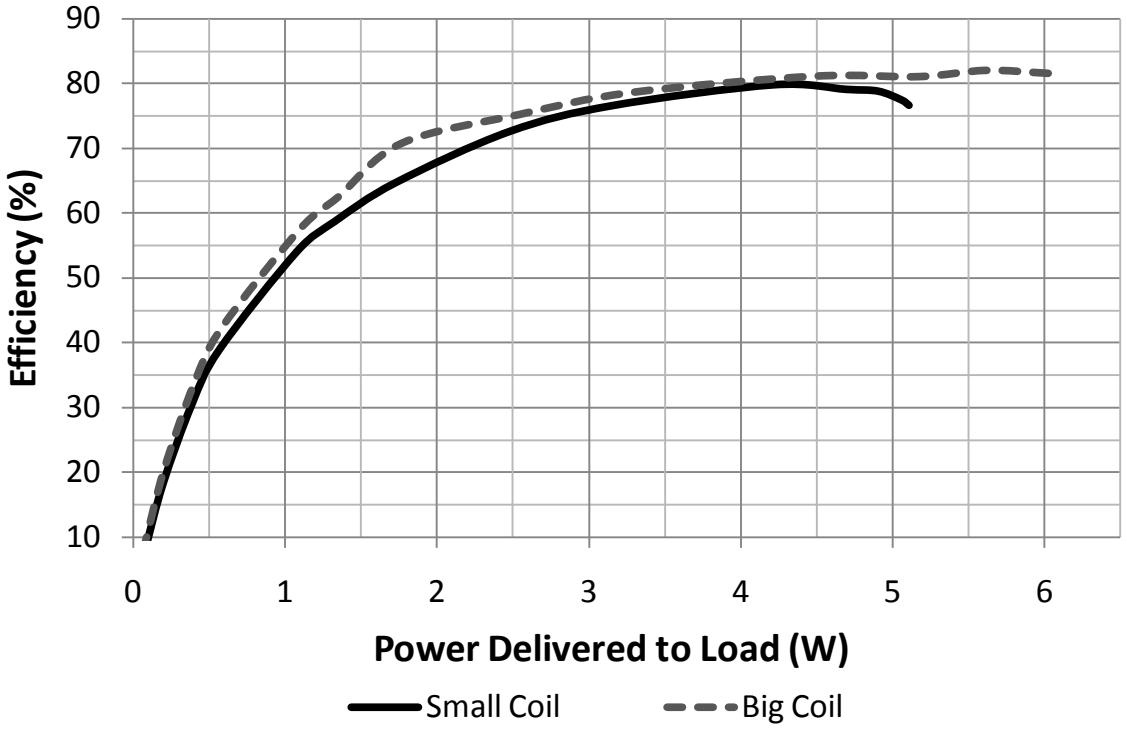

Figure 7-8. Efficiency-Power plot of single receiver setup (Solid black line: Small coil. Dashed gray line: Big coil)

Figure 7-8 shows the efficiency-power plot of a single receiver setup using the big and small receivers being placed on the same transmitting coil. Since both of the receiving coils are optimized for operation on the same transmitting coil, the efficiencies of both receivers are similar for the respective power level. Better than 60% efficiency can be achieved for power delivery level above 1.5 W, keeping absolute power loss of the system low at all times, which is important to ensure the system does not overheat. Due to stronger coupling, the big receiving coil has a slightly higher efficiency as well as power delivery. Power delivery is about 6 W using the big coil and about 5 W using the small coil.

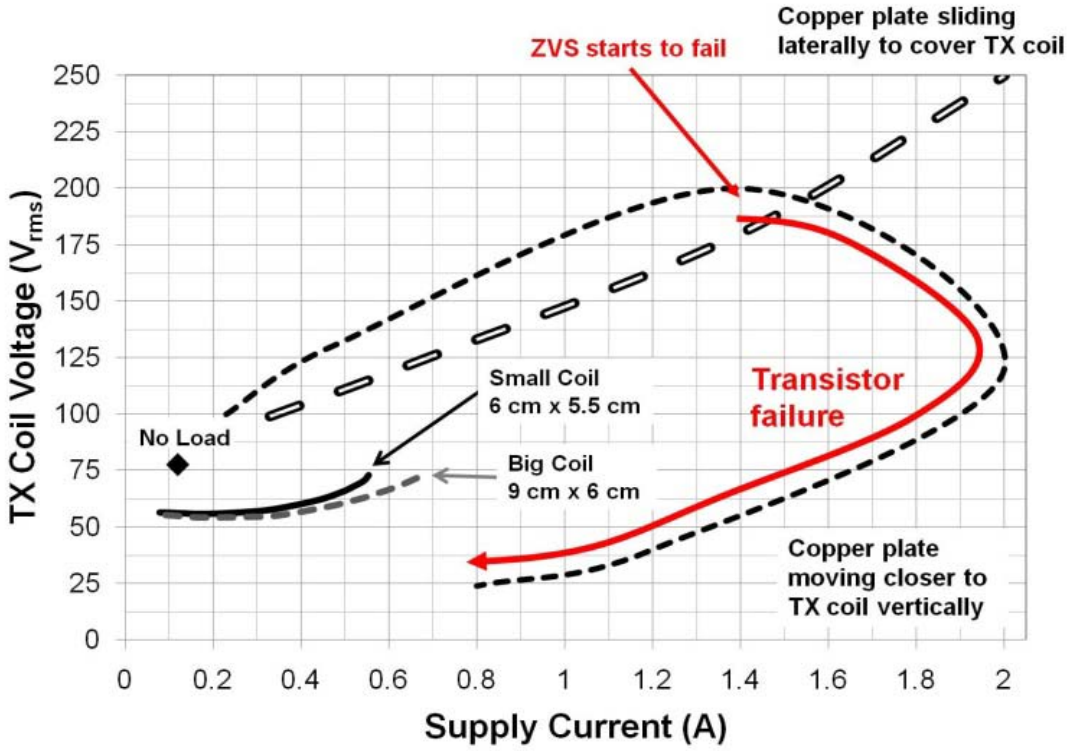

Figure 7-9. Examples of different loading conditions and fault modes on coil voltage versus supply current space.

Figure 7-9 shows the coil voltage and supply current space diagram which is used to determine the different operating modes. The system enters the no-load mode when the operating condition is in the vicinity of the diamond shape. A margin of ± 10 V and ± 50 mA can be use to frame the no load operating point so that the system will be more robust under component

variation. The safe zone is at lower coil voltage (less than 80 V_{rms}) and current (less than 0.85 A) region where two receivers are at their nominal operation without being over loaded. Therefore, safe zone is located at the bottom left corner of the coil voltage and supply current space as any excessive voltage or current will damage the transmitter. The small receiving coil generates a larger transmitting coil voltage because the same amount of power delivery is required over a smaller receiving area, which requires a stronger magnetic field. Two different potential fault scenarios, a large copper plate being brought closer to the transmitting coil and a large copper plate being slid over the transmitting coil, are shown in Figure 7-9. Although, there are other fault scenarios such as placing a smaller copper sheet in the middle of the transmitting coil, the two scenarios tested should be able to provide sufficient understanding on how the system will react under various fault modes. The solid dashed line shows the trend of coil voltage and supply current moving clockwise when the distance between the transmitting coil and a larger copper sheet becomes smaller. ZVS/ZDS starts to fail at the voltage inflection point as more energy is dissipated across the transistor instead of being transferred to the load (copper pate). If the system does not shut down immediately the transistor will be damaged due to heating. The hollow dashed line shows an increasing coil voltage and supply current when the overlapped area between the transmitting coil and a large copper plate increases. The trend of the line is expected to follow the same as the experiment which the copper plate is brought closer to the transmitting coil. However, the coil voltage and supply current is so excessive that the transistor will be damaged due to non ZVS/ZDS operation. Therefore, measurements were not carried out beyond 2 A supply current. Since high coil voltage will always lead to over-voltage problems at various points of the circuit and damage the components, it is not important to study the trend of the curve during fault operation as the priority is to shut down the system as quickly as possible.

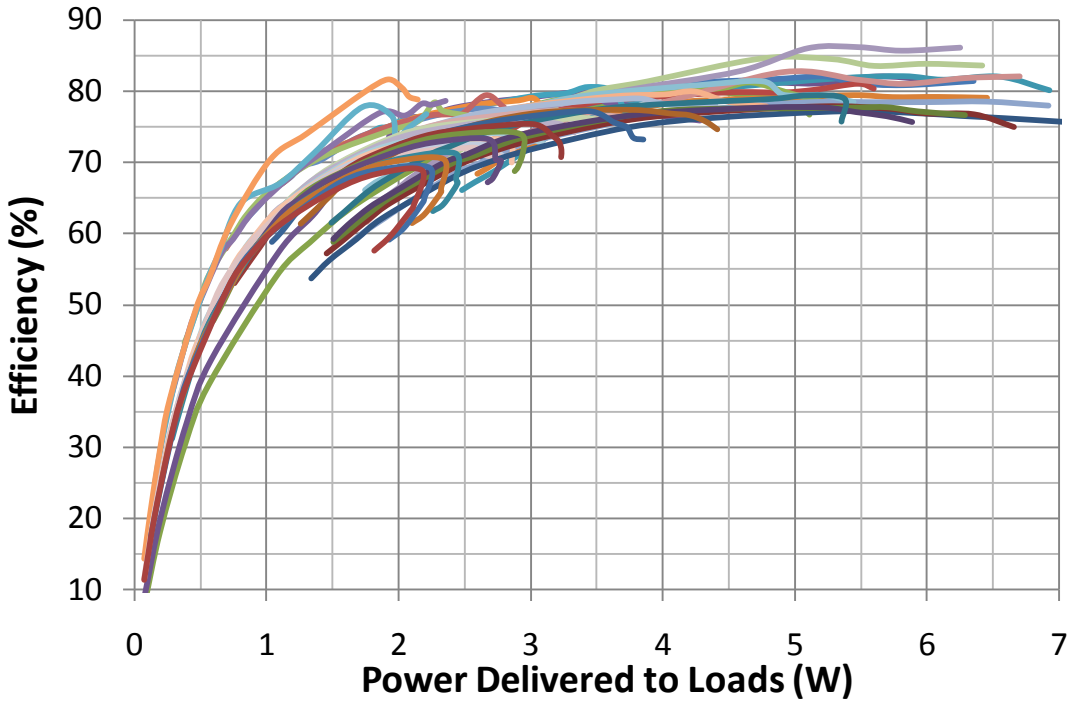

Figure 7-10. Efficiency-power plot of three sets of dual load measurements and two sets of single load measurements using a combination of big and small receiving coils.

Three sets of measurements were carried out on the system using two loads of load resistance ranging from 20Ω to 4000 Ω in 14 discrete steps. The three sets are two big coils, two small coils, and one big coil with one small coil. The pair of receiving coils are placed side by side in the middle of the transmitting coil with a 2 cm gap between each other. The efficiency-plots of the three measurements are shown in Figure 7-10. In addition, two single-receiver measurements are also shown in Figure 7-10 for comparison. DC-DC efficiency is above 70% for power delivery levels above 3W, crossing 85% for some load points. The spread of efficiency is approximately ±5% regardless of the number of receivers. All load conditions achieved ZVS/ZDS operation, maintaining high efficiency operation with minimum power loss. Since the efficiency of the system is well bounded regardless of loading conditions and their sizes, the spread in the coil voltage and supply current space should be limited as well.

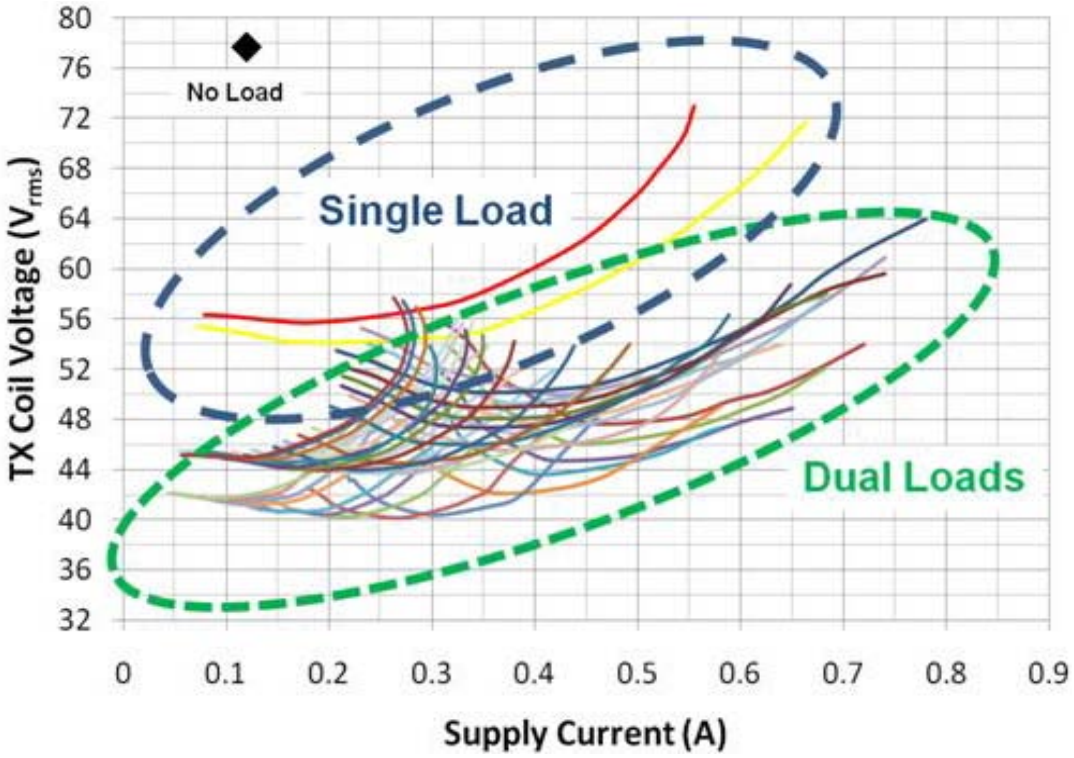

Figure 7-11. Transmitter coil voltage and supply current space illustrating three different zones: no-load, single load, and dual loads.

Figure 7-11 shows the transmitting coil voltage and supply space for a single load (big coil and small coil) and dual loads. Although, there is some overlapping between the 2 spaces, it is possible to detect the number of loads for most of the loading conditions. As shown in Figure 7-11 a sharp transition will be observed when an extra load is being placed on or removed from the transmitting coil. Therefore, the system can easily detect if an additional receiver is placed on the transmitting coil or being removed from it by tracking the transmitter coil voltage and supply current over time. It is also possible to detect the number of loads when the transmitter is powered on with valid loads on the transmitting coil because during the initial power-on states of most electronic devices, they will not draw much power. Therefore, the power delivery will slowly ramp up during the first few seconds when the transmitter is powered on. Due to this intrinsic characteristic of most electronic devices, the system will typically observe an initial coil voltage of 40 V_{rms} to 48 V_{rms} for dual loads and 52 V_{rms} to 58 V_{rms} for single loads. Under the

worst case situation, if it is not possible to differentiate the number of loads being placed on the transmitter, the system can track the loading conditions via techniques such as Markov Chains over a specific period of time and determine its loading conditions. This requires large amount of training data to perform load pattern analysis which is beyond the scope of this dissertation.

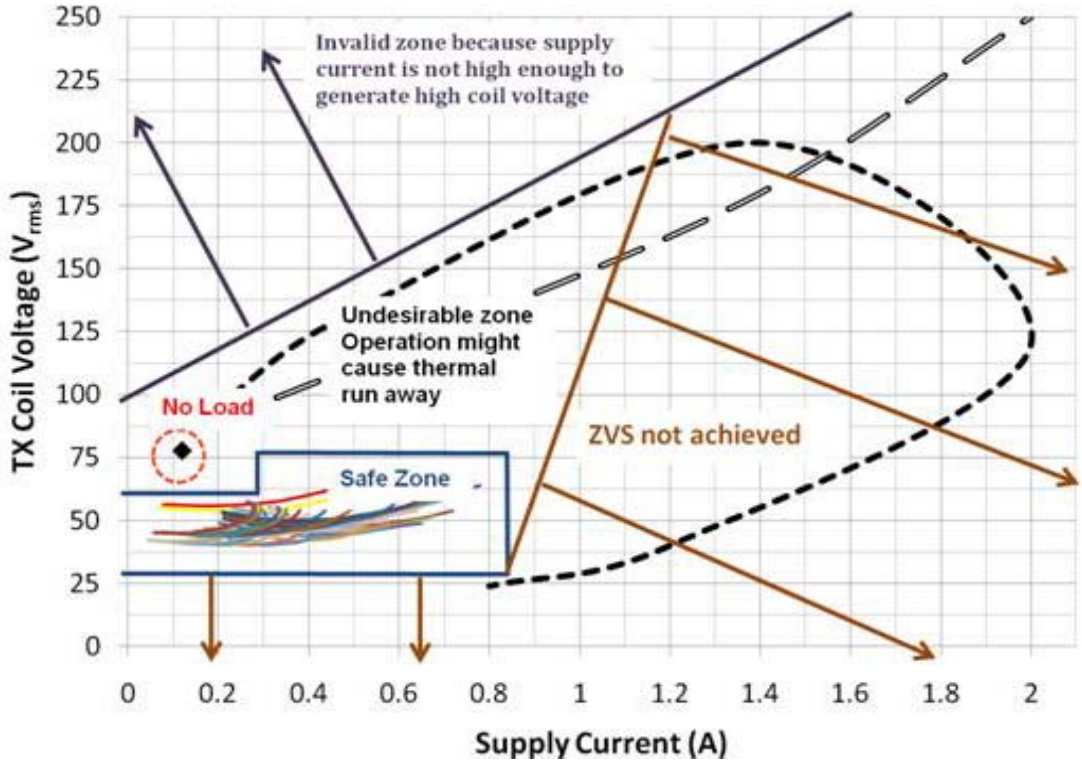

Figure 7-12. Transmitter coil voltage and supply current space diagram illustrating three different zones, no-load, safe and fault.

Summarizing the above discussions, Figure 7-12 shows the transmitter coil voltage and supply current space indicating the various zones. The no-load zone is enclosed by red circle and the safe zone is enclosed by blue lines. The no-load is basically a point solution with a radius for system tolerance purposes which can be simplified into a rectangle or square. The zone can be described using two points in the space or four data points for which each point is described using the transmitter coil voltage and supply current or simply the four sides of the rectangle/square. The safe zone has two steps. For supply current below 0.3 A, the transmitting coil voltage should be between 32 V_{rms} and 64 V_{rms} whereas for supply current above 0.3 A, the

transmitting coil voltage should be between 32 V_{rms} and 80 V_{rms}. Any supply current greater than 0.85 A is considered as a state of over current for this system and determined as fault mode. Five data points are required to describe the safe zone. In fact, any operating condition not within the safe or no-load zone is considered to be in the fault zone. Therefore, each unique supply voltage and operating frequency will require nine data points to describe its coil voltage and supply current space. The purple zone on the top left corner of Figure 7-12 is an invalid zone because the supply current is too low to generate such voltages of those magnitudes and would never occur. ZVS/ZDS operation is still valid to some extent in the area above the safe zone. However, the transmitting coil voltage is very high and might damage components. In addition, excessive transmitter coil voltage might lead to thermal run away on some components especially the transistor. The brown area on the right of the safe zone is when the transmitter no longer operates under the ZVS condition. When this happens, large amount of energy is dissipated across the transistor as the high voltage across the drain of the transistor and high current through the transistor are no longer orthogonal in time.

An interesting linear relationship between the supply current and the power delivered to the load is shown in Figure 7-13. The results from the five sets of measurements can be consistently described using the equation $y = 0.095x + 0.055$ where the y-axis is supply current to the transmitter and the x axis is the power delivered to the load. Based on the 12 V supply voltage, for every 1 W of power at the receiver the transmitter requires an input power of 1.14 W. Once the system is operating in the safe zone, using the proposed equation, Figure 7-14 shows the plot of calculated delivered power via measured supply current to the transmitter versus the actual delivered power. The results show relatively good agreement at all power levels with an average error of -0.08 W and standard deviation of 0.16 W for 616 sets of reading.

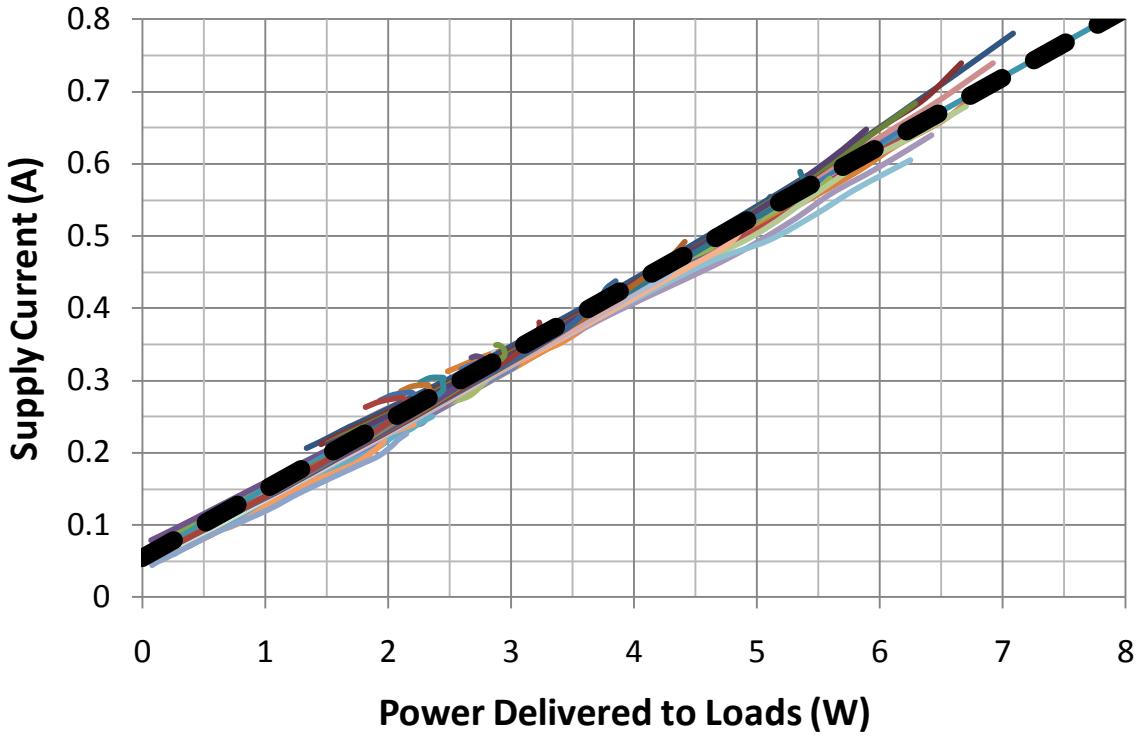

Figure 7-13. Linear relationship between supply current and power delivered to the loads for all 5 sets of measurements. Solid dashed line: y = 0.095x + 0.055.

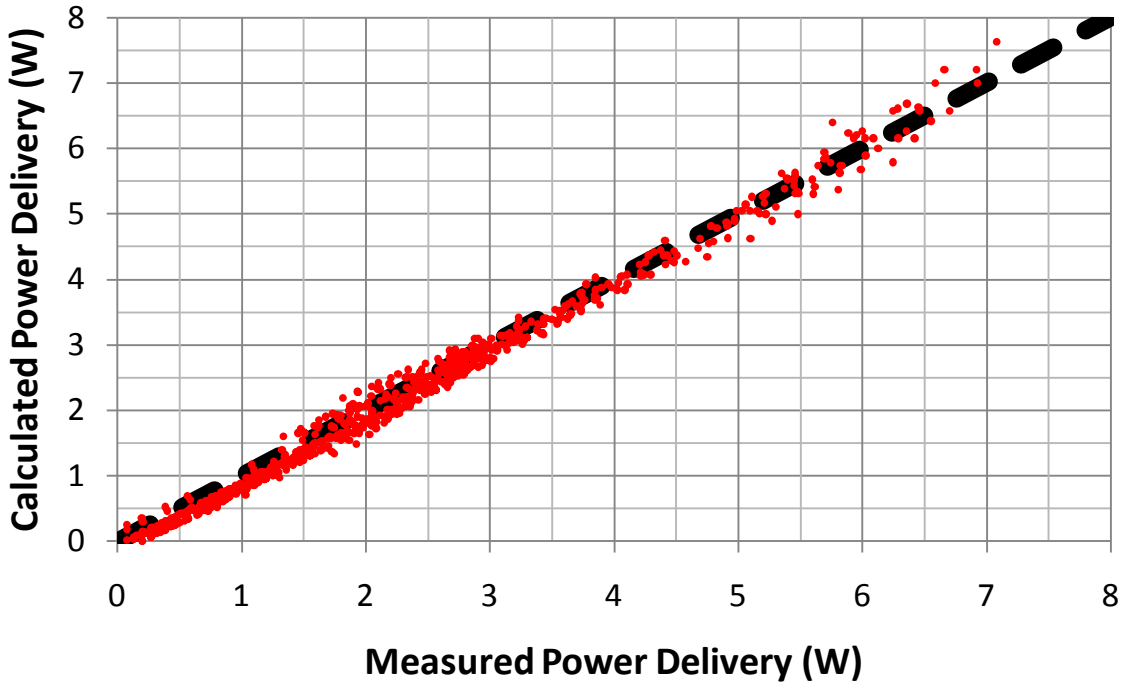

Figure 7-14. Power delivery error distribution plot. Calculated power delivery is based on measured supply current. Solid dashed line: ideal error free calculation.

Although the experimental verification shows the feasibility of the proposed load/fault mode detection scheme, the thresholds for different modes and the equation to track the power delivery are highly dependent on the supply voltage and operating frequency. Therefore, a voltage sensing mechanism is implemented to detect the supply voltage and make appropriate adjustments to the thresholds. The operating frequency is assumed to be stable for this case by using 1% tolerance components for the RC timing network. A more effective method is to use a crystal reference to generate the clock frequency; a low cost 30ppm crystal will generate a clock signal with negligible frequency offset. However, by using this technique the frequency will be locked to a single frequency or multiple/fraction of the operating frequency making fine frequency resolution control not possible.

7.3 Extension of Load/Fault Detection Scheme

7.3.1 M:N Coupling Structure

The analysis of the load/fault detection scheme is confined only to single transmitting coil architecture. As shown in Figure 5-23, placing two receivers concurrently onto a single transmitting coil will "choke" the power delivery, as the power delivery of one receiver is dependent on the loading condition of the other receiver. This observation is supported by Equation 4-6 for which the real part of Z_{tx} increases with each additional receiver while the reactance of Z_{tx} remains approximately the same. Therefore, the power delivery remains approximately the same but is being split between two receivers. Instead of using a single transmitting coil, a M:N coupling structure shown in Figure 7-15 is proposed. The M:N coupling structure can be implemented to support multiple portable devices with a one-to-one pairing or cover a large area by using a large array of transmitting coils to power compact sized receivers. In depth analysis of the M:N coupling structure is beyond the scope of the discussion as the focus will be on system level. For the following analysis and experimental verification, the focus

will be on a M:N coupling structure supporting two portable devices. A single class E transmitter is used to drive two similar transmitting coils (15.5 cm x 17.5 cm) being placed beside each other. Two identical receiving coils (9 cm x 6 cm) are being used. The design rules in Chapter 3 are used to select the components.

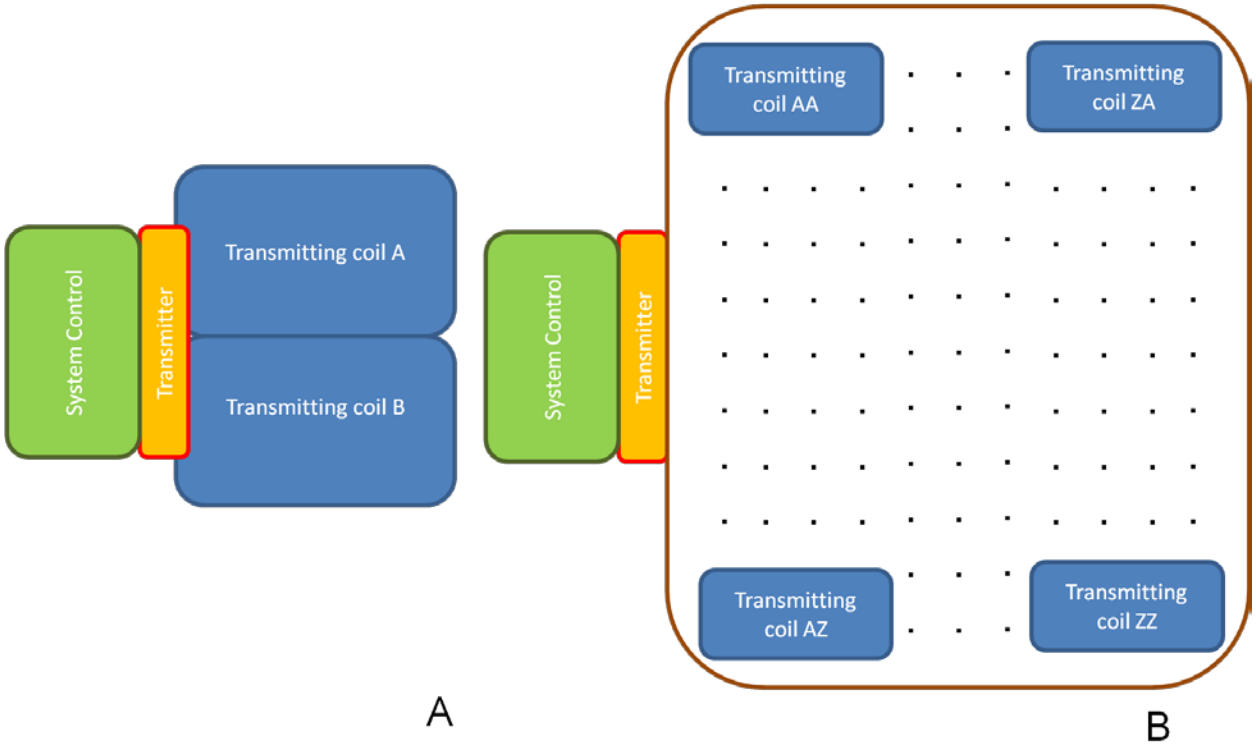

Figure 7-15. Examples of M:N coupling structures. A) Supporting two portable devices and. B) Large array of transmitting coils covering a large area.

Figure 7-16 shows the power "choking" delivery trend of a dual receiver setup when both receivers are being placed on a single transmitting coil while leaving the other coil unloaded. The power delivery is dependent on the other receiver with power level above 1W is observed, which is similar to the trend in Figure 5-23. The "choke" point is lower than that of Figure 5-23 because the bigger receiving coil results in stronger coupling. A stronger coupling between the transmitting and receiving coils will enhance the dependency of power delivery between two receivers being placed on a single transmitting coil. Figure 7-17 shows the power delivery trend

of a dual receiver setup when one receiver is being placed on each transmitting coil. The power "choking" phenomena is not observed for this case, power delivery to each receiver is independent of one another. This is because the coupling between each transmitting coil is very weak as they are placed next to each other instead of overlapping each other. Therefore, it can be assumed to be two independent single transmitting coils to a single receiving coil system. Power delivery to the individual receivers is not balanced because the coils are hand wounded with tolerance of self inductance as high as 10%. This problem will be eliminated during mass production as the coils will be machine wounded or PCB fabricated with much higher tolerance. As shown, by using the M:N coupling structure the problem of power "chocking" can be eliminated. To ensure that the design is feasible, further analysis on the efficiency, validity of transmitter coil voltage and supply current space as well as power delivery.

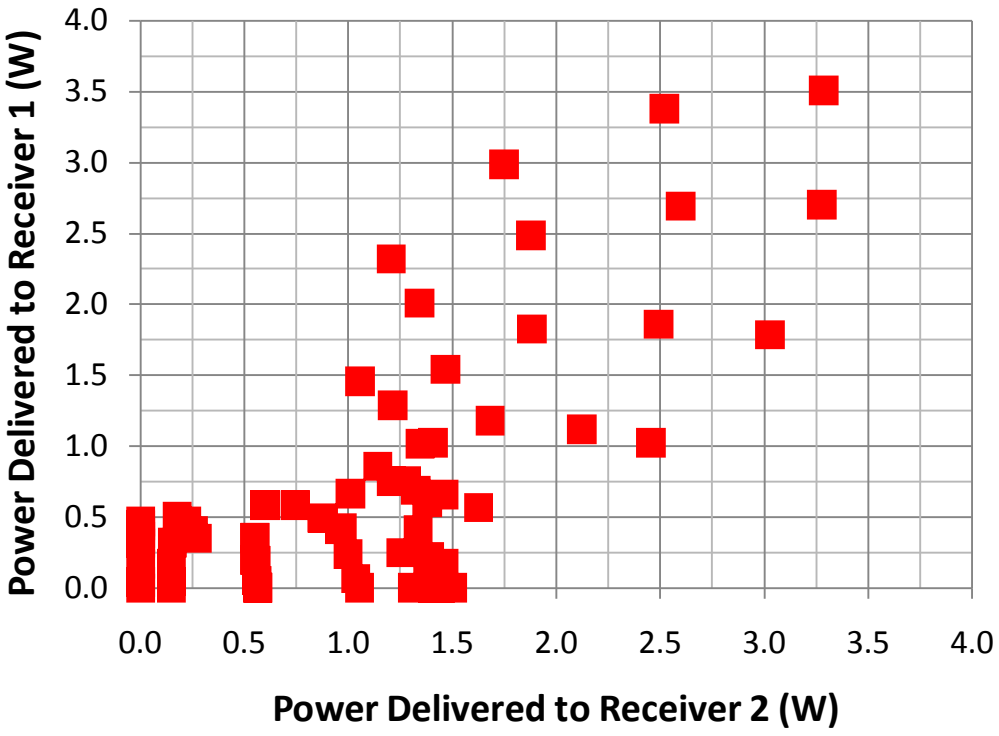

Figure 7-16. Measured power delivery of a dual receiver setup on a dual transmitting coil test bench with both receivers on a single coil leaving the other coil unloaded.

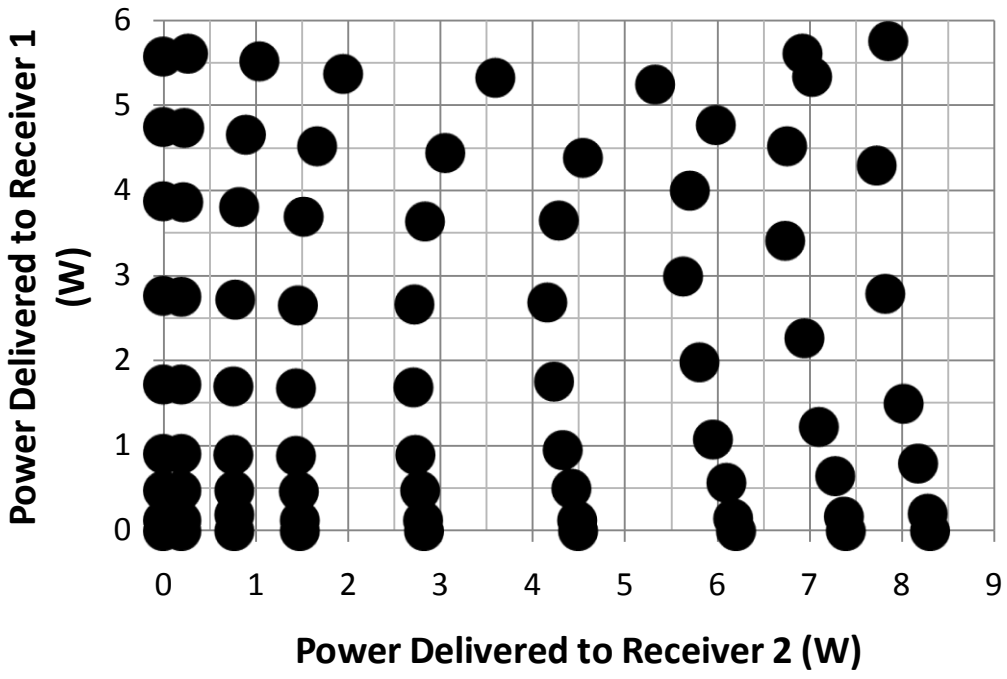

Figure 7-17. Measured power delivery of a dual receiver setup on a dual transmitting coil test bench with one receiver on each transmitting coil.

Figure 7-18 shows the efficiency-power plot for both test results of Figure 7-16 and Figure 7-17 including the results for a single receiver setup. Efficiency is high for both cases achieving a better than 75% efficiency for power level above 4 W. Efficiency follows the same trend for setup with single receiver and dual receivers on a single transmitting coil confirming the design rules presented in Chapter 3 can be applied to a M:N coupling structure. Slight efficiency improvement is observed for the setup with a receiver is placed on each of the individual coils. This can be explained by the fact that, although one of the transmitting coil is not loaded, current is still running through the coil. The current will cause energy to dissipate across the coil's parasitic resistance as high level of reactive power is being driven into the unloaded coil. However, if the coil is loaded, the resistance seen by the coil due to its load is much larger than the parasitic resistance of the coil and the losses can be neglected for this case, improving the efficiency of the system.

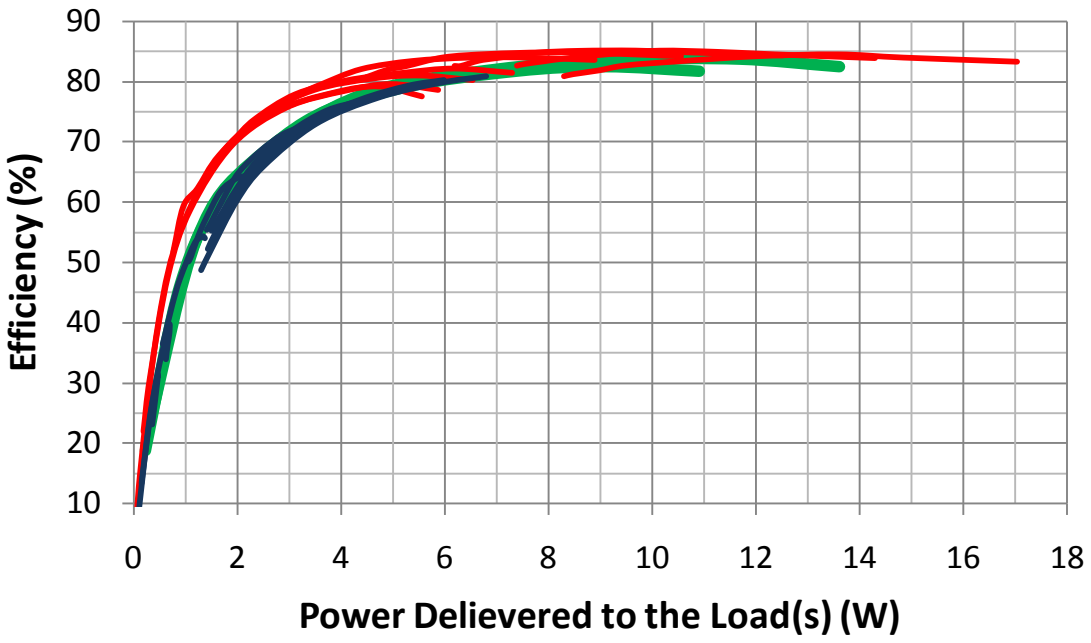

Figure 7-18. Efficiency-power plot of two sets of dual load measurements and two sets of single load measurements. (Green lines: Single receiver, Blue lines: Dual receivers on single transmitting coil, Red lines: Dual receivers on dual transmitting coil)

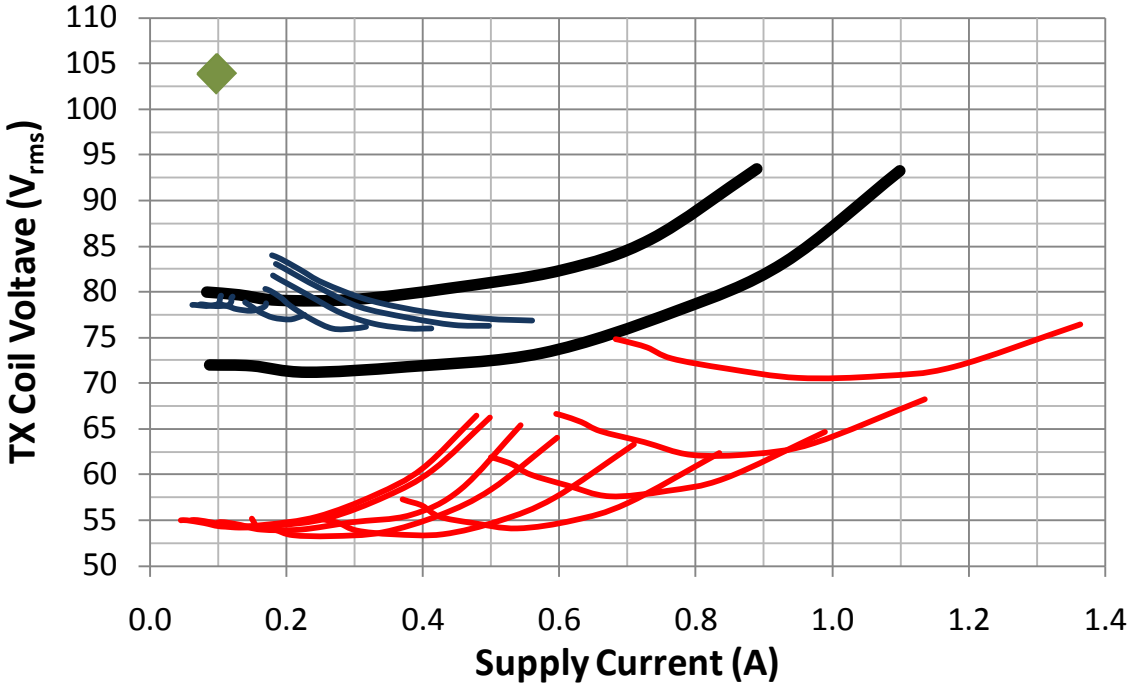

Figure 7-19. Transmitter coil voltage and supply current space. (Green diamond: No load, Black lines: Single receiver, Blue lines: Dual receivers on single transmitting coil, Read lines: Dual receiver on dual transmitting coil)

Figure 7-19 shows the transmitter coil voltage and supply current space for various loading conditions which is similar to Figure 7-12. Therefore, it is possible to extend the same load detection technique for a M:N coupling structure. The discrepancies shown in Figure 7-19 for the single receiver case is due to the tolerance of the hand wounded transmitting coil as discussed earlier. It is observed that the two different conditions of loading the transmitting coils with two receivers resulted in two distinctive zones in the transmitter coil voltage and supply current space. By using techniques of pattern recognition and sufficient training sample size, the transmitter is able to determine the number of receivers on each individual coil. Although there are some overlaps between a single receiver setup and the setup with two receivers on a single transmitting coil, the trends of the lines are distinctively different following a different charge profile trend. The trends can be modeled into different sets of Markov Chains for which over time the state of the system can be determined.

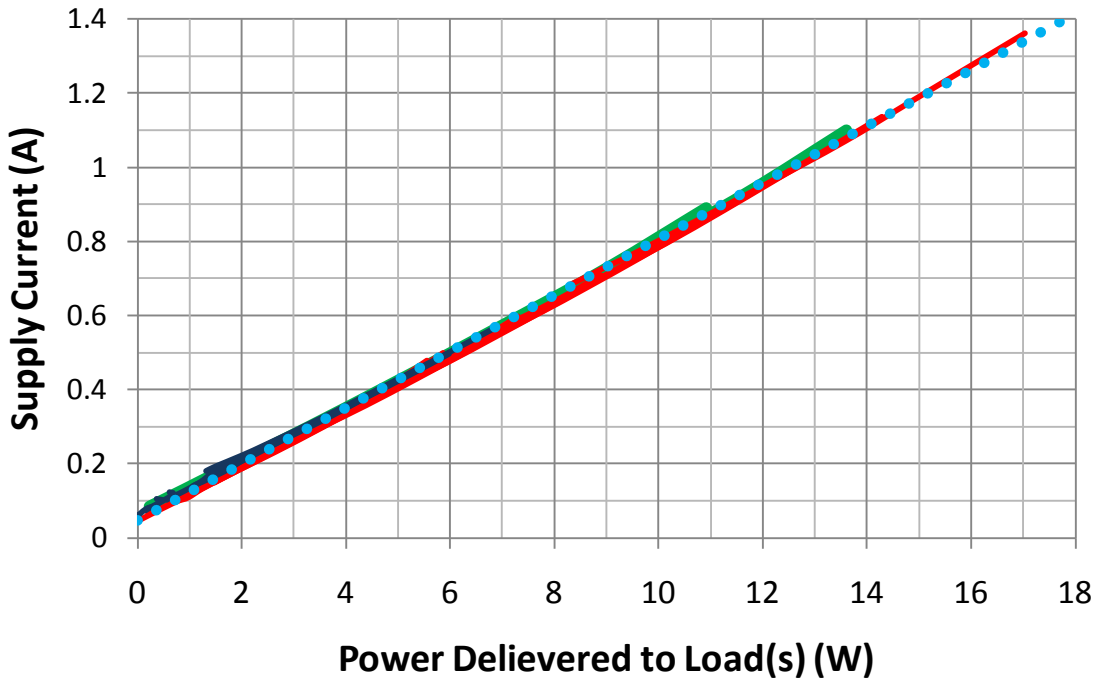

Figure 7-20. Linear relationship between supply current and power delivered to the loads for all 4 sets of measurements. Solid dashed line: y = 0.076x + 0.048.

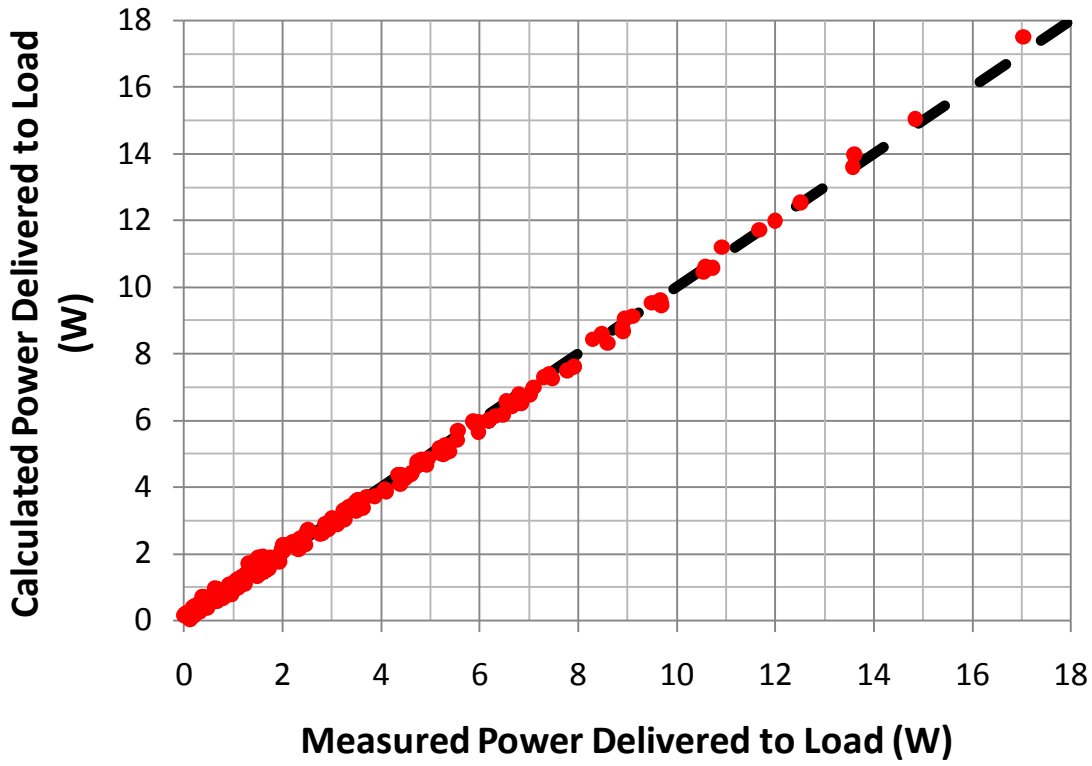

Figure 7-21. Power delivery error distribution plot. Calculated power delivery is based on measured supply current. Solid dashed line: ideal error free calculation.

Figure 7-20 shows that the linear relationship between the supply current and power delivered to the load(s) still holds for a M:N coupling structure regardless of the placement of the two receivers. The linear relationship can be described by the equation y= 0.067x + 0.048. Figure 7-21 shows the power delivery error distribution plot using the equation to calculate the delivered power. The average error is found to be 0.017W and standard deviation error is found to be 0.183W out of a maximum of 18W power delivery. This shows a very small spread in errors which verified the feasibility of using the power tracking scheme on a M:N coupling structure. Similar trends are expected for higher number of transmitting and receiving coils attached to the class E transmitter. However, as more transmitting coils are attached in parallel to a single transmitter, the effective inductance will be reduced causing the circuit to be more sensitive. Increasing the transmitting coil size or number of turns will help to mitigate the effect.

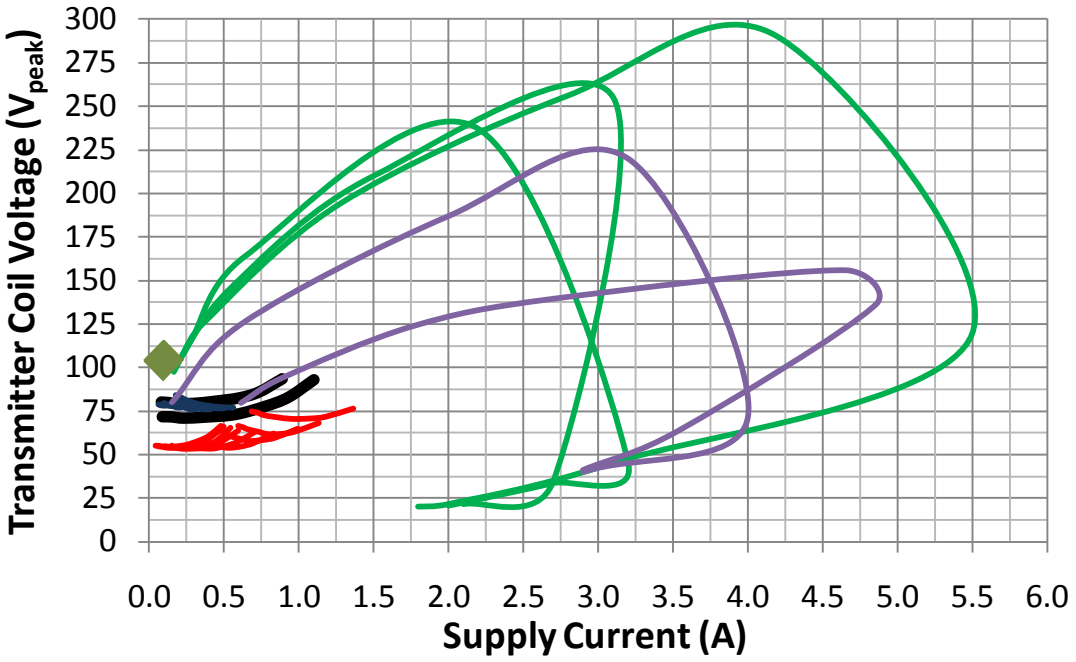

Figure 7-22. Transmitter coil voltage and supply current space with fault tests. (Green lines: Fault tests without valid receiver on one of the coil, Purple lines: Fault tests with a valid receiver on one of the transmitting coils)

Five different common fault scenarios are being studied for the M:N coupling structure. They all involved a large piece of copper sheet (30 cm x 30 cm) sliding across the coil or being brought to close proximity on the same plane. All of the fault lines green and purple follow a clockwise trend with increasing severity of the fault (proximity of copper sheet or amount of overlap). The green lines in Figure 7-21 show three different fault scenarios without any valid receiver being placed on one of the transmitting coils. The detection scheme is capable of detecting a fault condition when a valid load is not placed on one of the transmitting coil (green line), but there are some overlaps between the load conditions and fault conditions when a valid load is being place on one of the transmitting coils while a piece of copper sheet is being slide across or brought closer to the unloaded transmitting coil (purple line). Although the overlapping region is small, an analysis is required to determine if it is acceptable for a “minor” fault to be considered safe.

The analysis starts with looking at what happens when a sheet of copper is partially overlapped onto a transmitting coil. Due to the close proximity of the copper or any electric conductor of sufficient mass, the self inductance of the coil will be reduced. The reduction is due to the proximity and amount of overlap. For this setup, two coils are driven in parallel. Therefore, with the reduction of self inductance of one of the transmitting coils, due to a copper sheet in close proximity, the total effective inductance looking into the pair of coils will be reduced as well. The reduction in effective inductance of the dual parallel structure will cause a reduction in the phase angle of Z_{tx}, making Z_{tx} more capacitive. A more capacitive Z_{tx} will result in higher power being transferred or higher unregulated receiver voltage. This observation is similar to decreasing C_{out} which will be discussed in Chapter 8. Although a slight overlap between the unloaded transmitting coil and a piece of copper sheet may seem to of not a major problem, it will cause the voltage before the voltage regulator of the valid load to increase. Therefore, if the maximum input voltage of the voltage regulator used on the receiver has insufficient margin, the voltage regulator will be damaged. To prevent the voltage regulator from being damaged, the voltage regulator must have a high input voltage tolerance which makes the receiver bulking and costly. It will also limit the selection of voltage regulators available to the designer.

A potential solution to the problem is to design the transmitter unit so that each transmitting coil is driven by an independent transmitter using a master clock and a master micro-controller as shown in Figure 7-22. Load/fault detection is done by each individual pair of transmitters. Since the coupling between neighboring coils is weak, the system can be assumed to consist of multiple 1:1 or 1:N transmitting systems which the load/fault detection scheme is proven to be effective earlier in this chapter. Depending on the load conditions, the transmitters

can be turned on and off accordingly, making it more energy efficient when one of the coils is unloaded. In addition, if a fault occurs on one of the coils it can be shut down while power delivery is not affected by the other transmitting coil. Since each transmitting coil will require their respective set of class E transmitter circuitry, it will increase the board size, components count and potentially increase the cost. However, each class E transmitter will most probably be required to drive a single load instead of multiple loads. Thus, the power handling of each transmitter will be reduced, allowing the use of smaller and more compact components. Due to the reduction in component size and power handling, making each transmitter more compact and cheaper offset the cost of multiple units.

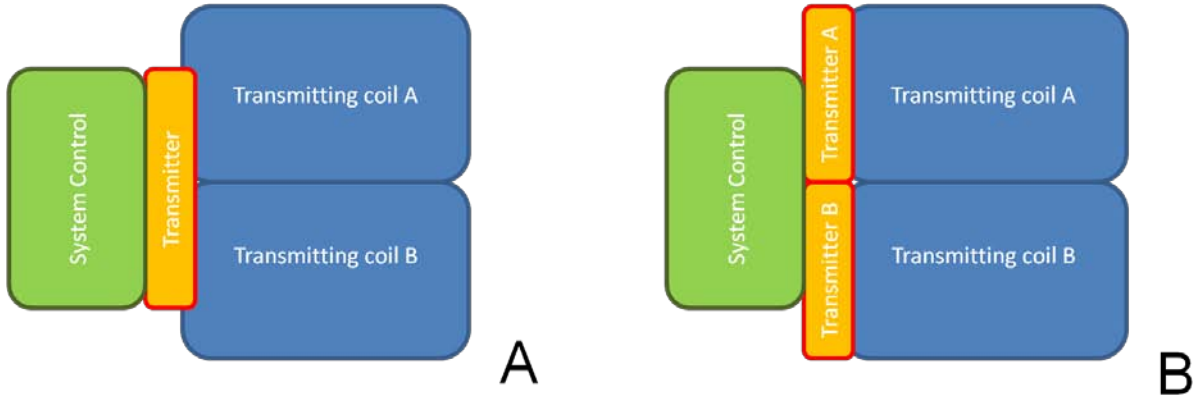

Figure 7-23. Different methods of driving a 2:N structure. A) Original M:N design for the experimental verification and B) proposed improved M:N design.

7.3.2 Removing L_{out} from Transmitter

Since a Class E power amplifier only requires a phase angle of Z_{tx} to be from 40° to 70°, it is possible to remove L_{out} from the transmitter load network using part of the leakage inductance (imaginary part of Equation 4-6) of the transmitting coil as L_{out} (shown in Figure 7-24) as long as the phase angle can be maintained within the high efficiency range across all receiver load resistances. Therefore, the design of the transmitting and receiving coils must be integrated as part of the design rule and can no longer be treated as a generic linear block. Since L_{out} is the

component with the highest loss in the class E transmitter, removing L_{out} will improve the efficiency by at least 5%. In addition, when the transmitting coil is not loaded, a significant amount of power is lost across the inductor and the transmitting coil. As Litz wire is being used to fabricate the transmitting coil, most of the losses will be across L_{out}. Therefore, by removing L_{out} from the system, the no load power consumption can be reduced significantly as well. However, doing so will cause the higher order harmonics content to be stronger across the coil as L_{out} also serves as a low pass mechanism. The radiation efficiency of the coil improves with the increase in frequency, resulting in the higher order harmonics being transmitted into free space. Therefore, care must be taken during the design to ensure the emission is low enough to pass the FCC part 18 test, this is important especially for high power system.

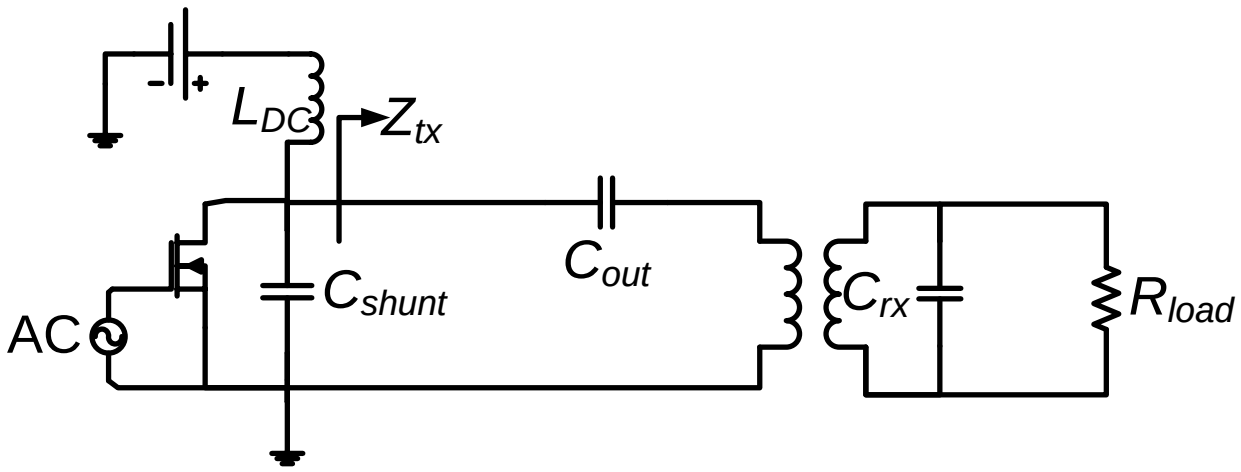

Figure 7-24. Block diagram of wireless system without L_{out}.

Using the same experimental setup as the M:N coupling structure, L_{out} is removed and C_{out} is tuned to compensate for the missing positive reactance by decreasing its capacitance value. The same fault test procedures are carried out on the test bench with Lout removed so that a fair analysis can be made. Results of the fault tests using the same format as Figure 7-22 are presented in Figure 7-25.

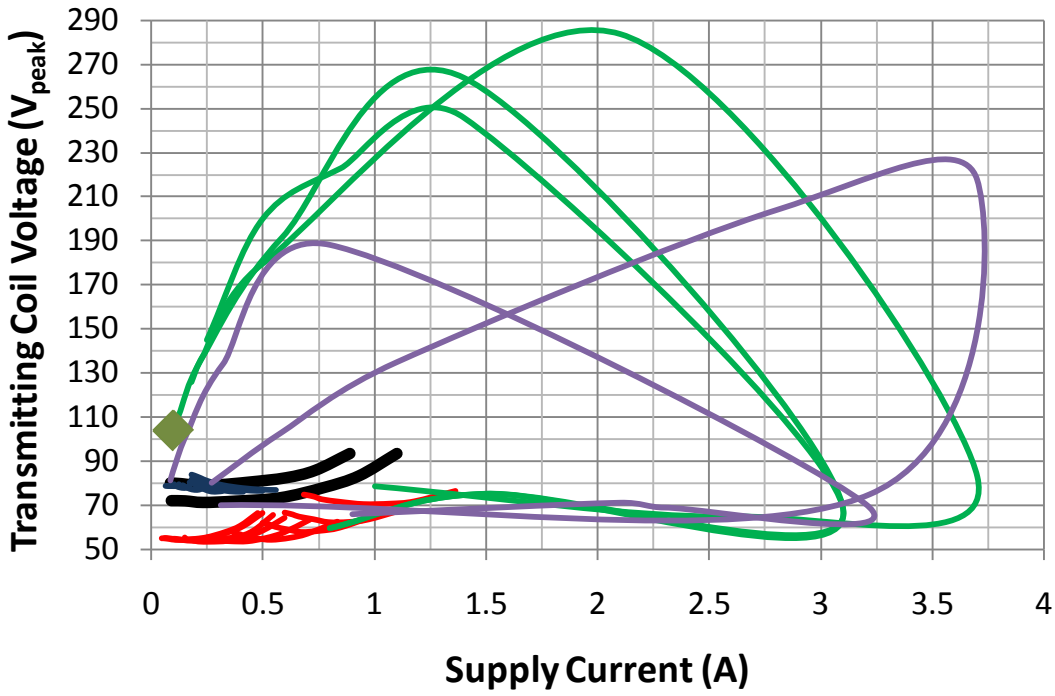

Figure 7-25. Transmitter coil voltage and supply current space with fault tests with L_{out} removed. (Green lines: Fault tests without valid receiver on one of the coil, Purple lines: Fault tests with a valid receiver on one of the transmitting coils)

Similar initial trend of the test results shown in Figure 7-22 was observed for all the five different fault tests with the lines going in a clockwise direction. However, the lines follow an upward trend while looping back and moving into the low voltage low current region instead of the downward trend as show in Figure 7-22. This results in the certain conditions of the fault mode overlapping with the safe or valid load region. All of the conditions involved the copper sheet being in close proximity or almost complete overlap onto the transmitting coil. This condition is a common case when the transmitting coil is accidentally flipped over onto a metallic table top or an unshielded transmitting coil being placed onto of a metallic table top. By removing L_{out}t from the transmitter using existing circuitry, the system will be unable to differentiate between a valid load and a fault mode under certain conditions. Therefore, to ensure robust operation while removing L_{out}, modifications of the detection circuit are required.

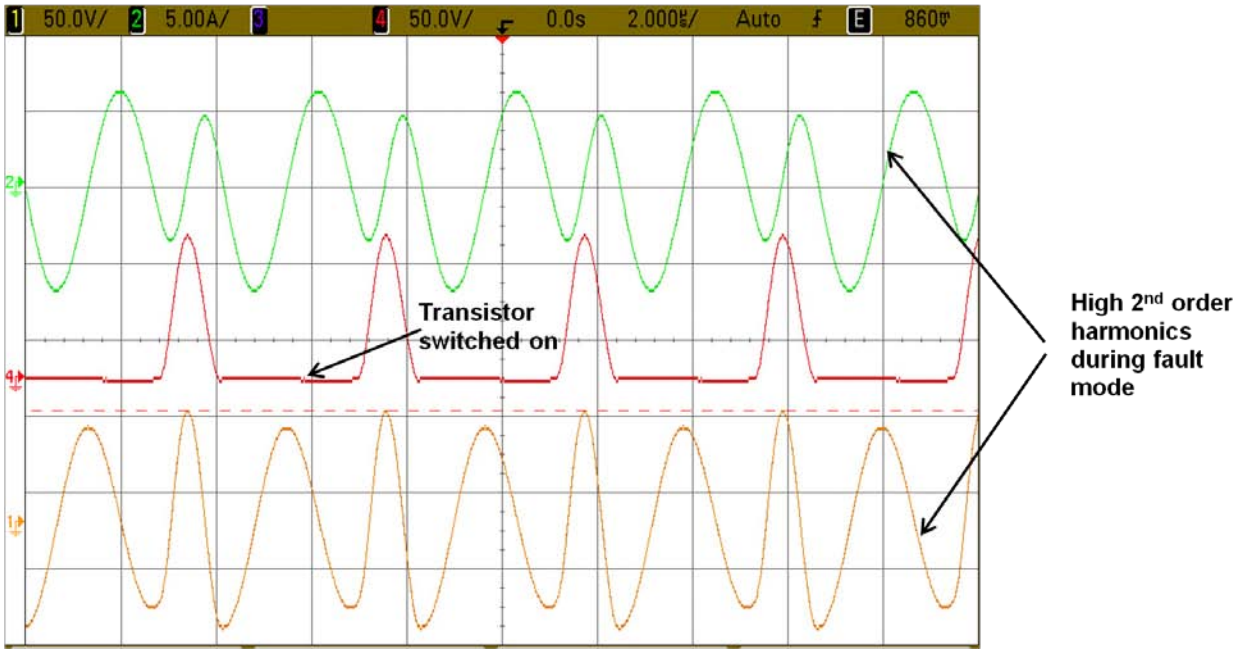

Figure 7-26. Waveform of the transmitter circuit without L_{out} when fault conditions overlaps with valid load conditions. (Red: Drain voltage, Orange: Coil voltage, Green: Coil Current)

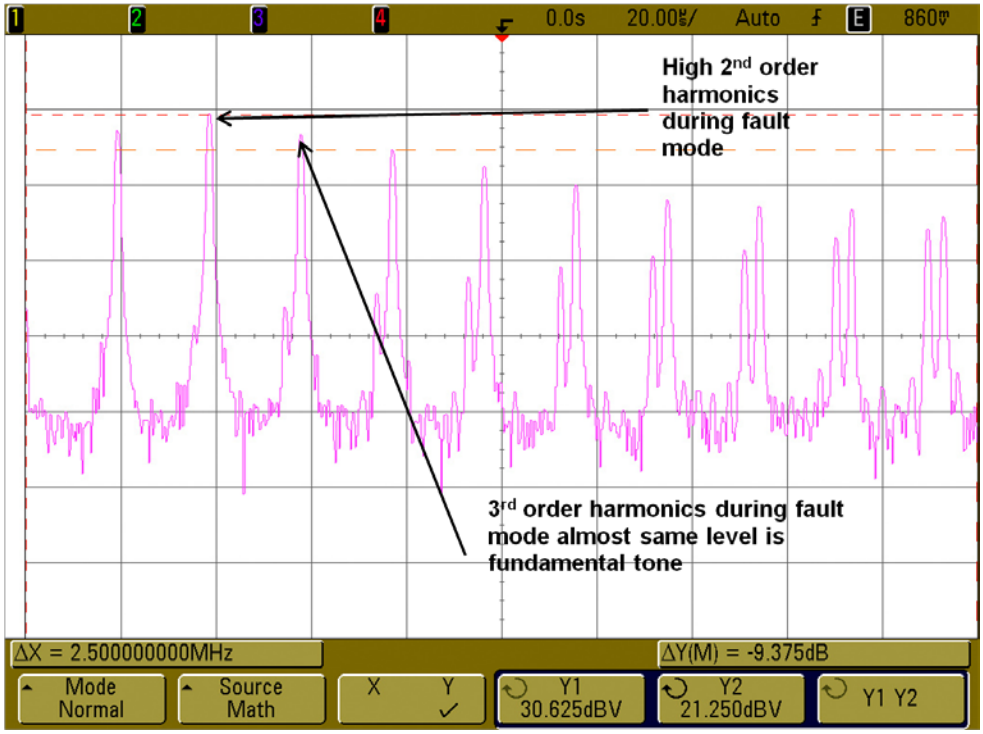

Figure 7-27. Spectrum of transmitter coil voltage without L_{out} when fault conditions overlaps with valid load conditions.

To better understand the mechanism which cause this upward trend to happen, the transmitting coil voltage and its spectrum was captured using an oscilloscope. As seen from Figure 7-26, the second harmonic is much stronger than the fundamental tone for both the transmitting coil voltage and coil current with the transmitting coil voltage at approximately 150 V peak to peak. This is supported by the measured spectrum of the transmitter coil voltage shown in Figure 7-27. The fundamental tone is approximately 27 dBV while the second harmonic is almost 31 dBV. The second harmonic can be considered as detection noise as the load/fault detection scheme neglects the effects of higher order harmonics. With a stronger second order harmonic on top of the fundamental tone, the transmitter coil voltage will be larger than expected, explaining why the transmitting coil voltage is larger than expected or has an upward trend into the valid load region under certain fault conditions.

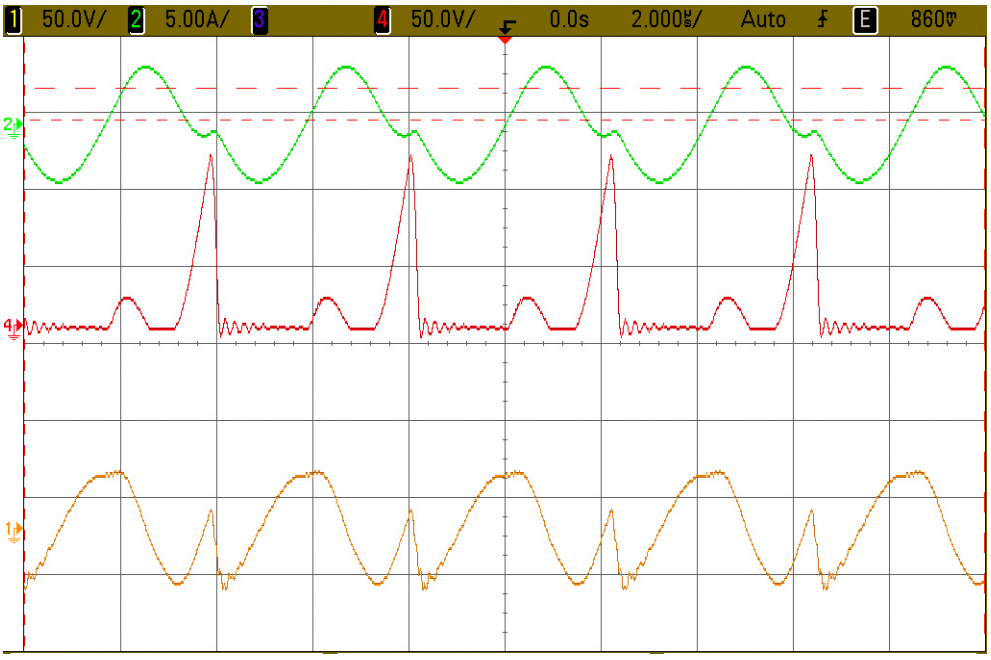

Figure 7-28. Waveform of the transmitter circuit with L_{out} when fault conditions overlaps with valid load conditions. (Red: Drain voltage, Orange: Coil voltage, Green: Coil Current)

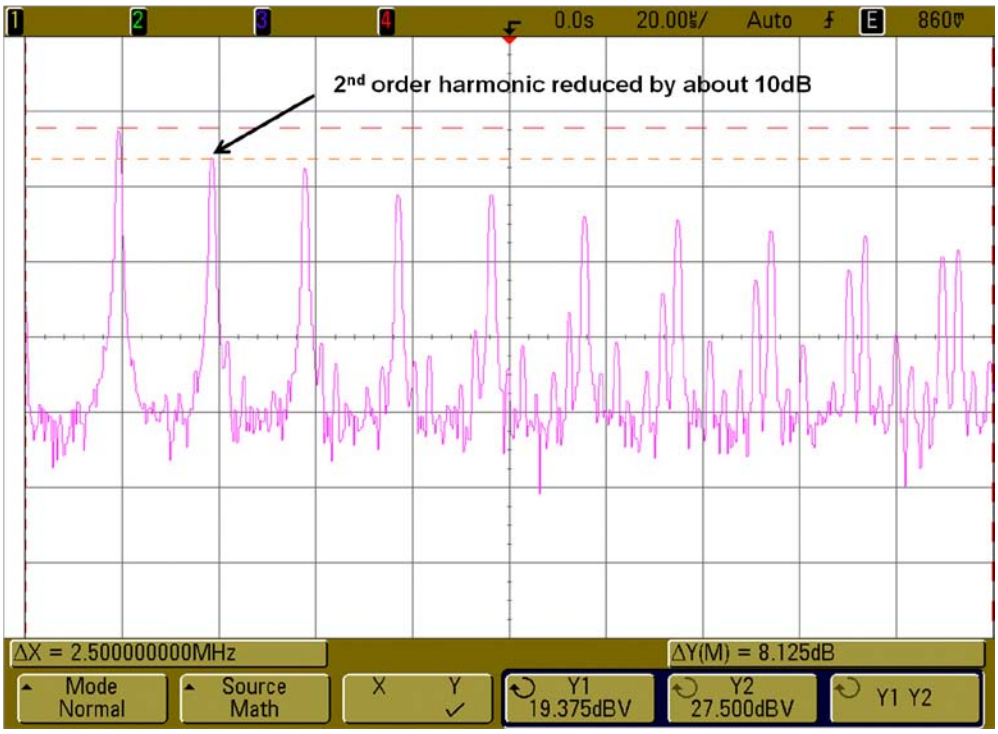

Figure 7-29. Spectrum of transmitter coil voltage with L_{out} when fault conditions overlaps with valid load conditions.

Figure 7-28 and Figure 7-29 show the same waveforms as Figure 7-25 and Figure 7-26 but with L_{out} added back to the transmitter circuit. The higher order harmonic are being suppressed by L_{out}. The second harmonic is reduced by approximately 10dB at 19 dBV with the fundamental tone remained at approximately 27 dBV. The transmitting coil voltage is reduced significantly from 150 V peak to peak to 70 V peak to peak. This brings the transmitting coil voltage below the safe zone lower threshold.

Although removing L_{out} is able to improve efficiency and reduce heating, higher harmonics contents which are filtered by L_{out} are allowed to pass. This affects the load/fault detection scheme as detection noise. The error in detection can also be mitigated by using a simple low pass RC filter before the detection diode to reduce the higher order harmonics. This can be realized by adding an appropriate capacitor to ground between R6 and D2 of Figure 7-7. If needed, a higher order low pass filter can be added in the coil voltage detection path to further

reduce the higher order harmonics. By adding the low pass filter, the original detection scheme can be used without causing any detection error. However, the higher order harmonics voltage across the transmitting coil will still be a potential issue during the emission test as the same transmitting coil will become a better radiator with the increase of operating frequency.

CHAPTER 8
RECEIVER VOLTAGE CONTROL

Although, the system is able to reduce the power delivered to the receiver when the effective load resistance increases, the unregulated DC voltage at the receiver will increase with increasing load resistance. The swing in receiver voltage is not important when the power level of the system is low as the voltage regulator at the receiver is able to tolerate such fluctuations. However, the range of voltage swing increases with increasing power rating of the system. A buck regulator will have poorer efficiency with a higher input voltage and tend to be larger in size as external switch transistors are required to perform the regulation. In addition, if a high input voltage is required for the receiver voltage regulator, the choices for the system designer will be limited and BOM cost will be higher as well. Therefore, it will be desirable for the unregulated voltage at the receiver to be bounded to a certain range.

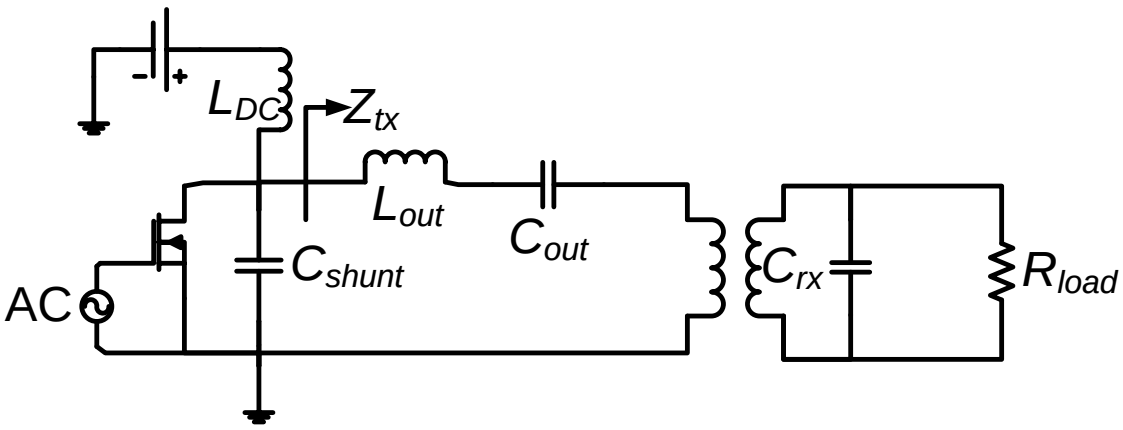

Figure 8-1. Block diagram of wireless power system.

From the simplified block diagram of the system as shown in Figure 8-1, there are limited parameters of the system that one can vary. Most probably the structure of the coil will be fixed, any attempt to vary the coil structure in terms of turns and area will make the system complicated. Capacitor C_{rx} can be tuned to control the received power level. There are two ways that C_{rx} can be tuned; it can be achieved by either using a varactor or switching between banks of

capacitors. Since the system is intended to operate with the frequency range of less than 1 MHz, it will take a considerable amount of capacitance to achieve an appropriate tuning range. Although, it is possible to achieve it with switchable banks of capacitors, it is not practical for the current implementation unless a high voltage and current switch is realized in the form of an integrated circuit. In addition, it is desirable to keep the receiver as simple as possible and move all the complexity to the transmitter as a transmitter will typically be used to power multiple receivers concurrently or at different instances. There are three possible ways to achieve voltage control of the unregulated receiver voltage on the transmitter. They are varying supply voltage, varying operating frequency and varying C_{out}. Each option will be studied with experimental results from a one-to-one setup test bench. The test bench used in the experiment is intended for high power applications (up to 80W) operating at 240 kHz and a supply voltage of 30V with the transmitting coil of 25 cm x 35 cm and the receiving coil is 12 cm x 12 cm. The findings should apply across all power levels and coil sizes with different level of tolerances.

8.1 Varying Supply Voltage to Achieve Receiver Voltage Control

The most straightforward way to achieve power control and receiver voltage control is to control the supply voltage of the transmitter. Experimental results by sweeping the supply voltage from 18 V to 30 V in steps on 1 V as shown in Figure 8-2 and Figure 8-3 further verify the feasibility of supply voltage control to achieve power control and receiver voltage control. From Figure 8-2, high efficiency is achieved across the whole range of supply voltages with efficiency peaking at different power level depending on the supply voltage. If the system is able to control the supply voltage from very low voltages such 6 V up to 30 V in sufficiently small steps, the system will be able to achieve better than 80% system efficiency regardless of loading conditions. However, this is not practical because it will require the system to be driven from a variable output voltage regulator instead of directly from a DC source. This will significantly

impact the system efficient especially when the supply voltage is very low e.g. 9 V. This is because a buck regulator becomes less efficiency when the difference between the input and output voltages increases. In addition, a high efficiency high power voltage regulator with a variable output is complex and costly. It is typically achieved by using an off the shelf variable voltage regulator and replacing one of the feedback resistors with a digital rheostat. The digital rheostat is then controlled by the micro-controller which is used for load and fault mode detection.

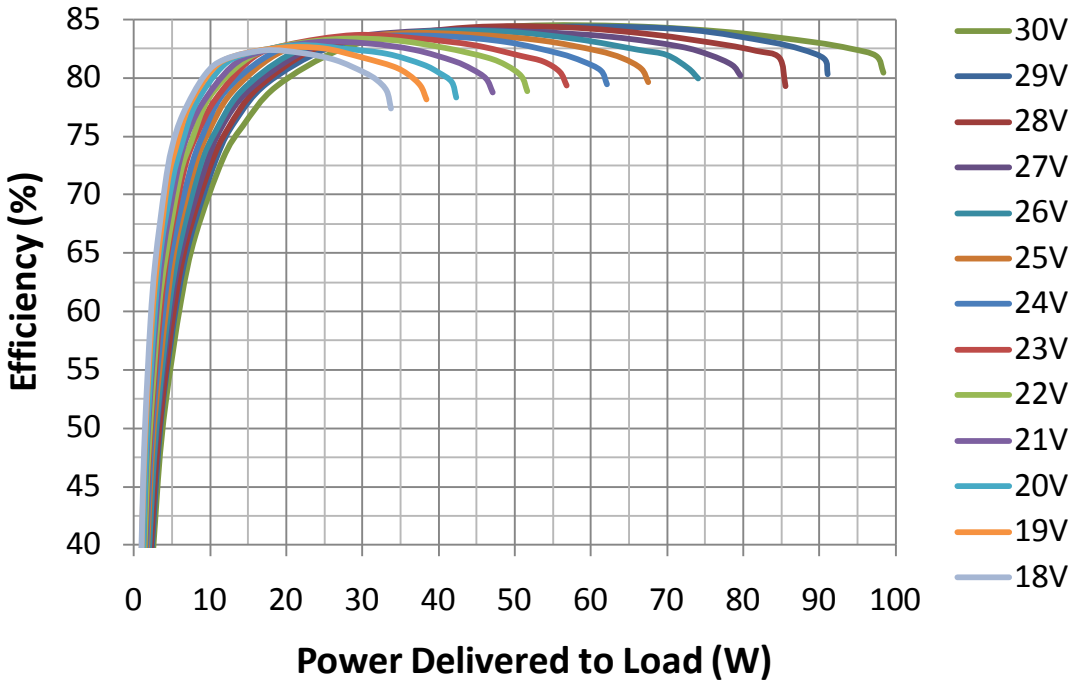

Figure 8-2. Efficiency-power plot for supply voltage from 18 V to 30 V in steps of 1 V.

Either the load tracking technique proposed in Chapter 7 or a communication link can be used to track the loading condition for a one to one load system. The supply voltage can be varied to optimize for the specific load condition. This technique can be applied to the other two following methods of controlling receiver voltage. Each supply voltage will have a different power delivery profile with respect to supply current. However, since the relationship between supply current and power delivered can be approximated by a linear relationship, the profile is

condensed into two data points, the gradient and intercept. As discussed in Chapter 7, the no-load requires four data points. The safe zone which was also discussed in Chapter 7 requires additional 5 data points. Therefore, each voltage point will require 11 data points and if each data point takes up 2 bytes of memory, each supply voltage point will require 22 bytes. A reasonable system will require a supply voltage resolution from 20 to 50 points, requiring 440 bytes or 1100 bytes of memory space on the micro-controller.

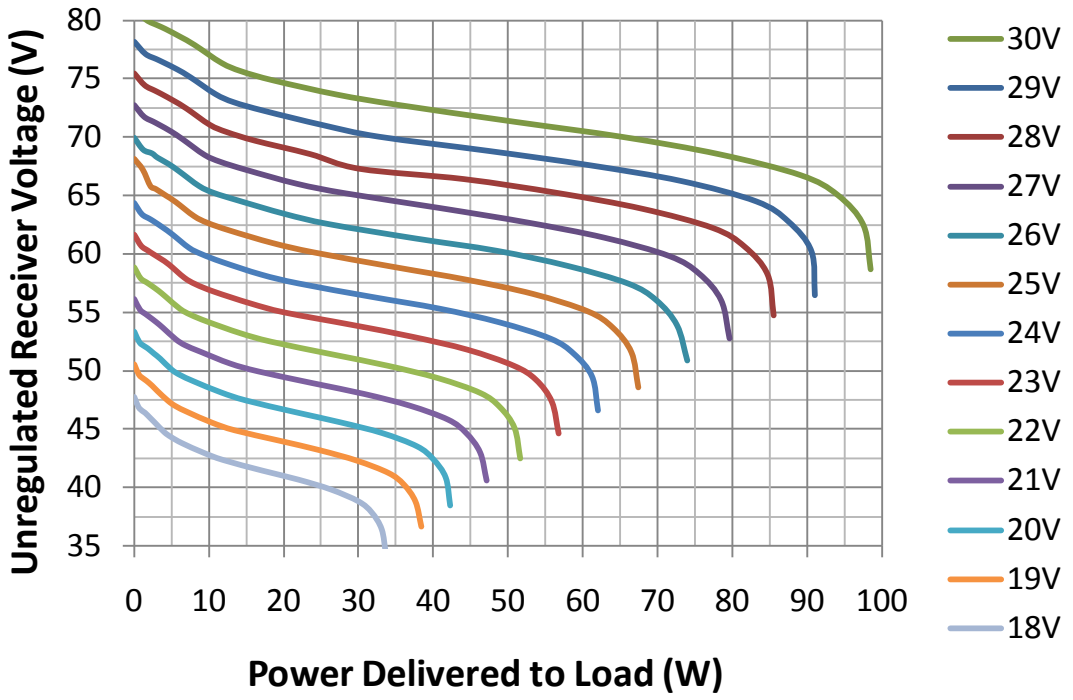

Figure 8-3. Receiver voltage-power plot for supply voltage from 18 V to 30 V in steps of 1 V.

As shown in Figure 8-3, the unregulated receiver voltage decreases with decreasing supply voltage at the same power level. Therefore, the receiver voltage can be kept within a tight bounded range for power delivery across a large power band. Depending on the acceptable voltage ripples and with sufficient resolution achieved on the supply voltage control, it is possible for the system to achieve wireless power transfer without a voltage regulator on the receiver. This is only true if and only if the coupling coefficient remains the same for all possible

placements. For a practical system, such a requirement will not be realistic unless the receiving coil is large enough to average the magnetic field variation or a locking mechanism is in place to ensure a fix placement. If so it will defeat the purpose of providing some level of mobility for a wireless power system unless it is used in some unique applications. Therefore, to ensure 100% stability without the system drifting in the wrong direction and still attain some level of mobility, a communication link is required to close the loop.

From Figure 8-3 it can be seen that if the system is to achieve a power handling of up to 40 W, the lowest possible voltage to achieve such a scheme without a voltage regulator on the receiver will be 42.5V (supply voltage 20 V line). The lowest voltage for such a power level is high because of high leakage inductances on both the transmitting and receiving coils. Such high leakage inductances are due to poor coupling coefficient which results from the size ratio between the transmitting and receiving coil (transmitting coil is 5 times larger than receiving coil). In order to bring the voltage lower, the receiving coil needs to become larger as relative to the transmitting coil (reduce leakage inductances) or have less turns (trading voltage for current at the expense of resistive losses in the receiving coil). This brings another set of constraints in the system design embedding the coil design into an integrated part of the system design. Such design constraints are unique to specific applications which are beyond the scope of this discussion and can be covered as potential future work for more tightly coupled one to one wireless power transmission system.

Figure 8-4 shows the linear relationship between the supply current and power delivered to the load for different supply voltage (18V to 30V in steps of 1V). The y-intercept for all the supply voltages remains approximately the same, but the gradient decreases with increasing supply voltage. The trend can be explain by the fact that for the same power level at similar

efficiency, the supply current decreases with increasing supply voltage to maintain similar power level and efficiency. The difference will become more significant with the increase of power delivered to the load resulting in a fan out plot from the y-intercept. Therefore, each supply voltage will require a new data set to describe the trend. It is possible to use a single y-intercept for all supply voltages if the tolerance for power tracking is relaxed. The difference will not be significant if the power handling of the system is sufficiently large (>50 W).

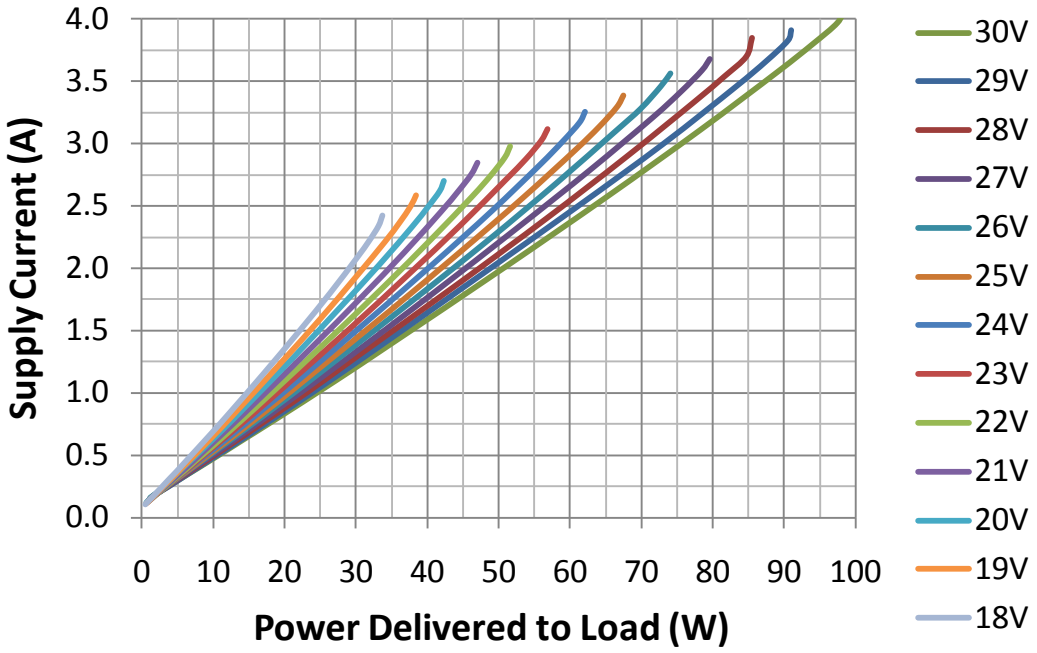

Figure 8-4. Linear relationship between supply current and power delivered to the load for supply voltage from 18 V to 30 V in steps of 1 V.

In conclusion, varying the supply voltage is an effective way to control the power delivery as well as the unregulated receiver voltage. With sufficient resolution, the system is able to deliver a stable receiver voltage for which the voltage regulator can be removed if and only if the coupling coefficient is sufficiently constant for all placement or both the transmitting and receiving coil is fixed in position. Since it is meaningless to design a wireless power system without any freedom in placement and it is also not possible to design a transmitting coil with a 100% even field distribution, the solution is not practical without a communication link to

provide a feedback loop. By adding a voltage regulator between the DC supply and the transmitter to control the supply voltage, the system will incur additional power losses which might result in thermal and efficiency issues. In addition, the complexity, size and cost added to control the supply voltage can be considerable. Therefore, varying supply voltage to control unregulated voltage and power delivery is an effective technique but not practical.

8.2 Varying Operating Frequency to Achieve Receiver Voltage Control

Varying the operating frequency can be used to indirectly tune to impedance looking into the transmitter load network after C_{shunt} as shown in Figure 8-1. The impedance looking into the transmitter load network (Z_{tx}) can be simplified into a series network of a capacitor, an inductor and a load resistance under any load condition. To ensure the effective Z_{tx} is inductive, the operating frequency is selected to be higher than the self resonance frequency of the LC network not taking the load resistance into account. Therefore, Z_{tx} will be less inductive with decreasing operating frequency, decreasing the phase of Z_{tx}, thus, increasing power delivery as well as unregulated receiver coil voltage, vice versa. However, the above assumption is true if and only if ZVS/ZDS operation still holds at the specification load impedance without changing C_{shunt} in Figure 8-1. Although making C_{shunt} tunable will improve the frequency dynamic range of a frequency tunable class E power amplifier, it will also increase its complexity. If the ZVS/ZDS operation is not valid, there will be an increase in device stresses and degradation in efficiency.

Due to the large amount of data and ease of using the nominal operating frequency as a reference point, the analysis is split into two different frequency ranges. The first frequency range (Figure 8-5 and Figure 8-6) will be for operating frequency above the selected operating frequency in steps of 2 kHz up to 250 kHz and the second frequency range (Figure 8-7 and Figure 8-8) will be for operating frequency below the selected operating frequency in steps of 1 kHz down to 235 kHz.

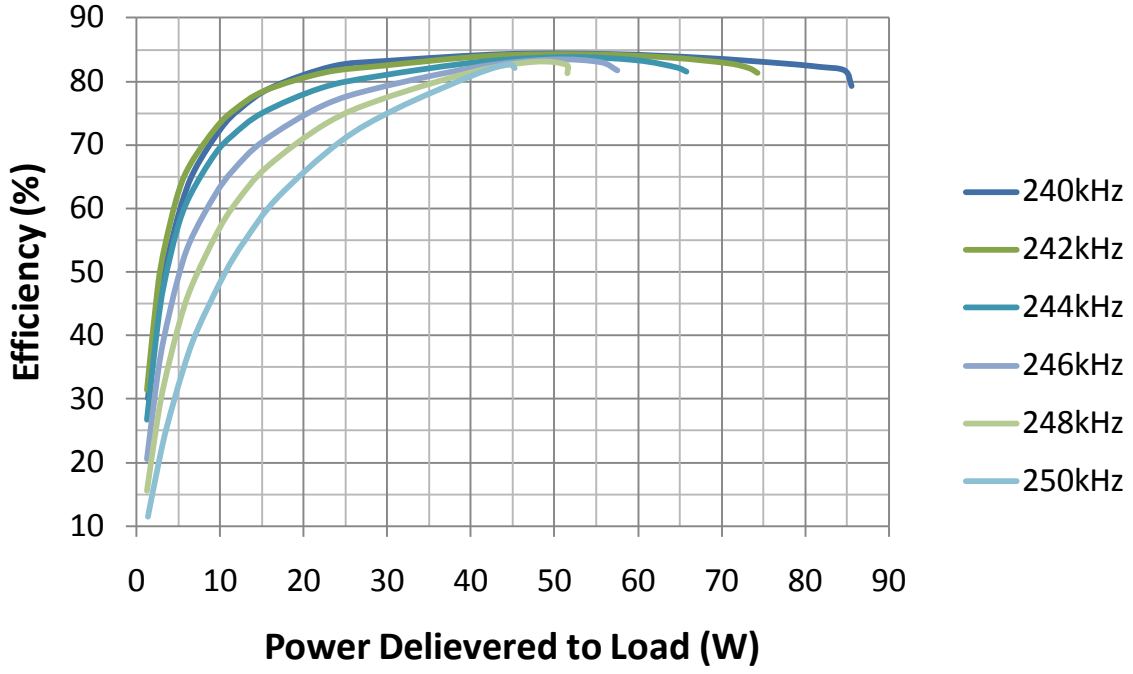

Figure 8-5. Efficiency-Power plot for operating frequency from 240 kHz to 250 kHz in steps of 2 kHz.

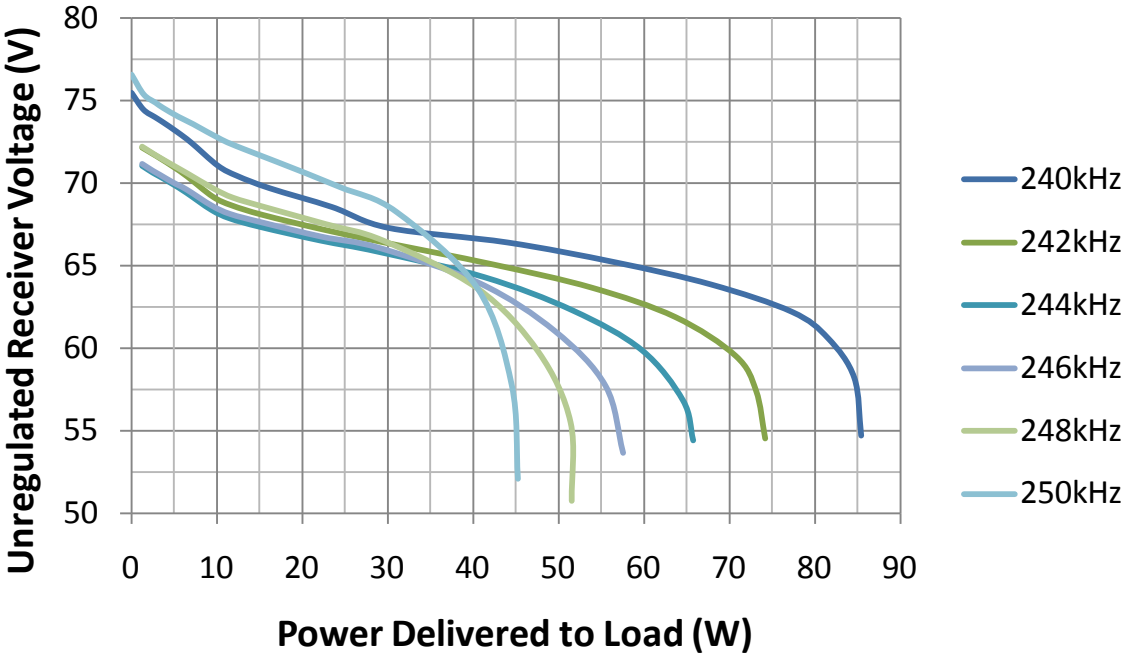

Figure 8-6. Receiver voltage-power plot for operating frequency from 240 kHz to 250 kHz in steps of 2 kHz.

As shown in Figure 8-5, the power delivered to the load decreases with increasing operating frequency because Z_{tx} becomes more inductive decreasing real power and increasing reactive power as discussed in Chapter 1. The unregulated receiver voltage decreases marginally with increasing operating frequency up to 244 kHz. However, as seen from Figure 8-5 the system efficiency starts to degrade at frequencies above 244 kHz. This is due to ZVS/ZDS operation does not hold anymore. The non-ideal waveform causes the switching losses across the drain to increase. The switching losses are predominately caused by the transistor being turned on before drain voltage drops to zero due to a shorter period with the increase in frequency. This results in the charges from C_{shunt} are being dumped across the transistor during turn on at high currents.

The unregulated receiver voltage also starts to become larger at lighter load especially during open circuit conditions when the operating frequency is increased to above 244 kHz as shown in Figure 8-6. Although Z_{tx} is more inductive with the increase in operating frequency limiting the power delivery, the coupling is also increased increasing the voltage induced on the receiver. As shown in Equation 2-6 the increase of coupling with respect to operating frequency is a square law effect. Therefore, there are two competing mechanisms affecting the power delivery and unregulated receiver voltage working against each other. In addition to the non ZVS/ZDS operation, Z_{tx} swings over a larger range with the same components on the transmitter and receiver load resistance at higher operating frequencies. Therefore, the range and value of unregulated receiver voltages increases with operating frequency as shown in Figure 8-6.

As shown in Figure 8-7, the power delivered to the load increases with decreasing operating frequency because Z_{tx} becomes more capacitive with decreasing frequency. The unregulated receiver voltage increases marginally with decreasing operating frequency down to

235 kHz and below. This trend is expected with the increase in power delivery. It can be observed from Figure 8-7 that the system efficiency starts to degrade much slower than increasing the operating frequency because ZVS/ZDS operation still holds. Although ZVS/ZDS operation does still hold, the zero crossing occurs earlier with decreasing frequency. With the decrease in operating frequency the period of each cycle gets longer but the drain waveform remains similar, causing the zero crossing of the drain waveform to occur earlier before the transistor is turned on. Minimum amount of power is still lost via the built in diode of the transistor causing a slight drop in system efficiency. The power loss via the built in diode can be reduced by adding an external diode such as a schottky diode with a faster transition time and smaller turn on voltage. The analysis is only valid if ZVS/ZDS operation still holds while the operating frequency is decreased.

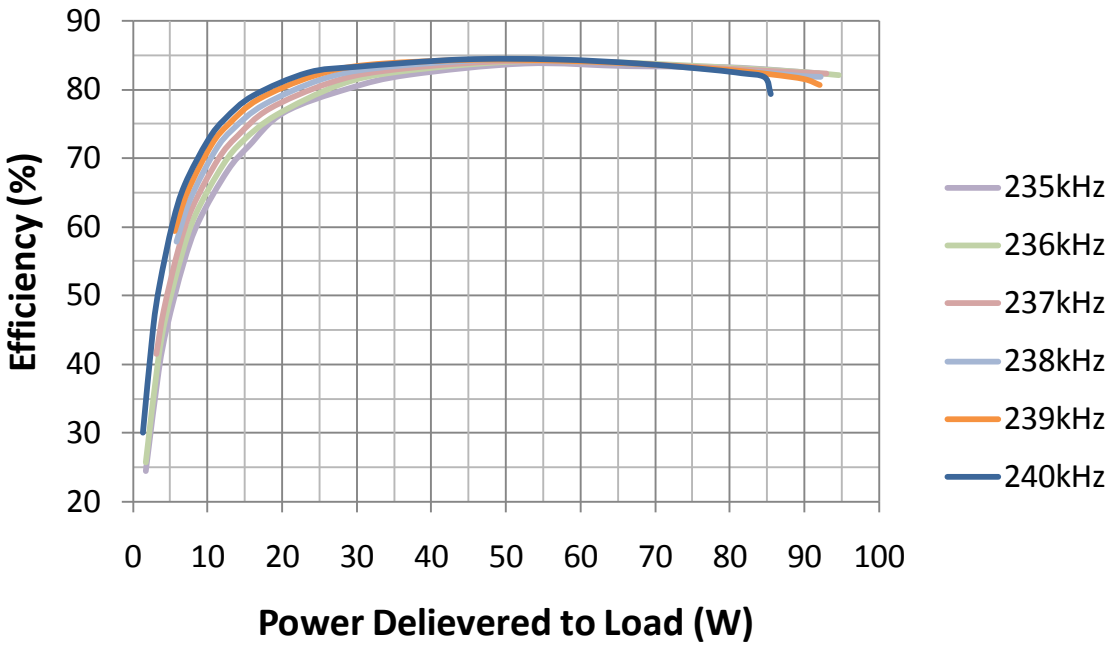

Figure 8-7. Efficiency-power plot for operating frequency from 235 kHz to 240 kHz in steps of 1 kHz.

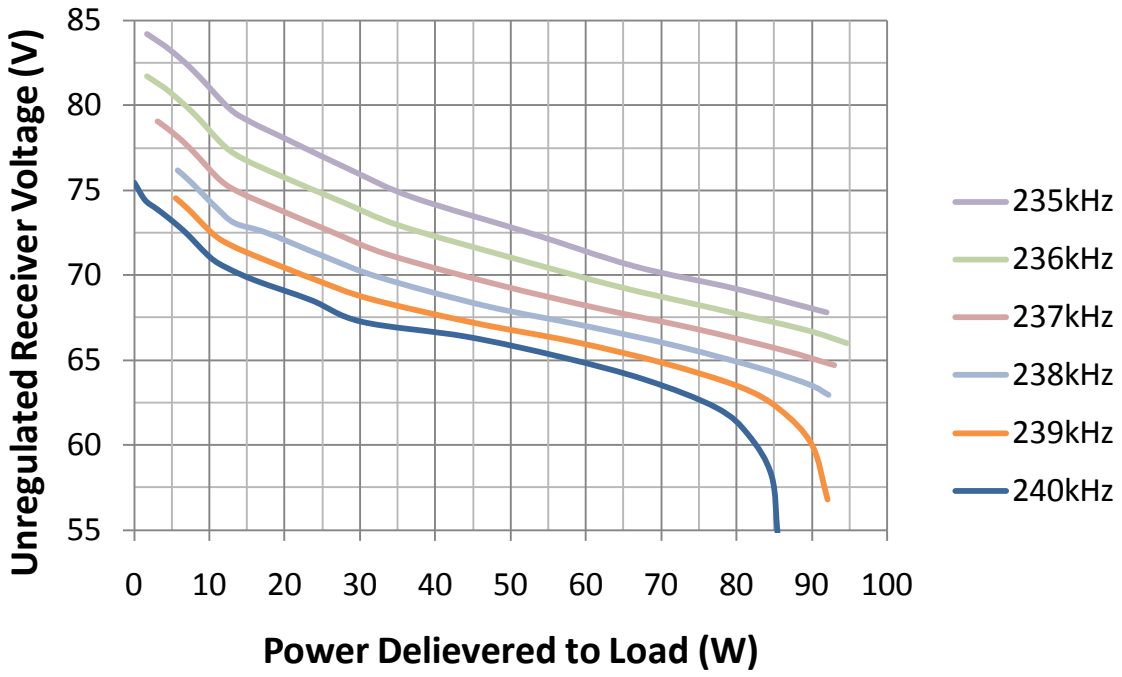

Figure 8-8. Receiver voltage-power plot for operating frequency from 235 kHz to 240 kHz in steps of 1 kHz.

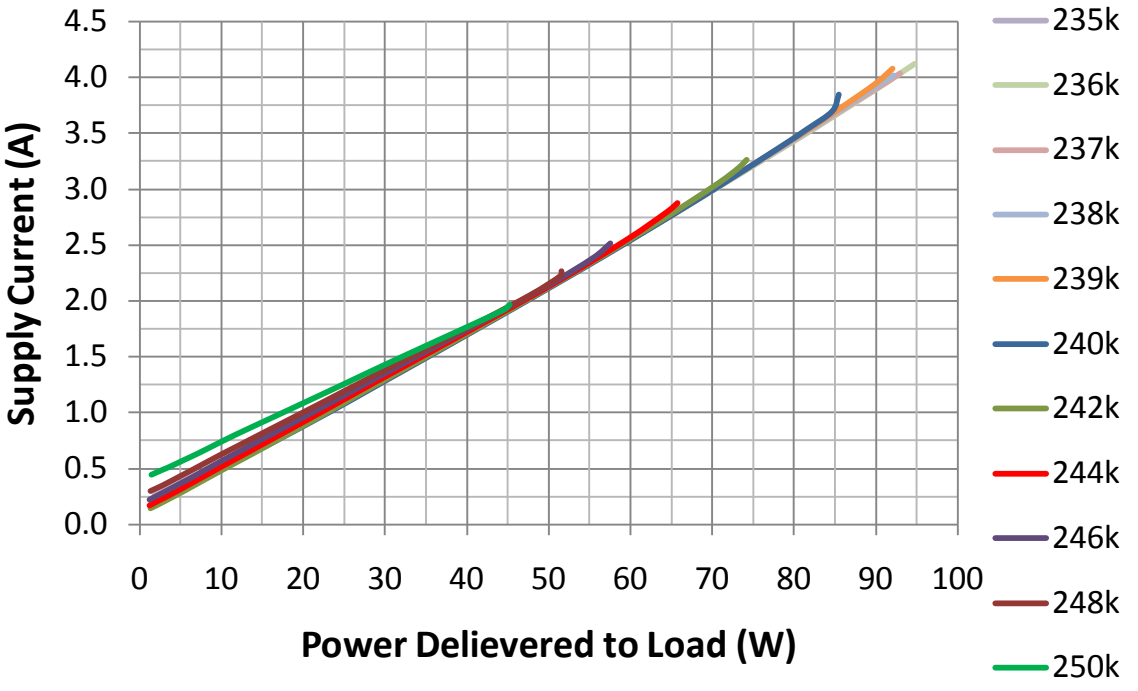

Figure 8-9. Linear relationship between supply current and power delivered to the load for operating frequency from 235 kHz to 250 kHz in steps of 1 kHz.

Figure 8-9 shows the linear relationship between the supply current and power delivered to the load for different operating frequencies (235 kHz to 250 kHz in steps of 1 kHz). The y-intercept and gradient of all the operating frequencies are different. Therefore, each operating frequency will require a different set of data set to describe the relationship. The fixed losses increases with operating frequency because the drain waveform deviates from the ZVS/ZDS conditions when the transistor is turned on earlier before the drain waveform settled down at ground. Therefore, more power is dissipated as heat across the transistor drawing a higher current regardless of loading conditions. This results in an increase of the y-intercept.

In conclusion, using frequency control as a form of power and unregulated receiver voltage control is not the optimum way. The useable frequency range to achieve high efficiency is limited unless the value of C_{shunt} can be tuned as well. This will increase the complexity of the system as two different parameters are being tracked concurrently. Although, the power delivery is reduced with increasing operating frequency, the maximum unregulated receiver voltage during light load actually increases after the frequency crosses a certain threshold which is 244 kHz for this setup. Therefore, the scheme is only able to reduce power delivery and not reduce high voltage device stresses for all loading conditions. In addition, if the operating frequency is varied across a considerable range, FCC regulations will require the system to be tested for each operating frequency.

8.3 Varying C_{out} to Achieve Receiver Voltage Control

The last method to control the receiver voltage is to vary the value of C_{out}. By increasing the C_{out} value, Z_{tx} will be made more inductive, reducing real power delivery to the receiver. The reduction in power delivery will reduce the unregulated receiver voltage for a specific load condition. This technique ensures a more consistent performance with respect to loading conditions as compared to that of varying operating frequency because the frequency is fixed.

The trend of unregulated receiver voltage as shown in Figure 8-11 shows a predictable trend as relative to the one shown in Figure 8-6. In addition, by using a fixed operating frequency instead of a variable operation frequency will make the FCC tests more straightforward.

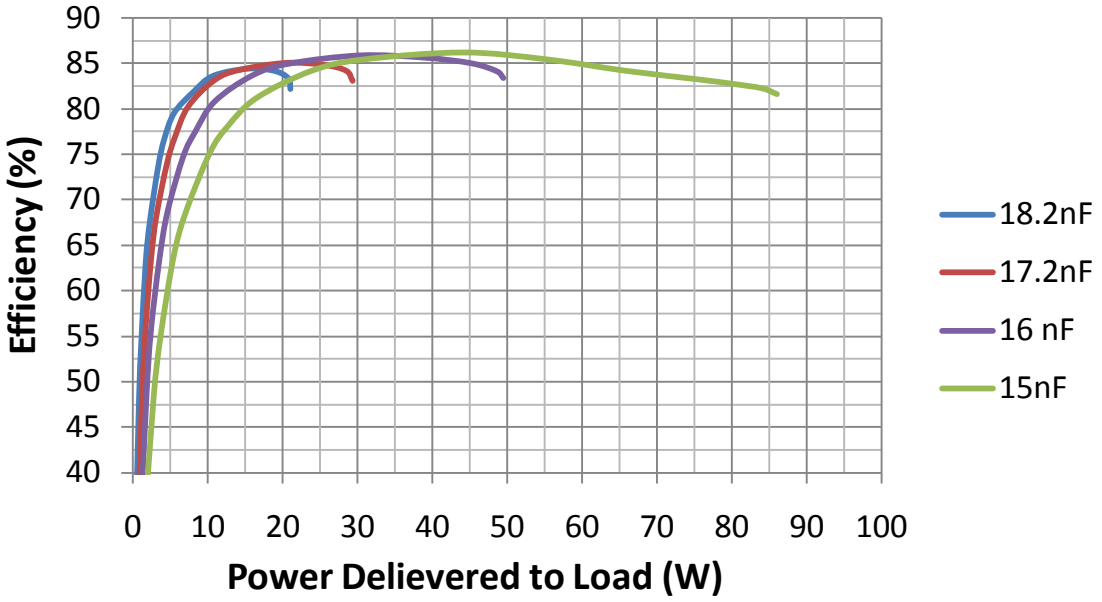

Figure 8-10. Efficiency-power plot for different C_{out} values.

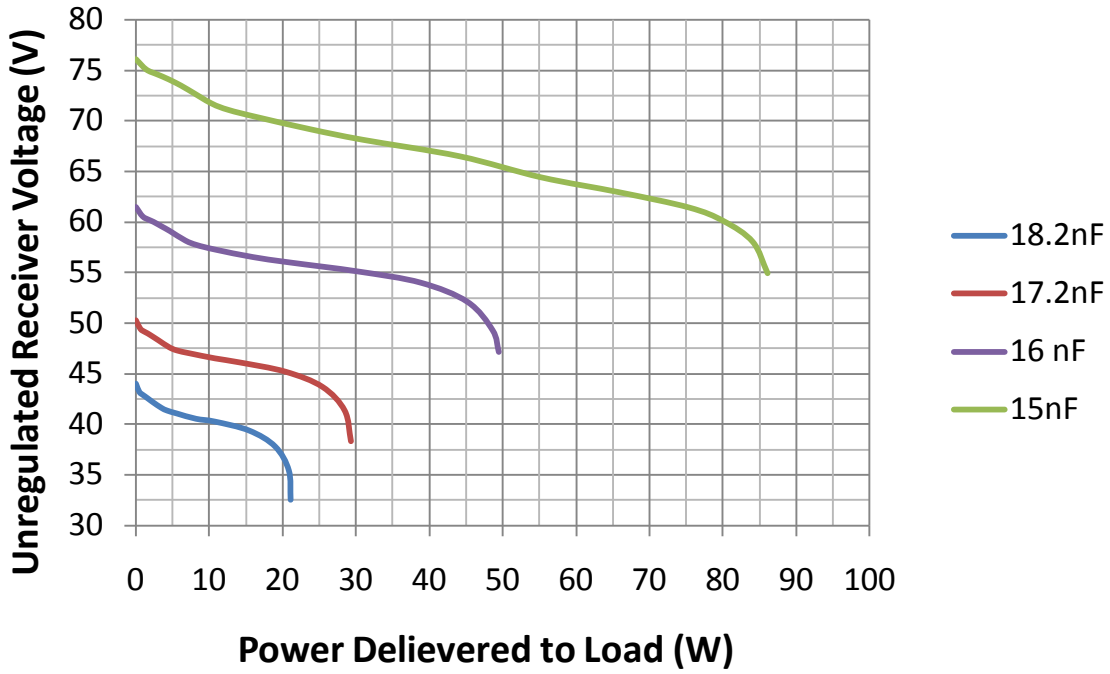

Figure 8-11. Receiver voltage-power plot for different C_{out} values.

C_{out} can be varied either by continuous tuning using a varactor or switching a bank of capacitors. Using a varactor across high AC voltage and current is not practical. Therefore, the more practical solution is to use discrete capacitors and relays to switch between the different capacitance values. Traditionally, high power relays are noisy and bulky but power relay technology has improved significantly that they are becoming more compact and does not produce much audible noise. An example is the P2 V23079 relay by Tyco electronics. Its dimension is 15 mm x 7 mm x 10 mm and is able to handle up to 5A current. The experimental results shown the Figure 8-8 and Figure 8-9 is based on a 2 relays design with the base capacitor value at 15 nF. The two extra capacitors' values are 1 nF and 2.2 nF. Therefore, it is able to achieve four different C_{out} values at 15 nF, 16 nF, 17.2 nF and 18.2 nF. The number of steps are two to the power of the number of relays, thus more relays can be added to increase the resolution. However, it is shown later than a single relay setup might be sufficient.

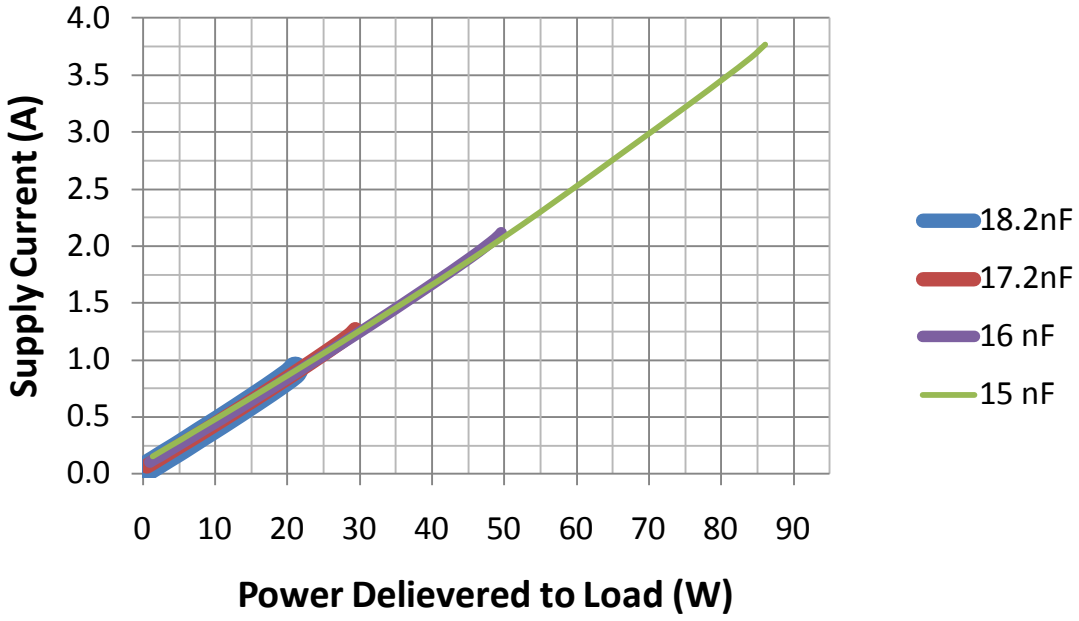

Figure 8-12. Linear relationship between supply current and power delivered to the load for C_{out} values of 15 nF, 16 nF, 17.2 nF and 18.2 nF.

Figure 8-12 shows the linear relationship between the supply current and power delivered to the load for difference C_{out} values (15 nF, 16 nF, 17.2 nF and 18.2 nF). Since all of the lines are overlapping one another, they can be approximated to a common y-intercept and gradient value regardless of C_{out} value. The only different between them is the length of the line which does not affect the load tracking algorithm. Therefore, by varying C_{out} to control unregulated receiver voltage and power delivery, a single set of data is sufficient to accurately track the power delivery of the wireless power system. This will simplify the system significantly.

As shown in Figure 8-10, the improvement in efficiency becomes less significant with the increase in C_{out} value; little difference is observed for C_{out} values of 17.2 nF and 18.2 nF. The unregulated receiver voltage value decreases significantly with increasing C_{out} value, for example, the unregulated receiver voltage decreases an average of 15 V for power level up to 50 W when the C_{out} is increased from 15 nF to 16 nF while limiting the maximum power delivery from 85 W to 50 W. For simplicity, it is still feasible to have only a single relay switching between two capacitance values of 15 nF and 16 nF. The maximum unregulated receiver voltage will be kept below 65 V with a single transition between the two states. In addition, a single set of values is sufficient to describe the supply current and power delivery relationship. This makes tracking and control simple and straightforward while keeping memory usage to the minimum. By reducing the number of times the relay switches, it will also extend the lifetime of the relay.

8.4 Conclusion

By studying the three different techniques of varying power delivery and unregulated receiver voltage, the simplest and most cost effective technique is to use a single relay to control between two different C_{out} values. Although, varying the supply voltage is an effectively technique, the complexity and added cost is too high to justify unless the system is able to completely remove the regulator at the receiver. However, by doing so, a communication link is

required to ensure the receiver's voltage is stabilized and not enter into a positive feedback loop. Finally, varying the operating frequency is not a good technique to control the unregulated receiver voltage due to the limited ZVS/ZDS operating frequency range and sensitivity of the system at increased frequency. Another method which was not discussed is the perform duty cycling on the transmitter. Although, it is a simple and straightforward technique, due to the large inductances of the transmitting coil, it will take considerable amount of time for the transmitter to reach steady state. Therefore, the duty cycling speed of the transmitter is limited. With a slow duty cycling speed, the receiver's DC charging holding capacitor at the input of the regulator will need to be significantly larger in capacitance value to provide a smooth DC input voltage to the regulator, making it not practical.

CHAPTER 9
SUMMARY AND FUTURE WORK

9.1 Summary

A new technique of designing a wireless power transfer system using the class E mode of operation for power transmission via inductive coupling is proposed. The history of wireless power transmission, background information is presented in Chapter 1. The system level design of the wireless power transfer system is discussed in Chapter 2. The design rules for two different impedance transformation network topologies, the series-parallel topology and parallel-parallel topology have been presented in Chapter 3. Instead of using complex detection schemes and variable tank circuits to seek resonance and high efficiency, the system is designed to achieve the desired power delivery profile via its natural response across a wide range of load resistances. A multi-channel topology is also proposed to achieve high efficiency for different power ranges. In addition, a Matlab program is developed to automatically generate the value for each component. Extending the work of a one-to-one system to support multiple receivers, a switch architecture is proposed in Chapter 4 to "decouple" the fully charged receiver from the system so that power delivery to the other receiver can be improved. The switch is able to pass high power signals as well as sustain high input voltages. Simulation results of the switch using Advanced System Design by Agilent verified the performance of the switch.

A dual channel system using the parallel-parallel impedance transformation network topology is fabricated and tested to verify the design. The experimental results are presented in Chapter 5. The fabricated system is capable of delivering nearly 300 W with forced air cooling and the power delivery can be varied via its supply voltage. Higher power delivery can be achieved if a power supply with higher output and transistors with higher breakdown voltages are used. With natural convection cooling, the system achieves a maximum power delivery of 69

W with end-to-end system efficiency of 74%. Another lower power system supporting multiple receivers using a single transmitting coil is also presented in Chapter 5. The system is designed for portable consumer products which are typically charged from a USB port at 5V, 500mA. Experimental results show the power choking phenomena or fish plot when two or more loads are placed on a single transmitting coil. However, when the fully charged device is decoupled from the system using the switch, power delivery to the other receiver is resume to normal.

It is found from the interoperability analysis in Chapter 6 that the system is sufficiently robust to power receivers designed for other platforms as long as the size ratio between the receiving coil and transmitting coil is kept within the range of 1:2 to 1:12. This enables a transmitting unit designed to power a specific model of cell phone to work for other cell phones or even mp3 players. Therefore, the consumer is not required to purchase a different transmitting unit or each device he owns, making it a universal system, reducing waste and power consumption.

A method of load/fault detection is presented in Chapter 7 to protect the transmitter from fault modes ranging from minor to fatal which will potentially damage the transmitter. An example of a fatal fault will be having a huge piece of metal sheet being placed on top of the transmitting coil affecting the self inductance of the transmitting coil. In addition, the load detection system is able to detect if a valid receiver is placed on the transmitting coil, powering down when the transmitter is not in use. This will reduce the no load power consumption significantly making it more energy efficient. A method of power delivery tracking scheme is also proposed to track the power delivery without a communication link. This enables the transmitter to track the charge profile of the receiver so that it can switch between different power handling mode or detect a damaged device or battery.

Finally, three different techniques to control power delivery as well as the unregulated receiver voltage are studied in Chapter 8. Although, varying the supply voltage is an effective way to perform power control, the implementation is too complex. Since a voltage regulator is able to tolerate a large range of input voltages, varying C_{out} in a single discrete step is more than sufficient to provide control to the power delivery and unregulated receiver voltage so as not to damage the receiver regulator. More steps can be added to bring down the voltage if needed.

In conclusion, depending on the requirements, the system can be reconfigured to transmit power wirelessly to different devices for a wide variety of applications. This technology can be applied to rugged electronics to enable the creation of hermetically sealed units and to eliminate the problem of charging port contamination and corrosion for operation in potentially harsh conditions. In environments where sparking and arching hazards exist, this technology can be applied to eliminate an electronic device's external metallic contacts. This technology can also be implemented in our everyday portable devices from cell phones to laptops for the convenience of the everyday consumer.

9.2 Future Work

Further extension of the load/fault detection scheme can be explored using more robust pattern recognition techniques to determine the number of receivers a transmitter is powering as well as their load profile. Although, the work presented is limited to close proximity of not more than 5 cm range and power handling of up to 300 W, the design rules and concepts presented in this dissertation laid the groundwork on how a wireless power system using magnetic induction can be designed. Using the same principles the system can be expanded to support power delivery for longer range and higher power levels e.g. 1 foot distance and >1 kW of power handling. This will enable many new technologies. One of which is contactless electric vehicle charging for which vehicles can be charged both in the garage at home or at work with a coil

embedded into the ground. The system will not require the owner to make an effort to connect a charging cable. The same technology can be applied to powering robotics at factories or warehouses so that they do not need to carry heavy batteries or to power small in-body or on-body sensors to monitor a patient vital signs. Therefore, there are various applied research topics that can be proposed base on this work. In addition, using the same pair of coils, near field high speed communication systems with data rates beyond 1 Gbps can be designed using wideband carrierless communication system.

APPENDIX A
FCC REGULATIONS

FCC regulations require any wireless power system via magnetic induction to pass 3 separate tests. They are Part 18.307 power line conduction test, Part 18.305 emission test and Part 15.109 part 15B test. Each individual test is intended for different purposes and will be discuss in the following sections.

Part 18.307 Conduction Test

The conduction test is to ensure that limited amount of power supply noise is being fed back into the power grid. The limits of the conduction test for various frequency bands are shown in Table A-1 [32]. The noise can be in the form of differential mode noise and common mode noise. However, since a typical DC power will have charging holding and decoupling capacitors along the power path, the predominant noise being fed back into the power system is common mode noise. Measurements of the conduction test are carried at the AC port of the DC power supply. The DC power supply is connected to a line impedance stabilization network (LISN) before connecting into the power grid. The LISN is fundamentally an electronic noise filter network so that the noise from the device under test (DUT) is not fed back into the power grid. The filtered noise is output from the LISN typically via a 50 Ω port which can be connected to a spectrum analyzer or an oscilloscope to analyze the noise signal.

Table A-1. FCC Part 18.307 conduction test limits

Frequency of emission (MHz)	Conducted limit (dBμV)	
	Quasi-peak	Average
0.15 - 0.5	66 to 56*	56 to 46*
0.5 – 5	56	46
5 – 30	60	50

*Decreases with the logarithm of the frequency

Part 18.305 Emission Test

FCC part 18 section 305 states that any device operating at non-ISM frequency below 500 kHz is allowed to have a maximum field strength of 15μV/m at a distance of 300 m. The emission limits are more relaxed if an ISM frequency is used (25μV/m). However, the worst case of operating in a non-ISM frequency is assumed.

It is not practical to conduct RF tests at 300 m range. Therefore, most measurements are conducted using a 10 m range or a 3 m range. By rule of thumb each decade reduction in distance will result in a 40 dB increase in field strength. Therefore the maximum field strength is converted to 82.6 dBμV/m at a 10 m range and 103.5 dBμV/m at a 3 m range. The measurement is typically performed using an antenna with a known correction factor so that the output spectrum into a 50 Ω port can be converted from dBμV to its equivalent field strength of dBμV/m. For a non-radiating system the field strength limit specified by FCC is extremely high and any wireless power system should be able to meet it unless the power level delivered is in excess of 1 kW.

Part 15.109 Part 15B Test

Table A-2. FCC Part 15.109 emission limits at 3 m range

Frequency of Emission (MHz)	Field Strength (μV/m)	Field Strength (dBμV/m)
38-88	100	40.0
88-216	150	43.5
216-960	200	46.0
Above 960	500	54.0

Since the wireless power transfer system neither sends data nor have a communication link, it is considered to be an unintentional radiator falling under Part 15B. The emission limits of Part 15B of various frequency bands at 3 m range are shown in Table A-2 [33]. The intention of Part 15B is to ensure that unintentional radiation is low enough not to interfere to surrounding electronics equipment. Most unintentional radiations are due to fast switching edges of clock

signals and high frequency noise riding on the supply bus. Radiation due to high speed clock edges can be easily suppressed by using a nulling resistor between the output of the gate driver and the gate of the switching transistor to slow down the clock signal. Supply noise can be easily suppressed by adding more decoupling capacitors with the appropriate self resonance frequency (SFR) and equivalent series resistance (ESR) specification.

LIST OF REFERENCES

1. C. E. Greene, D. W. Harrist, J. G. Shearer, M. Migliuolo, G. W. Puschnigg, "Implementation of an RF power transmission and network," U.S. Patent Application, US2007/0191075A1, Jan 23rd, 2007.

2. W. C. Brown, "The History of Power Transmission by Radio Waves," *IEEE Transactions on Microwave Theory and Techniques*, vol. 32, pp. 1230 – 1242, Sep 1984.

3. W. C. Brown, E. E. Eves, "Beamed microwave power transmission and its application to space," *IEEE Transactions on Microwave Theory and Techniques*, vol. 40, pp. 1239 – 1250, Jun 1992.

4. IEEE Std C95.1, 2005 Edition, *IEEE Standard for Safety Levels with Respect to Human Exposure to Radio Frequency Electromagnetic Fields, 3 kHz to 300 GHz*.

5. J. F. Showrow, G. H. MacMaster and W. C. Brown, "The super power CW amplitron," *Microwave Journal*, pp. 52, Oct 1964.

6. J. W. Coltman 'The Transformer," *IEEE Industrial Applications Magazine*, Jan – Feb 2002, pp. 8 – 15.

7. Inductive cooker [Internet]. Wikipedia (US); [updated 2009 May 25; cited 2009 May 27]. Available from http://en.wikipedia.org/wiki/Induction_cooker

8. Electric Toothbrush [Internet]. Wikipedia (US); [updated 2009 May 16; cited 2009 May 27]. Available from http://en.wikipedia.org/wiki/Electric_toothbrush

9. Cut Loose. Wireless power for portable devices [Internet]. SplashPower Limited (UK); [updated 2009 May 27; cited 2009 May 27]. Available from http://www.splashpower.com/

10. Welcome to the Evolution of Wireless Power [Internet]. eCoupled/Fulton Innovation (US); [updated 2009 May 21; cited 2009 May 27]. Available from http://www.ecoupled.com/

11. Leading and Partnering in Wireless Power [Internet]. ConvenientPower (HK); [updated 2009 May 27; cited 2009 May 27]. Available from http://www.convenientpower.com/

12. Wireless Charging [Internet]. PowerMat (Israel); [updated 2009 Jan 7; cited 2009 May 27]. Available from http://www.pwrmat.com/

13. Wireless Electricity Delivered Over Distance [Internet]. WiTricity (US); [updated 2009 Jan 7; cited 2009 May 27]. Available from http://www.witricity.com/

14. Wireless Power [Internet]. WiPower (US); [updated 2009 Apr 27; cited 2009 May 27]. Available from http://www.wipower.com/

15. Wireless Power for a Wireless World [Internet]. PowerCast (US); [updated 2009 May 21; cited 2009 May 27]. Available from http://powercastco.com/

16. M. K. Kazimierczuk "Class D voltage-switching MOSFET power amplifier", *IEE Proceedings-B*, Vol 138, No. 6, Nov 1991, pp. 285 – 296.

17. N. O. Sokal and A. D. Sokal "Class E – A New Class of High Efficiency Tuned Single-Ended Switching Power Amplifier" *IEEE Journal of Solid State Circuits*, Vol. SC-10, No. 3, pp. 168 – 176, June 1975.

18. F. H. Raab, "Effects of circuit variations on the class E tuned power amplifier," *IEEE Journal of Solid-State Circuits*, vol. 13, pp. 239 – 247, Apr 1978.

19. F. H. Raab, "Idealized operation of the class E tuned power amplifier," *IEEE Transactions on Circuits and Systems*, vol. 24, pp. 725 – 735, Dec 1977.

20. Nathan O. Sokal, "Class-E RF Power Amplifiers", QEX, pp. 9 – 20, Jan 2001.

21. X, Liu, S. Y. R. Hui, "An Analysis of a Double-layer Electromagnetic Shield for a Universal Contactless Battery Charging Platform," in *Proc. IEEE 36th Power Electronics Specialists Conference*, 16th June 2005, pp. 1767 – 1772.

22. C. Wang, G. A. Covic, O. H. Stielau, "Power transfer capability and bifurcation phenomena of loosely coupled inductive power transfer system," *IEEE Transactions on Industrial Electronics*, vol. 51, pp. 148 – 157, Feb. 2004.

23. C. Wang, G. A. Covic, O. H. Stielau, "Investigating an LCL load resonant inverter for inductive power transfer applications," *IEEE Transactions on Power Electronics*, vol. 19, pp. 995 – 1002, July 2004.

24. C. Wang, O. Stielau, G. A. Covic "Design consideration for a contactless electric vehicle battery charger," *IEEE Transactions on Industrial Electronics*, vol. 52, pp. 1308 – 1314, Oct. 2005.

25. J. J. Casanova, Z. N. Low, J. Lin, R. Tseng, "Transmitting Coil Achieving Uniform Magnetic Field Distribution for Planar Wireless Power Transfer System," in *Proc. IEEE Radio and Wireless Symposium*, 18th – 22nd January, 2009.

26. X. Liu, S. Y. R Hui, "Optimal design of a hybrid winding structure for planar contactless battery charging platform," *IEEE Transactions on Power Electronics*, vol. 23, pp. 455 – 463, Jan. 2008.

27. R. Laouamer, M. Brunello, J. P. Ferrieux, O. Normand, N. Bucheit, " A multi-resonant converter for non-contact charging with electromagnetic coupling," in *Proc. 23rd International Conference on Electronics, Control and Instrumentation*, Nov 1997, vol. 2, pp. 792 – 797.

28. G. Gwon, D. Park, S. Choi, S. Han, "Wireless charger decreased in variation of charging efficiency," International patent application, PCT/KR2006/001706, 4th May 2006.

29. Z. N. Low, R. A. Chinga, R. Tseng, J. Lin, "Design and Analysis of a Loosely Coupled Planar Wireless Power Transfer System using Magnetic Induction," *IEEE Transactions on Industrial Electronics*, vol. 56, pp. 1801 – 1812, May 2009.

30. Minsik Ahn, Chang-Ho Lee, Laskar, J., "CMOS High Power SPDT Switch using Multigate Structure", in *Proc. IEEE International Symposium on Circuits and Systems*, 25th – 27th May 2007, pp. 3283 – 3286.

31. M. Yu, R. J. Ward, G. M. Hegazi, "High power RF switch MMICs development in GaN-on-Si HFET technology", in *Proc IEEE Radio and Wireless Symposium*, 22nd – 24th Jan 2008, pp. 855 – 585.

32. United States Code of Federal Regulations (CFR) Chapter 47, Part 18, Section 307, 1st October 2001.

33. United States Code of Federal Regulations (CFR) Chapter 47, Part 15, Section 109, 10th July 2008.

BIOGRAPHICAL SKETCH

Zhen Ning Low was borned in Singapore. He attended the Nanyang Technological University in Singapore earning the bachelor's degree in electrical and electronic engineering in 2005 under the accelerated bachelors programme. He worked as an intern at the Institute for Infocomm Research for half a year developing Zigbee wireless sensor networks. During his undergraduate, he joined Positioning and Wireless Technology Centre as an undergraduate research working on GPS and UWB position location systems and authored two conference papers and two journal papers. After obtaining his bachelor's degree in February 2005, he joined the Institute for Infocomm Research as a Research Engineer to continue his work on Zigbee sensor networks and UWB position location system. In August 2006, he came to the University of Florida to pursue his Ph.D. in electrical engineering. For his Ph.D. research he worked under the guidance of Dr Jenshan Lin in the Radio Frequency Circuits and Systems group working on wireless power transfer systems. He has 18 publications in technical journals and conferences and 6 patent applications.